STRUCTURE-PROPERTY RELATIONSHIPS OF ELECTRON BEAM IRRADIATED MONOMERIC AND POLYMERIC SYSTEMS

by

Ha Chul Kim

Dissertation submitted to the Faculty of the

Virginia Polytechnic Institute and State University

in partial fulfillment of the requirements for the degree of

DOCTOR OF PHILOSOPHY

in

Chemical Engineering

APPROVED:

Garth L. Wilkes, Chairman

Thomas C. Ward

David F. Cox

James P. Wightman

William L. Conger

August, 1989

Blacksburg, Virginia

STRUCTURE-PROPERTY RELATIONSHIPS OF ELECTRON BEAM IRRADIATED MONOMERIC AND POLYMERIC SYSTEMS

by

Ha Chul Kim

Garth L. Wilkes, Chairman

Chemical Engineering

(ABSTRACT)

Structure-property relationships were investigated for electron beam(EB) irradiated monomeric and polymeric systems. The objectives were to study the feasibility of preparing systems of potential application, and to characterize these systems in terms of structure-property behavior. In this thesis, the basic theories on radiation chemistry were first reviewed. Next, five different studies on the application of EB radiation were discussed.

In the first study on the surface modification of the methacrylic acid derivative of the glycidyl ether of bis-phenol A(bis-GMA) substrates, considerable changes in wetting characteristics were observed using functionalized poly(dimethyl siloxane)(PDMS) oligomers as surface modifiers. Systematic studies were conducted to investigate the effects of the type of functionality, the molecular weight of PDMS and the radiation dosage, etc. The second subject was on the structure-property behavior of EB crosslinked caprolactone-allyl glycidyl ether(CL-AGE) copolymers. EB radiation was utilized to crosslink these materials at various temperatures both above and below the crystalline melting point. The final solid state properties were found to be strongly dependent on the morphological state of the CL-AGE copolymer at the time of EB irradiation. In the third study, models of time-temperature-energy(TTE) diagrams in an idealized EB radi-

ation curing system were developed to help provide a conceptual understanding of the TTE relationship. Three general adiabatic cases were presented with increasing degree of complexity: the first considered only heating through EB energy dissipation, while the second and third attempted to include a kinetic exotherm, and the effects of glass transition and vitrification behavior, respectively. The fourth study focused on the effects of EB irradiation on the mechanical and thermal properties of poly(phenylene sulfide). The effects of morphological state and atmospheric environment such as air or nitrogen during the irradiation process were investigated in terms of structure-property behavior. In the fifth study, two systems(symmetric and asymmetric) based on the controlled distribution of bis-GMA within a crosslinked nitrile rubber(NBR) network were prepared utilizing EB irradiation. The prepared symmetric and asymmetric distributions of bis-GMA and the morphological structure of the NBR/bis-GMA system were investigated by dynamic mechanical as well as by FTIR and polarizing optical microscopy analyses.

Acknowledgements

The author wishes to express utmost gratitude to his advisor, Prof. Garth L. Wilkes, for his constant encouragement, guidance and support during the course of study.

The author also wishes to thank Drs. Ward, Wightman, Cox and Conger for serving on his committee. The author would like to thank Drs. Smith, Yoo and Prof. McGrath for the synthesis of the siloxane and caprolactone materials, and Drs. Song and El-Naggar for the helpful discussion.

The author would like to gratefully acknowledge the financial support from 3M Corporation.

The author wishes to thank Wilkes' group members for their help and friendship.

Finally, the author wishes to thank his parents, for their support and encouragement.

Table of Contents

List of Illustrations

List of Tables

1.0 Introduction

Radiation chemistry can be defined as the study of the chemical effects induced by ionizing radiation such as electrons, protons, deutrons, alpha-particles, x-rays and gamma-rays. Probably one of the earliest observations in radiation chemistry was by Homer who recognized the sulfur-like smell in the atmosphere after lightening. With a knowledge of modern radiation chemistry, we now know this is due to the oxides of nitrogen and ozone from the reactions initiated by the lightening discharge. However, on a scientific basis, the history of radiation chemistry may not be said to have commenced until the end of nineteenth century when the discovery of radioactivity led to the isolation of radioactive sources.

The development of radiation chemistry began with the discovery of x-rays by Roentgen in 1895 and the blackening effect of a photographic plate exposed to uranium by Bequerel(1) in 1896. In 1899, M. Curie(2) reported that radiation caused the coloration of glass and the formation of ozone from oxygen. Jorrissen and Ringer(3) in 1906 demonstrated that hydrogen and chlorine combine at room temperature by radiation and Jorrissen and Woudstra(4) in 1912 showed that the penetrating radiation from radium caused the coagulation of some colloid solutions. Little additional progress was made during the years prior to the Second World War. In 1942, the first nuclear chain reaction was discovered and this opened a new era by giving a great impetus to the area of radiation chemistry. The development of the nuclear reactor generated the need for

in-depth information on the interaction of radiation with a wide variety of materials. Radiation sources also became more powerful and were readily available as non-natural radioisotopes e.g. cobalt-60, and were produced in atomic reactors.

It was by Dole and Rose(5) during 1947-1949 that polymers were introduced to radiation chemistry and their property changes by radiation were studied systematically. Dole and Rose observed that polyethylene chains were crosslinked by radiation and this induced significant effects on the stress-strain behavior and the yield properties of polyethylene. In 1952, Charlesby(6) published his first paper on the effects of radiation on polymers. About thirty years have now passed since the area of radiation chemistry of high polymers was reviewed in books by Charlesby and Chapiro in 1960(7,8). Since then, numerous valuable industrial applications and research from laboratories around the world have been made of the high-energy irradiation of polymeric systems.

Polymers are unique in so far as their response to high energy radiation is concerned since a few radiation-induced crosslinks can significantly modify the physical and mechanical properties of the irradiated material. For example in a polyethylene, with a molecular weight of 100,000 and weight to number average molecular weight ratio of 9, only one crosslink per 14,400 monomer units is needed to reach the incipient gelation point(9). In contrast, a few chain scissions can have significant effects in the properties of high molecular weight polymers. Even though crosslinking and degradation of macromolecules have been major subjects, radiation polymerization of prepolymers, graft copolymerization and various application studies have also been developed and studied especially over the last two decades.

The extensive studies of electron beam effects on polymeric systems are now approximately thirty years old. However, broad applications of this technology in industry have a much shorter history and it is only in recent years that this area is rapidly growing after a long period of acceptance. Hence, it seems to be appropriate in this thesis that basic theories of radiation chemistry which have been set forth by a number of researchers are first reviewed. Next, application studies of electron beam radiation have been discussed in the following chapters.

2.0 Literature Review

2.1 Primary Interaction of High Energy Radiation with Matter

High energy radiation often includes energetic charged particles such as electrons, protons, alpha and other heavy particles. Some of the high energy photons such as x-rays and gamma-rays are also included in this class of radiation. Upon interaction with matter, high energy radiation results in ionization(or some excitation) of the medium, hence, charged particles, x-rays and gamma-rays are called "ionizing radiation." In contrast, visible and ultraviolet photons interact with matter by mainly producing excited states although ionization can also be produced by photons with high energy. Thus, visible and ultraviolet photons are called "nonionizing radiation" and often need photoinitiators for polymerization and crosslinking. Photoinitiators absorb energy in the ultraviolet-visible spectra range and convert this light energy to chemical energy in the form of reactive intermediates such as free radicals and reactive ions. These reactive intermediate species subsequently initiate polymerization and crosslinking of monomers, oligomers, and polymers. Applications of this nonionizing radiation include photoimaging(10,11,12), UV curing of coatings(13,14,15,16), and inks(17), etc. In the subject of electron beam effects on monomeric and polymeric systems, the interaction

of ionizing radiation with matter has been discussed with an emphasis on electron beam radiation.

It is essential to understand the various primary processes by which radiation interacts with matter since it is in these processes that energy is transferred to the medium. Consequently this energy absorption leads to chemical changes in the irradiated material.

2.1.1 Primary Interaction of Gamma-rays with Matter

Gamma-rays are electromagnetic radiation of very short wavelength, about 0.01Å(0.001 nm) for a 1 MeV photon. Figure 2.1 shows wavelengths and energies for various types of radiation(18). When gamma-rays interact with matter, most of the energy is absorbed in the medium to eject electrons from the atoms of the matter. This process is dependent mostly on the atomic composition and slightly on the molecular structure. In contrast, the absorption of energy from light waves such as infrared, visible and ultraviolet generally depends on the molecular structure of the medium and only indirectly on the atomic composition. This is a fundamental difference between ionizing radiation and nonionizing radiation(19).

Absorption of gamma-rays by matter obeys the fundamental Lambert-Beer law:

$$I = I_0(-\mu x) \qquad [2.1]$$

where I, I_0 are intensities of the transmitted and incident radiations respectively, x is the thickness of the medium and μ is the total absorption coefficient of the material. This

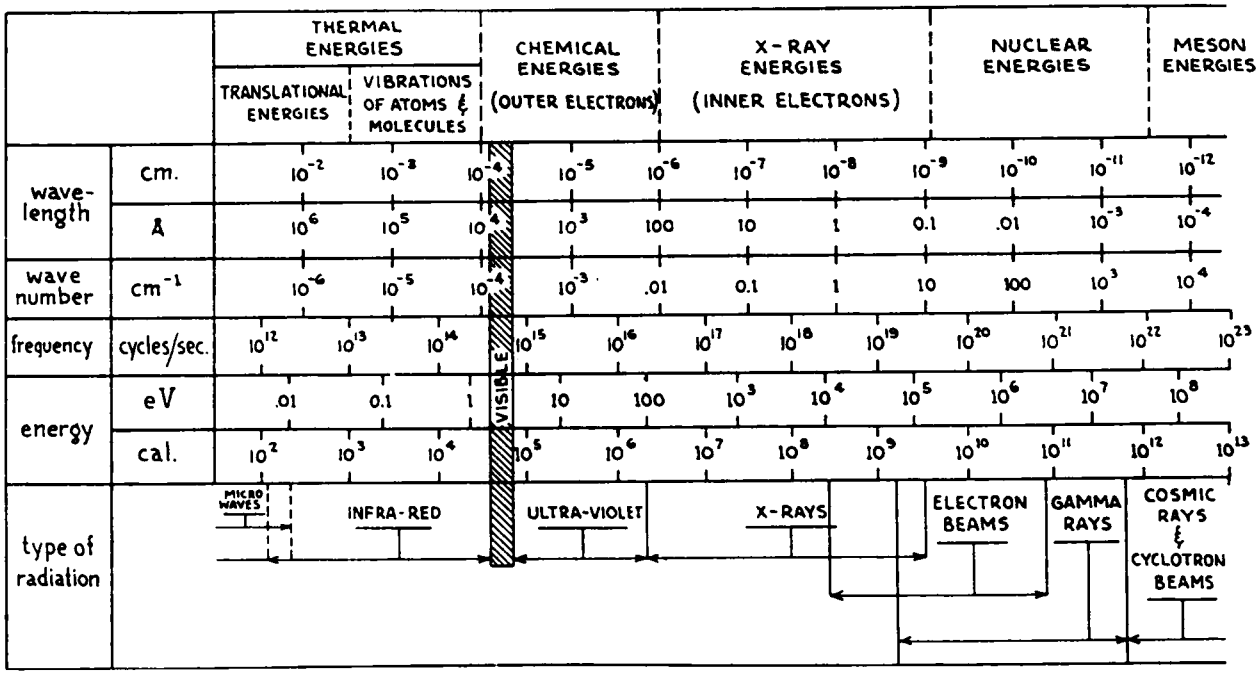

Figure 2.1. Wavelengths and energies for various types of radiation.: (ref.18).

coefficient is made up of contributions from three processes by which energy can be transferred from the radiation to the medium. These processes are called the photoelectric effect, the Compton effect and pair production.

In the photoelectric effect, the photon energy is transferred to an atomic electron with subsequent ejection of the electron. The ejected electron has an energy equal to that of the original quantity less the binding energy of the electron in the atom. Binding energy ranges from 100 eV for low atomic weight materials to 100 KeV for high atomic weight materials. It is known from the experiments that the maximum probability for this process occurs when the energy of a photon coincides with the binding energy of the electron with which it interacts. The photoelectric effect is greatest for low energy photon(< 0.1 MeV) and for elements of high atomic number.

In the Compton effect, the gamma-ray photon gives up only part of its energy to an electron which may be free or bound in an atom. In the latter case, the electron will be ejected from the atom. The incident photon is scattered and proceeds with an energy equal to that of the original quantity less the energy of the ejected electrons. The scattered photon may then undergo absorption by the photoelectric effect or the Compton effect. Compton absorption is important for photons of high energy.

In pair production, the gamma-ray photon is mostly absorbed in the vicinity of an atomic nucleus and produces a positron-electron pair. Note, in the case of the photoelectric as well as the Compton effect, the interaction of the photon is always with electrons of the atoms. The rest mass energy of an electron or a positron is 0.511 MeV. Hence, for a pair production to occur, the minimum photon energy must be 1.02 MeV. Any excess energy of the photon appears as kinetic energy of the electron and positron.

In annihilation process in which the electron and positron are slowed down, two photons, each with 0.511 MeV, are created(7,8).

Therefore, it can be concluded that, regardless of the process of interaction involving photons, secondary electrons are generated and these induce all the chemical changes in the matter following gamma-ray irradiation.

2.1.2 Primary Interaction of Electrons with Matter

Charged particles, upon penetration into a medium, interact with molecules, lose energy and slow down. They lose their energy by interacting either with the electrons or with the nuclei of the medium. The nuclear interaction has two different types which are bremsstrahlung production(high energy level) and Rutherford type of collisions(low energy level). These are not discussed here since only the electronic interactions are of dominating importance in the radiation chemistry of polymeric systems.

The "slowing-down" process of a charged particle is related to and often characterized by the stopping power of the material. Stopping power is defined as the rate of energy loss suffered by a charged particle in traversing a unit path length. As indicated by Pacansky(20), the electron beam irradiation process can be divided into three sub-stages which correspond to the "physical stage", the "physiochemical stage" and the "chemical stage." The stopping power is especially important in the first two stages since, in these two stages, the energy is transferred to the medium and produces excited states for ultimate chemical reactions(The chemical stage is discussed later in the section, Irradiation of Monomeric and Polymeric Systems). The stopping power is related to the charge

and velocity of the incident particle and also to the property of the target material. Electrons lose their energy by inelastic collisions with electrons of the stopping material resulting in ionic and electronic excitation in the medium. The equation describing the stopping power, also called linear energy transfer(LET), was first developed by H. A. Bethe(21). The details about the development and theories of the stopping power can be found in a number of reviews(22,23). A simplified and useful version shown by Pacansky(20) is as follows:

$$(\frac{dE}{dS}) = -7.8 \times 10^{10}(\frac{\rho}{E})\sum_i C_i(\frac{Z_i}{A_i}) \ln \gamma(\frac{E}{J_i}) \qquad [2.2]$$

where

$\gamma = 1.166$

ρ = mass density[g/cm^3]

E = electron energy[eV]

Ci = weight fraction of species

Ai = atomic weight

Ji = mean ionization energy

and Ji is given by Berger and Selzer(24) as:

$$J_i = (9.76 + 58.8Z_i^{-1.19})Z_i \qquad [2.3]$$

Several important features on the stopping power can be gleaned from the above equations as:

(1) The stopping power is proportional to density and therefore will be lower in gases than in solids or liquids.

(2) For energies up to 1 MeV, the stopping power increases as the energy decreases, i.e. as the electrons are slowed down. Figure 2.2 shows a plot for stopping power of polystyrene as a function of electron energy up to 1 MeV.

(3) This relation clearly illustrates the difference between electrons and photons. In a mixture medium, the most abundant component primarily absorb incident electron beam energy whereas, in UV light, extinction coefficient controls the absorption process as shown in Lambert-Beer law(20).

In this section, the process of interaction of electrons with matter has been reviewed with an emphasis on the stopping power theory as it concerns radiation chemistry. Only the interaction with medium electrons which results in ionic and electronic excitation has been considered among the various mechanisms of energy loss involved. In radiation chemistry, studies are concentrated on the formation of chemical products as a result of the energy deposition through this mechanism.

2.1.3 Energy Transfer

The energy consumed in radiation reactions is generally regarded equal to the amount of incident radiation energy absorbed directly by reactants. However, in some cases, the extent of the reaction is far greater than could be explained this way, implying that most of the energy absorption has occurred elsewhere and part of it has been transferred to the various reactive sites.

In the broadest meaning, the term, energy transfer, includes the mass transfer, the charge transfer and the excitation transfer. The mass transfer is the normal diffusion through

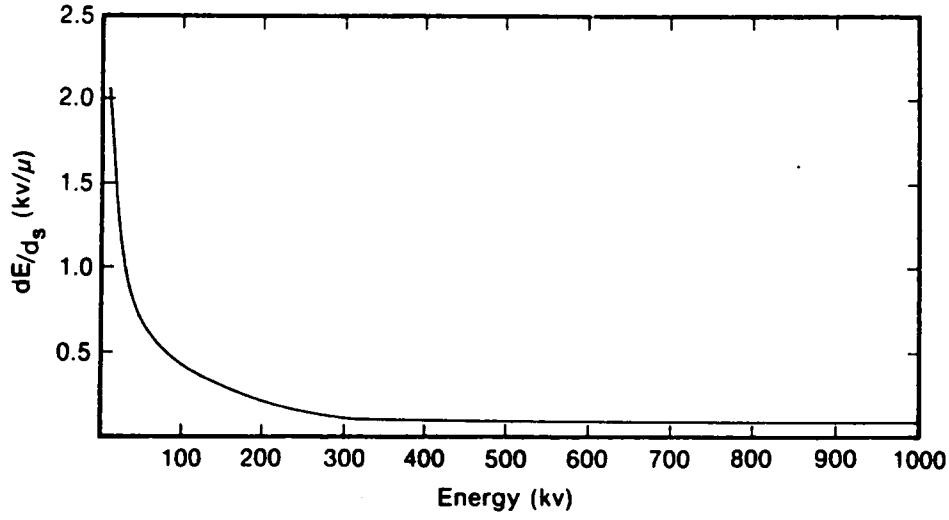

Figure 2.2. A plot of stopping power dE/dS vs. E for polystyrene.: (ref.24).

a particular matrix of small reactive chemical species such as hydrogen atoms, free radicals, ions, and excited molecules. This mass transfer may not be included in the energy transfer, however, for some cases, the mass transfer is accompanied by the charge or excitation transfer. Therefore, in general, the energy transfer is best defined by the transport of charge or excitation although for many polymeric system it is difficult to distinguish between these two processes.

Charge transfer in polymers can be electronic or ionic. Hirsch and Martin(25) showed that the electrical conductivity of various irradiated polymers consist of a "prompt" component by which a considerable amount of charge is transferred to a relatively short range of about 100Å, and a "delayed" component which is highly temperature dependent and indicates a thermally activated charge-hopping process between "shallow" traps. This "delayed" component is usually considered to be terminated after about 1 μ distance by trapping in deep traps or by recombinations. Therefore, it is best to assume that both positive and negative charge transfer are possible in most polymers, with the transfer distance small at low temperature but greater at higher temperature.

Electronic excitation transfer between molecules or molecular groups can occur by a number of different processes-these being the radiative transfer, exchange transfer, excimer transfer, Forster long range transfer, molecular exciton transfer, etc. These are well reviewed in a number of references on radiation chemistry(26). As an example, Forster long range transfer is caused by Coulombic interaction between two molecules which results in simultaneous coupled electronic transitions of equal energy. In this transfer process, one molecule goes from an excited state to the ground state while the other goes from the ground state to an excited state(27).

Energy transfer in polyethylene has been extensively studied in both direct and indirect methods. Studies on charge transfer showed that the charge carriers are predominantly positive species at relatively high temperature(above 80°C) and can migrate for about 1000Å, although migration is limited to about 100Å for temperatures below room temperature(25). Partridge(28) indicated that the efficiency of main-chain excitation transfer in polyethylene is dependent on chain length. The higher efficiency with increasing chain length is found partly due to the increased excitation migration distance and the increased excited state lifetime(29). Various energy transfer reactions have been observed in irradiated polyethylene and other alkanes, however it has been regarded very difficult to differentiate between the charge transfer and the excitation transfer.

Irradiation of solid 1,4-polyisoprene or 1,4-polyisobutadiene is found to produce isomerization of double bonds(30). This appears to be caused not by double bond migration but by excitation of the double bonds which causes them to rotate and then to stabilize in the second geometric isomer form.

The reduction in degradation of irradiated poly(methyl methacrylate)(PMMA) by addition of aromatic amines was shown by Borovkova(31). He ascribed such protection to the trapping of migratory polymer positive charges by the additives, thus preventing scission due to electron recombination with a positive polymer ion. And the excitation transfer due to the additives may be significant since only cations from the additives were observed. Ho and Siegal(32) showed that the addition of biphenyl or naphthalene to PMMA resulted in excited states of the additives upon irradiation and discussed on their observation in terms of excitation energy transfer.

Pacansky(33,34) discussed the role of energy transfer using electron beam irradiation of organic mixtures of some specific types. Concepts of energy deposition and chem-

ical cross section are mentioned here followed by a review of his experiments on the energy transfer.

A rough geometrical description for an electron beam exposure of a film containing N molecules per cm^2 is illustrated in Figure 2.3. E_0 is the energy of electron beam, I the current and the beam is travelling in the z direction which is normal to the film surface. Grun(35) showed that the penetration depth, Zp, also known as the Grun range(R_G), is proportional to the inverse of density and to the 1.75 power of electron energy. Grun also concluded that the shape of the depth dose function is generally invariant to the type of material when the penetration depth and the electron energy are normalized as given below:

$$\Lambda(f) = \frac{d(E/E_0)}{d(z/R_G)} \qquad [2.4]$$

$$\frac{dE}{dz} = \left(\frac{-E_0}{R_G}\right)\Lambda(f) \qquad [2.5]$$

in which the polynomial function, $\Lambda(f)$, has been found empirical in nature depending on the chemical composition of the target material. Figure 2.4 shows an example plot of dE/dz vs. z in the case of $R_G = 12.9\mu(E_0 = 25keV)$. Although dE/dz is not equal to dE/ds which is called the stopping power, since s is the actual electron pathlength, they are approximately equal if the film thickness is small compared to R_G. The chemical cross section, σ, is shown in:

$$\frac{N}{N_0} = e^{-\sigma D} \qquad [2.6]$$

where N_0 is the initial number of molecules and N is the number of molecules after a delivered dose D representing N/N_0 as the fraction of molecules surviving the dose. This chemical cross section provides important concepts on the rate at which chemistry is induced by an electron beam, or on energy transfer between electronic excited states. Figure 2.5 shows a plot of N/N_0 versus dose for a number of materials with experimentally determined cross sections(34).

A system, which consists of diazoketone(a guest additive) and phenolic resin(a host matrix), was chosen by Packansky(33) to illustrate the importance of energy transfer in electron beam chemistry. The chemical structures and a scheme for energy transfer in terms of electronic states are described in Figure 2.6 indicating that the first excited state of the diazoketone is considerably lower in energy than the phenolic resin. Also shown in Figure 2.7 is the N/N_0 for diazoketone decomposition versus plots for various weight ratios of the diazoketone to the resin in electron beam irradiated mixtures. Several conclusions were made from this experiment as follows. First, the cross section increases as the concentration of the diazoketone until the concentration reaches 0.038M where the cross section starts decreasing exponentially as shown in Figure 2.8 which is a replot of Figure 2.7. Therefore, the maximum cross section at 0.038M suggests that this concentration of the diazoketone in the phenolic resin for which energy transfer is most efficient. Second, the energy deposited in the resin matrix, which is highly resistant to chemical damage by the electron beam, is transferred to the diazoketone. Consequently this transferred energy induces chemical decomposition which is the major decay channel for diazoketone. Third, at a concentration of diazoketone below 0.038M, the increasing spatial distance between diazoketone molecules with decreasing concentration reduces the efficiency of the energy transfer as shown in Figure 2.8. These can be explained by the Forster energy

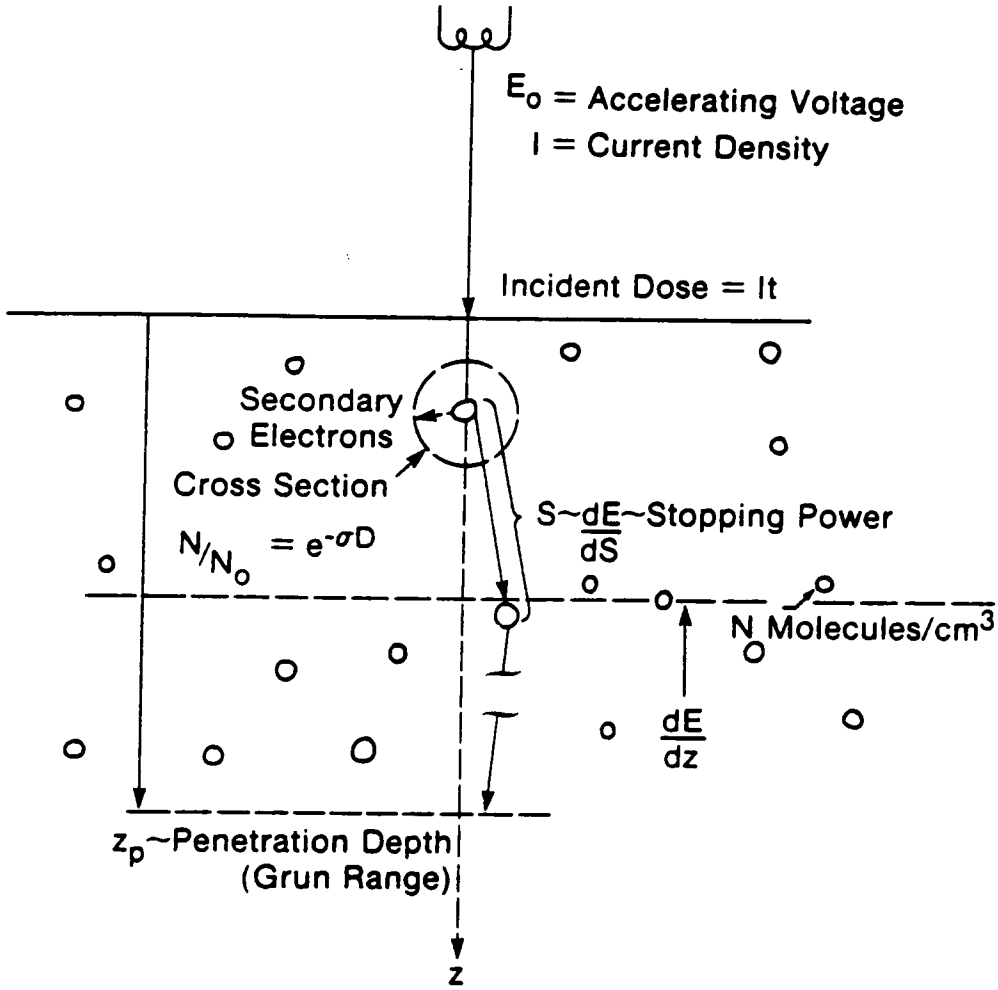

Figure 2.3. A simplified description for an electron beam exposure of a film containing N molecules/cm^3: (ref.33).

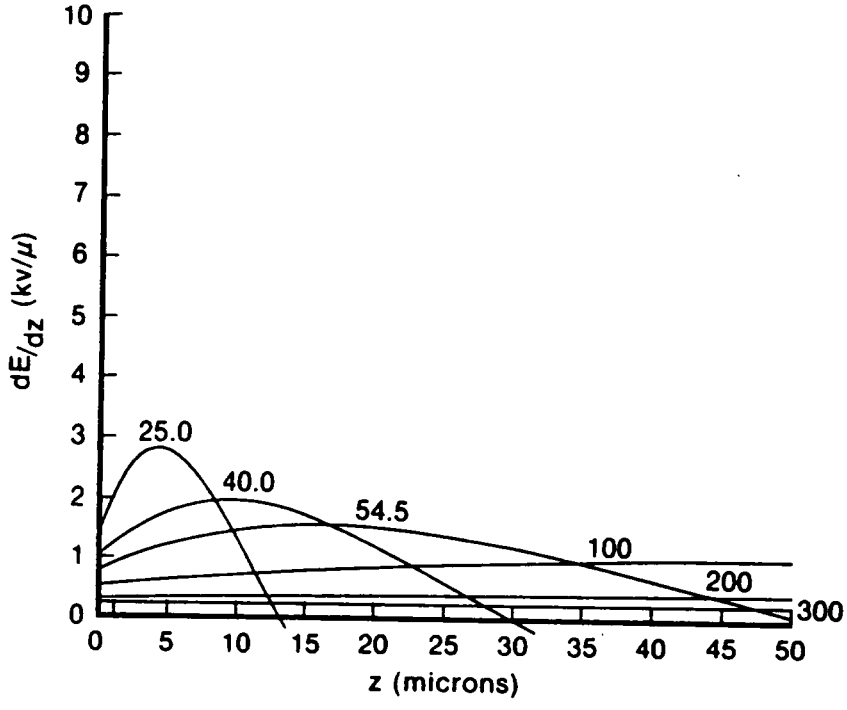

Figure 2.4. A plot for energy dissipation dE/dz vs. z.: (ref.33).

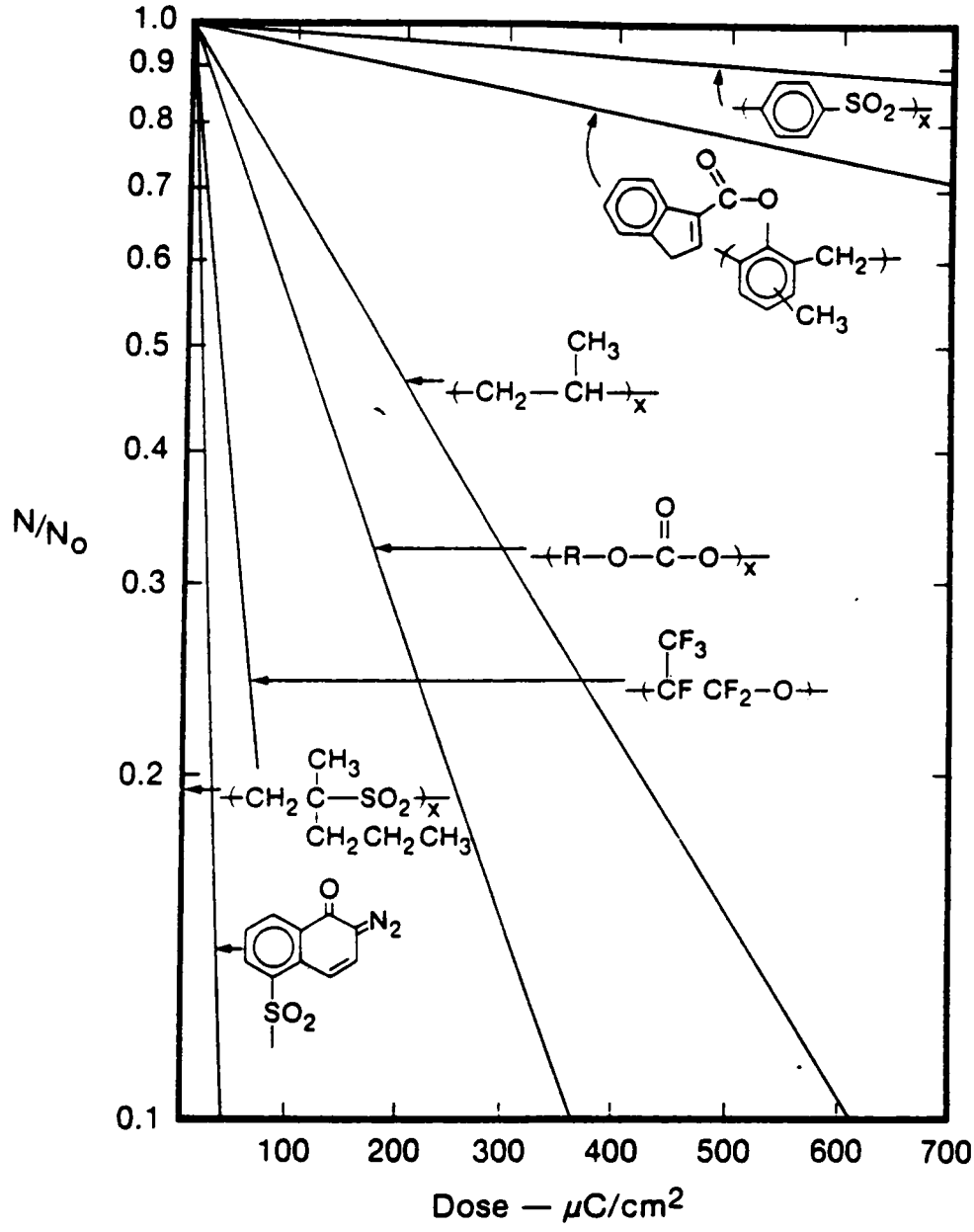

Figure 2.5. A plot for the log of N/No vs. incident electron beam dose for several systems.: (ref.33).

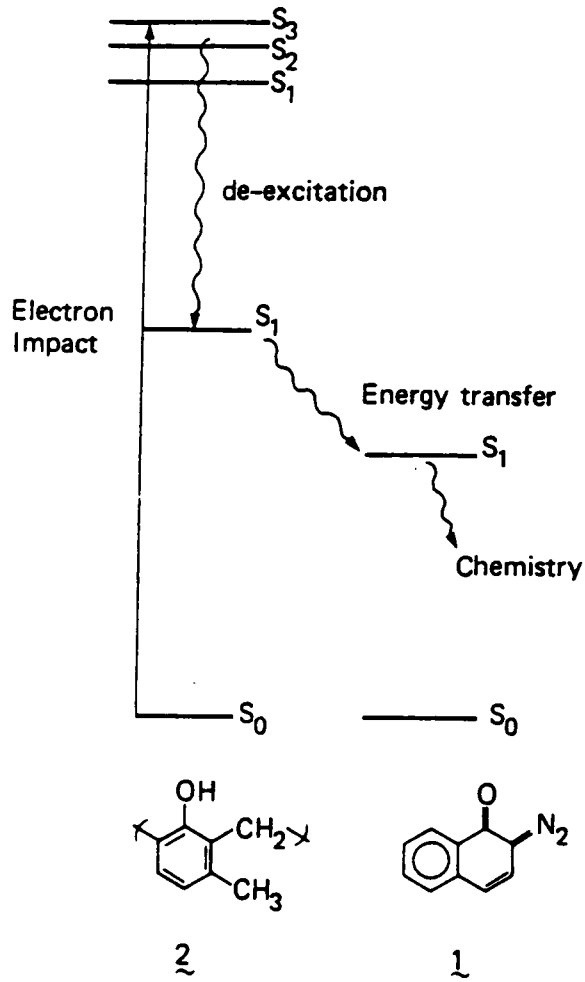

Figure 2.6. A scheme for transfer of energy between electronic states for the diazoketone(1), and phenolic resin(2) system.: (ref.33).

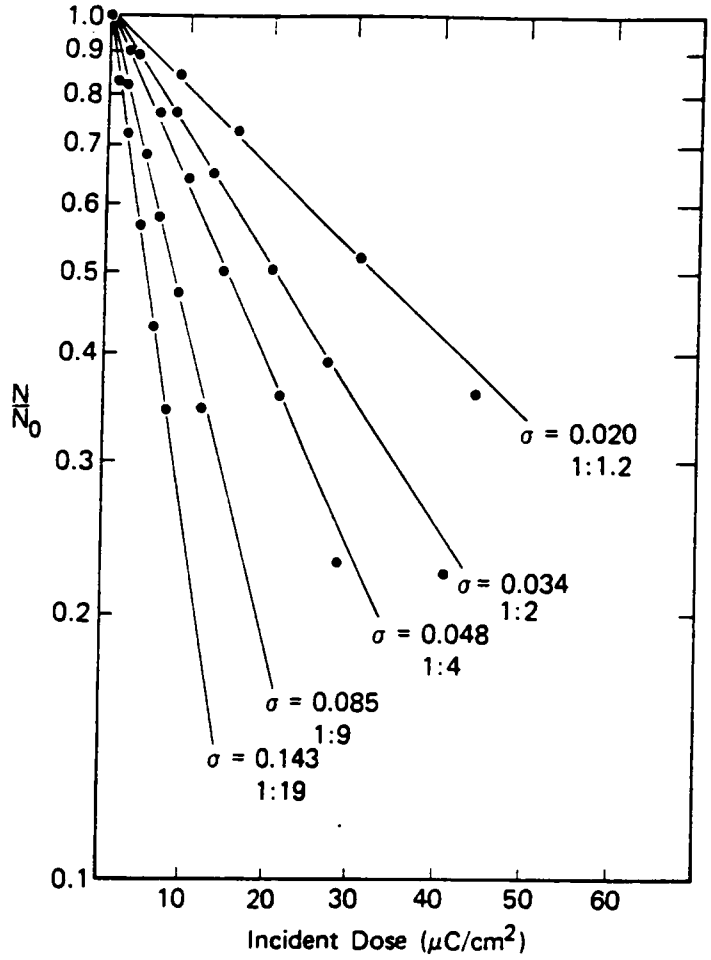

Figure 2.7. **The results for the electron beam exposure of the diazoketone(1)/resin(2) mixtures.:** The slope of each line is defined as the cross section, σ, which is changing with the diazoketone(1)/resin(2) weight ratio(ref.32).

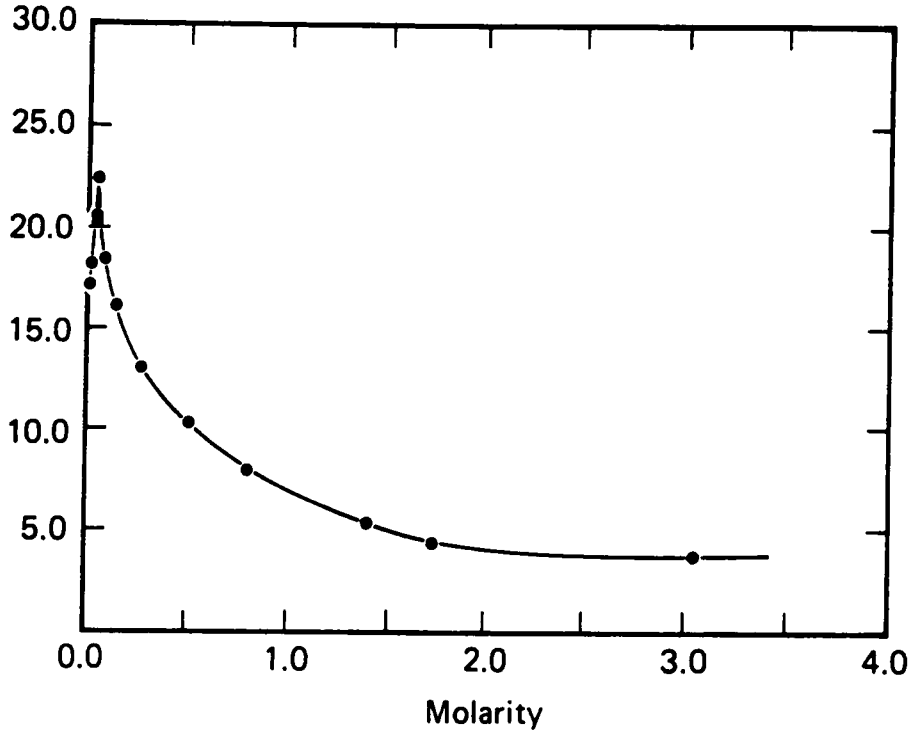

Figure 2.8. A plot of cross section vs. molar concentration of diazoketone.: (ref.32).

transfer mechanism(37), as discussed previously in brief, which describes the most effective distance between molecules for the electron exchange mechanism.

In this section, various aspects of energy transfer in radiation chemistry have been reviewed and the references are listed for the details. The importance of the energy transfer is obvious especially in the selection of chemical formulas and compositions for irradiation processes.

2.2 Radiation Effects on Organic Compounds

The response of organic compounds to radiation varies greatly depending on the physical state and the molecular composition. The importance of radiation effects on simple organic compounds lies in the fact that these compounds may provide models for polymeric systems and may suggest reasonable explanations for the behavior of macromolecules under radiation. In general, aromatic systems are known to be stable to radiation in a moderate temperature range. This must be due to highly delocalized energy of excitation instead of being concentrated on particular bonds. For example, polyphenyls have been used as coolants in nuclear reactors due to the relatively high stability under radiation although the stability has a wide variety of range depending on the exact chemical structure and the radiation condition, etc. In contrast, some olefines and vinyl compounds are readily polymerized often with extremely high yields. Radiation-induced reactions also occur in some oxidation, chlorination, sulfoxinations and isomerizations, etc. Reactivity upon radiation changes accordingly depending on the type of organic compounds with a wide range(36).

The study on reactive intermediate species in radiation- induced reactions has been regarded a very difficult area of investigation and heavy reliance on indirect experiments has occurred such as examination of the final products. This is due to the extremely short lifetime of the intermediate species. Therefore, conventional chemical analysis can be utilized to study these "stable" irradiation products which may have a relatively longer lifetime. In fact, the product can provide information on active intermediate species and reaction mechanisms that is often unique and valuable. On the

other hand, pulse radiolysis technique has been developed in recent years having a time resolution of pico-seconds(37). This technique has known to be a very powerful method to study primary processes in interaction of radiation with matter in "early" stages.

The amount of chemical change under radiation depends on the total radiation energy deposited in the material. And this concept has led to the definition of the G value as the method to express yields of the radiation induced chemical changes. The G value is best defined as the absolute chemical yield as the number of individual chemical events occurring per 100 eV of absorbed energy(8). For example, G(crosslink or X) represents the "absolute number of crosslinks produced per 100 eV" in a certain reaction. Therefore, this G value is widely used to represent the amount of chemical changes(or sensitivity) upon irradiation.

2.2.1 Saturated Hydrocarbon

Direct observation of the free radicals generated by irradiation of saturated hydrocarbons have been made by optical methods and electron spin resonance. The optical absorption spectrum is not specific about the nature of the free radicals, however it gives information on the reaction kinetics. In contrast, ESR experiments can be very informative about the free radical structure.

The ESR spectra of irradiated 3-methylpentane glasses have shown that a single type of radical, $CH_3C{\bullet}HCH(CH_3)CH_2CH_3$, is formed with G = 1.6(26). This result reflects the location of the weak secondary C-H bonds upon electronic or ionic excitation. The formation of a single or, at most, a small number of free radical types have been reported

as a general case in gamma or electron-irradiation of organic solids and liquids. The absence of other types of free radicals could be due to "cage effects" by which ruptured C-C bonds in an intermediate state are held in position by the neighboring molecules and consequently are recombined. The H atoms formed from broken C-H bonds, which are stronger than C-C bonds, however, have a much better chance to escape away without a recombination.

G. R. Freeman(38) studied the irradiation of liquid cyclohexane which has been widely utilized due to its simplicity. All the C-H bonds and all the C-C bonds are basically identical. Table 2.1 shows the complete list of the initial products and their yields with irradiation dose up to 5 Mrads by gamma-irradiation. As expected, hydrogen is formed as a major product. Most of the hydrogen molecules should be formed from the direct abstraction process of H_2 or by the reaction between "hot" hydrogen atoms and cyclohexane such as

$$H + C_6H_{12} \rightarrow H_2 + C_6H_{11}\bullet$$

Cyclohexene, which is a second major product, has been known to be formed by unimolecular decomposition of cyclohexane and disproportionation of cyclohexyl radicals:

$$C_6H_{12}^* \rightarrow C_6H_{10} + H_2$$
$$2C_6H_{11}\bullet \rightarrow C_6H_{12} + C_6H_{10}$$

Also the dimerization to form the dicyclohexyl can be explained by the reaction:

$$2C_6H_{11}\bullet \rightarrow (C_6H_{11})_2$$

Similar patterns of radiation products for cyclopentane were reported by L. Wojnarovits(39).

Oxygen has a profound effect on the irradiation of hydrocarbons due to its reactivity with electrons and free radicals(38). When cyclohexane is irradiated in oxygen, the yield of hydrogen is reduced significantly with the formation of hydroperoxides. The reactions of organic radicals and hydrogen atoms with oxygen being given as:

$$C_6H_{11}\bullet + O_2 \rightarrow C_6H_{11}O_2\bullet$$
$$H + O_2 \rightarrow HO_2$$

and which can be followed by:

$$2C_6H_{11}O_2\bullet \rightarrow C_6H_{10}O + C_6H_{11}OH + O_2$$
$$C_6H_{11}O_2\bullet + HO_2 \rightarrow C_6H_{11}OOH + O_2$$

For a useful comparison, products of electron beam irradiated n-hexane in the liquid state have been listed in Table 2.2(40). The results are more complex than for the case of cyclohexane since n-hexane does not contain C-C or C-H bonds of the same strength. The major products are in the order of hydrogen, trans-hexane, and various isomeric dodecanes. The mechanisms for these products are analogous to those for the products from cyclohexane discussed before. Although free radical reactions in irradiation of hexane are most important, J. H. Futrell(41) suggested that ionic reactions are responsible for some portion of the low molecular weight products.

Table 2.1. Products of γ-ray irradiated cyclohexane(38).

Product	G-value
Hydrogen	5.6
Cyclohexene	3.2
Dicyclohexyl	1.76
1-Hexene	0.40
Methylcyclopentene	0.15
Cyclohexylhexene	0.12
n-Hexane	0.08
Unidentified C_{12}	0.05
Ethylcyclohexane	0.04
Cyclohexylcyclohexene	0

Table 2.2. Products of electron beam irradiated n-hexane(40).

Product	G-value(vapor)	G-value(liquid)
H_2	5.0	5.0
CH_4	0.5	0.12
C_2H_2	0.3	--
C_2H_4	1.1	0.3
C_2H_6	1.0	0.3
C_3H_6	0.3	0.13
C_3H_8	2.3	0.42
C_4H_8	0.06	0.03
i-C_4H_{10}	0.5	0.0
n-C_4H_{10}	2.2	0.5
C_5H_{12}	0.6	0.3
C_6H_{12}	0.1	1.2
i-C_6H_{14}	0.3	0.0
C_7	0.5	0.15
C_8	1.1	0.53
C_9	0.47	0.45
C_{10}	0.14	0.43
C_{11}	0.1	0.02
C_{12}	0.4	2.0

2.2.2 Unsaturated Hydrocarbons

There is a significant difference between saturated hydrocarbons and unsaturated hydrocarbons. Due to the π-electrons, the unsaturated hydrocarbons have much lower ionization potentials and are better able to accept the addition of free radicals and ions.

Irradiation of cyclohexene in the liquid state were discussed by G. R. Freeman(42). As shown in Table 2.3, the effect of introducing a double bond into a molecule can be seen by comparison with the case of cyclohexane(Table 2.1). First, the yield of hydrogen is significantly reduced which is general for unsaturated hydrocarbons compared to the corresponding saturated hydrocarbons. The π-electrons in unsaturated hydrocarbons can be readily attacked by free radicals or cations including hydrogen atoms. Thus, this is believed to be the main reason for the decreased hydrogen yield. Second, the dicyclohexyl in the irradiation of cyclohexene is formed as a major product which can be compared with dicyclohexyl in the case of cyclohexane. The dicyclohexenyl is formed by dimerization reactions given as:

with negligible disproportionation to produce cyclohexadienes. However, in the irradiation of cyclohexane, a large number of cyclohexene was formed by disproportionation of cyclohexyl radicals. Third, the irradiation of cyclohexene resulted in a high yield of polymers. This is mainly due to the ability of free radicals to attack double bonds.

Table 2.3. Products of γ-ray irradiated cyclohexene(42).

Product	G-value
Hydrogen	1.28
Cyclohexane	0.95
2,2'-Dicyclohexenyl	1.94
3-Cyclohexylcyclohexene	0.60
Dicyclohexyl	0.23
Unidentified dimer	0.22
Polymer(C_6 units)	2.3

Unsaturated hydrocarbons are much more susceptible to oxidation under radiation than are saturated hydrocarbons. In the case of cyclohexene, it was reported by R. Montarnal(43) that peroxide has been found with high G values after irradiation in oxygen. Then, the peroxide radicals may be neutralized by "hot" hydrogens or may attack allylic hydrogen atoms leading to abstraction such as:

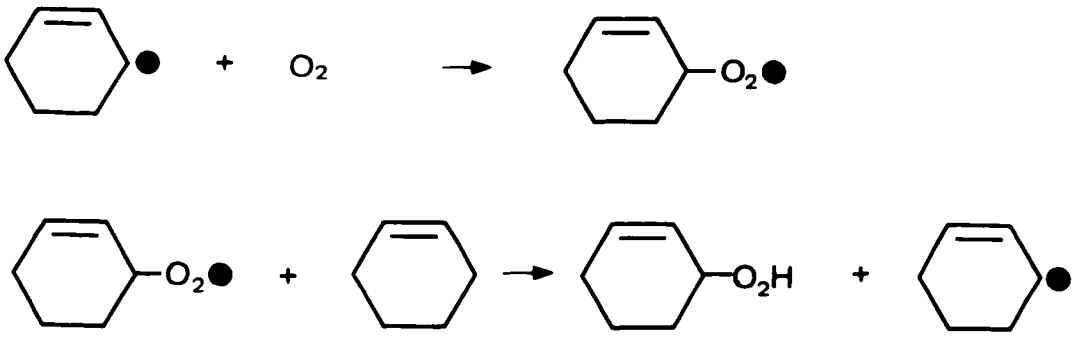

Oxygen has significant effects on the irradiation of monomeric and polymeric systems. As noted in a number of polymers, it decreases the tendency to crosslink and increases the tendency to degrade. Also, oxygen produces a number of side products such as peroxides, carbonyl, carboxylic groups, etc.

2.2.3 Aromatic Hydrocarbons

Aromatic compounds are known to be relatively stable to radiation than the alkanes and alkenes, which can be seen by comparing the yield values from irradiated(gamma-rays) benzene in Table 2.4(44) with those from cyclohexane in Table 2.1. In this comparison, small yield values of all products imply the ability of liquid benzene to absorb energy without decomposition. The π-electrons of the aromatic system are shared by the entire system and, consequently, the energy of excitation

is delocalized instead of being concentrated on particular bonds. And the excitation of π-electrons results in the lowest triplet excited states which are formed by internal conversion and intersystem crossing from higher singlet excited states. Therefore, a large portion of the excitation energy received by an aromatic molecule is transferred to relatively lower-energy triplet excited states which have lower probabilities of dissociation. The energy taken up can be retained for a relatively long time in the form of electronic excitation, and the aromatic system is also known as an energy sink for energy received by other parts of the molecule(44). The yields of hydrogen and low molecular weight products from substituted benzenes such as toluene(45), xylene(46), ethyl benzene(47) are generally no greater than those from benzene itself.

As shown in Table 2.4, the major gamma-radiation products from liquid benzene are higher molecular compounds which are often referred as "polymer." This has been shown to include C_{12} compounds(biphenyl, phenyl cyclohexadiene, phenylcyclohexene, and nonaromatic bicyclic compounds), C_{18} compounds(hydrogenated terphenyls), and higher molecular weight compounds of similar molecular weights. The average molecular weight has been shown to increase with increasing radiation dose(48).

2.2.4 Other Organic Compounds

Halogenated hydrocarbons are among the organic compounds which are most sensitive to radiation. In these compounds, the carbon-halogen bonds are weaker than either carbon-carbon or carbon-hydrogen bonds. A broken carbon-halogen bond by radiation results in giving an organic free radical and a halogen atom. As an exception, C-F bonds are relatively stronger than other bonds in the molecules and,

Table 2.4. Products of γ-ray irradiated benzene(44).

Product	G-value
Hydrogen	0.039
Acetylene	0.020
Ethylene	0.022
1,3-Cyclohexadiene	0.008
1,4-Cyclohexadiene	0.021
Phenyl-2,4 cyclohexadiene	0.021
Phenyl-2,5 cyclohexadiene	0.045
Biphenyl	0.065
Polymer(C_6 units)	0.8

thus, irradiation of these compounds leads more frequently to breaking of other bonds. According to the order in the reactivity in the series, F > Cl > > Br > I, chlorine atoms abstract hydrogens readily from organic molecules whereas bromine atoms do that less readily and iodine atoms do so rarely. Therefore, the initial radiation products from chlorine compounds tend to contain chloride, while bromine compounds tend to give hydrogen bromide or bromine or both, and iodine compounds give iodine(49).

Alcohols are very similar to water, as polar components, in the behavior upon irradiation. Radiation products from pure alcohols contain hydrogen, hydrocarbons, water, carbon monoxide, glycols and aldehydes or ketones. Primary alcohols tend to give mainly aldehyde, secondary alcohols tend to give a mixture of aldehydes and ketones and tertiary alcohols give ketones only. Also, alpha-glycol, RC(OH)-C(OH)R, are usually formed which is consistent with the postulate that a common radiation-induced reaction of alcohols (RCHOH) is abstraction of alpha-hydrogen atom to give the radical, RC•OH. The yield of hydrogen increases with the straight chain alcohols and decreases with increased branching, whereas hydrocarbon yields are greatest with branched-chain alcohols(50).

Irradiation of ethers is analogous to that of the alcohols except that the predominant bond cleavage happens mainly at the C-O, and C-C positions which are adjacent to the ether oxygen. They are decomposed by radiation to a somewhat greater extent than alcohols, in contrast to their stability toward to many chemical reagents(50).

Studies of irradiated acetone have given basic information on free radical reactions of carbonyl compounds. Major radiation products from acetone are in the order of CH_4, CO, and H_2. These indicate that cleavage in carbonyl compounds occurs

predominantly between the carbonyl group and the larger alkyl group to give $R_1C{\bullet}O + {\bullet}R_2$(51). Not much information has been given on the radiation chemistry of aldehydes although it has been known that they are reactive and produce polymers by irradiation even at low temperature(50).

A number of nitrogen compounds have been investigated on the reactions by radiation. Yields for nitrobenzene and aniline are low, and the aromatic system helps stabilize the molecule. Heterocyclic compounds which have aromatic character are also stable to radiation if the yield of hydrogen is taken as the criterion-however they give significant high yields of polymer. Pyrrole, pyrollidine, piridine, pyridazine, and pyrimidine have been reported to give high yields of polymer(52). Acetonitrile(CH_3CN), which is the simplest nitrile, also has been shown to give a significantly high G value of polymers(53).

In addition to the few relatively simple examples discussed in this section, the radiation chemistry of numerous other organic compounds has been studied. The results have given valuable information in understanding reactive intermediate species and reaction mechanisms. And the radiation chemistry of relatively simple organic compounds has been regarded essential in investigating the radiation effects on polymeric systems.

2.3 Irradiation of Monomeric and Polymeric Systems

Although the radiation chemistry of polymeric systems has a relatively short history, many industrial applications have already come into our daily life. This may both be represented by the growing interests in the area of radiation chemistry by increasing research and developments in both industry and academia. Clearly, in certain industrial processes, radiation techniques often serve as excellent alternatives due to their unique features.

Let us look at our most important means of local transportation-cars. The paint on the dash board is often cured by electron beams and much of the foamed plastics used for insulation of noise, shock and extreme temperatures are irradiated plastics. Insulation components of auto ignition system consist of radiation crosslinked materials. A number of dairy products we pick up from the stores are probably encased in a packaging material processed by electron beam radiation. We also encounter, in our everyday life, miscellaneous irradiated monomeric and polymeric materials such as magnetic tapes, optical fibers, paints, adhesives, etc(54).

The primary interaction of radiation with matter which leads to the electronic and ionic excitation has been discussed in the previous sections. These are represented by the "physical" and the "physiochemical" stages(20). The third stage, the "chemical stage," is discussed in this section. Although the overall effects of radiation on polymeric system are known, the basic mechanisms and kinetics of radiation-induced reactions are yet to be fully understood. Most reactions are often interpreted on the basis of free

radical processes. However, in recent decades ionic mechanisms have been studied in detail and shown that these may play a significant role in certain types of irradiation processes. In any case, a better understanding of basic reactions occurring in irradiated polymeric system will undoubtedly lead to new and widely opened applications of radiation technology in the future.

2.3.1 Polymerization

Polymerization of prepolymers may consist of three major steps which correspond to initiation, propagation, and termination, although these can be slightly modified by other reactions such as "chain transfer." In radiation-induced polymerization, a clear distinction can be found in the first step, where radiation may often be considered as an attractive alternative to chemical initiation by a thermally activated catalyst. Advantages of radiation-induced polymerization include absence of residual decomposition of a chemical catalyst, wide range of initiation rate, a choice of operating temperature, and possible polymerization in solid state or crystalline prepolymers, etc(8).

Conventional processes of addition polymerization are often characterized and categorized by the generation of a specific kind of intermediate, usually free radicals, anions or cations. In contrast to these conventional types of process, it should be admitted that high-energy radiation process is considerably less specific with regard to primary actions. A wide variety of reactive intermediates are known to be formed, and these may result in complicated overall kinetics with the simultaneous operation of more than one mechanism. As an example, free radical and ionic mechanisms

are operating together in the polymerization process of styrene. However, this situation can be somewhat simplified by the fact that one mechanism often predominates under well-defined process conditions. This simplification may also be rationalized if it is recalled that the rates of chain reactions are strong functions of the rate constants for the respective propagation and termination steps, and that the absolute values of k_p (rate constant for propagation) and k_t(rate constant for termination) are specified by the nature of the intermediate species.

What kind of mechanism predominates in a radiation-induced polymerization? Information about this critical question may be obtained in some general ways:

1.By checking the effects of well-known inhibitors such as oxygen, benzoquinone which inhibit free radical reactions, and methanol, acetone which inhibit cationic reactions,etc.

2.From the influence of process conditions(dose rate, temperature, etc.) on the polymerization rate.

3.By studying the reactivity of monomers with cationic, free radical, or anionic reagents in homopolymerization. Some of the examples are shown in Table 2.5(55).

Although, in this section, an emphasis has been placed on radiation-induced polymerization in the liquid state, the unique possibilities of high energy radiation for the initiation of solid state polymerization have been explored in a number of systems. The gel effect and vitrification in certain types of process are also important factors which limit the molecular motion of the reactive chains and influence the degree of polymerization.

Table 2.5. Response of monomers in homopolymerization to different initiation(55).

Cationic	Free radical	Anionic
Isobutylene	Vinyl chloride	Nitroethylene
Cyclopentadiene	Vinyl acetate	Vinylidene cyanide
Alkyl vinyl ethers	Acrylonitrile	Acrylonitrile
β-Pinene	Methyl methacrylate	Methyl methacrylate
α-Methylstyrene	Ethylene	α-Methylstyrene
Styrene	Styrene	Styrene
Butadiene	Butadiene	Butadiene

2.3.1.1 Free Radical Polymerization in the Liquid State

It is obvious that, in major cases, radiation-induced polymerizations take place predominantly by free-radical mechanisms. Applications of the kinetics of free-radical chain reactions to a number of processes have been proven to be successful(26).

A polymerization process should first be initiated by radiation or by some agent, and monomers should be added consecutively to a growing reactive molecule. This growing macromolecule may then be terminated by combination or dis-proportionation to give inactive polymer products. In general, three steps can be differentiated-these being initiation, propagation, and termination reactions.

In initiation, radicals are formed either from the monomer itself or some initiating agent if any is utilized:

$$M, I \rightarrow R\bullet$$

For the case of electron beam radiation, electrons themselves serve as an initiating agent by transferring their energy to the chains, so polymerization can be completed without initiators. The production of free radicals depends on the G values for radical formation from monomers or some initiating agents, however, due to the effects of energy transfer it is rarely an additive function of composition.

In the propagation step, initiating radicals are added to the double bonds of the monomers, giving other radicals which in turn add to monomers giving other radicals, and so forth:

$R\bullet + M \rightarrow RM\bullet$

$RM\bullet + M \rightarrow RM_2\bullet$

In general:

$RM_n\bullet + M \rightarrow RM_{n+1}$

Finally, in the termination step, the sequence of monomer additions is terminated by mutual interaction of two growing macromolecular radicals either by combination, by disproportionation or by mixture of these two processes. In any case, the rates of these reactions are additive for a given polymerization due to the common bimolecular terminations and second-order constants. In general,

$RM_n\bullet + RM_m\bullet \rightarrow$ Polymer

Under steady state conditions, the rate of polymerization, Rp, can be given by:

$$Rp = k_p[M]\sqrt{\frac{Ri}{k_t}} \qquad [2.7]$$

where k_p and k_t are rate constants for propagation and termination respectively, and Ri is the rate of initiation and [M] is monomer concentration. Ri is also equal to the rate at which free radicals are formed, and hence proportional to the G value for radical formation and to the dose rate. Based on the schemes shown above, the

degree of polymerization, DPn, is equal to the amount of polymer formed divided by the number of chains initiated. If termination is by disproportionation,

$$DPn = \frac{Rp}{Ri} = \frac{k_p[M]}{\sqrt{k_t Ri}} \qquad [2.8]$$

If termination is by combination, DPn becomes twice the right- hand side of equation[2.8].

As shown in the above discussions, the overall rate of polymerization, Rp, is proportional to the square root of the dose- rate. In contrast, the molecular weight is inversely proportional to the square root of the dose rate. This relationship has been reported experimentally in a number of cases where radiation-induced polymerization is applied in the homogeneous liquid phase. One of the earliest experiments indicating the validity of this relationship is shown in Figure 2.9 where pure styrene is polymerized at 20°C by radiation(56). In this plot, the slopes of log(Rp) vs. log(dose rate) and log(Mn) vs. log(dose rate) are close to -0.5 and +0.5 respectively over a wide range of dose rate.

It can be deduced that most polymer radicals in free radical polymerizations terminate predominantly by combination, although systematic studies in this regard are not found in plenty. In general, disproportionation should be more important for tertiary than secondary polymer radicals due to the effect of steric hindrances. These are shown in the examples of termination of poly(methyl methacrylate) radicals which tend to terminate by disproportionation, and polystyryl radicals which tend to terminate by combination(57). Therefore, as an example, it can also be expected that

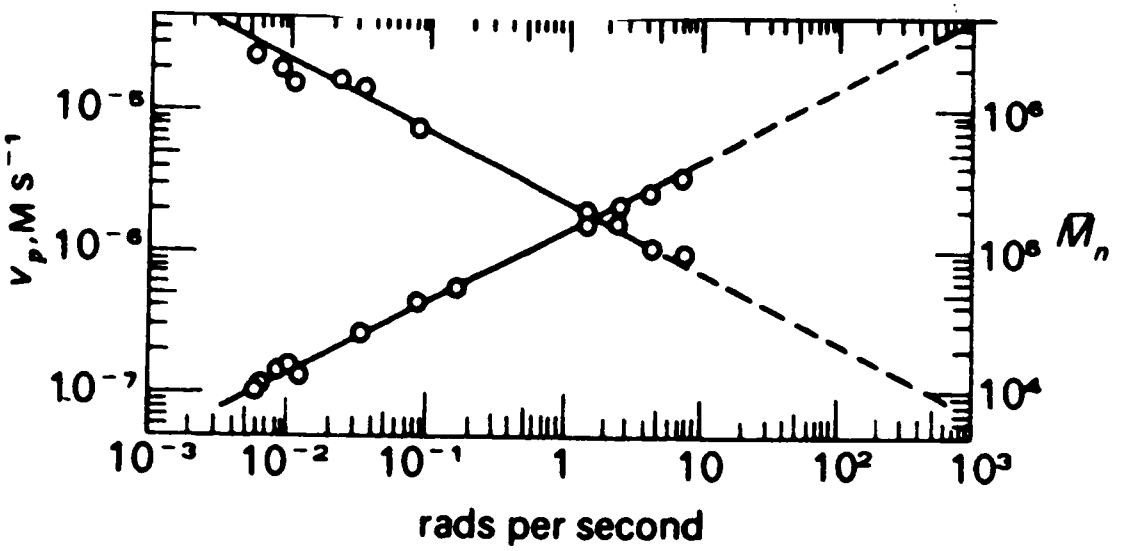

Figure 2.9. Dependence of the polymerization rate and m.w. on dose rate in the free radical polymerization of styrene.: (ref.56).

acrylate functional group is more efficient in radiation-induced polymerization than methacrylate functional group partly due to the steric hindrance effect.

It is possible for polymer radicals to terminate by reaction with monomer, additives or, at higher dose, already formed polymers resulting in formation of radicals. These reactions are called chain transfer processes.

$$RM_n\bullet + AB \rightarrow RM_nA + B\bullet$$

where AB can be a monomer , a polymer or any additives in the reaction mixture. The rate of polymerization remains the same as in the absence of the chain transfer processes provided that the radical B can initiate another chain. However, the degree of polymerization, or molecular weight decreases as shown by

$$\frac{1}{DPn} = \frac{\sqrt{k_t Ri}}{k_p[M]} + \frac{k_{trm}}{k_p} + \frac{k_{trs}[S]}{k_p[M]} \qquad [2.9]$$

where k_{trm} and k_{trs} are constants for transfer to monomers and additives respectively and [S] is the additive concentration(57).

As conversion of the polymerization increases, the viscosity of the system becomes high and hinders termination of growing polymer radicals. Hence the rate of polymerization reaction and molecular weight both show an increase at a relatively high conversion, which is known as the Tromsdorf effect. If the conversion increased further, diffusion limitation of reactive moieties including smaller molecules affects the propagation rate and may assist in inducing the vitrification of the system. As results from these combined effects, the reaction rate is depressed and, consequently, the

polymerization process ceases often without consuming all the reactive species. In certain cases, these trapped reactive species survive for a relatively long time as reported in a number of electron spin resonance experiments.

2.3.1.2 Ionic Polymerization in the Liquid State

Pinner and Worrall(58) in 1957 reported polymerization of isobutylene in the liquid state at -78°C with high energy radiation. This might be the first observation that an ionic polymerization could be radiation-initiated in the liquid state. Since that experiment, a number of studies have been developed to suggest an acceptable description of radiation- induced ionic polymerization.

Radiation-induced ionic polymerization proceeds via three basic steps of initiation, propagation and termination, which are analogous to free radical polymerization. In initiation, generally monomer ions are formed by the interaction with radiation:

$$M \rightarrow M^+ + e^-$$

While the generated electrons can react with other species subsequently, the positive ions can initiate polymerization by adding to monomer:

$$M^+ + M \rightarrow M_2^+$$

leading to the general propagation reaction

$$M_m^+ + M \rightarrow M_{m+1}^+$$

If termination is brought by an impurity, X, such as

$$M_n^+ + X \rightarrow M_m + X^+$$

the termination may occur by charge transfer, proton transfer or addition of an ion to a base. By following procedures similar to those of free radical polymerization, the rate of polymerization, Rp, can be obtained by

$$Rp = \frac{k_{pc} Ri[M]}{k_{tx}[X]} \qquad [2.10]$$

where k_{pc} and k_{tx} are the rate constants for reaction of propagation and termination, respectively. As shown above, the rate of polymerization, Rp, is proportional to the first power of Ri, that is, to the first power of dose rate. An analogous expression can be applied for termination by impurities in free radical polymerization, however, in free radical polymerization, impurities are generally consumed in the early stage of process so that polymerization rate tends to become proportional to the square root of the dose rate as previously discussed. However, in ionic polymerization, the impurity, X, seems to be capable of being regenerated by the charge neutralization so that the expression for Rp shown above is expected to be applicable except at a extremely high degree of purity.

If the amount of impurity is extremely low and the ions are regarded separate, termination would occur by reaction between the propagating ion and the counter-ion:

$$M_m^+ + M_n^- \rightarrow \text{Polymer}$$

and in cationic polymerization without consideration of impurity, the polymerization rate, Rp, is as follows:

$$Rp = k_{pc}[M]\sqrt{\frac{Ri}{k_t}} \qquad [2.11]$$

where k_t is the rate constant for termination in the scheme. An analogous expression can be applied to anionic polymerization. As shown in the equation above, the polymerization rate, Rp, is proportional to the square root of the dose rate, Ri, which is similar to the case of free radical polymerization. Figure 2.10 shows the expected dose rate dependence for this cationic polymerization at various impurity concentrations.

Radiation-induced ionic polymerization is often characterized by the propagation rate constants which are several orders of magnitude higher than those of free radical polymerization and very low activation energies. Therefore, provided that the concentration of the impurities is extremely low, the reaction rates of ionic polymerization might be thousands of times greater than those of free radical polymerization(59).

2.3.1.3 Polymerization in the Solid State

Solid state polymerization has been regarded as one of the novel subjects in polymer science developed since 1950s. Ionizing radiations such as gamma-rays and electron beam have been utilized in the development of radiation-induced polymerization in the solid state. The first report on this subject was given by Schmitz and Lawton(60) who

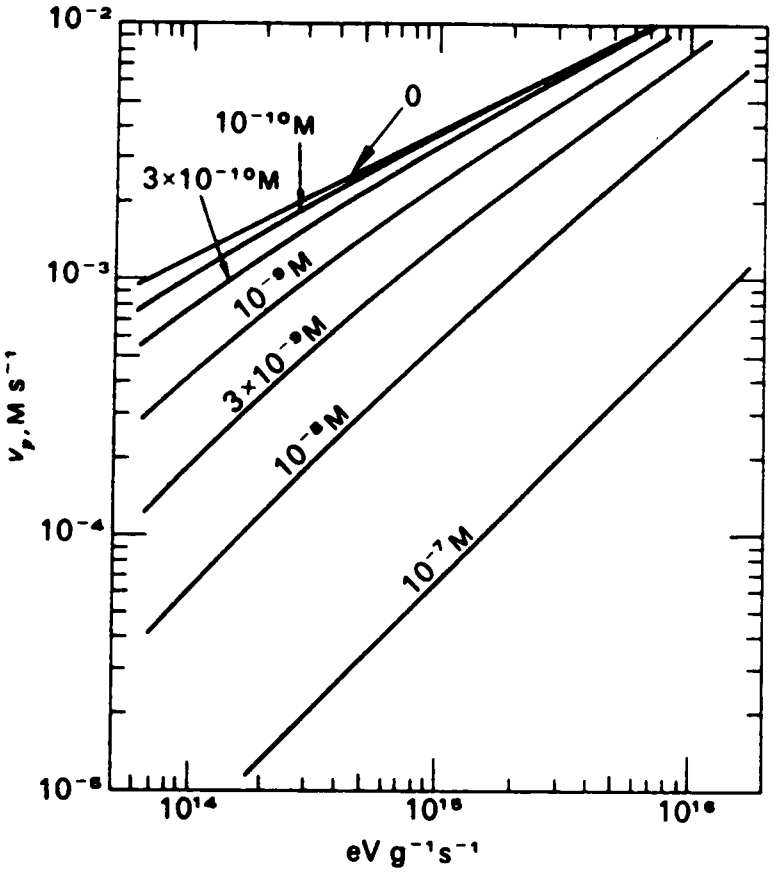

Figure 2.10. Dependence of cationic polymerization rate of styrene on dose rate at various concentration of impurities.: (ref.37).

obtained a polymer product from a solid ethylene glycol dimethacrylate by electron beam irradiation. A number of monomers have been subsequently found to polymerize when irradiated in the solid state. In particular, Mesrobian(61) and Lawton(62) first demonstrated by x-ray diffraction and other techniques that crystalline solid monomers such as acrylamide(Tm = 84°C) and hexamethyl cyclotrisiloxane(Tm = 64°C), undergo radiation-induced polymerization within the crystal. Other monomers which have been polymerized by irradiation in solid state, sometimes at temperatures as low as -196°C, include styrene, vivyl acetate, isoprene and acrylonitrile.

These early studies gave rise to the question as to whether the radiation-induced polymerization could indeed proceed in the solid or the crystalline state. It seemed to be necessary for the molecules to move, at least, about a distance between neighboring molecules if they are to be polymerized, and this process is expected to be strongly hindered in the solid state. Thus, it had been widely presumed that the reaction which proceeds in monomer crystals occurred by local melting by the heat of polymerization or irradiation itself, or that the radicals formed by irradiation are trapped in a glassy or crystalline lattice and initiate polymerization upon subsequent heating. However, there has been very strong evidence that polymerization does occur at extremely low temperatures. For example, potassium acrylate(Tm = 360°C) has been polymerized by radiation at room temperature, in which the heat of polymerization does not have much effect(63). Depending on the type of the material, high conversion can be reached in radiation-induced polymerization of solid monomers and, in some cases, the rate of polymerization is far greater than in the liquid state suggesting some unusual kinetics for molecular motion in crystalline solids(64,65) .

It seems to be necessary to emphasize that the physical state of the crystal is one of the most important factors in solid state polymerization. Samples irradiated under identical conditions have shown differences in polymerization behavior depending on the degree of supercooling as an example. Therefore, the molecular arrangement in the crystal or possibly a hindered rotation of a molecule may influence the initiation, propagation and termination reactions. Interesting features shown by the morphological structure of the prepolymer in solid state polymerization have been reported in recent decades. When little change occurs in the distance between the reacting prepolymer units in a polymerization process, the structure of a monomer lattice can impose order and certain orientation on the polymer product. Certain ring compounds offers an example showing this effect. When the distance between the units in an original monomer crystal is larger than in the polymer product, i.e. if monomer molecules should move to be incorporated into the polymer product, often a volume contraction happens and the produced polymers tend to be amorphous(59). Defects in crystalline solids have been known to play an important role, either increasing the polymerization rate by favoring the mobility of monomer molecules, or decreasing the rate terminating the chain.

O'Donnell and coworkers(66) investigated the radiation- induced polymerization of methacrylic acid derivatives in the solid state. It was shown by electron spin resonance that the major initiating radicals were formed by addition of hydrogen atoms to the vinyl double bond.

Westlake and Huang(67) showed that gamma-ray induced polymerization of styrene in the solid state resulted in a bimodal molecular weight distribution. This has been

attributed to the postulated coexistence of two distinct propagating species, one of which is a radical and the other is a cation.

It has been very difficult to establish the mechanism of radiation-induced polymerization in the solid state. One of the major reasons is that many of the diagnostic methods which have been used in the liquid phase cannot be used readily in the solid state. At the present time, it is widely acknowledged that both free radical and ionic polymerization can occur depending on the type of the prepolymer and conditions of the irradiation process.

2.3.2 Crosslinking

2.3.2.1 Responses of Polymers upon Irradiation

Crosslinking and scission of polymers induced by high energy radiation are simultaneous phenomena and the ratio of these two yields determines the net effect of the process. Depending on the value of this ratio, most polymers might be categorized into two distinct classes-those which crosslink and those which degrade. Miller et al.(68) made an interesting suggestion that the steric factors must be at least responsible for the different behavior of polymers. In the case of vinyl polymers particularly, it has been suggested that crosslinking predominates when the formula is [-CH_2-CHR-] or [-CH_2- CH_2-], however degradation predominates when the formula is [-CH_2-CR_1R_2-]. In the latter case the steric strain introduced weakens the carbon-carbon links in the main chain and enhances the main chain scission. Even though there are several examples where this rule can not be applied, it provides a useful

criterion to most of the observed effects in polymers with a carbon backbone. The main responses for several polymer are shown in Table 2.6(69). And yield values of crosslinking, G(X), and scission, G(S), for several irradiated polymers are given in Table 2.7.

2.3.2.2 Theoretical Aspects of Crosslinking

Flory(70) and Stockmayer(71) first developed a theory of network formation for approximation of the molecular weight changes in a system beginning with species of the same initial molecular weight, M. Without considering links between monomers in the same original polymer, the number of final molecules was calculated on the molecular weight M, 2M, 3M, ---, iM, due to combination of the appropriate number of the original molecules. It was also shown that the number of polymer molecules unaffected by crosslinking decreases exponentially and the number of crosslinked molecules of a certain size, iM, reaches a maximum, then decreases as the crosslink density increases, and eventually a network is formed.

Charlesby(7,72) later proposed the case when an arbitrary molecular weight distribution is initially assumed. It was emphasized that the important parameter in network formation is not γ, the average number of crosslinked units per number average molecule, but δ, the average number of crosslinked units per weight average molecule. The physical properties of the network are also expected to be significantly different depending on the resulting molecular weight distribution.

Below the gel point where a network is formed, it has been shown that the average molecular weights, Mn, Mw, and Mz, increase as follows:

Table 2.6. Effect of radiation on polymers(69).

Predominant crosslinking	Predominant degradation
Polyethylene	Polyisobutylene
Polypropylene	
Poly(vinyl chloride)	Poly(vinylidine chloride)
Chlorinated polyethylene	Polychlorofluoroethylene
Chlorosulfonated polyethylene	Polytetrafluoroethylene
Polyacrylonitrile	Polymethacrylonitrile
Poly(acrylic acid)	Poly(methacrylic acid)
Polyacrylates	Polymethacrylates
Polyvinylpyrrolidone	
Poly(vinyl alkyl ethers)	
Poly(vinyl methyl ketones)	
Polystyrene	Polyα-methylstyerne
Sulphonated polystyrene	
Natural rubber	
Synthetic rubber(except polyisobutylene)	
Polysiloxane	
Polyamide	
Poly(ethylene oxide)	
Polyesters	

Table 2.7. Approximate crosslink and scission yields of irradiated polymers.

Polymer	G(Crosslink)	G(Scission)
Polyethylene	3.0	0.88
Low density polyethylene	2.53	0.4
Polypropylene	0.6	1.1
Natural rubber	1.1	0.22
Polybutadiene	3.8	--
Butadiene-styrene copolymer	2.8	0.39
Polystyrene	0.045	< 0.018
Polydimethylsiloxane	2.7	< 0.54
Poly(alkyl acrylates)		
methyl	0.55	0.18
n-butyl	0.63	0.18
iso-butyl	0.63	0.18
sec-butyl	0.47	0.18
tert-butyl	0.16	0.18
neopentyl	0.57	0.18
Poly(alkyl methacrylates)		
methyl	--	1.2--3.5
n-butyl	--	2.7
iso-butyl	--	3.9
sec-butyl	--	5.3
tert-butyl	--	9.6
Poly(ethylene terephthalate)	0.04--0.14	0.07--0.17
Poly(propylene oxide)	0.15	0.22
Poly(vinyl chloride)	2.15	--
Polycaprolactam(nylon-6)	0.5	0.6
Pol(hexamethylene adipamide)(nylon-6,6)	0.5	0.6
Poly(vinyl acetate)	0.1--0.3	0.06--0.17

$$Mn(r) = \frac{Mn(0)}{1 - \frac{1}{2\gamma}} \qquad [2.12]$$

$$Mw(r) = \frac{Mw(0)}{1 - \delta} \qquad [2.13]$$

$$Mz(r) = \frac{Mz(0)}{1 - \delta^2} \qquad [2.14]$$

with the relation as shown below:

$$\frac{\delta}{Mw(0)} = \frac{\gamma}{Mn(0)} \qquad [2.15]$$

where r is the irradiation dose applied to the system. Therefore, it is possible with proper assumptions to approximate number, weight, and z-average molecular weight. Starting from a linear polymer, the increase in molecular weight is represented by a branched polymer, although below the gel point there is an average of less than one link per average molecule so that the degree of branching is relatively low. At the gel point($\delta = 1$), Mw and Mz become infinite as illustrated in Figure 2.11. A dramatic change in many properties occurs when δ exceeds unity and this occurs whatever the original molecular weight distribution may be.

Above the gel point, a part of the system becomes an infinite network which is insoluble in solvents and this part is called the gel fraction. The other molecules are still soluble, although some of them have become crosslinked. This part is called the sol fraction. For molecules which have an initially random distribution of molecular weights, the following Charlesby-Pinner relationship holds:

$$s + \sqrt{s} = \frac{p_0}{q_0} + \frac{1}{q_0 r DPn} \qquad [2.16]$$

where s is the sol fraction, p_0 the proportion of monomer units fractured per unit radiation dose, q_0 the proportion of monomer units crosslinked per unit radiation dose, DPn, the number- average degree of polymerization. This relationship is not strictly valid for polymers without an initial random distribution of molecular weights. However, even for such a polymer, it might be applied in a relatively high dose range. One of the useful utilities is to calculate G values for crosslinking and degradation providing the number average degree of polymerization is known as shown in Figure 2.12.

2.3.2.3 Mechanism of Crosslinking

Mechanisms by which the chemical changes in polymers are produced should be essentially equivalent to those in lower molecular weight species of similar chemical composition. A number of reaction mechanisms have been proposed to account for radiation-induced crosslinking(73), although the subject is yet to be completely explained. Polyethylene has been one of the most thoroughly studied and serves as a model for long chain paraffin molecules. Several simplified model reactions which can be expected to occur in irradiated polyethylene molecules are as shown in Figure 2.13 and described by the following steps:

step(I): cleavage of a C-H bond to form a hydrogen atom and a polymeric radical.

step(II): direct elimination of molecular hydrogen leading to unsaturation of the polymer.

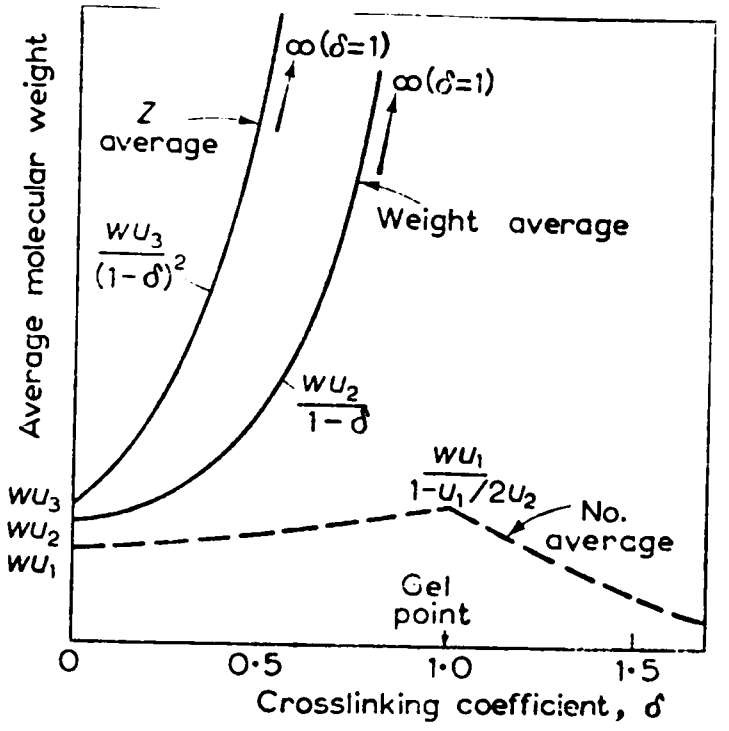

Figure 2.11. Changes in number average, weight average, and z average molecular weight due to radiation induced crosslinking.: (ref.7)

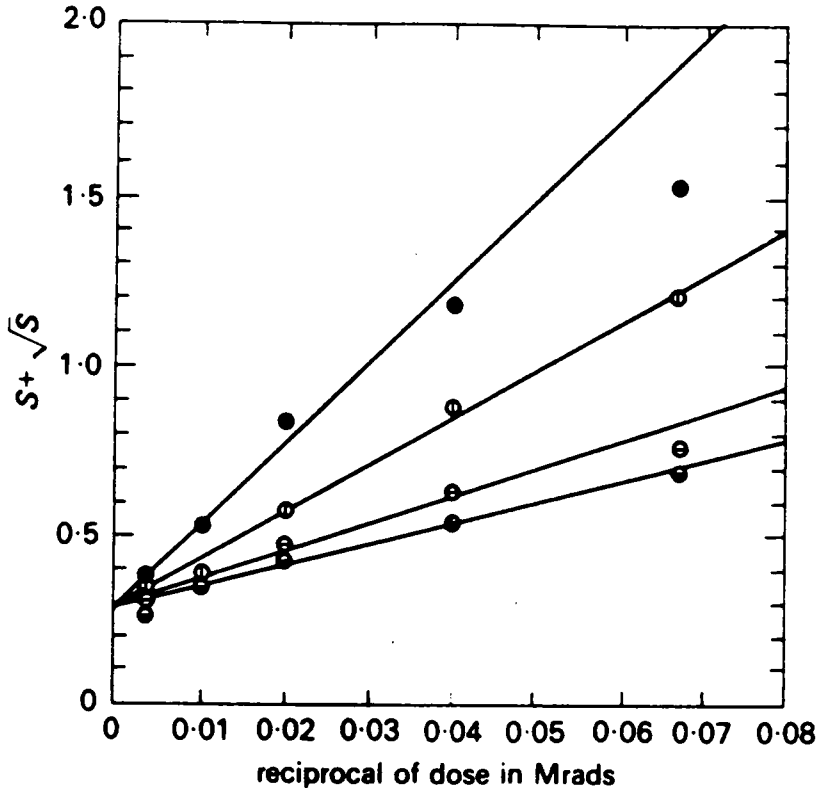

Figure 2.12. Dependence of $s+\sqrt{s}$ on reciprocal of radiation dose in irradiated polyethylene.: (ref.7)

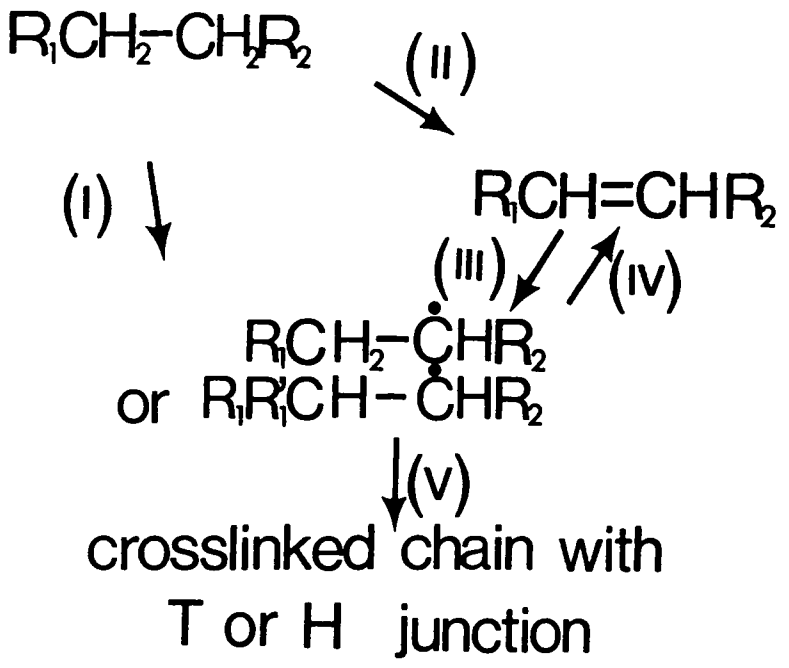

Figure 2.13. A simplified model of a proposed free radical reaction in irradiated polyethylene.

step(III): elimination of a double bond on the polymer by an hydrogen atom or other radical species leaving a polymeric radical.

step(IV): direct formation of unsaturation by abstraction of a hydrogen atom.

step(V): combination of adjacent polymeric radicals to form the crosslink.

One of the most important phenomena is that produced radicals can migrate along a molecular chain or, possibly, between molecules. These intra-chain and inter-chain migrations of radicals have been widely studied(74,75,76). Therefore, it can be deduced from the capability of radicals to migrate that each formation of a radical, an unsaturation and a crosslink can occur without strong dependence on the original location of the reactive site. Although ionic mechanisms have gained strong attention, most of the existing theories on crosslinking have been suggested based on some form of radical reaction.

Pearson(77) proposed a theory of crosslinking based on the reactions of unsaturated groups, either present in the original polymer, or formed subsequently by radiation as shown in Figure 2.14. According to the generalized crosslinking reactions discussed previously, the formation of the radical and the unsaturation can be represented by step(I)(II), and the reaction by step(III). And it was also shown that the migration of radicals is essential to account for the rapid disappearance of initial vinylidene groups.

Dole et al.(78) reported that principally two types of ring structures can arise, depending on whether inter- or intramolecular cyclization takes place. Such structures are shown in Figure 2.15. Structure(I) can likely be derived from an intramolecular crosslinking process since the geometrical configuration occurs with a high probability in a flexible hydrocarbon chain molecule. The formation of

structure(II) by intermolecular cyclization appears to be more difficult to explain. Structure(III) has been assumed to result from the interactions of two neighboring double bonds.

One of the advantages of using irradiated polyethylene, or possibly other polymers which are similar in behavior, lies in the so-called "memory" effect. Polyethylene is generally crystalline at room temperature, and these crystals can lock polymer chains into a configuration quite different from their thermodynamic equilibrium. This configuration may be retained indefinitely by radiation-induced crosslinking until the crystals are melted when the polymer can be stressed to a new temporary shape. Industrial use of this "memory" effect may include shrinkable connectors in cable and other electrical devices in which a controlled shape change is desired, triggered by a simple temperature change.

Types of intermediates and effects by radiation on natural rubber and synthetic elastomers are shown in Table 2.8, 2.9, respectively(79).

2.3.2.4 Enhanced Crosslinking

In the cases which have been discussed so far, crosslinking does not necessarily require unsaturation or other more reactive groupings. It has been assumed that each crosslink is formed independently and requires at least one radiation event on each chain. In order to provide the minimum crosslink density for an incipient network with one crosslink unit per each molecule, a radiation dose(r_0) follows the relation(79,80) as shown by:

Table 2.8. Intermediates in irradiated elastomers(79).

Polymer	Radical structure	Esr line spectrum
polyisoprene	$-CH_2-\dot{C}H-C(CH_3)=CH-CH_2-$	septet
	$-CH_2-CH=CH-\dot{C}H_2$ ⟷ $-CH_2-CH=C(\cdot CH_2)-CH_2-$	sextet
	$-CH_2-CH(C(CH_3)=CH)-CH_2-$ ⟷ $-CH_2-CH(C(\cdot)(CH_3)-CH_2)-CH_2-$	quintet
polybutadiene	$-CH_2-\dot{C}H-CH=CH-CH_2-$	septet
polyisobutylene	$-C(CH_3)_2-\dot{C}H_2-$	broad doublet
ethylene–propylene rubbers	$-CH_2-\dot{C}H-CH_2-$	sextet
	$-CH_2-\dot{C}(CH_3)-CH_2-$	quartet
polychloroprene	$-CH_2-C(Cl)=CH-\dot{C}H_2$ ⟷ $-CH_2-\dot{C}(Cl)-CH=CH_2$	broad singlet
	$\cdot CH_2-C(Cl)=CH-CH_2-$ ⟷ $CH_2=C(Cl)-\dot{C}H-CH_2$	
fluoroelastomers	$-CF_2-\dot{C}F-CF_2-$	doublet of quintets
	$-CF_2-\dot{C}F_2$	triplet

Table 2.9. G values in irradiated elastomers(79).

Polymer	G(Crosslink,X)	$G(H_2)$	G(Scission,S)
Polyisoprene	0.9--1.1	0.43--0.67	0.16
Polybutadiene	3.6	0.23	0.1--0.2
Styrene-butadiene copolymer	1.8--3.8	0.45	0.4--1.9
Polyisobutylene	0.05	1.3--1.6	1.5--5.0
Ethylene-propylene rubber	0.26--0.5	3.3	0.1--0.25
Viton elastomer	1.7	0.27	1.36

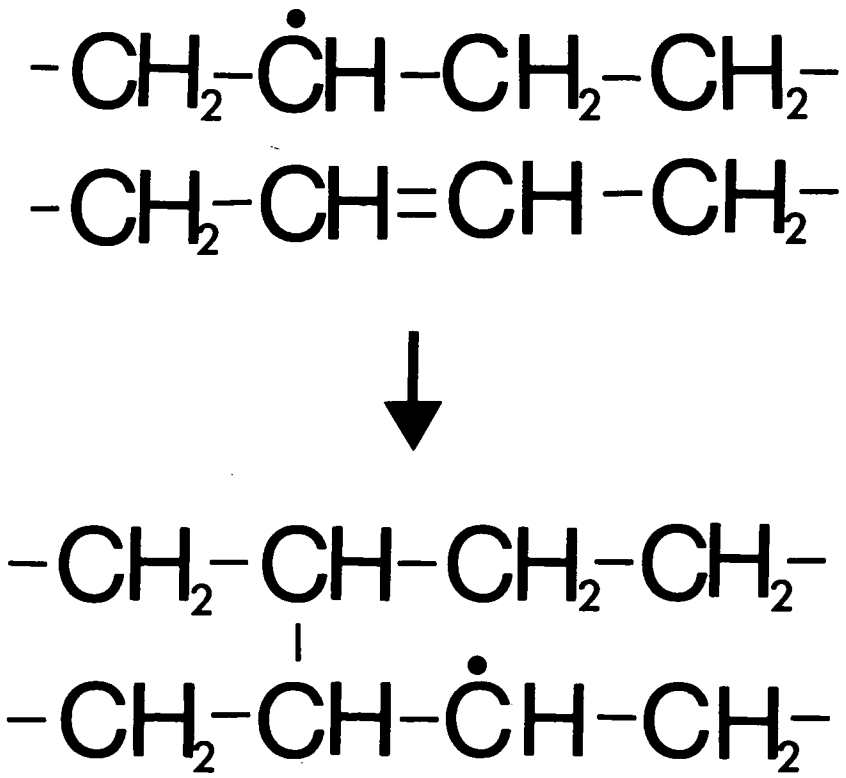

Figure 2.14. Crosslinking based on the reactions of unsaturated groups in irradiated polyethylene.: (ref.77).

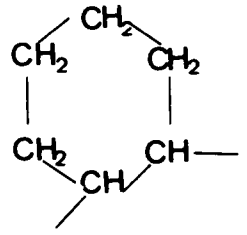

(I)

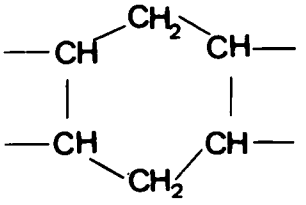

(II)

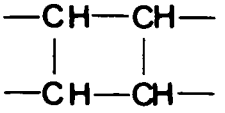

(III)

Figure 2.15. Inter- or intramolecular cyclization in irradiated polyethylene.: (ref.78).

$$r_0 = \frac{0.96 \times 10^6}{G(c.u.)Mw} \qquad [2.17]$$

where r_0 is in Mrad. For a typical crosslinkable polymer with, as an example, $Mw = 2x10^5$ and $G(c.u.) = 2$, r_0 is about 2.4 Mrads. For a low-molecular-weight polymer with $Mw = 10^4$, or a prepolymer with $Mw = 500$, the dose requires 48 Mrads or 1,000 Mrads, respectively, at least for initial network formation. This does not appear to be economically feasible in industrial applications. Therefore, reactive species including the vinylidene group should be introduced for crosslinking of low-molecular-weight polymeric or monomeric systems. In an analogous way, polymers carrying a number of reactive groups on each molecule can be crosslinked as if they are polyfunctional monomers. Using polyfunctional monomers which serve as links and chain propagators, a similar reaction can be obtained with a saturated polymer. Therefore, these types of crosslinking can result in a highly crosslinked structure and even a glassy rigid network at relatively small doses. And it has been reported that crosslinking of low-molecular weight reactive monomers, oligomers or polymers by low energy radiation occurs almost exclusively by free radical mechanism(81).

2.3.2.5 Time-Temperature-Transformation(TTT) Diagram

The curing phenomena of thermosetting resins by either thermal or radiation initiation can generally be characterized by the property changes such as gelation and vitrification. In gelation, an incident infinite network is formed, and vitrification describes a transformation from the liquid or rubbery state to the glassy state due to an increase in molecular weight and/or crosslink density. In vitrification, an increase in viscosity in-

fluences the kinetics while viscosity is also affected by the extent of reaction and temperature, etc. As the curing reaction proceeds with increasing molecular weight, the glass transition temperature of the system also increases. When the glass transition temperature reaches the cure temperature, the material undergo vitrification with retardation of the chemical conversion which is often characterized by diffusion limitation. Therefore, radiation or thermally induced reaction can be quenched due to vitrification without complete consumption of reactive moieties.

Gillham and coworkers(82,83) developed a time-temperature- transformation(TTT) diagram showing a plot of cure temperature and times required to reach gelation and vitrification in an isothermal curing process. This TTT diagram is represented by distinct regions of the thermosetting process such as liquid, gelled rubber, gelled glass, ungelled glass and char as shown in Figure 2.16. The gelled rubber and gelled glass may still contain sol components. Isoviscosity contours in addition to gelation and vitrification are also included.

Isothermal curing processes at various cure temperatures based on the TTT diagram can be described as follows. Tg_0 is the temperature of the uncured resin and below this temperature there is generally no reactivity. Tg(gel) is the temperature at which gelation and vitrificaton coincide. Between Tg_0 and Tg(gel) the system reaches vitrification before gelation by quenching any chemical reactions. The system vitrified below Tg(gel) is of relatively low molecular weight and thus upon subsequent heating the material is readily processable. In the temperature range between Tg(gel) and Tg_∞ which is the glass transition temperature of the fully cured resin, the material starts as a liquid, reaches gelation by entering the gelled rubber region and vitrifies due to the effect of Tg raised to the cure temperature. As the cure temperature is increased in this region, less time

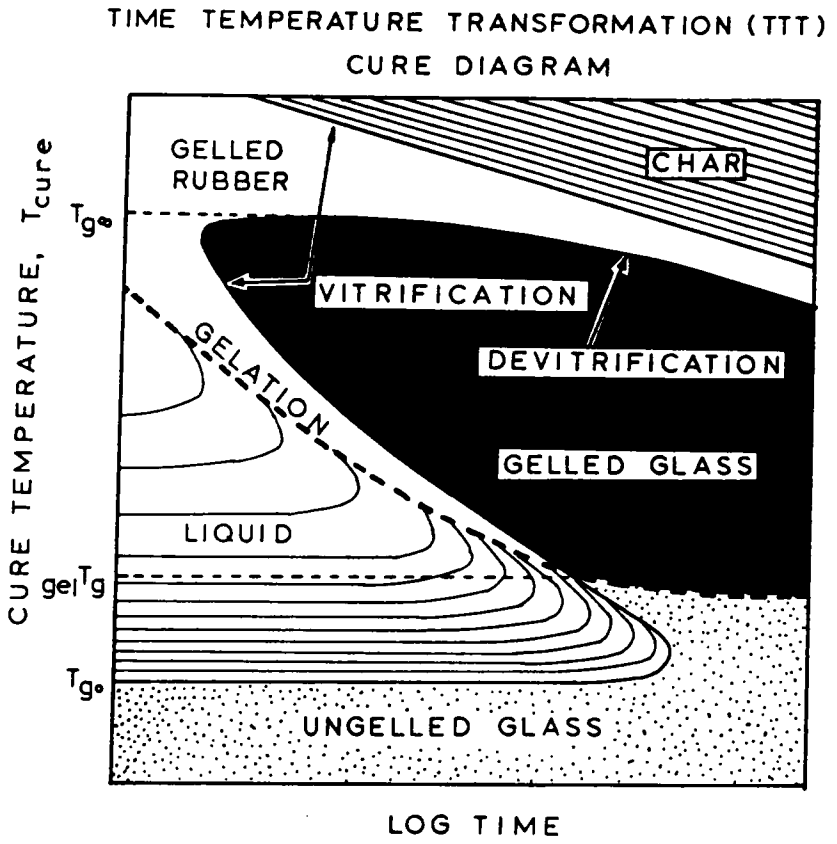

Figure 2.16. Time-Temperature-Transformation Diagram proposed by J. K. Gillham.: (ref.82).

is needed to reach the gelation curve which can be considered as a isoconversion state. At temperatures above Tg_∞, the material gels without vitrification and then reaches fully cured state before the char region is reached.

The curing process of a thermosetting system can therefore be summarized conveniently by the TTT diagram showing the times to gelation and vitrification as a function of isothermal cure temperature. In EB radiation-induced curing processes, however, the temperature change can often be significant due to the energy dissipation of the incident electrons and the exothermic reaction. Therefore, a successful modeling of time, temperature and their relationships with radiation energy may provide useful information in describing the curing processes in conjunction with the TTT diagram.

2.3.2.6 Curing and Phase Behavior of Polymer Blends

Polymers used in composites and structural adhesives are generally glassy materials that are highly crosslinked. Thermosets such as cured epoxy resins and polyimides often exhibit an inherent brittleness due to the typical glassy crosslinked nature. While, in some cases, this brittleness is not important in obtaining a high modulus and to minimize long term creep, these brittle polymers must be toughened in a number of areas where neither brittleness nor loss in glass transition temperature can be tolerated. One of the successful methods used to toughen crosslinked epoxy systems is the addition of an elastomer that phase separates during the cure process. The curing process can be controlled so that the final material is a matrix with elastomer particles dispersed in and usually bonded to the matrix(84). Improvement in toughness is dependent on the particle size, volume fraction, and size distribution of the dispersed rubbery phase as well as the chemical nature of the matrix and the dispersed phase(85).

In most cases of rubber-toughening processes, the system is initially homogeneous, however, at a certain thermoset conversion, rubber-rich domains begin to phase-separate from the matrix. The morphology continues to change until the system gels or vitrifies. On the other hand, temperature is another important factor which controls the phase separation process. Polymer blends which are homogeneous at one temperature may undergo liquid-liquid type phase separation at other temperatures. In radiation curing processes, the phase separation becomes more complicated since the reaction generally proceeds rapidly with temperature increases which are due to the exothermic reactions and radiation energy dissipation. Therefore, in order to control the rubber toughening process in radiation curing, the understanding of the effects of time, temperature, radiation energy in addition to the reaction kinetics is obviously important.

In 1942, Flory(86) and Huggins(87) developed the liquid lattice theory for estimating the combinatorial entropy of mixing as described in Figure 2.17. The relatively smaller entropy change is shown for the mixing of high molecular weight polymers in contrast to the solvent-solvent and solvent-polymer systems. It is also expected that the heat of mixing is positive or endothermic as shown in the equation by:

$$\Delta Hm = RT\chi N_1\phi_2 \qquad [2.18]$$

where N_1 is the number of molecules of component 1, ϕ_2 the volume fraction of component 2, and χ the Flory-Huggins interaction parameter. These combined considerations makes it unfavorable to provide negative free energy of mixing due to the smaller entropy change shown by:

$$\Delta Gm = \Delta Hm - T\Delta Sm \qquad [2.19]$$

which is required for miscibility. The idea, "like- dissolves-like," supported by the solubility parameter approach(88) appears to fail in identifying many miscible polymer pairs.

Progress has been made in systematic studies of miscible polymer blends by shifting an emphasis from entropy to heat of mixing as a driving force for miscibility. The effects of negative exothermic heat of mixing are well reviewed by Harris et al.(89). An initial polymer blend that are homogeneous at one temperature may undergo in-situ phase separation during radiation cure in which the temperature rise is often significant. In many cases such as mixtures of low molecular weight species and polymer solutions, an upper critical solution temperature(UCST) which is shown for phase separation to occur on cooling and characteristic of a positive entropy of mixing. However, for blends of relatively higher molecular weight polymers, phase separation on heating caused by a lower critical solution temperature(LCST), as shown in Figure 2.18, appears to be more prevalent(90). LCST is characteristic of a negative entropy of mixing and it is not explained by the Flory-Huggins theory although there are theories predicting LCST behavior(91). Random copolymers often form miscible blends with other polymers such as poly(methyl methacrylate)(PMMA) with styrene-acrylonitrile copolymer, poly(vinyl chloride)(PVC) with ethylene-vinyl acetate copolymer, or PVC with nitrile rubber, etc.(92).

The curing process of an initially homogeneous solution of epoxy resin and rubber is generally represented by the sequential processes-these being phase separation, gelation and vitrification. As the molecular weight of the rubber increases, the system undergoes in-situ phase separation due to the lowered compatibility between the rubber and the epoxy resin. Separation is eventually ceased by gelation or vitrification with the increased viscosity(93). As discussed previously, temperature change play a most impor-

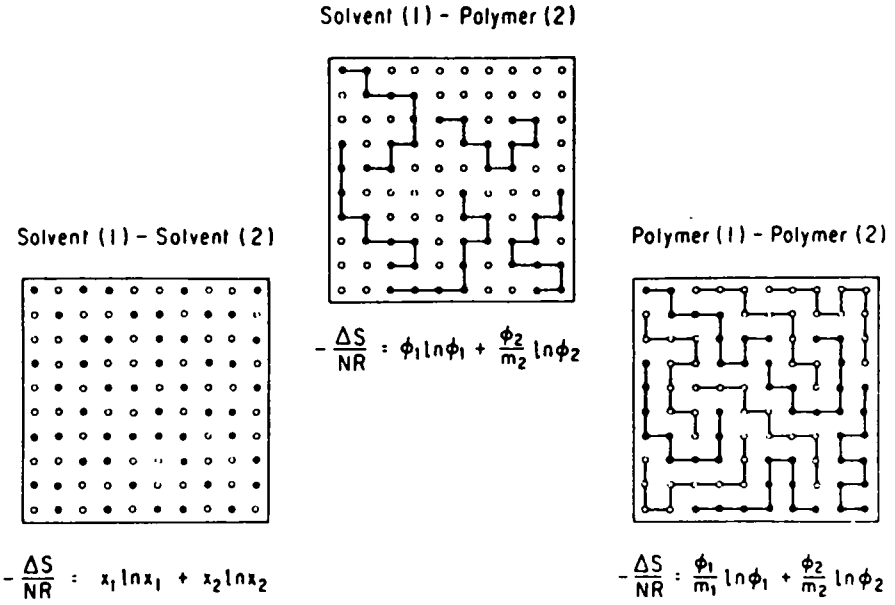

Figure 2.17. Lattice model for combinatorial entropy of mixing.: (ref.86,87).

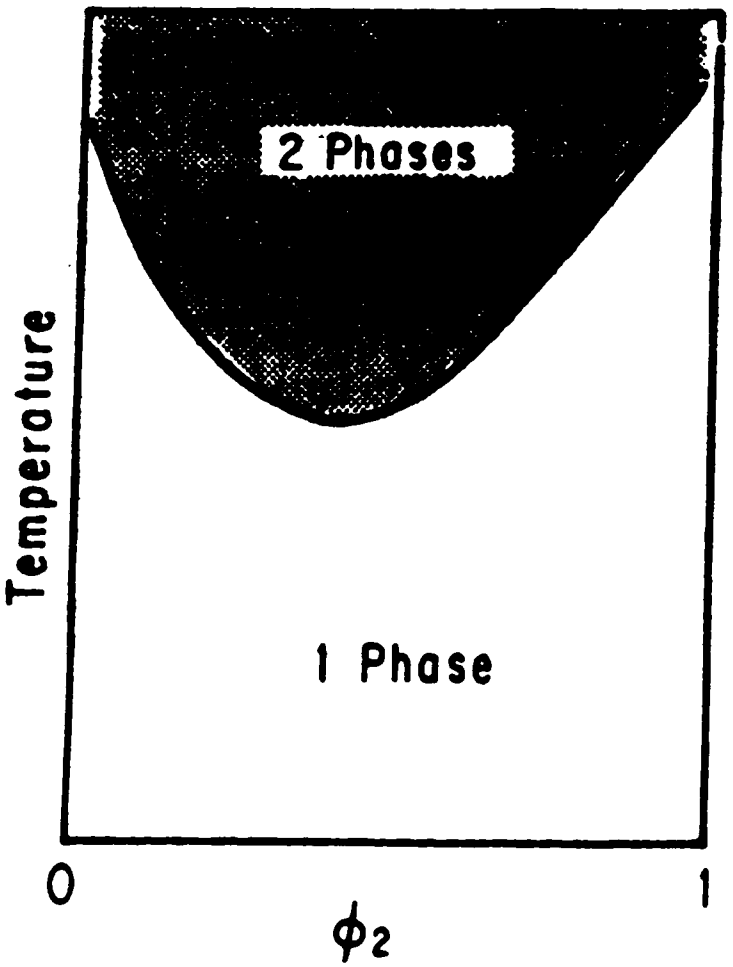

Figure 2.18. A liquid-liquid phase diagram showing LCST behavior.: (ref.90)

tant role in the development of morphology in terms of the rate of nucleation and growth of the dispersed phase, compatibility of rubber, and the kinetics of the cure reaction(94).

Williams et al.(95) developed a model describing phase separation during a thermoset polymerization for a rubber- modified epoxy system. Although some simplifications were made such as an isothermal curing condition and inertness of the rubber component, it was suggested that the temperature and the reaction rate have profound effects on the dispersed-phase fraction and the concentration of dispersed particles.

Interpenetrating polymer network(IPN) provides a new way of blending two polymers. IPN is defined as an alloy of two polymers synthesized by two non-interfering reactions and it can be prepared by two methods. For a sequential IPN, prereacted network A is swollen by monomer B and this blend is polymerized. For a simultaneous IPN, two networks are polymerized simultaneously but by independent reactions(96). Both the sequential and simultaneous IPN's are utilized in producing toughened elastomers and reinforced plastics. The sequential IPN often has relatively small size domains(97). Although literatures on the utilization of radiation process to produce IPN's are found to be scarce, it appears to be a potential research subjects with regard to the curing conditions, the morphology and mechanical behavior of IPN's produced by radiation-induced polymerization.

2.3.2.7 Effects of Radiation Induced Crosslinking on Crystallization and Crystalline Morphology

The effects of radiation on the structure and properties of semicrystalline polymers has been a subject of continuing research since the radiation induced crosslinking phenom-

enon was observed by Dole and Rose(5). Extensive studies have been performed on the effect of crystallinity on the radiation induced crosslinking especially in polyethylene. Two basic models have been developed on this subject-one of them suggesting that crosslinking occurs preferentially at the folds outside the crystalline cores and the other being based on an observed orthorhombic-to-hexagonal transition in a single crystal of polyethylene at a relatively high dose(98). There appears to be a dependence of crosslinking not only on ordering intrinsic to the crystal and the inter or intrachain contact due to chain folding, but also on the macroscopic morphology. In this section, a brief review is presented on the effect of crosslinking on crystallinity, particularly for polyethylene due to its importance and generality. Also, similar effects on other polymers such as polycaprolactone are reviewed.

Kawai et al.(99) showed the great differences in gel content vs. irradiation dose data between solution grown crystals and melt crystallized samples as shown in Figure 2.19. It is indicated that the most important morphological factor for gel formation is the intimacy of lamellar contact. The bulk crystallization provides compactly stacked layer aggregates which facilitate the interaction of chain folds between each layer, while in solution grown crystals the lamellar layers are loosely apart. A rough illustration of this effect is shown in Figure 2.20. Radicals are generated by irradiation randomly throughout the crystal and they can not be easily combined within the crystal lattice to form crosslinks. However, these radicals can migrate along the straight stems until they have chances to form crosslinks in the surface region of chain folds. If layers are closely located to each other, intermolecular crosslinks can be formed. On the other hand, if layers are not in close contact with each other, intramolecular links can primarily be formed without any effective network formation.

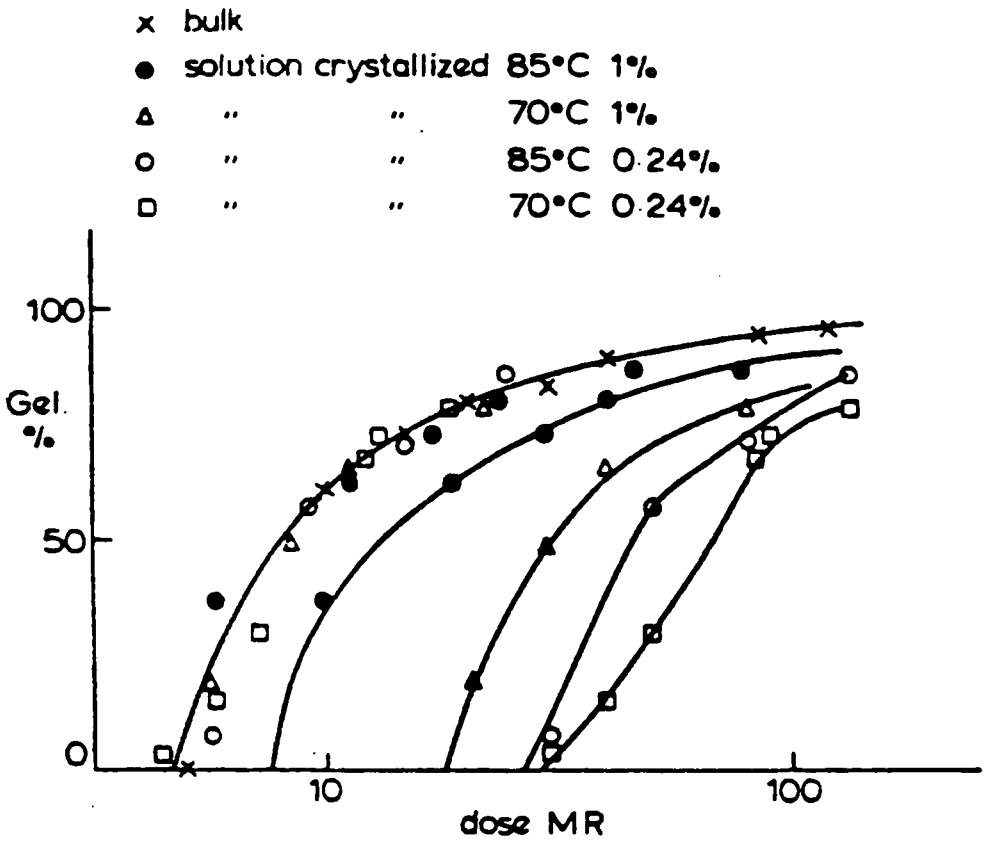

Figure 2.19. **Plots of gel content vs. log dose for gamma-irradiated polyethylenes.:** Samples were prepared by bulk(curve on the extreme left) and four different solution crystallizations(ref.99).

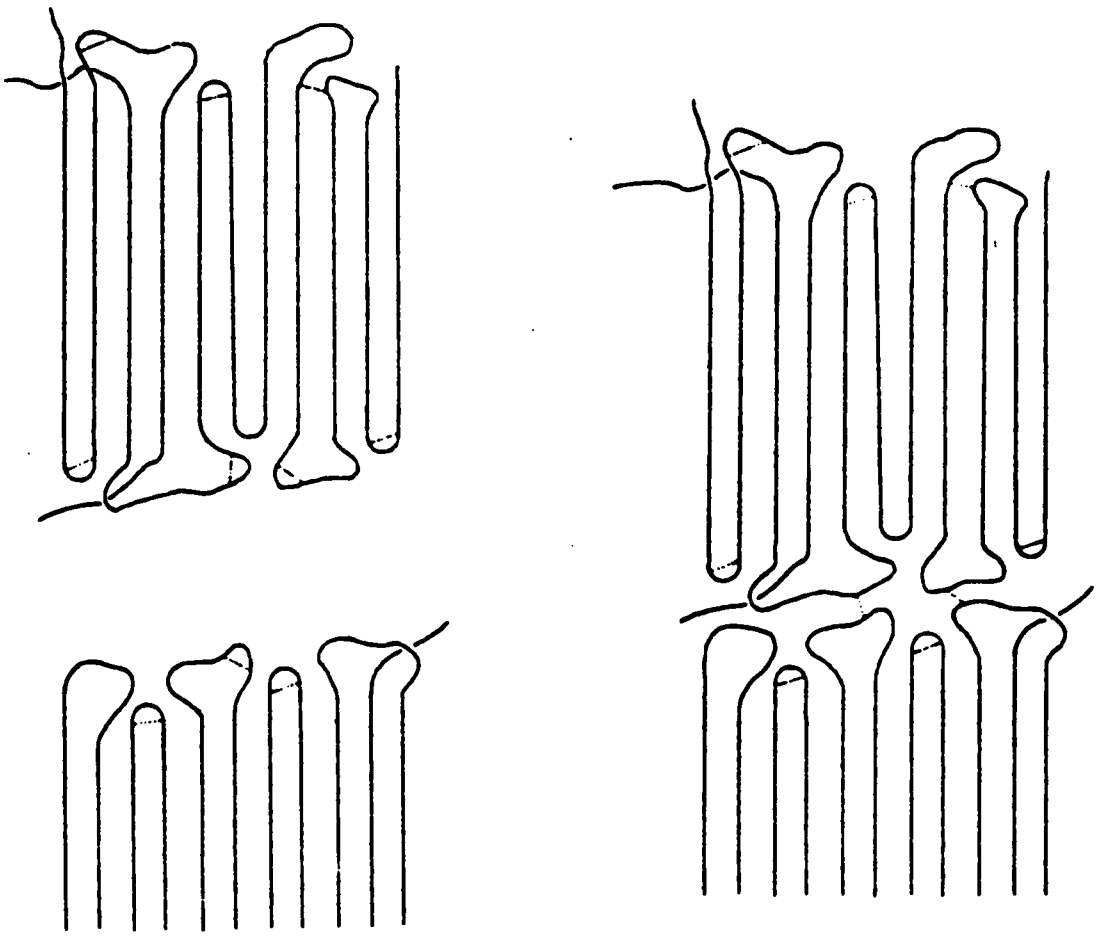

Figure 2.20. **A schematic illustration of crosslinking model in chain folded crystalline layers.:** Formation of crosslinks(dotted line) for large(left) and small(right) inter-lamellar spacings.

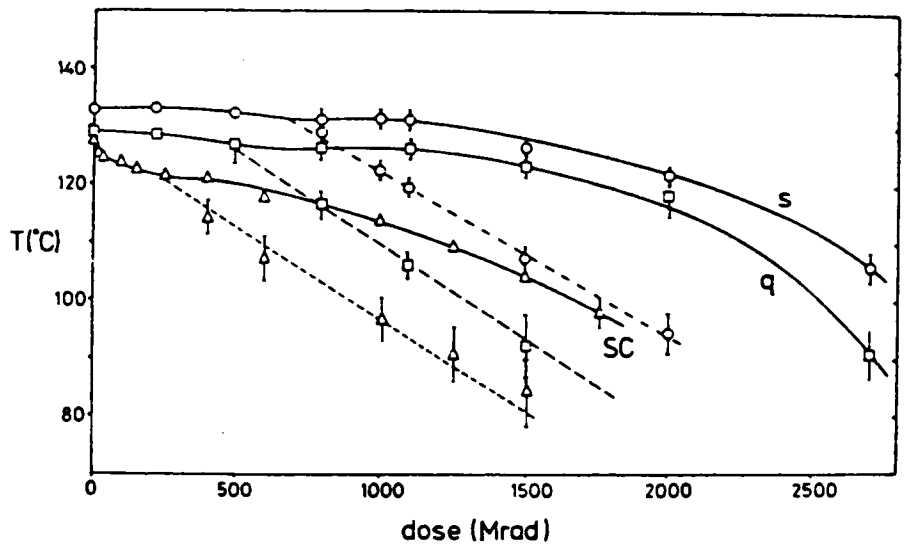

Figure 2.21. Melting(continuous line) and orthorhombic-to-hexagonal(dashed line) transition temperatures vs. irradiation dose.: Slowly crystallized(s), quenched bulk(q), and single crystals grown at 85°C(sc)(ref.101).

Ungar(100) observed that the crystallinity of polyethylene is significantly impaired and eventually disappeared only at relatively high irradiation doses. It was shown that the crystallinity fades out at doses above 200 Mrad and the increasing imperfection of the crystals is more significant for quenched than for slow cooled material. As shown in Figure 2.21(101), samples beyond a certain radiation dose display two unusual endothermic peaks in the course of DSC heating as also observed by Ahmad and Charlesby(102). The lower transition temperature corresponds to a crystallographic phase transition from the original orthorhombic to a new hexagonal phase and the endotherm at higher temperature is the true melting point of hexagonal-to-liquid transition. Also shown in Figure 2.21 is the difference between three sample types having different lamellar thickness. As the lamellar thickness decreases, both first and second transition occurs at lower temperatures, and the onset of the orthorhombic-to-hexagonal transition takes place at lower doses.

Yoda and Oadjima(103) indicated on the crystalline destruction in a low dose range crosslinks are introduced preferentially in the chain fold surface and these subsequently disrupt the lattice structure in their vicinity, thus making it possible to crosslink on further irradiation. Therefore, crystallinity destruction at a higher dose range proceeds by thinning the lattice toward the inside.

Narkis et al.(104) studied γ-radiation effects on semicrystalline linear saturated polyester using polycaprolactone. It was suggested that, upon irradiation, reorganization and ordering in the crystalline phase occurs presumably by scission of the constrained tie molecules. These are followed by subsequent crosslinking in the reorganized state with the increased crystal size. Melting point depressions, and corresponding changes in crystallinity were also studied.

It can be deduced from the review shown above that radiation induced crosslinking events in a semicrystalline material such as polyethylene or lower molecular paraffin are far from randomness. Indeed, it was suggested with evidence that at least for short paraffin($C_{23}H_{48}$) the crosslinked species can migrate and phase-separate suggesting a surprising possibility of molecular mobility within the crystal(99).

2.3.2.8 Crosslinking of Acrylated Systems

Acrylic prepolymers are now commonly utilized to produce highly crosslinked polymers that are needed in a wide variety of industrial applications such as coating technology. The polymerization can usually be initiated by gamma-rays and electron beam irradiation. Effects of the molecular weight, functionality and kinetics of the crosslinking polymerization have been studied, however the exact elucidation of the process appears yet to be achieved. In this section, a brief review is given in the relatively recent advancements on the crosslinking of acrylated urethanes. Also, the percolation model, which illustrates the spatial inhomogeneity in the curing of diacrylates, is introduced.

Seto et al.(105) studied the effects of molecular structure and reaction mechanism on the electron beam curing process of multifunctional acrylic prepolymers including urethane modified systems. It was observed that at a certain irradiation dose the percent conversion of the acrylate functional group is higher for prepolymers with greater molecular weight per functional group,. While the gel fraction is greater for samples with a smaller molecular weight per functional group. Similar behaviors were also observed for the acrylate urethane materials. It was indicated that the lower conversion for prepolymers with greater number of functional group is due to the reduced molecular chain mobility as highly crosslinked gels are formed. The rate of polymerization, Rp, for multifunc-

tional acryalte prepolymers was suggested to be proportional to the first order of the the dose rate, which is quite different from the proportionality to the half order of dose rate as shown in section 2.3.1.1 of free radical polymerization kinetics.

This observation implies that multifunctional acrylate prepolymers polymerize in condensed phase by different kinetics. Various explanations(106,107) have been suggested to account for this unusual kinetics including the presence of trapped radicals in radiation cured multifunctional acrylate coatings. The monomolecular termination due to the radical trapping appears to result in the deviation from the kinetics of the half order proportionality of dose rate to reaction rate. Indeed, it was shown by Kloosterboer et al.(108) that the radical trapping occurs often from the beginning of the reaction at the stage of 10% conversion and where the resin is still liquid. And the maximum degree of reaction conversion is often limited by vitrification of the sample when reactive radicals are trapped(109).

Spatial inhomogeneity indicated by highly crosslinked microgel particles in the curing of diacrylates were described by Kloosterboer(110) using a random walk percolation model. Figure 2.22 shows the difference between a step reaction model which produces small homogeneously distributed polymer molecules, and a chain reaction model which shows large inhomogeneous structures in the same volume fraction. Also shown in Figure 2.23 is the plot of the fraction, b, of monomer units which carry a pendant double bond in the polymer versus the polymer weight fraction, p, for the classical kinetic model, the percolation model, and the experimental data. At low conversion, pendant double bonds in the growing polymer appear to be more reactive than those in the free monomer as highly crosslinked microgel particles are formed. At high conversion, pendant double bonds seem to be less reactive than those in the free monomer resulting in

limitation of reactivity for double bonds and radicals inside the microgel, and consequently resulting in vitrification. For $p > 0.3$, Both the classical and the percolation model appear to deviate from experimental data, although the classic model fits better for $p > 0.8$.

Urethane prepolymers have been utilized for many years in industrial applications such as varnishes, coatings, sealants and in conjunction with curatives as castable elastomers. In particular, radiation-curable urethane materials have been of great interest since polyurethanes are capable of providing excellent properties such as toughness, wear-resistance and flexibility. These are for many respects in contrast to acrylic resins, acrylated epoxies, vinyl ester resins, or unsaturated polyesters which are generally brittle and less tough. The acrylated polyurethane prepolymer can readily be cured by radiation and has received the most attention in this regard. The general chemical structure can be shown as follows:

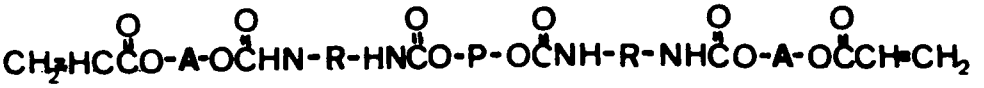

where P is generally polyesters or polyethers, R is from diisocyanate reacted with the hydroxyls, and A is from the chain extender. Although the acrylated prepolymer mentioned above is the most important in industrial practice, it is apparent that a large variety of radiation-curable polyurethane prepolymers can be made because of the ability of the isocyanate group to react with generally any molecule having active hydrogen atoms(111).

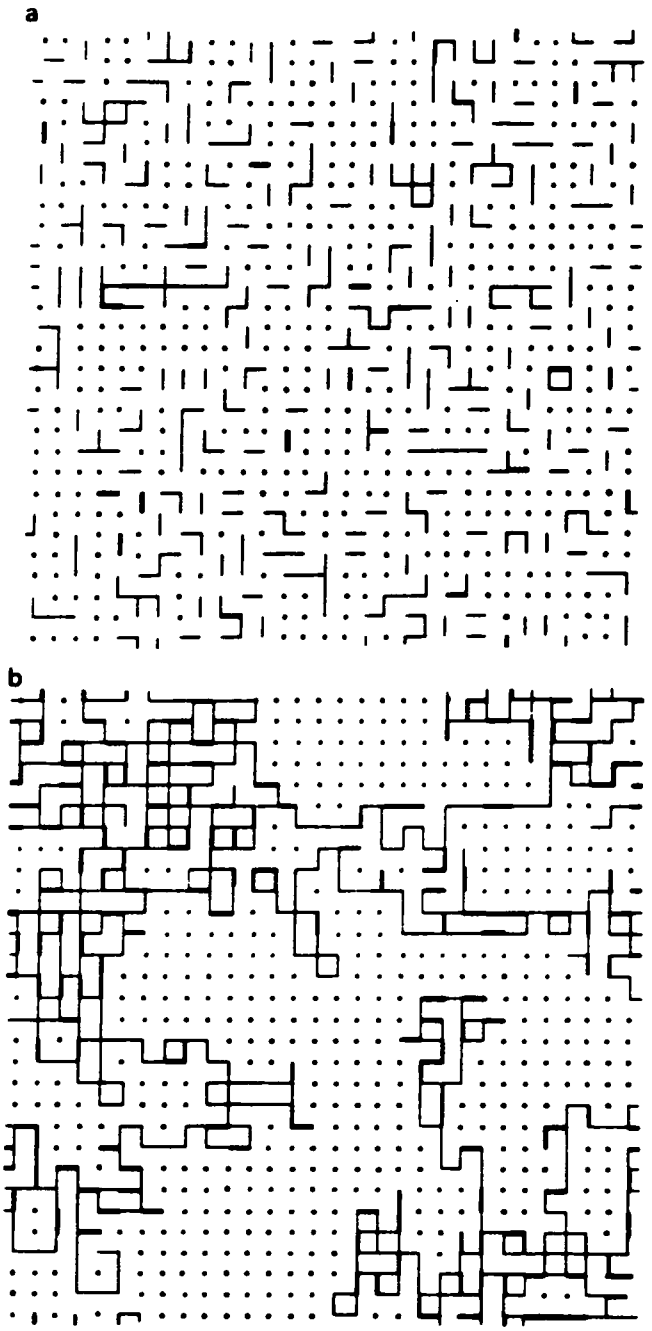

Figure 2.22. Simulations of a step reaction(a), and a chain reaction(b) for tetrafunctional monomers.: (ref.110).

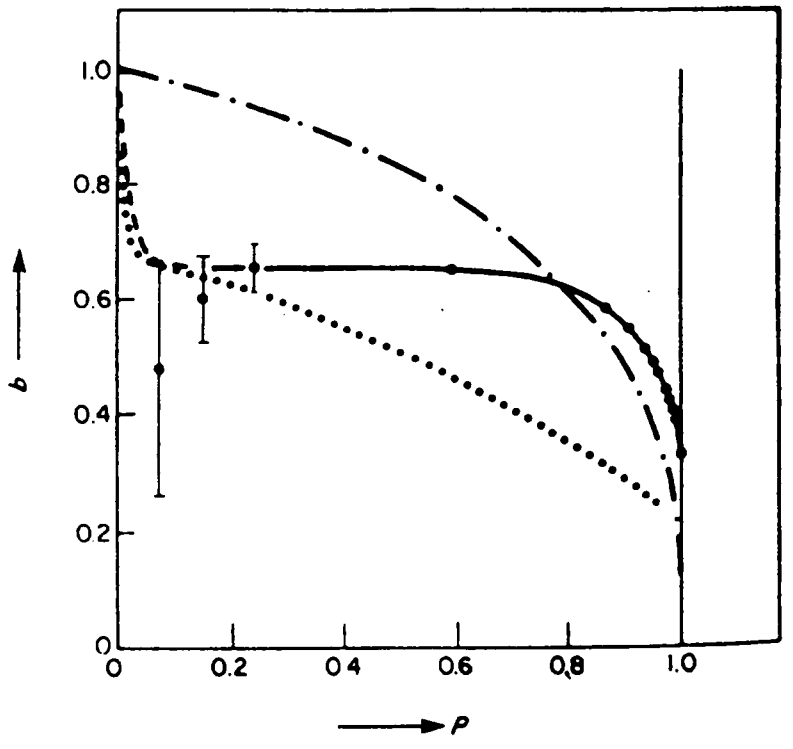

Figure 2.23. Fraction, b, of pendant double bonds per monomeric unit in the polymer vs. the weight fraction, P, of polymer.: Experimental data(continuous curve), classical kinetic model(dashed-dotted curve), and percolation model(dotted curve)(ref.110).

Joseph et al.(112) studied the structure-property relationships of electron beam cured urethane prepolymers. It was indicated that, upon irradiation of the acrylated semi-crystalline prepolymer at temperature below melting point, crosslinking occurs mainly at the acrlylic double bonds and possibly along the polymer backbone, and this irradiated material shows a measurable amount of order in the melt state. While, upon irradiation above the melting temperature, no order is present in the melt state implying the occurrence of random crosslinking. Morphology, crystallization kinetics and mechanical properties were also studied in conjunction with the irradiation dose level and the irradiation temperature.

Ando and Uryu(113) studied the characteristics of electron beam(EB) and ultraviolet(UV) light solid state polymerizations using acrylated polyurethane prepolymers. It was shown that EB irradiation below the melting point of the prepolymer can result in crosslinking without the destruction of the crystalline structure, while the UV polymerization can proceed with the melting of the crystalline structure. The material crosslinked by EB irradiation, which has higher crosslinking density, showed higher mechanical strength than the UV polymerized urethane prepolymer.

Ando and Uryu(114) investigated the structure and properties of the gel film obtained from the electron beam solid-state polymerization of urethane-acrylate prepolymer. It was observed that spherulite size decreased drastically from 5 to 20 Mrads. The crystallinity was reduced with increasing dose, while crystallite size decreased remarkably in the range of 0-1 and 5- 15 Mrads. They indicated that these changes in crystallinity in the dose range below 5 Mrads were due mainly to crosslinking by the terminal acrylate, whereas, at a higher dose range (above 5 Mrads), they were due to the crosslinking related to polymer backbones under EB heat damage.

Ando and Uryu(115) studied the structure and properties of EB irradiated urethane prepolymers with three different reactive terminal groups-these being acrylate, methacrylate, and acylamide. The polarity of the terminal group appeared to result in the difference in crystallinity which is maintained upon subsequent EB-polymerization. Spherulitic texture was observed on the EB-polymerized gel film surfaces for urethane- acrylate and urethane-methacrylate, while it was not observed for urethane-acrylamide. Respective mechanical properties of EB- irradiated urethane materials showed agreement with morphological observations.

Nagarajan et al.(116) investigated the effects of soft segment molecular weight, hard segment type and radiation crosslinking on radiation cured acrylated polyurethane materials. An increase in the soft segment molecular weight was found to result in higher soft segment crystallinity, lower soft segment glass transition temperature, longer chain length between crosslinking sites in the cured material, and an increased elongation at break. It was also observed that the radiation-induced crosslinking process depresses crystallization of the soft segment and improves tensile properties. In addition to the soft segment molecular weight, the diisocyanate type was also found to be important in determining mechanical and thermal properties of the materials.

2.3.3 Degradation

2.3.3.1 Factors Affecting Degradation

Bovey(18) reported in 1958 that G(S) should be greater than 4G(X) to hinder gel formation, and this explains the occurrence of gelation in irradiated polypropylene or

poly(propylene oxide) in spite of the generally greater G(S) than G(X). Thus, in this regard the polymers whose value of G(S) is greater than 4G(X) are often considered as polymers that primarily degrade on irradiation. Poly(methyl methacrylate)(PMMA) and poly(isobutylene) are among the most widely studied nongelling polymers in terms of this classification.

In addition to the classification made by Miller(68)as discussed previously, Wall(117) pointed out that polymers in which degradation predominates have low heats of polymerization due to steric hindrance. As shown in Table 2.10, the division of polymers between the nongelling and gelling types is in agreement with the rule of Miller.

Among the factors promoting degradation is the rate of recombination of the free radicals at the chain ends after scission has occurred. The more readily the radiation damage is repaired, the less the degradation. A low heat of recombination which is partly due to the steric hindrance may lower the free energy of recombination. Alexander et al(118) reported that no recombination occurred in the case of PMMA dissolved in CCl_4 containing 1% benzoquinone, which was the same as in CCl_4 containing no benzoquinone. It was expected that the benzoquinone would have reacted with free radicals and thus prevented recombination.

Waterman and Dole(119) in 1970 reported that the lack of an alpha-hydrogen might suppress crosslinking since free radical migration via hydrogen atom migration should be retarded. They also pointed out that, for polyethylene, free radical migration is clearly promoted by hydrogen hopping because of the catalytic effect of molecular hydrogen in promoting the conversion of alkyl to allyl free radicals.

Table 2.10. Heats of polymerization for gelling and nongelling polymers(117).

Gelling polymers	Heat of polymerization(kcal/mole)
Polyethylene	22
Polypropylene	16.5
Poly(methyl acrylate)	19
Poly(acrylic acid)	18.5
Polystyrene	17
Non-gelling polymers	
Poly(methacrylic acid)	15.8
Polyisobutylene	13
Poly(methyl methacrylate)	13
Poly(α-methyl styrene)	9

Table 2.11. Effect of radiation on commercial polymers(122).

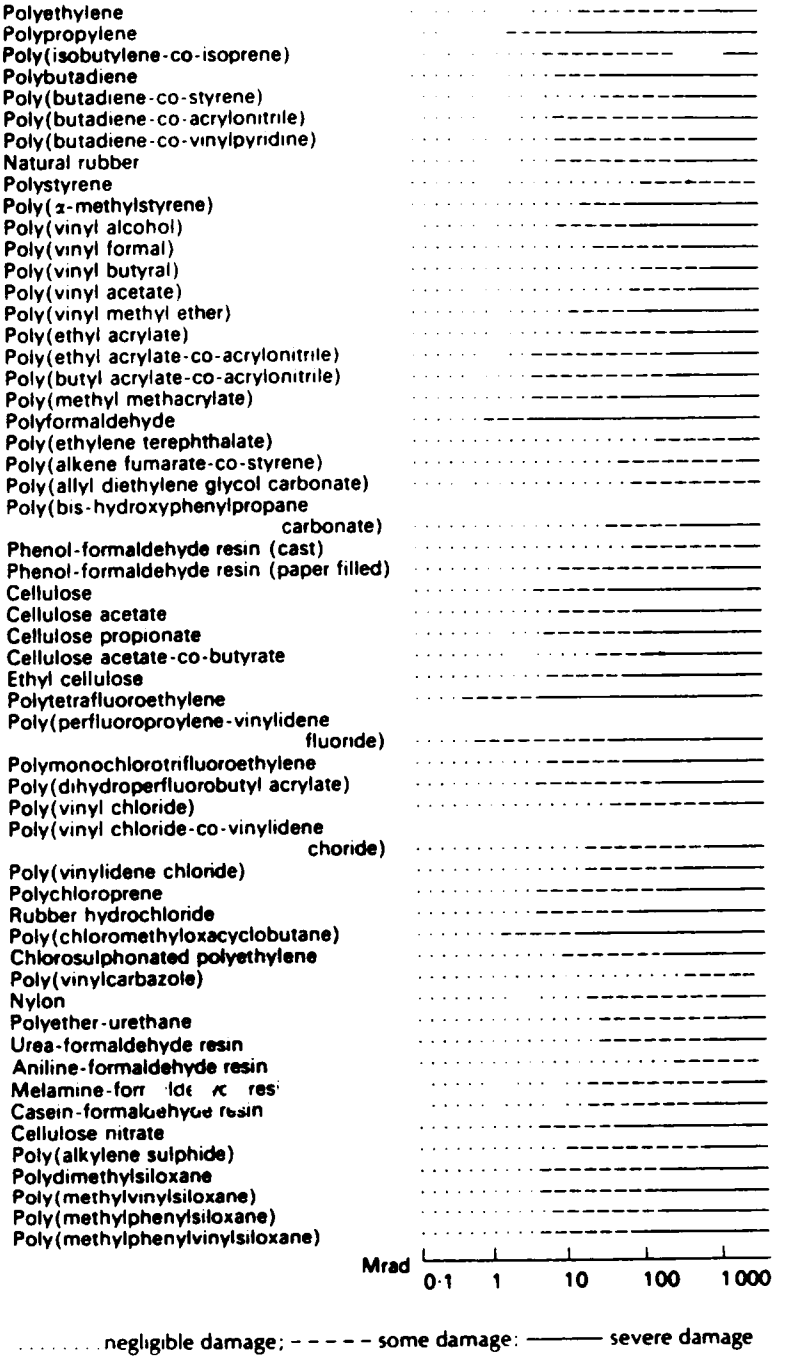

..... negligible damage; - - - - - some damage: ——— severe damage

Campbell(120) suggested that, in addition to the above factors, highly branched polymers favor scission predominantly over crosslinking and the presence of the C-O linkage as a repeating group or in a group which bridges the main chain polymer is often effective to cause scission.

The European Organization for Nuclear Research(121) provided very useful results of investigation on the irradiated generic polymers in addition to the materials with commercial trade names. Although these tested materials were irradiated in the environment of a nuclear reactor with accumulated doses, these types of investigation give helpful information in the initial selection of materials in terms of general response to irradiation as shown in Table 2.11(122).

2.3.3.2 Molecular Weight Changes in Degrading Polymers

The simplest case in degradation might be when the scission occur at random along polymer molecules. The exact location of scission is generally irrelevant to the effect on overall molecular weight changes. Each main chain rupture adds one to the number of molecules as shown by:

$$\frac{Na}{Mn} = \frac{Na}{Mn,o} + \frac{G(S)r}{100} \qquad [2.20]$$

where Na is Avogadro's number, Mn,o the initial number average molecular weight, r the absorbed dose, G(S) the number of chain scissions produced per 100 eV of energy absorbed. Therefore, using this relation, Mn can be determined from known G(S), or G(S) can be evaluated by plotting the irradiation dose r and Mn.

One of the assumptions made in above relation is that there is no intermolecular cross-linking, although complete absence of crosslinking can not reasonably assumed. Therefore, equation[2.20] shown above should be modified to:

$$\frac{Na}{Mn} = \frac{Na}{Mn,o} + \frac{[G(S) - G(X)]r}{100} \qquad [2.21]$$

where G(X) is the G value for intermolecular crosslinks. An analogous equation in terms of weight average molecular weight was reported by Kilb(123) as shown by:

$$\frac{Na}{Mw} = \frac{Na}{Mw,o} + \frac{[G(S) - 4G(X)]r}{200} \qquad [2.22]$$

There are several important assumptions related to these equations. First, the crosslinking and scission processes occur randomly. Second, G(S) and G(X) are independent of dose. Third, the initial molecular weight distribution is random.

2.3.3.3 Mechanism of Degradation

The two most intensively studied polymers which primarily degrade under irradiation are poly(methyl methacrylate)(PMMA) having the structure:

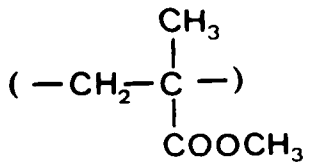

and polyisobutylene having the structure:

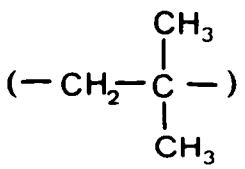

The degradation mechanisms of these two polymers are briefly reviewed here.

PMMA is a good example of a nongelling polymer and it has relatively high glass transition temperature of about 105°C. Free radicals and liberated gases by radiation are readily trapped and persist in vacuum for days. Therefore, ESR has been widely utilized for free radical studies in the degradation process(124). Shultz(125) proposed the formation of a diradical by elimination of HCO_2CH_3 resulting in either of

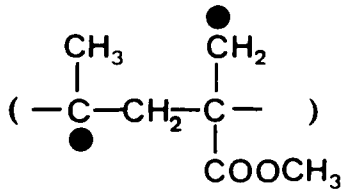

or

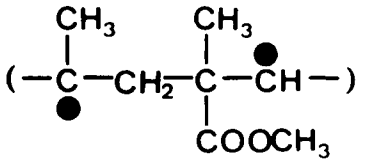

then, these diradical species undergo a further process giving either of

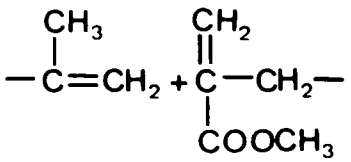

or

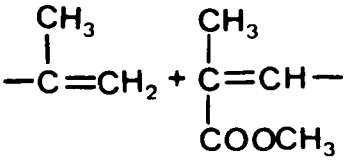

Kircher et al.(126) suggested that the radical

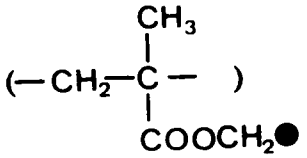

can abstract a hydrogen from another chain to produce the radical

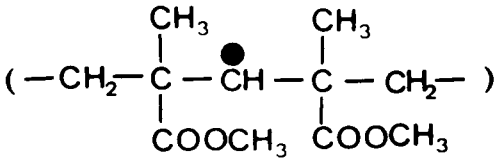

which then results in

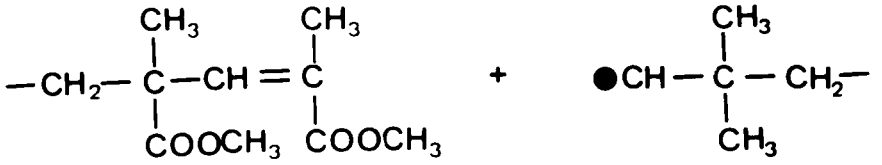

PIB is the simplest polymer which degrades under radiation, and has been found to have a head to tail structure. It has an amorphous structure shown by x-ray studies, and may be readily depolymerized thermally due to the steric hindrance between methyl groups.

Shultz(125) suggested a mechanism of degrading PIB as shown by the following sequence:

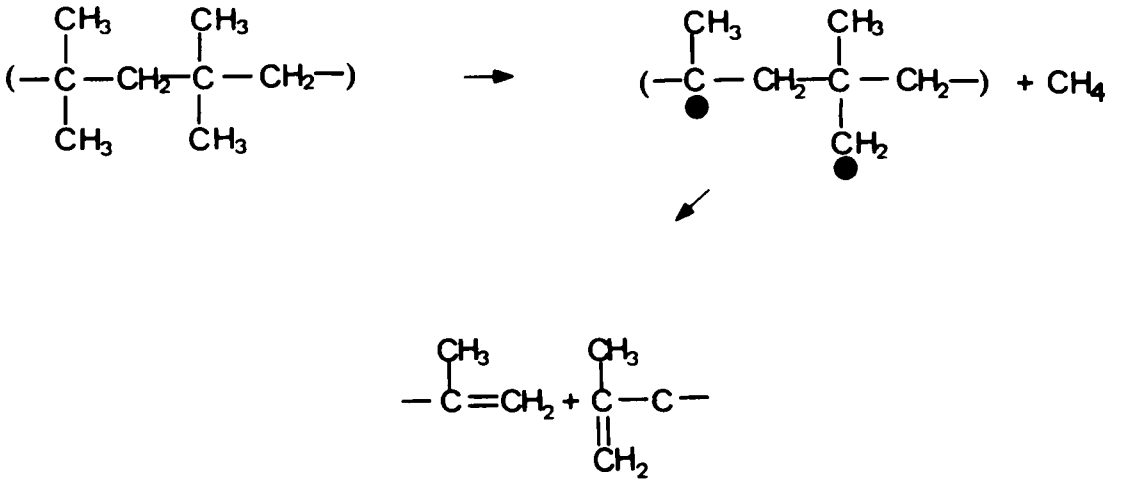

Turner(81) proposed an alternative mechanism such as:

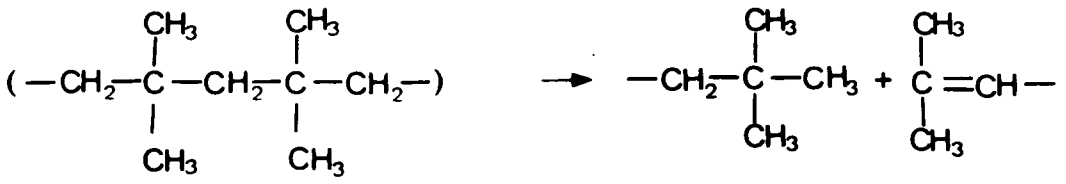

and

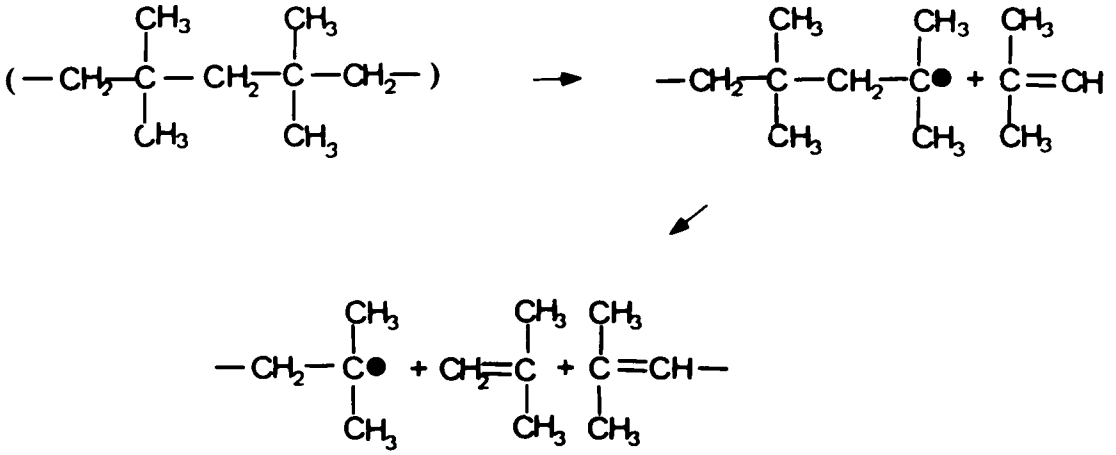

Partirige(128) predicted that, in consideration of $G(CH_4)$ values previously reported by Turner(127) and others for PIB and polypropylene, excitation results in side chain scission with a higher efficiency if side chains are symmetrically attached to the main chain in pairs as is the case of the comparison between PIB and polypropylene. In addition, Barron(129) showed that electron beam irradiation induces changes in tacticity in isotactic polypropylene as observed by n.m.r. It was suggested that the mechanism was chain scission followed by bond rotation and recombination.

2.3.4 Graft Copolymerization

Graft coplymerization using high energy radiation has been studied since the 1950's. However, it is only in the recent decade that radiation grafting had drawn a great deal of industrial interest and extensive studies are under way in conjunction with a wide variety of commercial applications.

A graft copolymer can be represented by a polymer backbone with lateral covalently linked side chains of various length. There are two main procedures to generate a A-B graft copolymer type(8).

I. Polymer A(backbone) + Polymer B(side chain) → A-B graft copolymer
High energy radiation has been utilized to synthesized these types of copolymers, and as an example, Spennadel(130) reported that a crosslinking of ethylene-propylene rubber(EPR) with low density polyethylene(LDPE) occurred using electron beam irradiation.

II. Polymer A(backbone) + Monomer B(side chain) → A-B graft copolymer
This method has been studied intensively and developed successfully according to three different types of techniques-direct grafting, preirradiation grafting, and peroxide technique.

In direct grafting technique, the backbone polymer is irradiated in the presence of the reactive monomer, and this monomer forms the side chain polymer by irradiation itself or "hot" radical species from the irradiated backbone polymer. The most important requirement to optimize the formation of graft copolymer with the minimum

of contaminating homopolymer is that the yield(G value) of radicals from the polymer should exceed that from monomer as much as possible. The opposite way is highly unfavorable resulting in a low degree of grafting. To overcome this problem with similar G values of the polymer and the monomer, a low concentration of the monomer or the polymer swollen by the monomer can be utilized.

In the preirradiation grafting technique, the backbone polymer is irradiated in the absence of the monomer, and subsequently this irradiated polymer is brought into contact with the reactive monomer. This method is generally limited to glassy and semicrystalline polymers since the free radicals trapped in the polymer are supposed to react consequently with the monomer forming the graft copolymer. With amorphous polymers in the rubbery state, the radicals produced by radiation do not survive long enough to initiate graft copolymerization. This technique is known to be suitable for electron beam irradiation with regard to the generation of trapped radicals followed by post-polymerization.

In the peroxide technique, the process can be illustrated in the following schematic:

Polymer A + O_2 -(i)→ Polymer AOOH -(ii-a)→ PolymerAO• + •OH

Polymer A + O_2 -(i)→ Polymer A-O-O-A Polymer -(ii-b)→ 2 Polymer AO•

If stage (ii) is performed in the presence of reactive monomers in an inert atmosphere, graft copolymerization will occur. Initiation of homopolymerization by •OH radicals in step(ii-a) can be hindered using a redox system as an example:

PolymerAOOH + Fe^{++} → PolymerAO• + OH^- + Fe^{+++}

Although the extensive literature on radiation-induced graft copolymerization has concentrated on free radical processes, ionic grafting has also been studied since it was successfully demonstrated by Jendrychowska-Bonamour(131) in 1968 with isobutylene grafted to PVC in the glassy state. The progress in this area up to 1975 has been well summarized by Chapiro(132).

At the present time, although some problems such as relatively low yields and extreme process conditions remain to be solved, radiation-induced graft copolymerization appears to draw a major industrial interest due to its uniqueness in a number of aspects.

In summary, literatures on primary interaction of high energy radiation with matter were reviewed with an emphasis on the stopping power theory and energy transfer process. Secondly, the radiation effects on relatively simple organic compounds were discussed due to their importances in providing models and explanations for the behavior of macromolecules under radiation. Finally, kinetics, mechanisms and various aspects on radiation crosslinking and scission in the liquid or the solid state were addressed in addition to graft copolymerization.

References

1. Becquerel, H. *Compt. Rend.* 1896, *122,* 420.

2. Curie, M. *Compt. Rend.* 1899, *129,* 823.

3. Jorissen, W. P.; Ringer, W. E. *Brigchte* 1906, *39,*2093.

4. Jorissen, W. P.; Woudstra, H. W. *Zeit. Chem. u. Industrie d. Kolloid* 1912, *10,* 280.

5. Dole, M. *Chemistry and Physics of Radiation Chemistry; Report of Symposium IX* Army Chemical Center, Maryland, 1950.

6. Charlesby, A. *Proc. Roy. Soc.* 1952, *A215,* 187.

7. Chrlesby, A. *Atomic Radiation and Polymers* Pergamon Press, Oxford, 1960.

8. Chapiro, A. *Radiation Chemistry of Polymeric Systems* Wiley-Interscience, New York, 1962.

9. Saito, O.; Kang, H. Y.; Dole, M. *J. Chem. Phys.* 1967, *46,* 3607.

10. Thompson, L. F.; Wilson, C. G.; Bowden, M. J. *Introduction to Microlithography, ACS Symp. Ser.* 1983, *219.*

11. Green, G. E.; Stark, B. P.; Zahir, S. A. *J. Macro. Sci., Revs. Macro. Chem.* 1981, *C21,* 187.

12. Delzenne, G. A. *Adv. Photochem.* 1979, *11,* 1.

13. Pappas, S. P. *UV Curing: Science and Technology, Vol. II* Technology Marketing Corp., Norwalk, CT, 1985.

14. Senich, G. A.; Florin, R. E. *J. Macro. Chem., Revs. Macro. Chem. Phys.* 1984, *C24*, 239.

15. Pappas, S. P. *UV Curing: Science and Technology* Technology Marketing Corp., Norwalk, CT, 1978.

16. Roffey, C.G. *Photopolymerization of Surface Coatings* Wiley-Interscience, New York, 1982.

17. Wentink, S. G.; Koch, S. D. *UV Curing in Screen Printing for Printed Circuits and the Graphic Arts* Technology Marketing Corp., Norwalk, CT. 1978.

18. Bovey, F. A. *The Effects of Ionizing Radiation on Natural and Synthetic High Polymers* Interscience, New York, 1958.

19. Evans, R. D. *The Atomic Nucleus* McGraw-Hill, New York, 1955.

20. Pacansky, J. *Radiation Curing* 1983, *10*, 4.

21. Bethe, H. A.; Ashkin, J. *Experimental Nucleus Physics* Wiley, New York, 1953.

22. Bishel, H. *Radiation Dosimetry* Academic Press, New York, 1968.

23. Fano, U. *Ann. Rev. Nucl. Sci.* 1963, *13*, 1.

24. Berger, M. J.; Seltzer, S. M. *NAS-NRC Publ. 1133* Washington, D. C., 1964.

25. Hirsch, J.;Martin, E. *J. Noncrystallogr. Solids* 1970, *4*, 133.

26. Ausloos, P. *Fundamental Processes in Radiation Chemistry* Interscience, New York, 1968.

27. Forster, Th. *Energetics and Mechanism in Radiation Biology* Academic Press, New York, 1968.

28. Partridge, R. H. *J. Chem. Phys.* 1970, *52*, 2491.

29. Hirayama, F.;Rothman, W.;Lipsky, S. *Chem. Phys. Lett.* 1970, *5*, 296.

30. Golub, M. A. *J. Phys. Chem.* 1965, *69*, 2639.

31. Borovkova, L. Ya.;Bagdsaryan, Kh. S. *High Energy Chem.* 1967, *1*, 295.

32. Ho, S. K.;Siegal, S. *J. Chem. Phys.* 1969, *50*, 1142.

33. Packansky, J.;Waltman, R. *Radiat. Phys. Chem.* 1985, *25*, 625.

34. Packansky, J. *IBM Res. J.* 1983, 3884.

35. Grun, A. E. *Naturforsch* 1957, *12a*, 89.

36. Bolt, R. O.; Carrol, J. G. *Radiation Effects on Organic Materials* Academic Press, New York, 1963.

37. Artandi, C. *Radiat. Phys. Chem.* 1977, *9*, 183.

38. Ho, S. K.; Freeman, G. R. *J. Phys. Chem.* 1964, *68*, 2189.

39. Foldiak, G. *Radiation Chemistry of Hydrocarbons* Elsevier, Amsterdam, 1981.

40. Dewhurst, H. A. *J. Am. Chem. Soc.* 1961, *83*, 1050.

41. Futrell, J. H. *J. Am. Chem. Soc.* 1959, *81*, 5921.

42. Wakeford, B. R.; Freeman, G. R. *J. Phys. Chem.* 1964, *68*, 2635.

43. Brun, M.; Montarnal, R. *Compt. Rend.* 1958, *247*, 2361.

44. Gaumann, T.; Hoigne, J. *Aspects of Hydrocarbon Radiolysis* Academic Press, New York, 1968.

45. Hoigne, J.; Burns, W. G.; Marsh, W. R.; Gaumann, T. *Helv. Chim. Acta.* 1964, *47*, 247.

46. Verdin, O. *J. Phys. Chem.* 1963, *67*, 1263.

47. Hofer, H.; Heusinger, H. *Z. Phys. Chem.* 1970, *69*, 47.

48. Gaumann, T. *Helv. Chim. Acta.* 1963, *46*, 2873.

49. Benson, H. L.; Willard, J. E. *J. Am. Chem. Soc.* 1966, *88*, 5689.

50. Teply, J. *Radiat. Res. Rev.* 1969, *1*, 361.

51. Akhtar, S. M. S.; Woods, R. J.; Bardwell, J. A. E. *Int. J. Radit. Phys. Chem.* 1975, *7*, 603.

52. Berk, S.; Gisser, H. *Radit. Res.* 1973, *56*, 71.

53. Baptista, J. L.; Burrows, H. D. *J. Chem. Soc. Faraday Trans. I.* 1974, *70*, 2066.

54. Silverman, J. *J. Chem. Educ.* 1981, *58*, 168.

55. Schildknecht, C. E. *Polymer Processes* Interscience, New York, 1956.

56. Chapiro, A.; Wahl, P. *Compt. Rend.* 1954, *238*, 1803.

57. Rudin, A. *The Element of Polymer Science and Engineering* Academic Press, 1982.

58. Davidson, W. H. T.; Pinner, S. H.; Worrall, R. *Proc. Roy. Soc.* 1959, *A252*, 187.

59. Hayashi, K. *Radiat. Phys. Chem.* 1981, *18*, 183.

60. Schmitz, J. V.; Lawton, E. J. *Science* 1951, *113*, 718.

61. Mesrobian, R. B.; Ander, P.; Ballatine, D. S.; Dienes, G. J. *J. Chem. Phys.* 1954, *22,* 565.

62. Lawton, E. J.; Grubb, W. T.; Balwit, J. B. *J. Polym. Sci.* 1956, *19,* 455.

63. Restaino, A. J.; Mesrobian, R. B.; Morawetz, H.; Ballantine, D. S.; Diene, G. J.; Metz, D. J. *J. Am. Chem. Soc.* 1956, *78,* 2939.

64. Sobue, H.; Tabata, Y. *J. Polym. Sci.* 1960, *43,* 459.

65. Bensasson, R.; Mart, R. *J. Polym. Sci.* 1960, *48,* 53.

66. Bowden, M.; O'Donnell, J. H.; Sothman, R. D. *Macromolecules* 1972, *5,* 269.

67. Westlake, J. F.; Huang, R. Y. *J. Polym. Sci. A1.* 1972, *10,* 2149.

68. Miller, A. A.; Lawton, E. J.; Balwit, J. S. *J. Polym. Sci.* 1954, *14,* 503.

69. Swallow, A. J. *Radiation Chemistry of Organic Compounds* Pergamon Press, New York, 1960.

70. Flory, P. J. *J. Am. Chem. Soc.* 1941, *63,* 3096.

71. Stockmayer, W. H. *J. Chem. Phys.* 1944, *12,* 125.

72. Charlesby, A. *Proc. Roy. Soc.* 1954, *A222,* 542.

73. Charlesby, A. *Advan. Chem. Ser.* 1967, *66,* 1.

74. Shimada, S.; Kashiwabara, H.; Sohma, J. *J. Polym. Sci. A2.* 1970, *8,* 1291.

75. Seguchi, T.; Tamura, N. *J. Phys. Chem.* 1973, *77,* 40.

76. Waterman, D. C.; Dole, M. *J. Phys. Chem.* 1970, *74,* 1913.

77. Pearson, R. W. *J. Polym. Sci.* 1957, *25*, 189.

78. Dole, M.; Milner, D. C.; Williams, T. F. *J. Am. Chem. Soc.* 1958, *80*, 1580.

79. Bohm, G. G. A.; Treekrem, J. O. *Rubber Chem. Technol.* 1982, *55*, 575.

80. Charlesby, A. *Radit. Phys. Chem.* 1981, *18*, 59.

81. McGinniss, V. D. *National Symposium on Polymer in the Service of Man* ACS, Washignton D. C., 1980.

82. Peng, X.; Gillham, J. K. *J. Appl. Polym. Sci.* 1985, *30*, 4685.

83. Chan, C. C.; Gillham, J. K. *J. Appl. Polym. Sci.* 1984, *29*, 3307.

84. Sultan, T. N.; McGarry, F. J. *Polym. Eng. Sci.* 1973, *13*, 29.

85. Riew, C. K. *Rubber Chem. Technol.* 1981, *54*, 374.

86. Flory, P. J. *J. Chem. Phys.* 1942, *10*, 51.

87. Huggins, M. L. *J. Chem. Phys.* 1942, *46*, 151.

88. Krause, S. J. *Macromol. Sci. Rev. Macromol. Chem.* 1972, *C7*, 251.

89. Harris, J. E.; Paul, D. R.; Barlow, J. W. *Polym. Eng. Sci.* 1983, *23*, 676.

90. Paul, D. R.; Barrow, J. W. *J. Macromol. Sci. Rev. Macromol. Chem.* 1980, *C18*, 109.

91. Sanchez, I. C. *Annu. Rev. Mater. Sci.* 1983, *13*, 387.

92. Paul, D. R.; Barlow, J. W. *Polymer* 1984, *25*, 487.

93. Manzione, L. T.; Gillham, J. K.; McPherson, C. A. *J. Appl. Polym. Sci.* 1981, *26*, 889.

94. Williams, R. J. J.; Borrajo, J.; Adabbo, H. E.; Rojas, A. J. J. *Polym. Prep., Am. Chem. Soc., Div. Polym. Mater. Sci. Eng.* 1983, *49*, 432.

95. Williams, R. J. J.; Borrajo, J.; Adabbo, H. E.; Rojas, A. J. *Advances in Chemistry Series* 1984, *208* 195.

96. Sperling, L. H. *Interpenetrating Polymer Networks and Related Materials* Plenum, New York, 1981.

97. Yeo, J. K.; Sperling, L. H.; Thomas, D. A. *Polymer* 1983, *24*, 307.

98. Minkova, L.; Ninkolova, M.; Nedkov, E. *J. Macromol. Sci. Phys.* 1988, *B27*, 99.

99. Bassett, D. C. *Development in Crystalline Polymers* Applied Science Publisher, Barking, Essex, 1981.

100. Ungar. G. *Polymer* 1980, *20*, 1284.

101. Ungar, G.; Keller, A. *Polymer* 1980, *21*, 1273.

102. Ahmad, S. R.; Charlesby, A. *Int. J. Radiat. Phys. Chem.* 1976, *8*, 585.

103. Yoda, O.; Oadjima, A. *Jap. J. Appl. Phys.* 1980, *19*, 1241.

104. Narkis, M.; Sibony-Chaouat, S.; Siegmann, A.; Shkolnik, S.; Bell, J. P. *Polymer* 1985, *26*, 50.

105. Seto, J.; Nagai, T.; Noguchi, T.; Arakawa, S.; Shibata, A.; Ishimoto, C.; Miyashita, M. *Radiat. Phys. Chem.* 1985, *25*, 567.

106. Tryson, C. R.; Shultz, A. R. *J. Polym. Sci. Polym. Phys.* 1979, *17*, 2059.

107. Decker, C. *ACS Symp. Series* 1984, *266*, 208.

108. Kloosterboer, J. G.; Lippits, G. J. M. *Polym. Prep. Am. Chem. Soc.* 1985, *26(2)*, 351.

109. Thompson, D.; Song, J. H.;Wilkes, G. L. *J. Appl. Polym. Sci.* 1987, *34*, 1063.

110. Kloosterboer, J. G.; Van de Hei, G. J. M.; Boots, H. M. J. *Polym. Comm.* 1984, *25*, 354.

111. Martin, B. *Radiat. Curing* Aug. 1986, 4.

112. Joseph, E.; Wilkes, G. L.; Park, K. *J. Appl. Polym. Sci.* 1981, *26*, 3355.

113. Ando, M.; Uryu, T. *J. Appl. Polym. Sci.* 1987, *33*, 1793.

114. Ando, M.; Uryu, T. *Polym. J.* 1987, *19*, 367.

115. Ando, M.; Uryu, T. *Radiat. Phys. Chem.* 1988, *31*, 607.

116. Nagarajan, C. Li. R. M.; Chiang, C. C.; Cooper, S. L. *Polym. Eng. Sci.* 1986, *26*, 1442.

117. Wall, L. A. *J. Polym. Sci.* 1955, *17*, 141.

118. Alexander, P.; Charlesby, A.; Ross, M. *Pro. Roy. Soc.* 1954, *A223*, 392.

119. Waterman, D. C.; Dole, M. *J. Phys. Chem.* 1970, *74*, 1913.

120. Campbell, F. J. *Radiat. Phys. Chem.* 1981, *18*, 109.

121. Schonbacher, H.; Stolavr-Izycha, A. *Compilation of Radiation Damage Data, Part I, II* European Organization for Nuclear Research, Geneva, 1979.

122. Swallow, A. J. *Radiation Chemistry* Longman Group Ltd., 1973.

123. Kilb, R. W. *J. Phys. Chem.* 1959, *63*, 1838.

124. Campbell, D. *Macromol. Rev.* 1970, *4*, 91.

125. Schultz, A. R. *J. Polym. Sci.* 1959, *35*, 369.

126. Kircher, J. F.; Slimers, F. A.; Markle, R. A.; Gager, W. B.; Leininger, R. I. *J. Phys. Chem.* 1965, *69*, 189.

127. Turner, D. T. *J. Polym. Sci.* 1964, *A2*, 1699.

128. Partridge, R. H. *J. Chem. Phys.* 1970, *52*, 2501.

129. Barron, P. F.; Busfield, W. K.; Hanna, J. V. *Polym. Comm.* 1988, *29*, 70.

130. Spenandel, L. *Rad. Phys. Chem.* 1979, *14*, 683.

131. Jendrychowska-Bonamour, A. M. *Eur. Polym. J.* 1968, *4*, 627.

132. Chapiro, A. *J. Polym. Sci. Symp.* 1976, *56*, 431.

3.0 Surface Modification of Bis-GMA Substrates by Functionalized Siloxane Oligomers Through EB Irradiation

Surface modification of polymer films via electron beam irradiation was studied using the methacrylic acid derivative of the diglycidyl ether of bisphenol A, commonly called bis-GMA, as a curable substrate. Functionalized poly(dimethyl siloxane)(PDMS) oligomers were utilized as surface modifiers. Considerable changes in the wetting characteristics were observed for the siloxane modified bis-GMA surfaces by critical surface tension analysis. For dose up to 5 Mrad, the dose level strongly affects the critical surface tension which implies differences in the concentration of the attached PDMS oligomers to the bis-GMA substrate. The methacrylate terminated PDMS was observed to be more effective in lowering the critical surface tension than a similar vinyl terminated PDMS. Higher molecular weight and multifunctional PDMS coatings resulted in lower critical surface tensions in the dose range applied in this study. The surface thickness of the functionalized PDMS coatings which were bonded to the substrate surface depended on the molecular weight of the surface modifiers as obtained by XPS analysis. Peel tests of the uncoated and PDMS coated bis-GMA clearly resulted in agreement with the critical surface tension data. Chemical inertness and poor wettability of PDMS provided the PDMS coating enhanced resistance to chemical degradation by a brief exposure to aqueous nitric and acetic acid.

3.1 Introduction

Electron Beam(EB) curing offers a solvent- and initiator-free process for coating and film applications which may consume less energy than conventional thermal processes. Recently, pollution standards and increasing energy costs have accelerated the utility of the EB radiation process and the number of available EB radiation curable materials.

EB techniques usually involve the use of reactive formulations composed of an unsaturated monomer or oligomer, either by itself, or by compounding with other reactive components which will bring about improvements of system properties. Relatively low-energy EB radiation generated from a linear filament(electrocurtain) can easily polymerize materials containing reactive "double bonds" by electronic and ionic excitation. The penetration capability of this low energy EB depends on the electron energy(beam kV) and properties of the material which is to be irradiated. The thickness of the coating material which is applied on a substrate, is often of the order of a few mils and the curing process is initiated and often completed within seconds. Hence, EB processes are generating a number of industrial applications such as pressure sensitive adhesives(1), coatings for metallic and polymeric substrates(2), optical fibers(3), coatings and laminates of paper, electrical printed circuits(4), sterilization, and food packaging.

Of the newer areas for EB applications, surface modification of organic polymer films is now receiving attention. This is due to the importance of surface properties of organic polymer films in a variety of applications such as for protective coating processes and paper release coatings, etc. Many physical or chemical methods have been employed for

the purpose of altering wetting characteristics, resistance to abrasion, and chemical inertness(5). The utility of a polymer coating may depend critically on surface free energy which is related to wettability or will depend on the abrasion and adhesion properties. Low surface free energy reduces the wettability and frictional force and hence often lengthens the lifetime of the coatings. With regard to these concerns, silicone- based materials offer unique chemical and physical properties which are brought about by their inorganic characteristics and surface properties. Much effort has been concentrated on the utilization of a compatible polysiloxane as a second component in EB curable systems(6). Also silicone-containing graft copolymers and block copolymers have been employed for the purpose of being used as additives in a polymer film and considerable changes of surface properties have been reported even when they were used with a composition less than one weight percent(7, 8).

As an alternative to the methods using organic compatible siloxane materials, relatively low molecular weight polydimethylsiloxane(PDMS) having radiation-curable functional groups were utilized in this study in an attempt to chemically attach these species onto the surface of the curable substrate for altering surface properties through EB irradiation. This method possibly possesses potential merits with regard to lower cost and *in situ* processabilities for altering surface properties.

In this study, monofunctionally end-capped PDMS as well as multifunctionalized siloxanes were investigated as surface modifiers in conjunction with radiation variables.

3.2 Materials and Experiments

3.2.1 Materials

Shown in Figure 3.1 is the methacrylic acid derivative of the diglycidyl ether of bisphenol A, [2,2-bis-{4(2-hydroxy- 3-methacryloxy-propyloxy)-phenyl}-propane], commonly referred to as bis-GMA (Freeman Chemical, Nupol 46-4005). It is used for dental restorative application and offers excellent chemical and solvent resistance in its cured form. The methacrylate functional group of bis-GMA provide reactive sites upon thermal or radiation curing process. The synthesis and characterization studies on bis-GMA material were done by Yilgor st al(9). This material served as the substrate upon which the PDMS modifiers were placed. The poly(dimethyl siloxane)(PDMS) generally provide following characteristics in a relatively wide temperature range:

- low surface energy
- thermal stability
- chemical inertness
- oxidative stability
- stable viscosity with temperature change
- non-flammability
- dielectric stability, etc.

Siloxane molecules possess a unique chain flexibility due to the extremely low energy barrier for rotation resulting in low glass transition temperature. Relatively low surface energy of PDMS materials, which ranges from 15 to 30 dyne/cm depending on the chemical structure and molecular weight, provides unique wetting characteristics and

resistance to abrasion, etc. PDMS terminated by reactive functional groups are generally employed as reactive prepolymers in producing high molecular weight silicone elastomer or block copolymers. It is also attracting interest in the surface modification area. Figure 3.2 shows the chemical structures of the PDMS containing surface modifiers. One was monofunctionally end-capped with a methacrylate(PDMS-M) having different molecular weights{Mn = 1,000(1K), 5,000(5K), 10,000(10K)}, while a second possessed a vinyl(allyl) functional group(PDMS-V). These were synthesized and characterized as described elsewhere(10). The reaction scheme to achieve these different structures is shown in Figure 3.3. A low molecular weight(ca. 25,000) multifunctional dimethylsiloxane vinylmethylsiloxane copolymer(DMS-VMS) was purchased from Petrarch System Inc. and utilized as the third surface modifier. This system had 1, 7.5, and 19 wt% content of vinylmethylsiloxane and a viscosity of 1,000 centistokes at room temperature.

3.2.2 Sample Preparation

A liquid bis-GMA coating(ca. 5 mil thickness) was applied on steel plate coupons(0.75″x0.75″). Thermal heating(50°C) was used to promote a smooth liquid surface by lowering the resin viscosity. A 10 wt% solution of one of the siloxane oligomeric modifiers in n-hexane was then spray-coated on the surface of the bis-GMA liquid substrate film. A coating thickness (dried) of the siloxane material deposited on bis-GMA was controlled to less than 2 μm. EB irradiation of this two-layered liquid system was then performed. Any remaining unreacted PDMS oligomers were then removed using n-hexane via Soxhlet extraction for 24 hours. After extraction, the samples were dried at atmospheric conditions for 24 hours before further testing. Uncoated

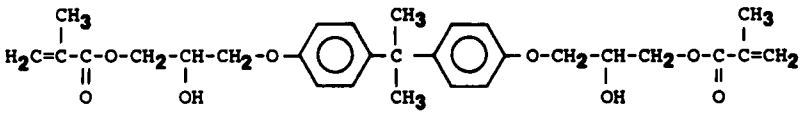

Figure 3.1. Chemical Structure of bis-GMA.

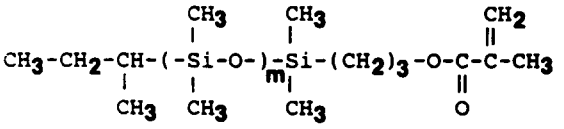

(a)

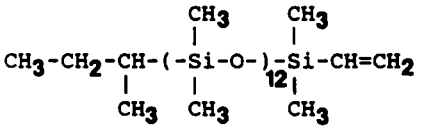

(b)

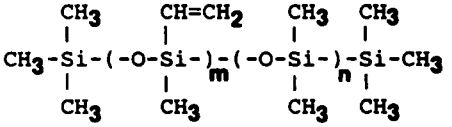

(c)

Figure 3.2. **Chemical structures of functionalized siloxane surface modifiers.:** (a)PDMS-M(MW 1k, 5k, 10k);(b)PDMS-V;(c)DMS-VMS.

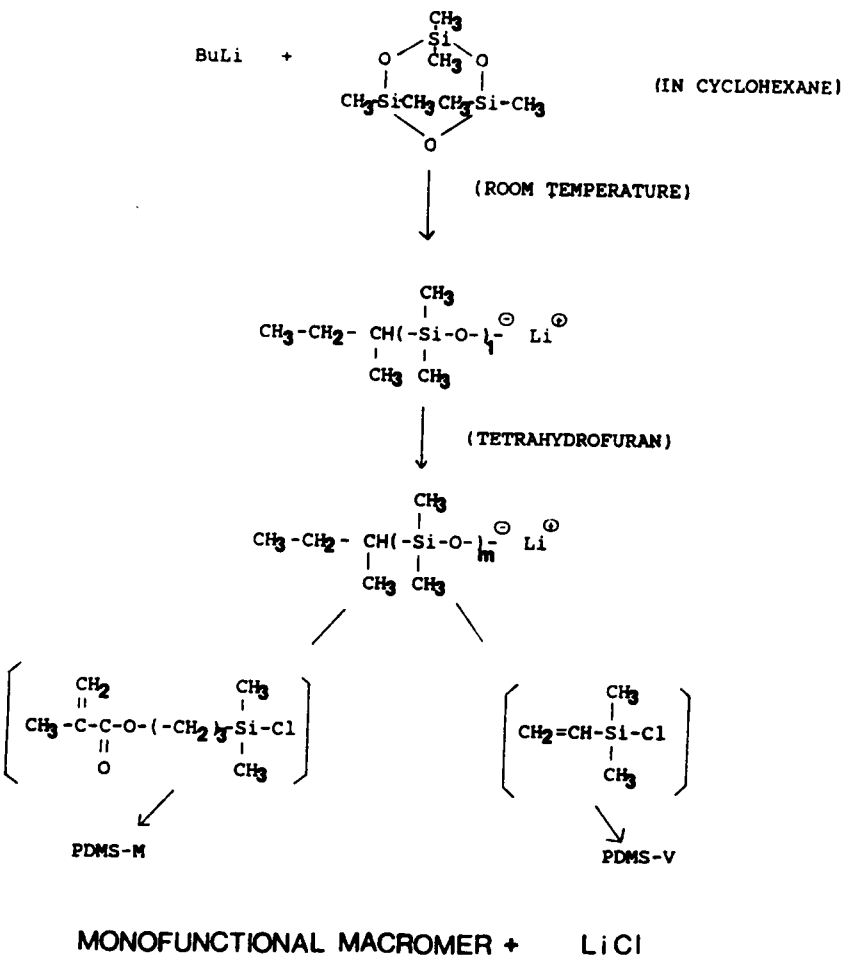

Figure 3.3. Reaction scheme for monofunctional end-capping.

bis-GMA materials were treated similarly as a "control". For the samples utilized for later peel tests, the same procedures were performed except that the bis-GMA was first applied on a titanium plate coupon(1"x5.2").

3.2.3 Irradiation and EB Apparatus

An Electrocurtain CB/150/15/180(Energy Science Inc.) equipped with a linear tungsten filament was used to irradiate the samples. A diagram of the instrument is shown in Figure 3.4. It can operate at a voltage between 150 and 175 kilovolts(kV) with an electron beam current up to 10 milliampere(mA). The accelerating voltage determines the electron energy which is related to the penetration capability of the electron into the target material. Typical depth-dose profiles are shown as a function of the beam energy in Figure 3.5. Hence, in order to provide a uniform dose throughout the film sample, penetration depths at these voltages limit sample thickness to ca. 4 mils. A constant voltage of 175 kV was utilized throughout this study. A conveyer speed of 40 feet per minute(fpm) was used for single pass dosages up to 10 Mrads. Dosage of 20 Mrads/pass was obtained at a line speed of 20 fpm such that the current requirement(half of that for the 40 fpm treatment) was within the operating range. Operating parameters were set according to

$$D = \frac{KI}{S} \qquad [3.1]$$

where K = 66.1(Mrad ft/mA/min). This K value was determined by the calibration of the dosage received by the sample and the other variables in above equation. The line speed is given by S(fpm) and I is the electron beam current measured in milliAmperes. Sam-

ples were placed on wood inserts in aluminum trays and passed through the conveyor system of the EB instrument.

3.2.4 Surface Tension Determination

3.2.4.1 Contact Angle Measurements

The characterization of solid surface wettability can be performed simply by measuring the contact angle of some selected liquids. The contact angle is defined as the tangent line angle of contact of a liquid drop sitting on a solid surface as schematically shown in Figure 3.6. Contact angles were measured by the sessile drop technique utilizing a Rame-Hart goniometer(Model 100-00). First, the reservoirs of the environmental chamber were filled with the test liquid to provide the equilibrium condition of the contact angle. Next, in order to measure the advancing contact angle, a 2 μl liquid drop was delivered to the sample surface using a microliter syringe. The angle measurement was taken as soon as possible after the liquid drop was placed to ensure the true advancing angle was obtained(11). An average was taken from ten measurements for each sample surface.

3.2.4.2 Zisman Method for Surface Tension Determination

An empirical equation proposed by Zisman(12) by measuring contact angles of a number of liquids is shown as follows:

$$\cos\theta = 1 + b(\gamma_c - \gamma_{lv}) \qquad [3.2]$$

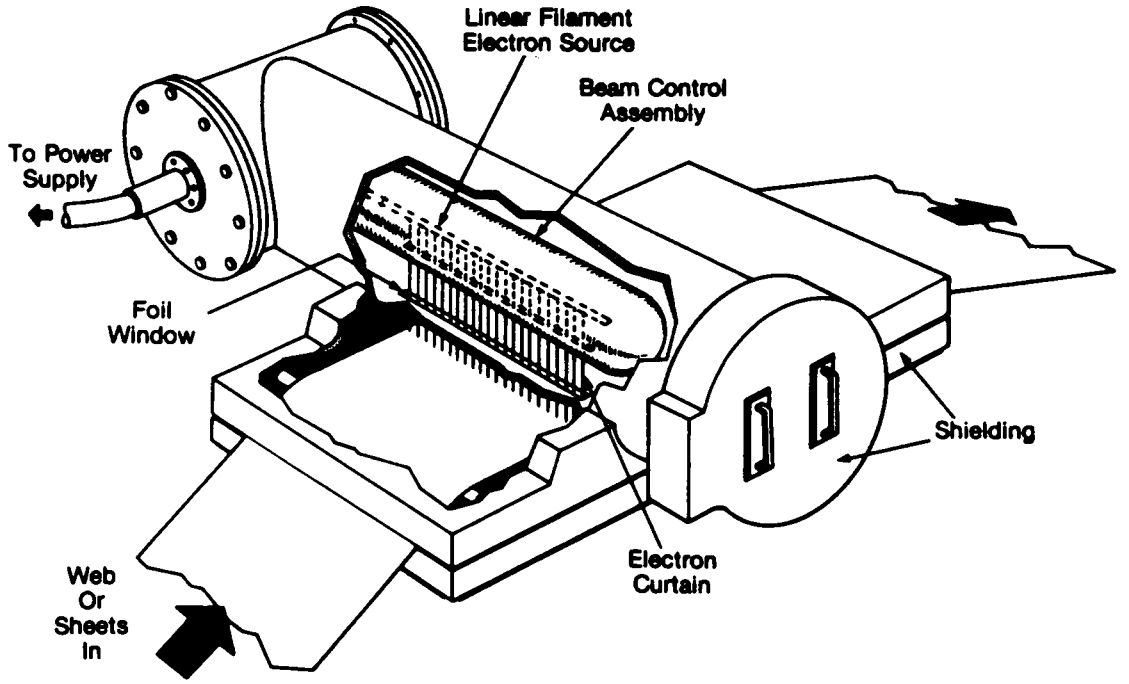

Figure 3.4. General schematic of electrocurtain instrument.

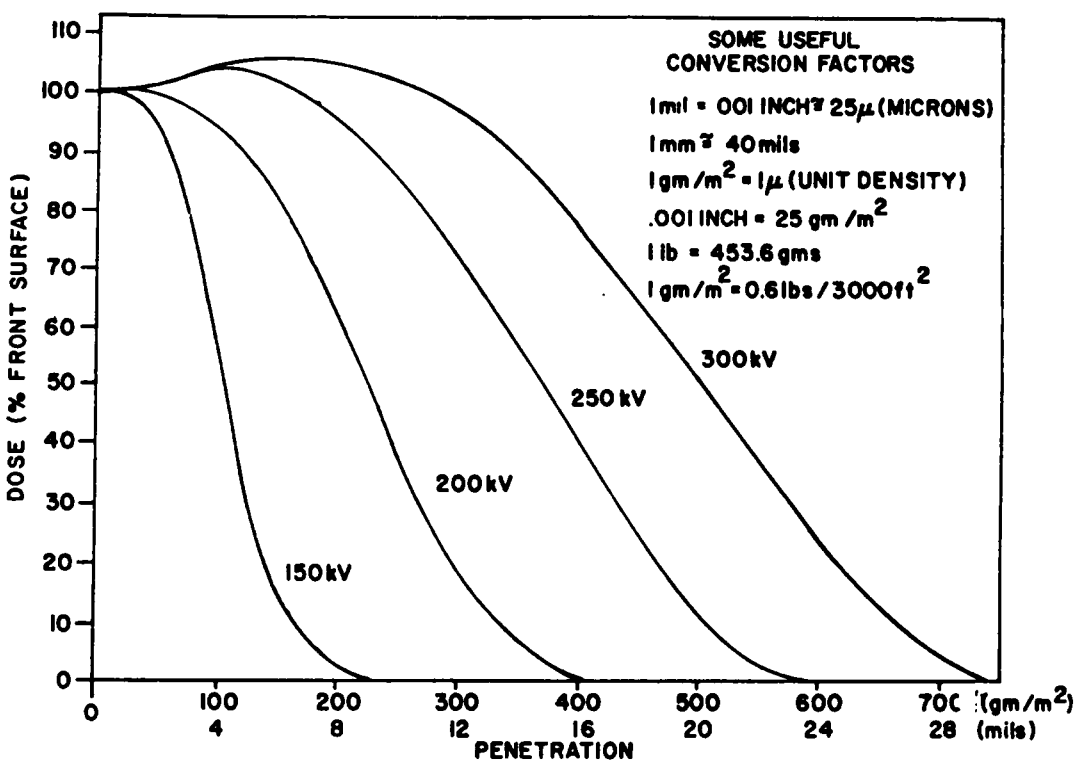

Figure 3.5. A depth-dose profile as a function of electron energy of EB processor.

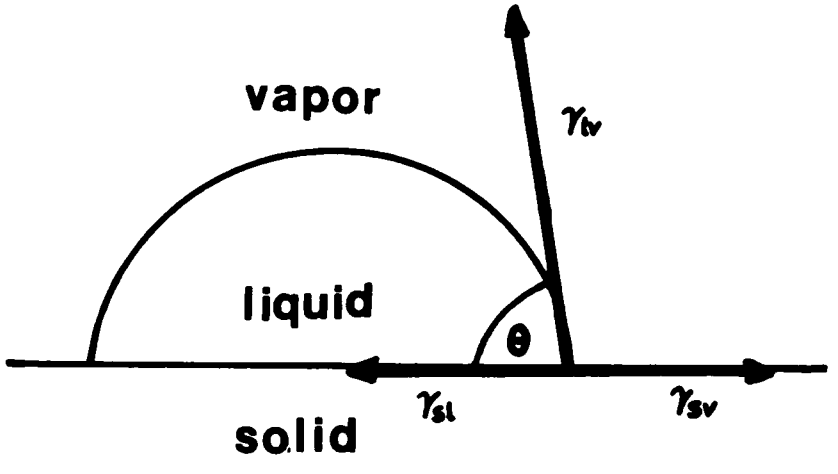

Figure 3.6. Schematic diagram of force balance with regard to a contact angle.

where b is the slope of the plot, $\cos\theta$ vs. γ_{lv}, and γ_c are called the critical surface tension. In order to obtain the critical surface tension, γ_c , the plot of the data, $\cos\theta$ vs γ_{lv}, is extrapolated to the point where $\cos\theta = 1$ and the value of γ_c coincide the surface tension of the liquid that wets the solid surface. This method provides estimates of the surface free energy of the sample. Using the values of the liquid surface tensions which were reported by Dann(13) as shown in Table 3.1, the critical surface tension of the bis-GMA, and functionalized PDMS coatings on bis-GMA substrates were determined.

3.2.5 X-ray Photoelectron Spectroscopy(XPS) Analysis

XPS spectra were obtained using a Kratos Xsam 800 X-ray photoelectron spectrometer with a Mg Kα x-ray source. Take-off-angle dependence studies were conducted to investigate the degree of surface enrichment of the siloxane surface modifiers. Both 90° and 10° take-off-angles were utilized for the surface analysis. The measured photopeak areas were obtained and used to calculate atomic concentration(14).

3.2.6 Peel Tests

Samples of 10 Mrads radiation cured bis-GMA samples with and without the methacrylate-terminated PDMS coating(MW 1,000) were prepared on rectangular titanium coupons(1″x5.2″). A masking tape(Permacel-Avery Int. Co.) was applied with a rolling 2 kg weight at a speed of 50 mm/min. Details of the controlled sample preparation for the peel test is shown schematically in Figure 3.7. The controlled rolling weight was reapplied twice more for each sample to ensure contact of the masking tape

Table 3.1. Surface tensions of Zisman liquid series reported by Dann(11).

Liquid	Γ [dyne/cm]
Water	72.2
Glycerol	63.4
Formamide	58.2
Methylene chloride	50.6
1-Bromonaphthalene	44.6
Hexadecane	26.5
Decane	23.8
Octane	21.6
Hexane	18.3

to the sample surface. A 180° peel test was conducted to measure the peeling force as a function of peel rate using an Instron Testing Machine(model 1122). These peel tests were performed carefully following the procedure, ASTM D100-78, as shown in Figure 3.8. Peeling rate was changed from 0.1 to 10 cm/sec.

3.2.7 Tests for Chemical Resistance

Hexane-extracted samples of bis-GMA with and without PDMS-M(MW 1,000, 10 Mrads) coatings were treated with aqueous nitric acid(70 %) and acetic acid(99 %) by placing each acid on the sample surface for 24 hours. After the acid treatment, each sample was washed with deionized water and dried for 24 hours. Scanning electron microscopy(SEM) pictures were taken of these acid-treated sample surfaces to allow comparisons between the uncoated bis-GMA and siloxane- coated bis-GMA surfaces.

3.3 Results and Discussion

3.3.1 Surface Tension Measurements

Contact angle measurements of the uncoated bis-GMA, PDMS-M(MW 1,000) coatings, and PDMS-V(MW 1,000) coatings were performed as summarized in Table 3.2. Critical surface tensions of these samples were determined as a function of the EB irradiation dosage as shown in Figure 3.9. In each case, for dosages up to 5 Mrads, dosage level strongly affects the critical surface tension which implies a difference in the concen-

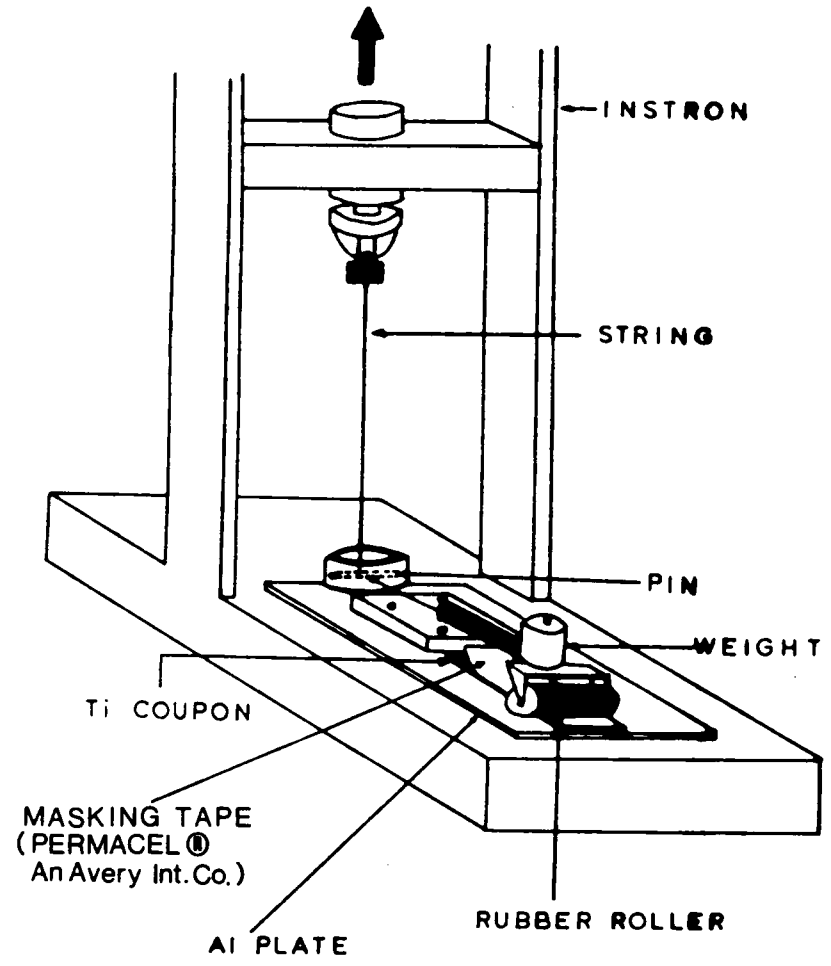

Figure 3.7. Schematic of the controlled masking tape application technique.

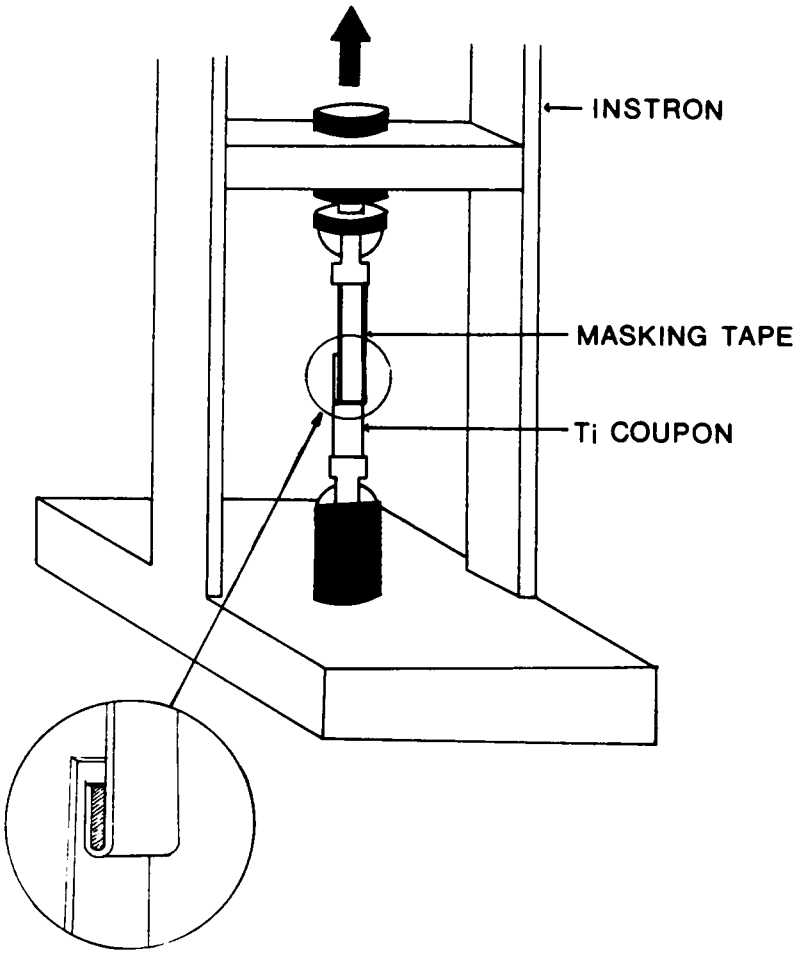

Figure 3.8. Schematic of 180 degree peel test.

tration of the attached PDMS oligomers to the bis-GMA surface. The dosage effect levels off above 5 Mrads. It is important to note that the methacrylate end-group is observed to be more effective in lowering the critical surface tension than the vinyl end-group. This may be due to a greater reactivity or possibly a greater copolymerizability of the methacrylate terminal group with bis-GMA relative to the vinyl terminal group(15). These features would facilitate the reaction at the time of irradiation.

Contact angle measurements of unmodified bis-GMA as well as those treated with PDMS-M(MW 1,000), PDMS-M(MW 5,000), and PDMS-M(MW 10,000) were performed with the results listed in Table 3.3. The critical surface tensions of these samples were determined as a function of EB irradiation dosage (Figure 3.10) Differences in critical surface tension between the uncoated bis-GMA and PDMS-coated bis-GMA surfaces ranged from 10 to 20 dyne/cm. Changing the molecular weights of PDMS also resulted in noticeable differences of the critical surface tension in the dosage range above 5 Mrads, whereas it resulted in scattered data below 5 Mrads. As shown previously in Figure 3.9, the effect of dosage on the critical surface tension levels off above 5 Mrads and hence the differences in critical surface tension in this dosage range as shown in Figure 3.10 are believed due to the difference in molecular weight of the PDMS materials. PDMS coatings of higher molecular weight resulted in a greater final thickness on the surface of the bis-GMA layer. This will be proven by XPS analysis later in this paper. Therefore a thicker PDMS coating gives a greater distance between the surface of the bis-GMA substrate and the free "air-side" surface of the PDMS coating. We believe these "final" thicker coatings assist in promoting a lower critical surface tension. It was reported by G. Gaines(16) that higher molecular weight of polymer liquid resulted in a higher surface tension based on the free volume theory. However, in our study, the monofunctionalized PDMS-M and PDMS-V possess a very low probability to be

Table 3.2. **Contact angle measurements of uncoated, PDMS-M, and PDMS-V coated bis-GMA.**

Sample	water	hexa-decane	glycerol	bromo-naphthalene	form-amide
bis-GMA(0.5Mrad)	79		68	20	62
bis-GMA(2Mrad)	79		70	24	62
bis-GMA(5Mrad)	84		75	25	67
bis-GMA(10Mrad)	82		74	27	65
bis-GMA(20Mrad)	84		78	33	66
PDMS-M(1k,0.5Mrad)	86	13	79	42	70
PDMS-M(1k,2Mrad)	87	17	92	61	85
PDMS-M(1k,5Mrad)	90	23	91	62	88
PDMS-M(1k,10Mrad)	92	22	92	66	88
PDMS-M(1k,20Mrad)	93	22	94	67	89
PDMS-V(1k,0.5Mrad)	81	6	71	33	65
PDMS-V(1k,2Mrad)	85	8	79	43	72
PDMS-V(1k,5Mrad)	86	10	81	51	74
PDMS-V(1k,10Mrad)	93	16	82	53	74
PDMS-V(1k,20Mrad)	95	19	93	62	87

*Each contact angle was averaged over 10 measurements.

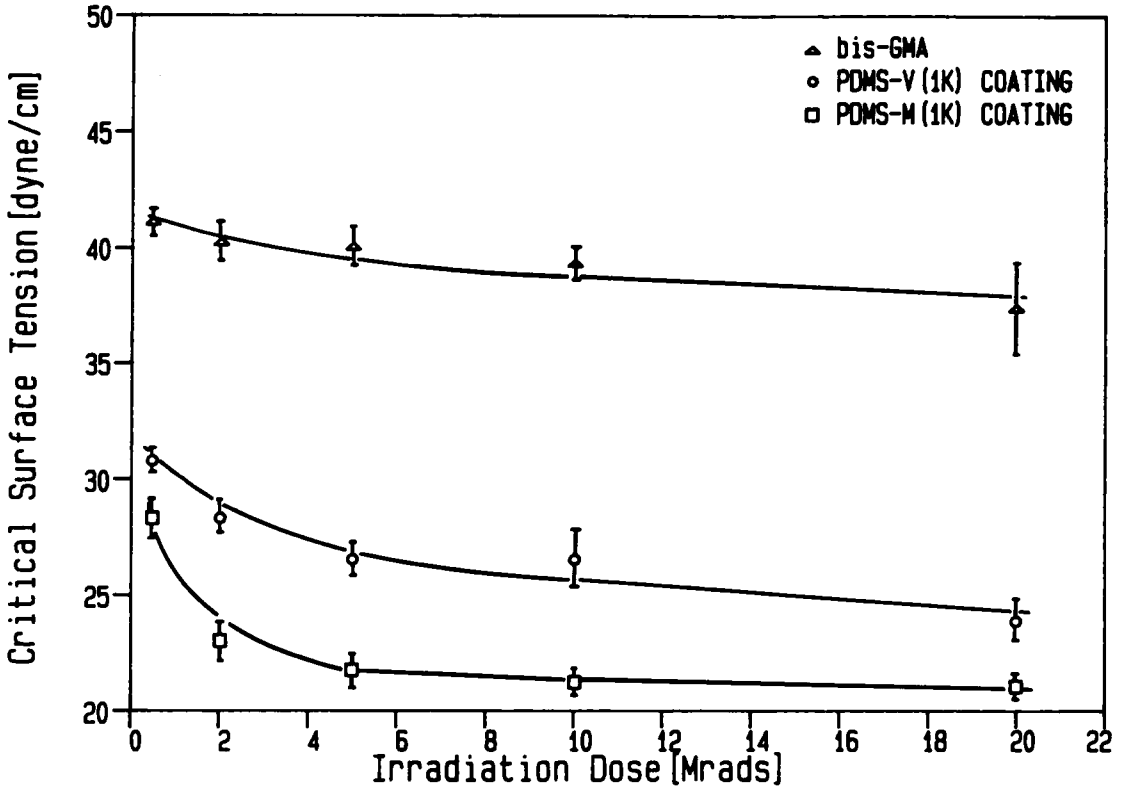

Figure 3.9. Irradiation dose vs. critical surface tension for bis-GMA control, PDMS-M, PDMS-V coatings.

crosslinked by our relatively low-energy EB irradiation although they can be dimerized or possibly trimerized. Therefore, once the oligomers are attached to the bis-GMA surface through their monofunctionality, the other EB-polymerized species on the surface are expected to be removed by the solvent extraction. Hence, no matter what molecular weight the chemically attached PDMS oligomers have, there should be a relatively low dependence on the free volume for the range of molecular weight addressed here. In the dosage range below 5 Mrads, the concentration of the functional end-group in addition to EB irradiation dosage can be regarded as the important process variables. For a higher molecular weight of PDMS in the dosage range below 5 Mrads, these two variables appear to somewhat counterbalance each other in the final critical surface tension data. First, a higher molecular weight PDMS has a tendency to form a greater coating thickness which results in a lower critical surface tension(see later discussion). However, a higher molecular weight PDMS offers a lower concentration of the functional end-group which is of importance at dosage levels below 5 Mrads. For lower molecular weight of PDMS in this same dosage range, the critical surface tensions as influenced by these same variables were expected to be somewhat reversed.

Contact angle measurements of bis-GMA, monofunctional PDMS-V coatings and multifunctional DMS-VMS copolymer coatings were performed-the results being summarized in Table 3.4. Figure 3.11 also shows the critical surface tensions determined as a function of EB irradiation dosage. The molecular weight was 1,000 for PDMS-V and about 28,000 for the DMS-VMS copolymer. In the dosage range both above and below 5 Mrads, the multifunctional DMS-VMS material resulted in lower critical surface tensions and showed a greater sensitivity of the critical surface tension on EB dosage in the lower dosage range. This behavior again is in agreement with the earlier considerations based on the concentration of the functional groups and molecular weight in the PDMS

Table 3.3. Contact angle measurements of uncoated, PDMS-M(1k), PDMS-M(5k), and PDMS-M(10k) coated bis-GMA.

Sample	water	hexa-decane	glycerol	bromo-naphthalene	form-amide
bis-GMA(0.5Mrad)	79		68	20	62
bis-GMA(2Mrad)	79		70	24	62
bis-GMA(5Mrad)	84		75	25	67
bis-GMA(10Mrad)	82		74	27	65
bis-GMA(20Mrad)	84		78	33	66
PDMS-M(1k,0.5Mrad)	86	13	79	42	70
PDMS-M(1k,2Mrad)	87	17	92	61	85
PDMS-M(1k,5Mrad)	90	23	91	62	88
PDMS-M(1k,10Mrad)	92	22	92	66	88
PDMS-M(1k,20Mrad)	93	22	94	67	89
PDMS-M(5k,0.5Mrad)	78	17	75	34	68
PDMS-M(5k,2Mrad)	91	27	83	40	70
PDMS-M(5k,5Mrad)	95	28	91	61	75
PDMS-M(5k,10Mrad)	102	36	95	64	87
PDMS-M(5k,20Mrad)	105	35	95	69	88
PDMS-M(10k,0.5Mrad)	84	10	74	43	65
PDMS-M(10k,2Mrad)	87	29	88	48	77
PDMS-M(10k,5Mrad)	106	31	97	60	91
PDMS-M(10k,10Mrad)	108	33	99	69	93
PDMS-M(10k,20Mrad)	102	43	103	73	97

*Each contact angle was averaged over 10 measurements.

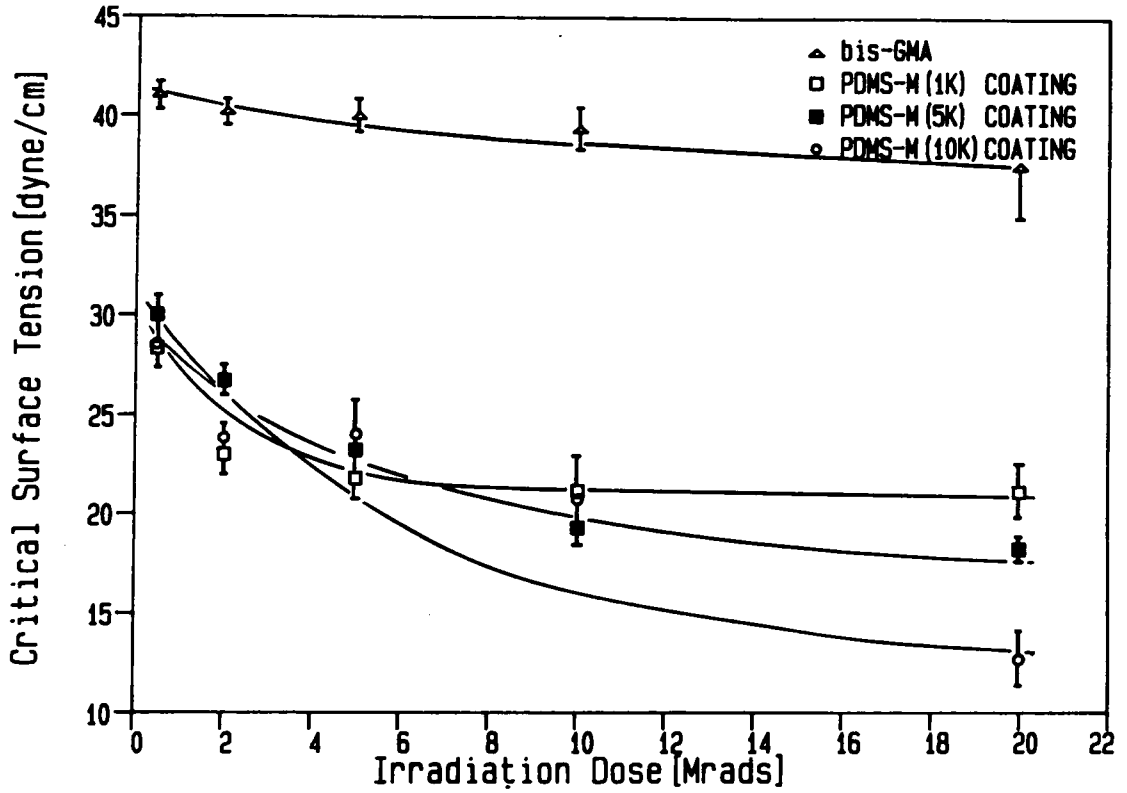

Figure 3.10. Irradiation dose vs. critical surface tension for bis-GMA control, PDMS-M(1k, 5k, 10k) coatings.

system. First, in the dosage range below 5 Mrads, both higher molecular weight and higher concentration of functional groups of the DMS-VMS material in comparison with the PDMS-V material contributes to lower the critical surface tension. However, in the previous data of Figure 3.10, these two variables appear to counterbalance each other in the critical surface tension data. Secondly, in the dosage range above 5 Mrads, the concentration of functional groups becomes insensitive to EB dosage since the bis-GMA surface portion unattached by PDMS materials decreases and vanishes as the EB dosage increases further in this higher dosage range. Therefore the molecular weight becomes the major variable as discussed in the previous data.

It should be stated that, while high molecular weight PDMS will crosslink with sufficient radiation treatment irrelevant of functional end-groups, no gelation occurred for any of the PDMS materials except that of the high molecular weight PDMS with multifunctional groups-i.e. DMS-VMS. These multifunctional DMS-VMS copolymers were found to form a gel in the dosage range above 10 Mrads. Using this knowledge regarding gelation, bis-GMA substrates spray-coated with this DMS-VMS copolymer (19 wt% VMS) and given a 20 Mrad-cure were then fractured in the direction perpendicular to the surface at room temperature. An example of a SEM micrograph taken on this gel-coated system is shown in Figure 3.12. From the SEM results, the thickness of the initial siloxane layer(ca. 2μm) applied(sprayed) on the liquid bis-GMA substrate could be easily determined.

Table 3.4. Contact angle measurements of uncoated, PDMS-M, and DMS-VMS coated bis-GMA.

Sample	water	hexa-decane	glycerol	bromo-naphthalene	form-amide
bis-GMA(0.5Mrad)	79		68	20	62
bis-GMA(2Mrad)	79		70	24	62
bis-GMA(5Mrad)	84		75	25	67
bis-GMA(10Mrad)	82		74	27	65
bis-GMA(20Mrad)	84		78	33	66
PDMS-V(1k,0.5Mrad)	81	6	71	33	65
PDMS-V(1k,2Mrad)	85	8	79	43	72
PDMS-V(1k,5Mrad)	86	10	81	51	74
PDMS-V(1k,10Mrad)	93	16	82	53	74
PDMS-V(1k,20Mrad)	95	19	93	62	87
			methylene iodide		
DMS-VMS(25k,0.5Mrad)		14	51	32	67
DMS-VMS(25k,2Mrad)		22	64	57	81
DMS-VMS(25k,5Mrad)		40	79	60	93
DMS-VMS(25k,10Mrad)		47	103	82	112
DMS-VMS(25k,20Mrad)		44	110	89	113

*Each contact angle was averaged over 10 measurements.

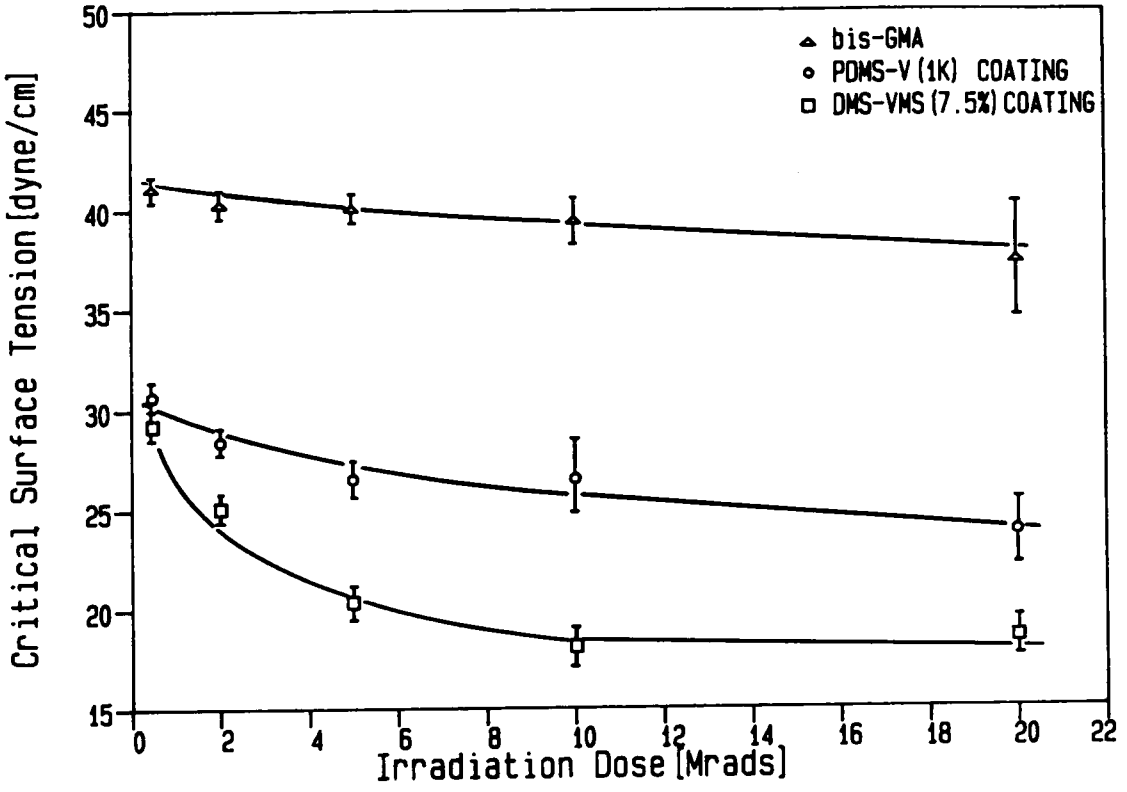

Figure 3.11. Irradiation dose vs. critical surface tension for bis-GMA control, PDMS-V, DMS-VMS coatings.

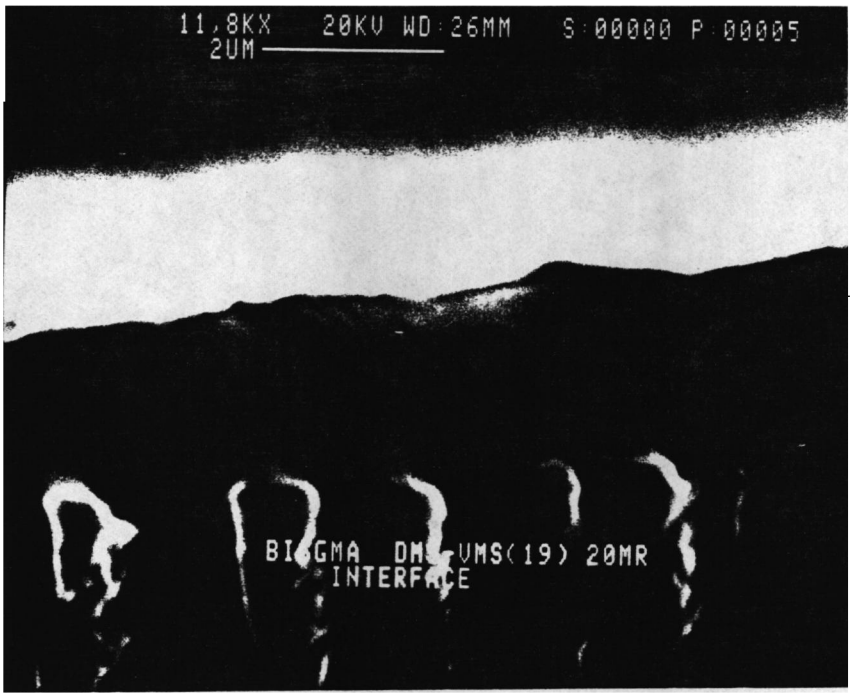

Figure 3.12. Scanning electron micrograph showing the thickness of DMS-VMS coating.

3.3.2 XPS Analysis

As discussed by the critical surface tension measurement, the thickness of final extracted monofunctionalized PDMS coating was suggested to vary with its molecular weight. In order to approximate the "size" of the PDMS coil which is attached to the substrate surface by a chemical bonding between the functional end-group and the bis-GMA, radius of gyration of the PDMS coil was approximated by using Gaussian chain statistics(17). High molecular weight PDMS is known to display Gaussian behavior. However, due to the relatively low molecular weights of the PDMS utilized in this study, they were not expected to be truly Gaussian especially with an attached end to the bis-GMA substrate. Nevertheless, as indicated above, the radius of gyration of PDMS(MW 1,000, MW 10,000) was calculated for the purpose of estimating coil dimensions and using these results to compare with the information obtained from XPS take-off-angle experiments.

Figure 3.13 shows the schematic of XPS take-off-angle analysis which incorporates the thickness dependence upon molecular weight of PDMS in conjunction with the approximate radius of gyration. Figure 3.14 shows the XPS spectra of the PDMS-M(MW 1,000 at 10 Mrads) coating with a 90° take-off-angle, the PDMS-M(MW 10,000 at 10 Mrads) coating with a 90° take-off-angle and the PDMS-M(MW 10,000 at 10Mrads) coating with a 10° take-off-angle. In each XPS spectrum, four major signals were detected as a function of core binding energy-these signals being the carbon atom C(1s) at 284(eV), the oxygen atom O(1s) at 532(eV), the silicone atom Si(2s) at 149(eV) and Si(2p) at 100(eV)(18). To test for the consistency of the signals, the peak areas were taken as ratios and compared as shown in Table 3.5.

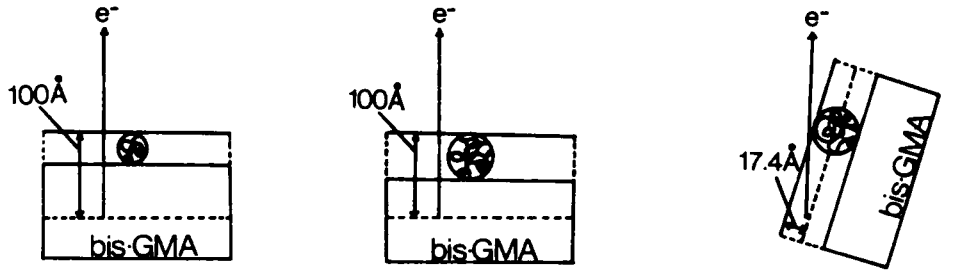

Figure 3.13. Schematic diagram of XPS analysis using different take-off-angles.: (a)PDMS-M(1k), 90 degree;(b)PDMS-M(10k), 90 degree;(c)PDMS-M(10k), 10 degree.

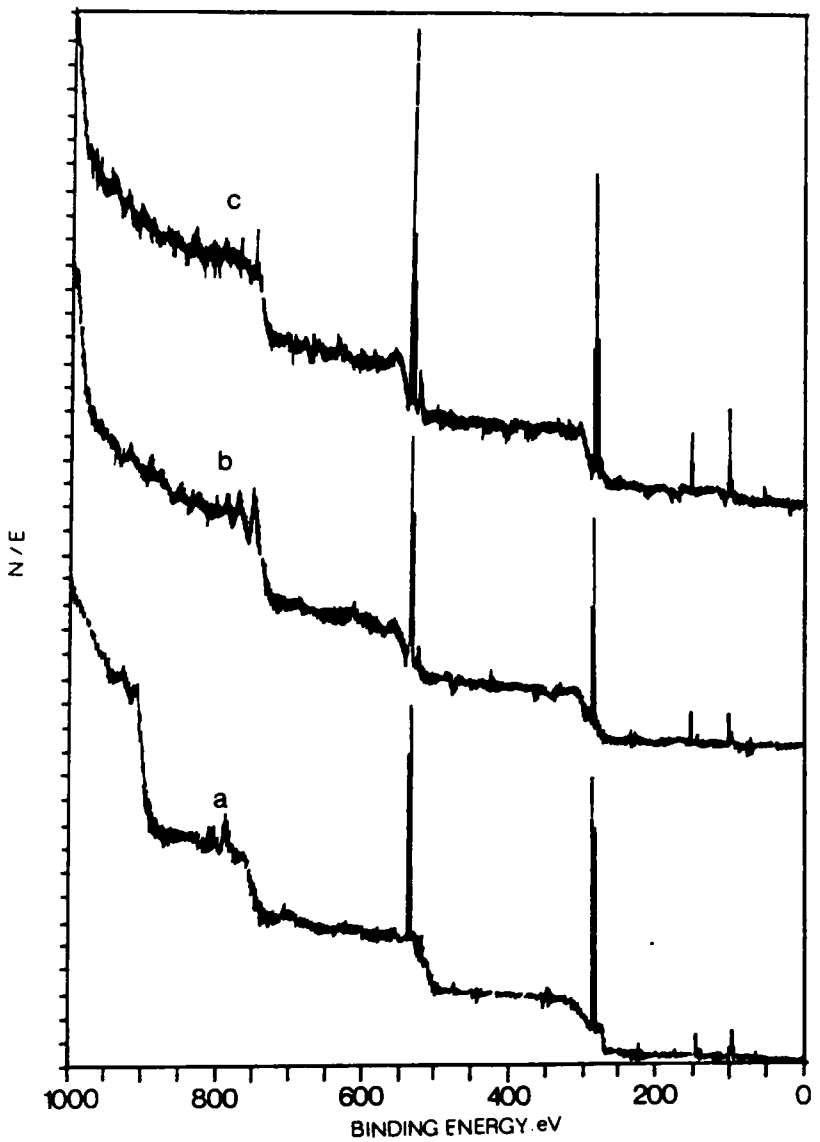

Figure 3.14. **XPS spectra of the PDMS-M coated bis-GMA surfaces.:** (a)PDMS-M(1k), 90 degree;(b)PDMS-M(10k), 90 degree;(c)PDMS-M(10k), 10 degree.

By increasing the molecular weight of PDMS-M from 1,000 to 10,000 but with a constant 90° take-off-angle, the C/Si ratio decreased from 13.2 to 9.6. By decreasing the take-off-angle from 90° to 10° with a constant 10,000 molecular weight, the C/Si ratio decreased further from 9.6 to 3.9. This C/Si ratio of PDMS-M(MW 10,000 at 10 Mrads) with the 10° take-off-angle approached the C/Si ratio of pure PDMS-M(MW 10,000) material since the analyzed depth was smaller than the diameter of the 10,000 molecular weight PDMS-M coil obtained from the crude Gaussian approximation of the radius of gyration. Therefore, these XPS data at least support the relative dependence of surface thickness of the functional PDMS on its molecular weight and the speculation that **a monomolecular thickness** of the PDMS component is obtained as would be expected. It should be mentioned that, in the case of the 10° take-off-angle analysis of the PDMS-M(MW 10,000) coating as shown in Table 3.5, the electrons should escape from a depth of about 20 Å. However actual XPS data indicate that some electrons were escaping from the bis-GMA substrate. This result can be rationalized as follows. The general sampling depth of XPS analysis with a conventional x-ray source for organic materials is known to be approximately 100 Å. However, it can deviate from this value depending on the type of the material to be analyzed. The accurate determinations of atomic density and mean free paths of the photoemitted electrons are therefore of importance if quantitative results are to be extracted from analytical sampling depth profiling experiments(19). For our investigation it is believed that there should be a significant difference in the atomic density between the PDMS layer and the crosslinked bis-GMA substrate thereby affecting the magnitude of electron mean free paths. We also believe that the siloxane layer could have lower density than that of crosslinked bis-GMA substrate even though the precise estimation of the magnitude of electron mean free path has been known to be difficult(19). If this is true, the sampling depth may be greater than that expected analytically as the thickness of PDMS increases and

the take-off-angle decreases in consideration of the atomic density difference. From this point of view, it is possible for some of electrons to escape from the bis-GMA layer although the sampling depth was smaller than the approximated thickness of the PDMS layer. Whatever the case may be, the XPS results still clearly support the conclusions reached above.

An attempt was made to verify that the coupling of PDMS molecules to the bis-GMA substrate surface has been achieved only by chemical bonding. Electron spin resonance(ESR) spectra of the irradiated(2 Mrad) bis-GMA with increasing aging time were obtained as shown in Figure 3.15. The well-known 9 line spectra of alternating intensity(20), which has been interpreted as a result due to the methacrylate radical species, were obtained. The concentration of the trapped radical appears to decrease with increasing aging time. These phenomena had been well discussed by D. Thompson(21). In another XPS experiment, bis-GMA **without** a PDMS coating was EB irradiated and then **completely thermal cured(150°C for 2 hours)** the latter which completes the polymerization leading to a high degree of a network formation and eliminating any remaining free radicals. PDMS-M(MW 1,000) was then spray-coated on this **previously cured** bis-GMA and aged for 24 hours followed by the same extraction procedure. The XPS spectrum of this sample surface is shown in Figure 3.16 and resulted in a signal which shows **no existence of the Si component.** This result very strongly supports at least two important premises of this study. First, PDMS oligomers are able to be attached onto the surface of bis-GMA only by chemical bonding between the EB reactive functional end groups of PDMS and the bis-GMA through EB irradiation. Second, there is no possibility for PDMS to remain on the substrate following extraction unless chemical bonding occurs.

Table 3.5. XPS take-off-angle analysis data.

Sample	radius of gyration	take-off-angle	sampling depth(Å)	C/Si ratio
PDMS-M(1k,10Mrad)	7.2	90	100	13.2
PDMS-M(10k,10Mrad)	19.9	90	100	9.6
PDMS-M(10k,10Mrad)	19.9	10	17.4	3.9

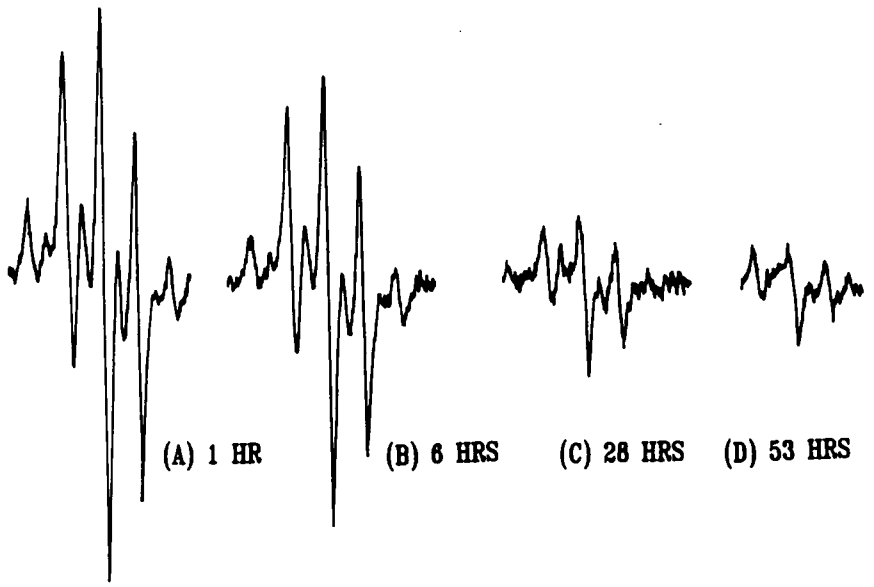

Figure 3.15. ESR spectra of irradiated(2 Mrad) bis-GMA with time after irradiation.

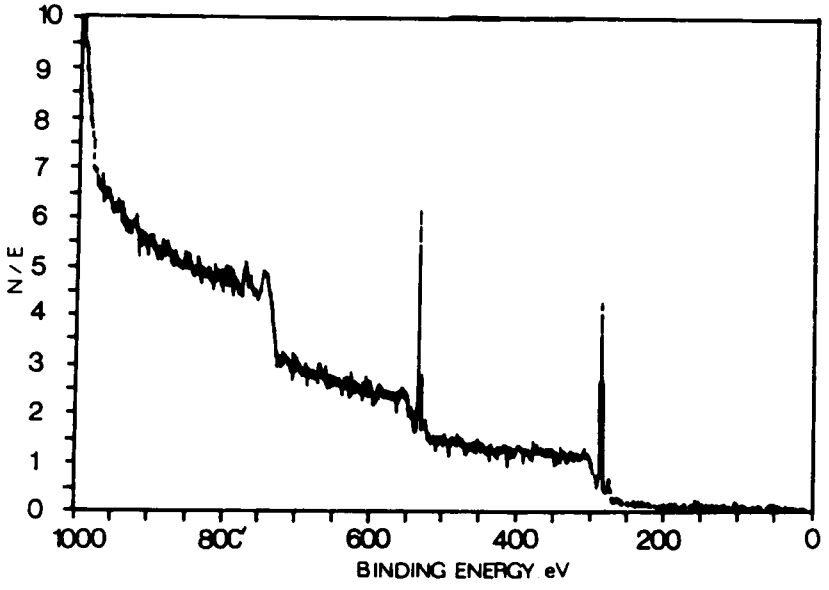

Figure 3.16. XPS spectra of cured bis-GMA followed by siloxane coating without EB.

3.3.3 Adhesion Studies-Peel Tests

Figure 3.17 shows the peeling forces for the uncoated bis-GMA and for methacrylate-terminated PDMS(MW 10,000) coatings. Both samples had been irradiated with 10 Mrads. As expected(22) peeling force increased with increasing peel rate reflecting the viscoelastic behavior of the adhesive. This is not the major issue here. At a lower peel rate of 0.1 cm/sec, the peeling forces were about 0.11 N/cm for the uncoated bis-GMA(10 Mrads) and 0.01 N/cm for the methacrylate-terminated PDMS(MW 10,000 at 10 Mrads) coatings. These results show a nearly 90 % peel force **reduction** for the siloxane-coated bis-GMA when compared to the uncoated material. At the higher peel rate of 10 cm/sec, peeling forces were approximately 0.34 N/cm for the uncoated bis-GMA and 0.14 N/cm for the same methacrylated PDMS(MW 10,000) coatings which gives a nearly 60 % peel force reduction for the PDMS modified surface. Clearly, the peel force behavior is in direct agreement with the surface tension measurements.

3.3.4 Tests for Chemical Resistance

Polysiloxanes are relatively inert to many hostile chemicals. Also, aqueous solutions of any kind generally have little effect on polysiloxanes. This behavior is principally due to the poor wetting characteristics of silicone. Thus dilute aqueous acids, metal salt solutions, dilute hydrogen peroxide, etc. have little effect on silicone polymers(23).

Aqueous nitric acid and acetic acid were used as an indicators in a brief test of the chemical resistance of the modified and unmodified bis-GMA surfaces as investigated by SEM. Nitric acid treated surfaces of the uncoated bis-GMA and PDMS coated

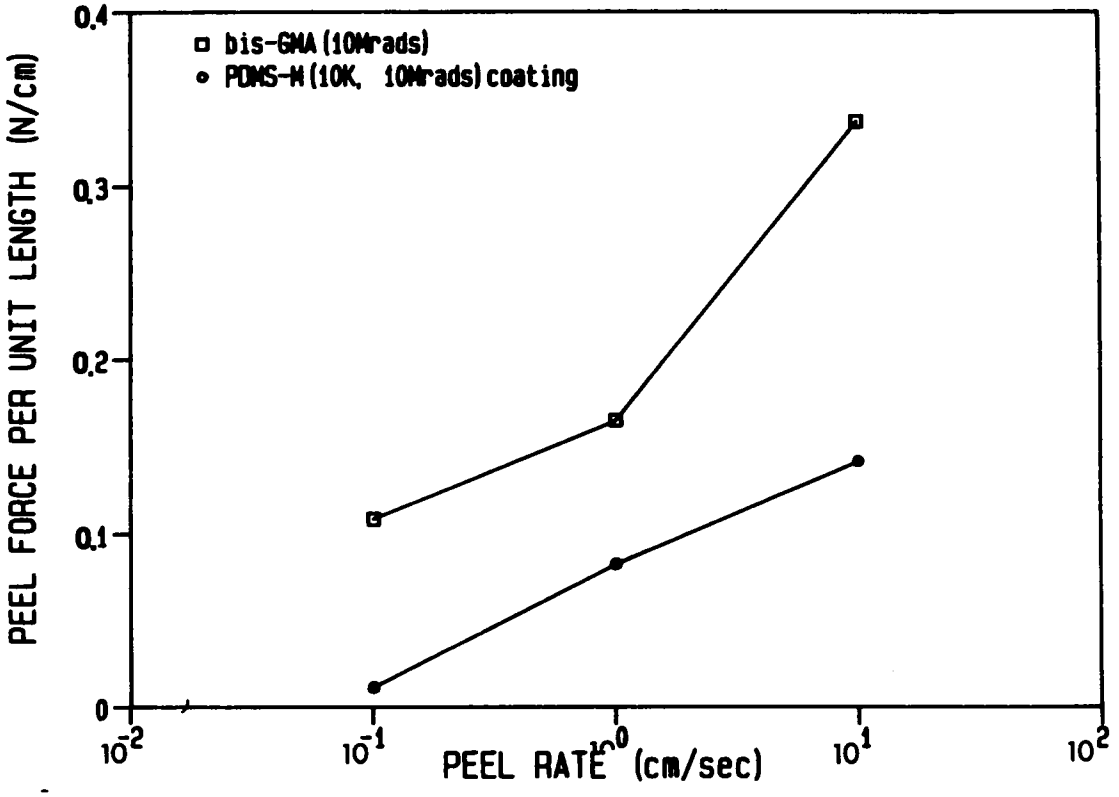

Figure 3.17. Peel test results for uncoated bi-GMA and PDMS-M(10k) coated bis-GMA.

bis-GMA are shown in Figures 3.18(a) and 3.18(b), respectively. Acetic acid treated surfaces of the uncoated bis-GMA and PDMS coated bis-GMA are also shown in Figures 3.19(a) and 3.19(b), respectively.

After being contacted with these acids at the surface for 24 hours, uncoated bis-GMA surfaces in Figure 3.18(a)(treated by nitric acid) and Figure 3.19(a)(treated by acetic acid) resulted in severe degradation by nitric acid and a somewhat roughened surface by acetic acid. The uncoated bis-GMA is suspected to be oxidized by nitric acid from the fact that the uncured bis-GMA monomer showed high reactivity with nitric acid in a short time period. Therefore it can be deduced by the reactivity between nitric acid and the bis-GMA monomer and Figures 3.18(a) and 3.19(a) that nitric acid is a hostile chemical with regard to bis-GMA. Aromatic substituent groups in organic polymers are known to be susceptible to bond cleavage by strong acids(23). It is important to add that bis-GMA monomer forms a gel in nitric acid within an hour when they are brought into contact to each other.

In contrast to the uncoated bis-GMA, the methacrylate- terminated PDMS coated bis-GMA offers extremely low wettability that could repel many organic chemicals as well as aqueous-based systems. Therefore aqueous acid is not able to contact the bis-GMA layer since the PDMS coating serves as a blocking layer between acid and substrate. Secondly, the chemical inertness of siloxane resists chemical changes by acids at least in the relatively low temperature range(24). Acetic acid was utilized as a weak acid for the test of chemical resistance. Similar comparisons between uncoated bis-GMA and PDMS coated bis-GMA resulted in the SEM observation given in Figures 3.19(a) and 3.19(b).

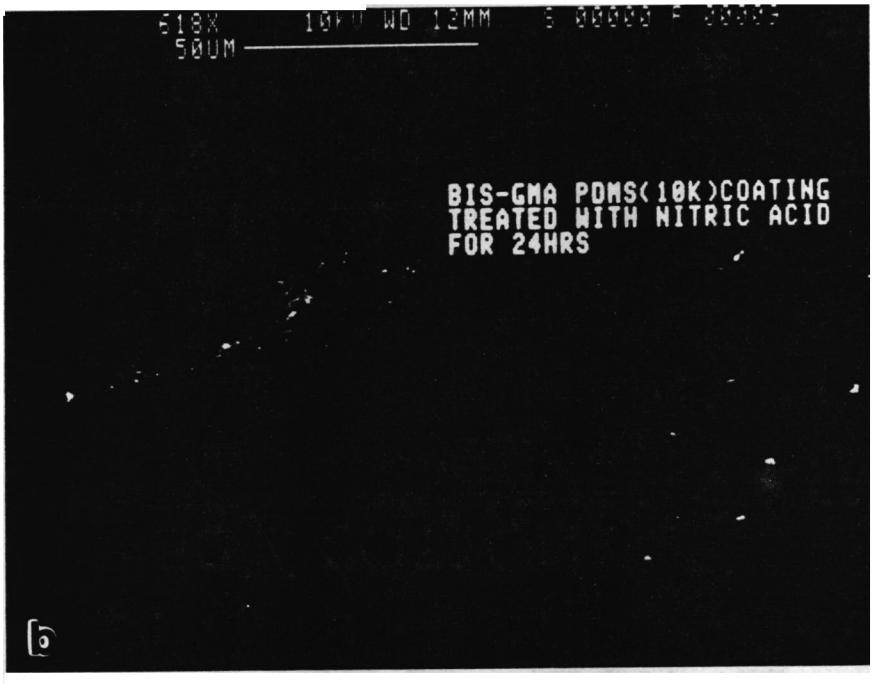

Figure 3.18. Scanning electron micrographs of the surface treated with nitric acid.: (a)uncoted bis-GMA;(b)PDMS-M coated bis-GMA.

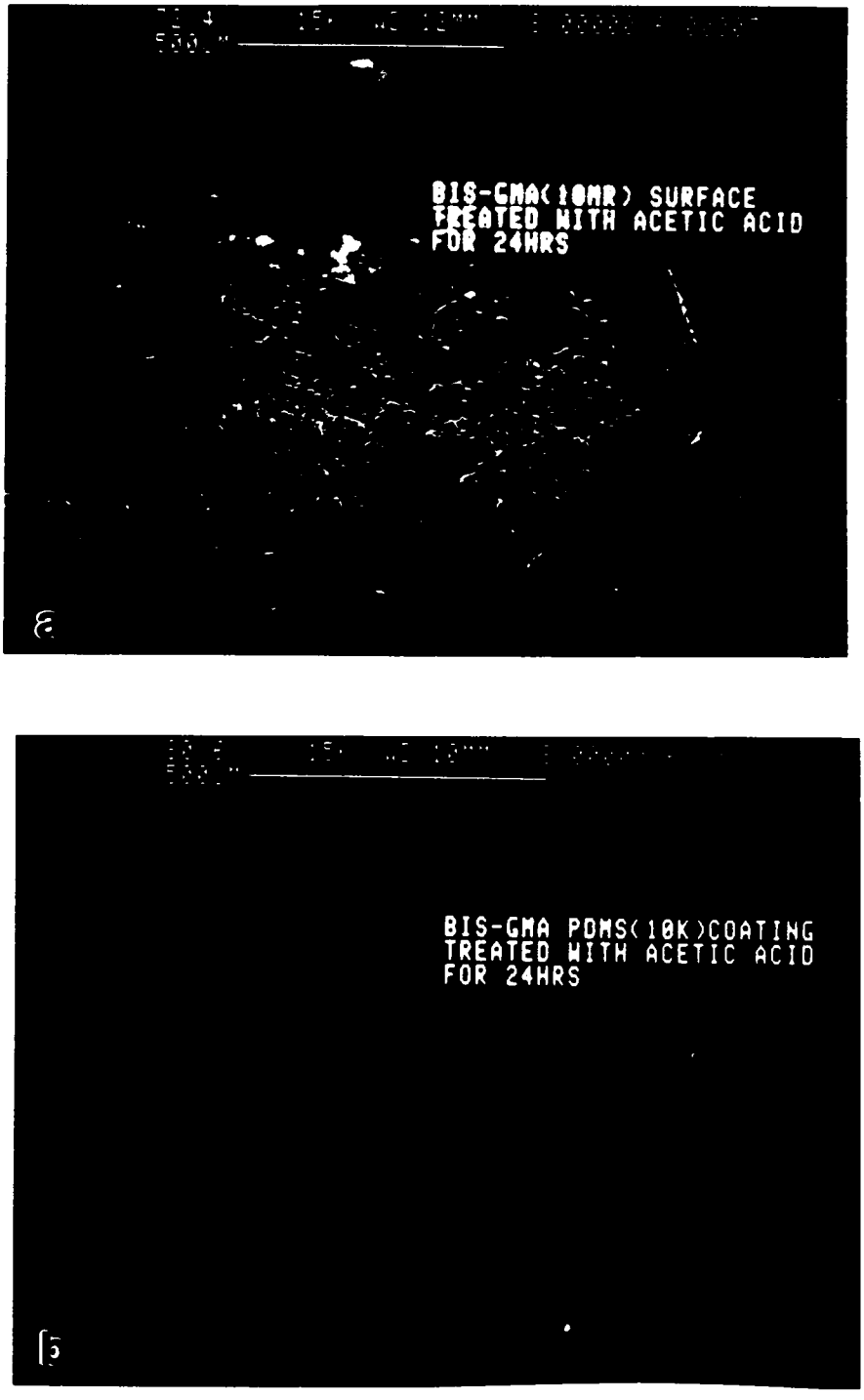

Figure 3.19. Scanning electron micrographs of the surface treated with acetic acid.: (a)uncoated bis-GMA;(b)PDMS-M coated bis-GMA.

3.4 Conclusions

A number of conclusions can be made from this study on the topic of surface modification of bis-GMA substrates using siloxane surface modifiers. The degree of chemical attachment of the EB reactive functionalized siloxanes onto the substrate surface increases with dosage up to 5 Mrads and shows nearly constant values above this irradiation dosage level. The methacrylate functional end-group was observed to be more effective in bonding to the substrate than the vinyl end-group which might be due to the reactivity of these two functional groups to the bis-GMA liquid substrate. Molecular weight of the monofunctionalized PDMS also played an important role in this study. Increasing molecular weight induces a greater thickness of the PDMS coating on the bis-GMA substrate but lowers the concentration of functional end groups. In the lower EB dosage range, these two variables counter-balanced each other with regard to the final critical surface tension data. Only the molecular weight becomes a variable at higher EB dosage in which the concentration of functional group became insensitive to changing dosage above about 5 Mrads. This tendency to provide a greater "coating thickness" from the higher molecular weight PDMS was also proven by XPS analysis. As expected, an increased number of functional groups in PDMS resulted in a higher sensitivity of bond attachment capability in the lower dosage range and showed lower critical surface tensions in all dosage ranges. Reductions of peeling forces by introducing these surface modifiers provided a strong agreement with the critical surface tension data. Inertness and poor wettability of siloxane provided the PDMS coatings with a strong resistance to chemical degradation by nitric and acetic acid in contrast to the uncoated bis-GMA.

References

1. Takiguchi, R.; Uryu, T. *J. Appl. Polym. Sci.* 1986, *31*, 2083.

2. Fujita, S.; Fujigawa, J.; Ueno, N.; Okamoto, A. *Radiat. Phys. Chem.* 1981, *18*, 864.

3. Chandan, H. C.; Kalish, D. *J. Am. Ceram. Soc.* 1982, *83*, 171.

4. Shinka, J. V.; LieBerman, R. A. *Radiat. Curing* 1983, *10*, 18.

5. Lee, L. H. *Characteristics of Metal and Polymer Surfaces* Academic Press Inc., 1977.

6. Gordon, D. J. *Technical Paper, Soc. Manuf. Engrs.* FC76-505(1976).

7. Kawakami, Y.; Murphy, R. A.; Yamashita, Y. *Polym. Bull.* 1983, *10*, 368.

8. Gaines, G. L. *Macromolecules* 1981, *14*, 208.

9. Yilgor, I.; Yilgor, E.; Banthia, A. K.; Wilkes, G. L. *Polymer Composites* 1983, *4*, 120.

10. Smith, S. D.; McGrath, J. E. *Polym. Prep.* 1987, *28*, 150.

11. Penn, L.; Miller, B. *J. Coll. Interface Sci.* 1980, *77*, 574.

12. Zisman, W. A. *Contact Angle, Wettability, Adhesion* Advan. Chem. Ser. 43, ACS, 1964.

13. Dann, J. R. *J. Coll. Interface Sci.* 1970, *32*, 302.

14. Wagner, C. D. *Anal. Chem.* 1972, *44*, 1050.

15. Lee, L. H. *J. Coll. Interface Sci.* 1968, *27*, 751.

16. Legrand, D. J.; Gaines, G. L. *J. Coll. Interface Sci.* 1969, *31*, 162.

17. Flory, P. J. *Principles of Polymer Chemistry* cornell Univ. Press, 1953.

18. Brundle, C. R.; Baker, A. D. *Electron Microscopy* Academic Press, New York, 1981.

19. Clark, D. T.; Thomas, H. R. *J. Polym. Sci. Polym. Chem.* 1977, *15*, 2843.

20. Borden, M. J.; O'Donnell *J. Phys. Chem.* 1968, *72*, 1577.

21. Thompson, D. T. *Ph.D. Thesis* VPI&SU, 1986.

22. Gent, A. N.; Petrich, R. P. *Proc. Roy. Soc.* 1969, *A310*, 433.

23. Stone, F. G. A.; Graham, W. A. G. *Inorganic Polymers* Academic Press, New York, 1962.

24. Noll, W. *Chemistry and Technology of Silicones* Academic Press, New York, 1968.

4.0 Structure-Property Behavior of Caprolactone-Allyl Glycidyl Ehter Copolymers Crosslinked by EB Radiation

Semicrystalline copolymers of caprolactone and allyl glycidyl ether(CL-AGE) have been crosslinked at various temperatures both above and below the crystalline melting point by electron beam irradiation. Gel fraction increases with irradiation dose up to 40 Mrad and shows slightly higher values when irradiated above the melting point compared to irradiation below the melting point. A stable spherulitic crossed polarizer optical microscopy pattern of the CL-AGE copolymer crosslinked in the semicrystalline state persisted over a wide range of temperature even in the melt. In contrast, random introduction of crosslinks into this material in the melt state resulted in some restriction on the crystallization process limiting the development of ordered superstructure upon solidification. Measurements of thermal and mechanical properties support the gel fraction results and the microscopy observations. It was concluded that the final solid state properties of the EB-irradiated CL-AGE copolymers are strongly dependent on the morphological state of the material at the time of the EB irradiation process.

4.1 Introduction

Crosslinking and chain scission of polymers induced by high energy radiation are generally simultaneous phenomena and the ratio of these two events determines the net effect of the process. Depending on the value of this ratio, most polymers are often categorized into two distinct classes-those which crosslink and those which degrade. Polyethylene which usually crosslinks and polyisobutylene which primarily degrades by radiation are two opposing examples with polypropylene often being considered as intermediate with regard to the chemical structure and the response to radiation(1,2).

Crosslinkable semicrystalline polymers such as polyethylene can be irradiated by an electron beam source at any desired temperatures to produce a network by crosslinking, while many other network forming processes such as peroxide crosslinking are typically undertaken with best results at temperatures above the melting or softening point. Polyethylene or other semicrystalline polymers crosslinked in the melt state generally result in changes in crystallinity as well as in mechanical response when compared to the same system crosslinked in the semicrystalline state. Therefore, it can be deduced that radiation effects on semicrystalline polymers are strongly dependent on sample morphology(and/or chain mobility) at the time of irradiation(3).

The overall net effect of radiation on saturated linear aliphatic polyesters has been known to depend on the ratio of the methylene group concentration to that of the ester group. D'alelio et al.(4) showed that the increased methylene to ester ratio resulted in a higher gel content for a given dose. Poly(glycolic acid), which possesses a one-to-one concentration of methylene groups to ester groups, degrades at a relatively low radiation dose while high density polyethylene (no ester group) predominantly crosslinks repres-

enting extreme cases in this regard. Radiation effects on polycaprolactone, a semi-crystalline polymer with the methylene to ester group ratio of 5, has been reported to show an initial gel formation in a critical dose range of 20-30 Mrad when irradiated at room temperature(5). It is this latter polymer that will be of interest within the present study.

In order to achieve lower gelation doses for saturated linear aliphatic polyesters such as polycaprolactone, certain functional groups including unsaturation can be incorporated. In this regard, and as will be discussed here, ε-caprolactone has been copolymerized with a relatively small amount of allyl glycidyl ether. Therefore, the randomly distributed allyl glycidyl ether units(2-6 mole percent) in the synthesized caprolactone-allyl glycidyl ether(CL-AGE) copolymers(semicrystalline at room temperature) provide crosslinkable sites by electron beam irradiation in a relatively low dose range thereby limiting damage to the backbone. It has been of interest to investigate whether the radiation-induced crosslinking of the CL-AGE copolymers in the semicrystalline state will result in a network which differs considerably in properties from that produced by crosslinking in the amorphous or melt state.

4.2 Materials and Experiments

4.2.1 Materials

Caprolactone-allyl glycidyl ether(CL-AGE) copolymers were synthesized as shown in Figure 4.1. First, the aluminum-porphyrin catalyst, which is an effective initiator of

alkylene oxide and lactone polymerization, was prepared following the general procedure reported by Aida and Inoue(6). Secondly, after the catalyst had been synthesized, a mixture of purified ε-caprolactone and allyl glycidyl ether(Aldrich Chemical Co.) was added to a reactor. The monomer feed which was composed of primarily ε-caprolactone with 5, 10, 15 mole % of allyl glycidyl ether was brought into reaction by stirring under a nitrogen atmosphere at 60°C. After an appropriate period of time, the reaction mixture was cooled down to room temperature and the final product was isolated by precipitation in methanol. Although, 5, 10, 15 mole percent of allyl glycidyl ether was included initially, approximately 2, 4, 6 mole percentages of allyl glycidyl ether were found in the final respective copolymer product when subjected to proton-NMR analysis(7). The number average molecular weight was found to be nearly 30,000 as determined by GPC analysis calibrated with polystyrene and polymethyl methacrylate standards. The glass transition temperature and the crystalline melting temperature of the prepared CL-AGE copolymer(6 mol% AGE) were found to be ca. -45°C and 56°C, respectively. A melting point depression of ca. 4°C by the introduction of AGE units(6 mol%) was observed in comparison to pure polycaprolactone of same molecular weight(Tm = 60°C)-this behavior being discussed in more detail later.

4.2.2 Preparation of Samples for Irradiation

The synthesized CL-AGE copolymers were dissolved in tetrahydrofuran(THF) at room temperature to give a homogeneous solution. After film casting and drying at an atmospheric condition for 24 hours, the CL-AGE copolymer films of ca. 3-mil-thickness were additionally vacuum-dried for 48 hours. Two sample temperatures, 25°C(semi-crystalline state) and 80°C(melt state), were utilized for irradiation. For the higher

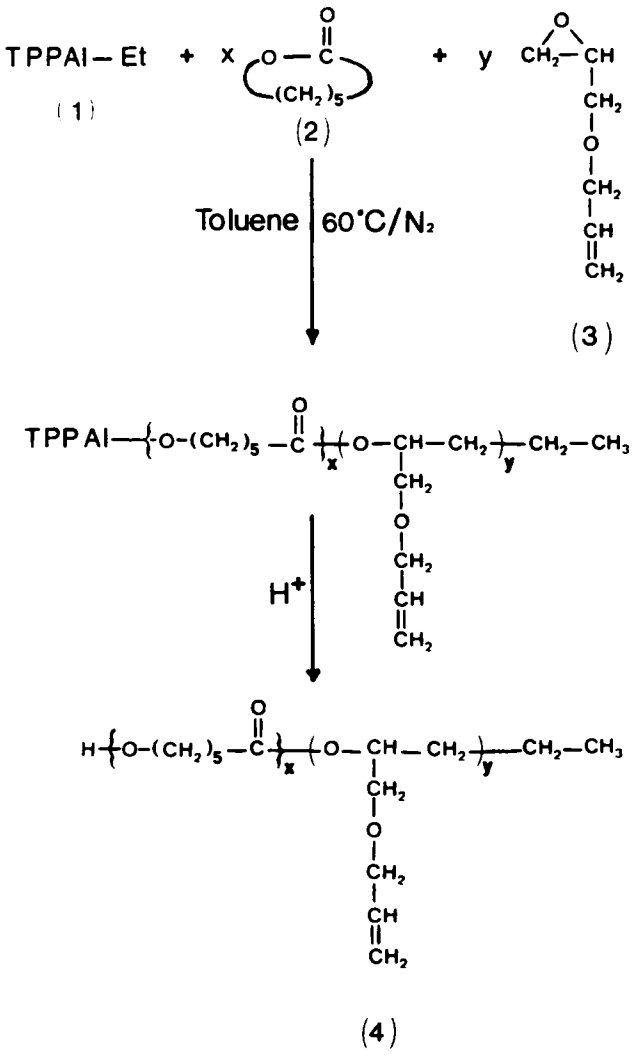

Figure 4.1. Synthetic scheme for the CL-AGE copolymers.: (1)Aluminum-Porphyrin Catalyst;(2)ε-caprolactone;(3)Allyl Glycidyl Ether;(4)CL-AGE copolymer.(ref 7).

temperature of 80°C, a heated steel plate was used as the substrate for the copolymer. The film sample was placed on this temperature-controlled steel plate and passed through the electrocurtain system described below. For the irradiation process which required two passes, following the first pass the sample was again immediately placed on another 80°C steel plate and passed through the electrocurtain system a second time.

4.2.3 Irradiation and EB Apparatus

Electron beam irradiation has been carried out with an electrocurtain accelerator manufactured by Energy Sciences, Inc.(model CB/150/15/180). The samples were placed on steel plates in aluminum trays and passed through the conveyor system of the electron beam apparatus. The maximum available dose per pass was 20 Mrad, hence, for the highest dose used in this study(40 Mrad), two passes were utilized. In light of the depth-dose profile at 175 kilovolts electron energy level of the EB system, the radiation dose will be nearly uniform throughout the sample thickness(3 mil).

4.2.4 Gel Percent Measurement

The respective gel fraction of the irradiated CL-AGE copolymer materials was evaluated as follows. First, a 10 to 40 milligram sample of the irradiated CL-AGE copolymer film was immersed and stirred in 200 ml of THF at room temperature for 72 hours. Then, the sample was removed from THF and dried in a vacuum oven at room temperature for 96 hours and the weight of the dried sample was measured. The gel content was given by the percent ratio of the final dried gel weight to the initial weight.

4.2.5 Optical and Scanning Electron Microscopy Analysis

A Zeiss polarizing microscope equipped with a Leitz 350 heating stage and a 35 mm camera was utilized to investigate the change in the crystalline structure by changing temperature. The temperature calibration of the heating stage was performed with naphthalene, indium, anthraquine and sodium nitrate. A scanning electron microscope(SEM, Cambridge Stereoscan 200) was also utilized for morphological investigations.

4.2.6 Thermal Test

Measurements of thermal properties were performed using a differential scanning calorimeter(Perkin-Elmer DSC-4). The samples were run from 15°C up to 75°C with a heating rate of 10°C per minute and the data obtained were labeled as "first run." After cooling to 10°C with a cooling rate of 10°C per minute, samples were again heated up to 75°C at the same scan rate. These data were labeled as "second run." The crystalline melting point of the CL-AGE material was determined as functions of the radiation dose and the morphological state at the time of irradiation.

4.2.7 Mechanical Analysis

The irradiated samples were tested for mechanical properties such as Young's modulus at room temperature using the ASTM D638 specification. Samples were prepared in a

dog-bone shape of initial dimensions corresponding to gauge length of 10 mm and width of 2.8 mm. An Instron tensile tester(model 1122) was utilized throughout this study with an extension ratio of 50 % per minute based on the initial sample length.

4.3 Results and Discussion

4.3.1 EB Crosslinking of CL-AGE Copolymers

CL-AGE copolymers having different contents(2, 4, 6 mole percent) of allyl glycidyl ether were EB-irradiated at room temperature by changing the irradiation dose from 0 to 40 Mrad. Figure 4.2 shows the gel fraction of these CL-AGE copolymers as a function of the irradiation dose. Up to 20 Mrad, the gel fraction increases as the content of AGE increases suggesting an improved crosslinking reactivity of the copolymers upon EB irradiation. However, at 40 Mrads the differences in the gel fraction values between the samples of different AGE contents were somewhat reduced and, in fact, the order was partly reversed. It was reported by Narkis et al.(5) that the critical gelation dose level for pure polycaprolactone(MW 35,000), which is the major backbone of the CL-AGE copolymers in this study, is 26 Mrads and, above this irradiation dose, measurable gel contents are formed with about 15% gel at 40 Mrads. Therefore, in the data shown in Figure 4.2, it can be deduced that, up to 20 Mrads, the crosslinking of the CL-AGE copolymers is principally attributed to the AGE content although the CL content likely affects the gel fraction data particularly at the higher dose level. To support this discussion, samples of pure polycaprolactone(MW 30,000) were EB-irradiated with a dose of up to 20 Mrads. Figure 4.3 shows typical chromatograms

obtained by gel permeation chromatography(GPC) as a function of irradiation dose in the pregelation stage of pure polycaprolactone. By irradiation with 5 Mrad, the average molecular weight appears to be shifted slightly to a higher value suggesting an increased molecular weight by EB irradiation. Then, the narrower molecular weight region of the distribution gradually widens with increasing dose and, at 20 Mrad, low and high molecular weight tails become clearly evident. It would be expected that this high molecular weight fraction shown in the tail would be transformed to the gel fraction upon further irradiation. Therefore, it can be deduced that when the CL-AGE copolymers are EB irradiated in the dose range up to 20 Mrad, the randomly distributed allyl glycidyl ether along the poly(ε-caprolactone) backbone provides readily crosslinkable sites without any major gelling contribution to the gel fraction from the caprolactone chain component. On the basis of these data, the CL-AGE copolymer with a 6 mole percentage of AGE units was chosen as the system for further analysis of radiation effects as will now be discussed below.

Shown in Figure 4.4 are the gel fractions measured for the CL-AGE(6 mol% AGE) copolymer irradiated at room temperature(semicrystalline state) and at 80°C(melt state) with increasing irradiation dose up to 40 Mrad. Although irradiation in the melt state results in higher gel fractions, the data suggest that a considerably high degree of crosslinking also occurred for irradiation in the semicrystalline state(room temperature irradiation). As discussed later in this chapter, when the copolymer is irradiated in the semicrystalline state, a certain degree of the ordered crystalline state which is present at the time of irradiation is maintained in the process of the network formation. In addition, this ordered state is shown to persist beyond the crystalline melting transition.

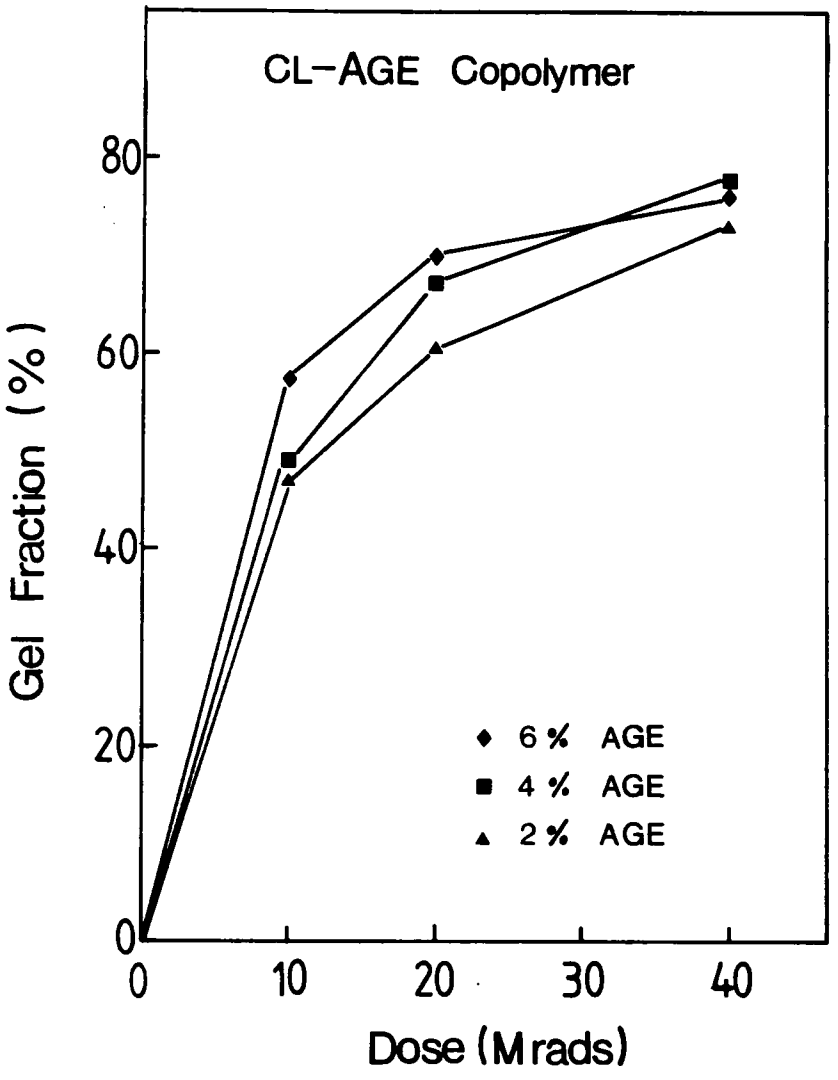

Figure 4.2. Percent gel vs. irradiation dose for the CL-AGE copolymers.

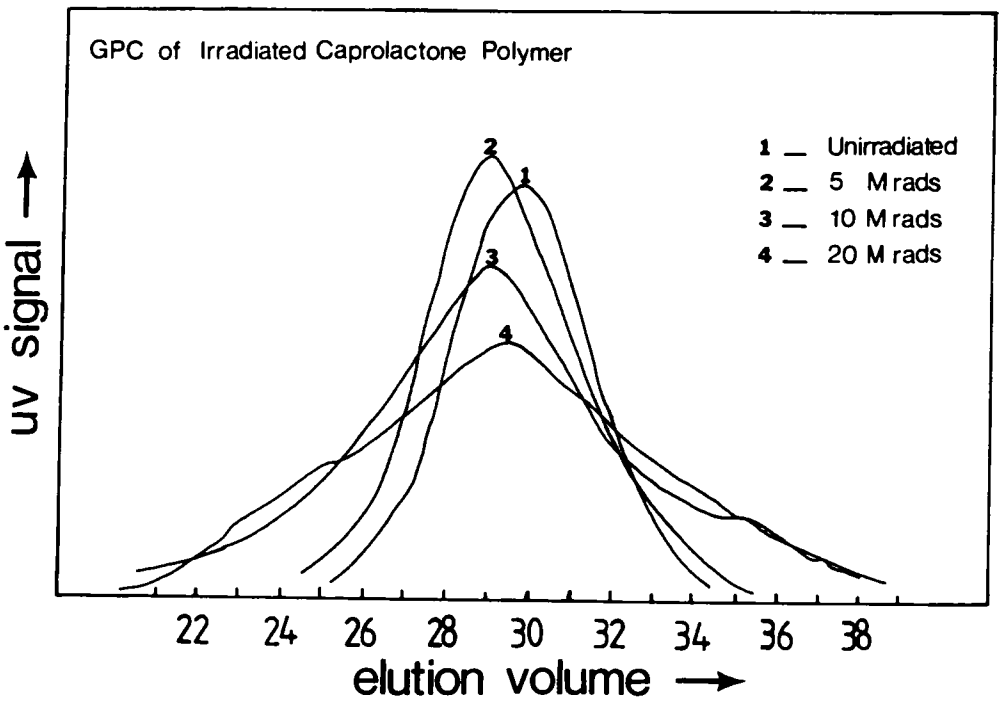

Figure 4.3. GPC chromatograms of irradiated pure polycaprolactone in the pregelation stage.

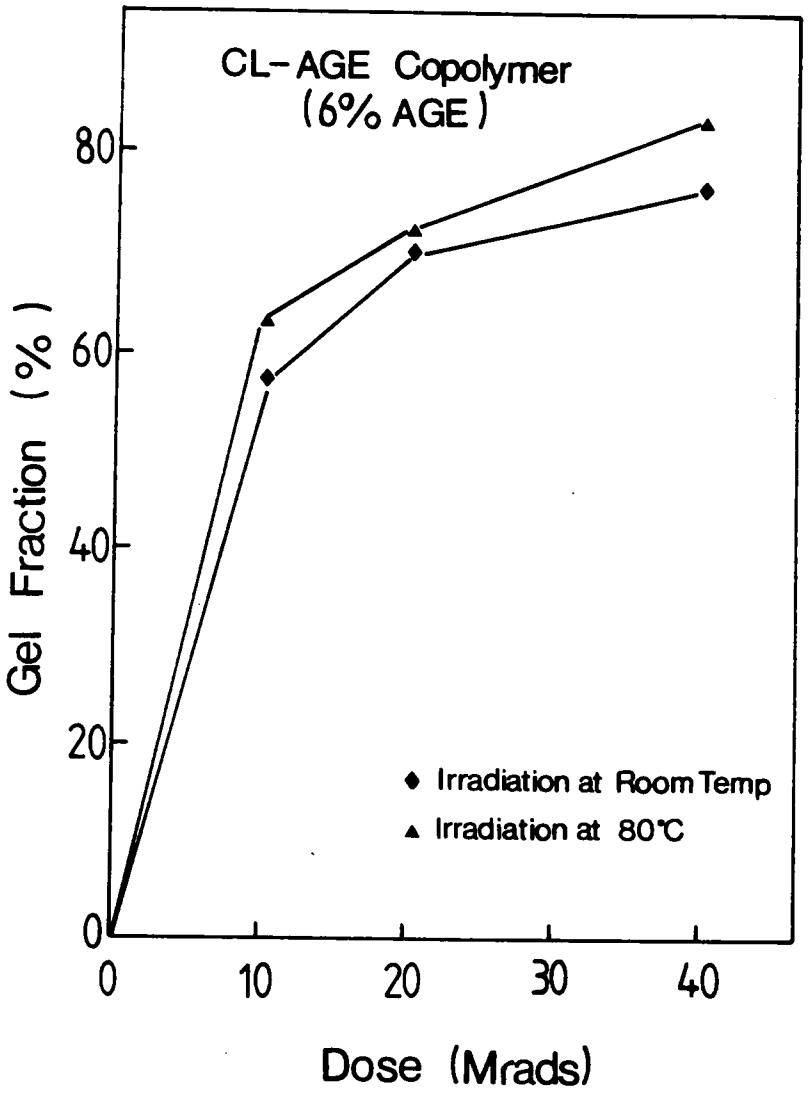

Figure 4.4. Percent gel vs. irradiation dose for the CL-AGE(6 mol% AGE).

4.3.2 Optical and Scanning Electron Microscopy Analysis

Shown in Figures 4.5, 4.6, and 4.7 are the cross-polarized optical micrographs of the CL-AGE copolymers crosslinked by EB irradiation with 20 Mrad at room temperature(semicrystalline state) and at 80°C(amorphous melt state) along with the control sample(no EB treatment). In order to study the morphological structure at different temperatures, a microscope heating stage was used for the irradiated sample. The sample temperature was raised to 120°C and then cooled down to room temperature in a step-by-step comparison with the control sample given the same thermal history in the hot stage.

At 25°C as shown in Figure 4.5, the micrograph of the CL-AGE sample EB-irradiated in the semicrystalline state shows a strong birefringent spherulitic pattern although the irradiated sample is highly crosslinked. It is very similar to that found for the control sample. As previously indicated in Figure 4.4, the gel fraction of this room-temperature-irradiated(20 Mrad) sample is approximately 70 percent. On the other hand, the sample, which was first irradiated in the amorphous melt state at 80°C and subsequently cooled down to room temperature, shows a relatively lower order and somewhat disrupted spherulitic pattern. The random introduction of crosslinks into the molten CL-AGE copolymer distinctly plays an important role in the restriction on the crystallization process since these crosslink units would be excluded from the crystalline regions and hence interfere with the kinetics of the crystallization process.

Micrographs of the samples which have been heated up to 120°C and which well exceed the crystalline melting temperature(ca. 55°C) are illustrated in Figure 4.6. The birefringent spherulitic pattern of the room-temperature-irradiated polymer continues to

persist beyond 120°C, while the birefringent pattern of the control sample and the copolymer crosslinked in the amorphous melt state were shown to disappear after exceeding the crystalline melting temperature(sample becomes black between crossed polarizer). Therefore, it is clear that irradiation of the sample in the spherulitic semicrystalline state results in a persisting optical anisotropy or order that exists well beyond the melting point although clearly the spherulites will have undergone the crystalline melting transition as shown in the micrographs or by later DSC results that will be presented shortly.

Upon isothermal cooling at 25°C from the melt state(120°C) as shown in Figure 4.7, some recrystallization of the room-temperature-irradiated sample was observed to occur within the former persisting spherulitic pattern. On the other hand, the unirradiated control sample underwent the usual transformation from an isotropic liquid to a spherulitic semicrystalline state. In a striking contrast to the samples irradiated at a temperature below the melting point, the formation of the spherulitic order was observed to be hindered for the case of 80°C-irradiated sample. Therefore, these microscopy results clearly emphasize the importance of the morphological state at the time of EB irradiation.

Scanning electron micrographs of the unirradiated copolymer and the copolymers irradiated with 20 Mrad at room temperature and 80°C are shown in Figure 4.8. All micrographs show spherulitic structure although the surface textures are clearly different. The initial smooth surface texture of the unirradiated copolymer sample was significantly roughened when irradiated with a single pass of 20 Mrad at room temperature, while the overall shape and size of the spherulites were maintained. The increased roughness for this room-temperature-irradiated sample is considered to be due to melt-

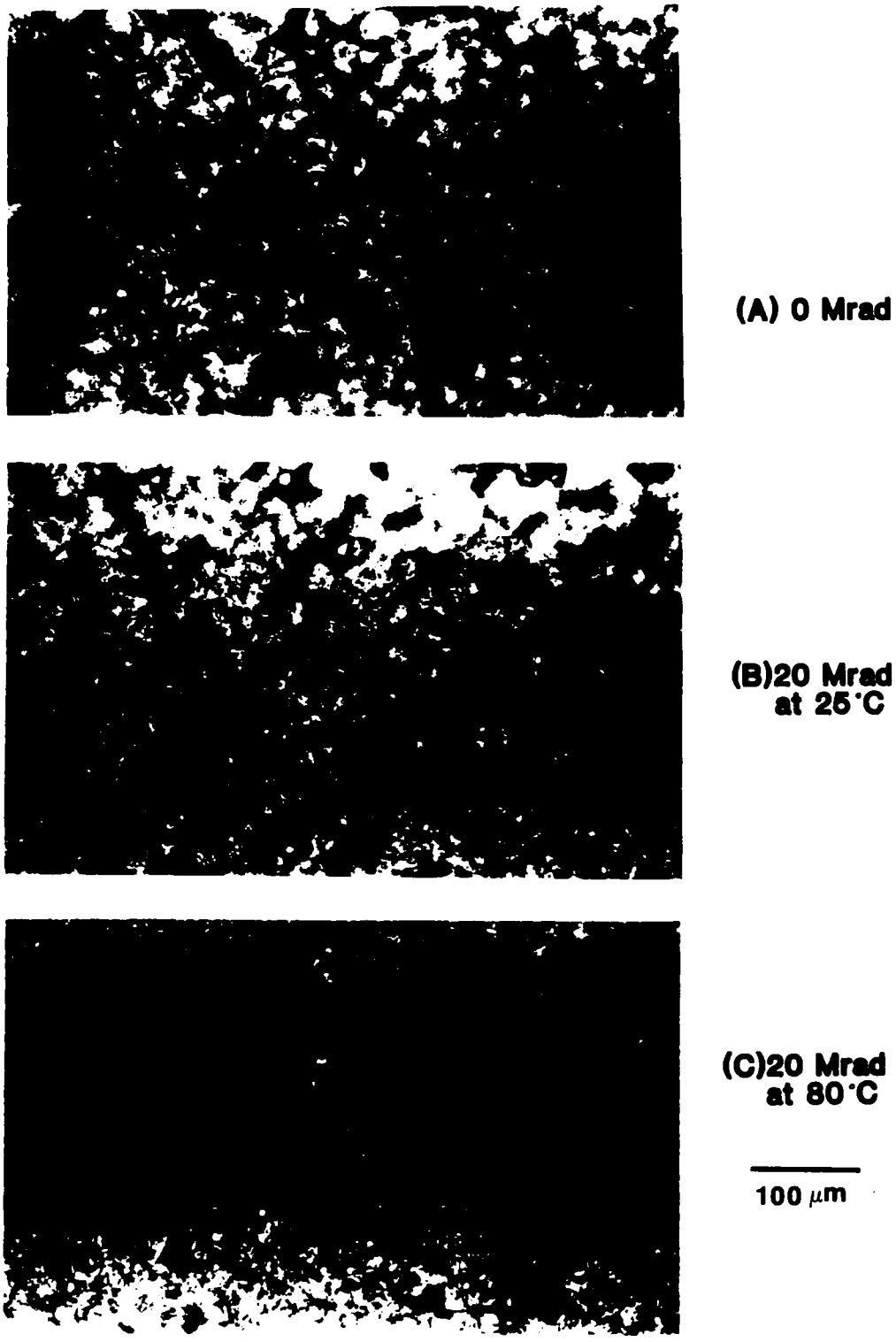

Figure 4.5. Cross polarizer optical micrographs taken for the CL-AGE copolymers at 25C.

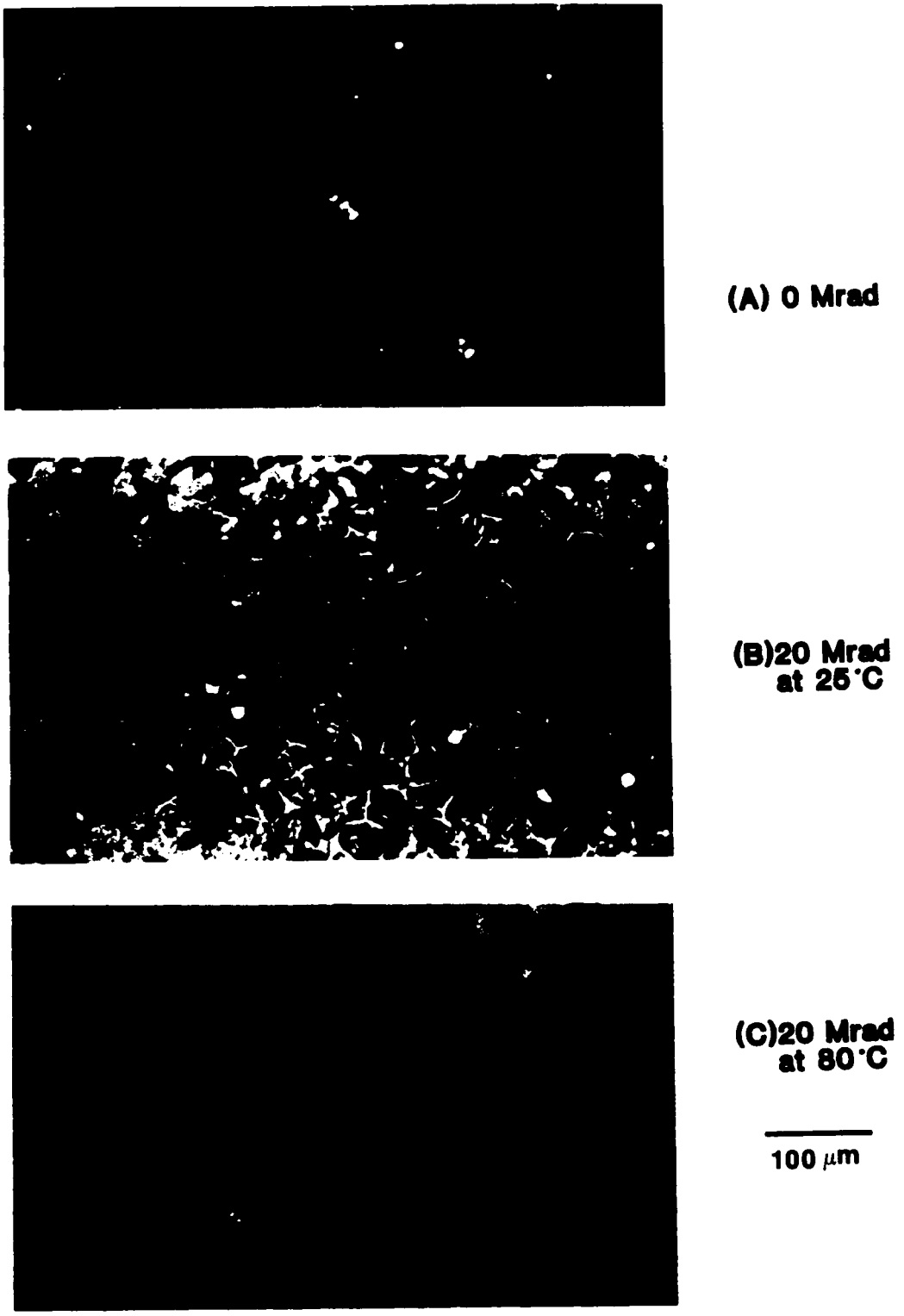

Figure 4.6. Cross polarizer optical micrographs taken for the CL-AGE copolymers at 120C.

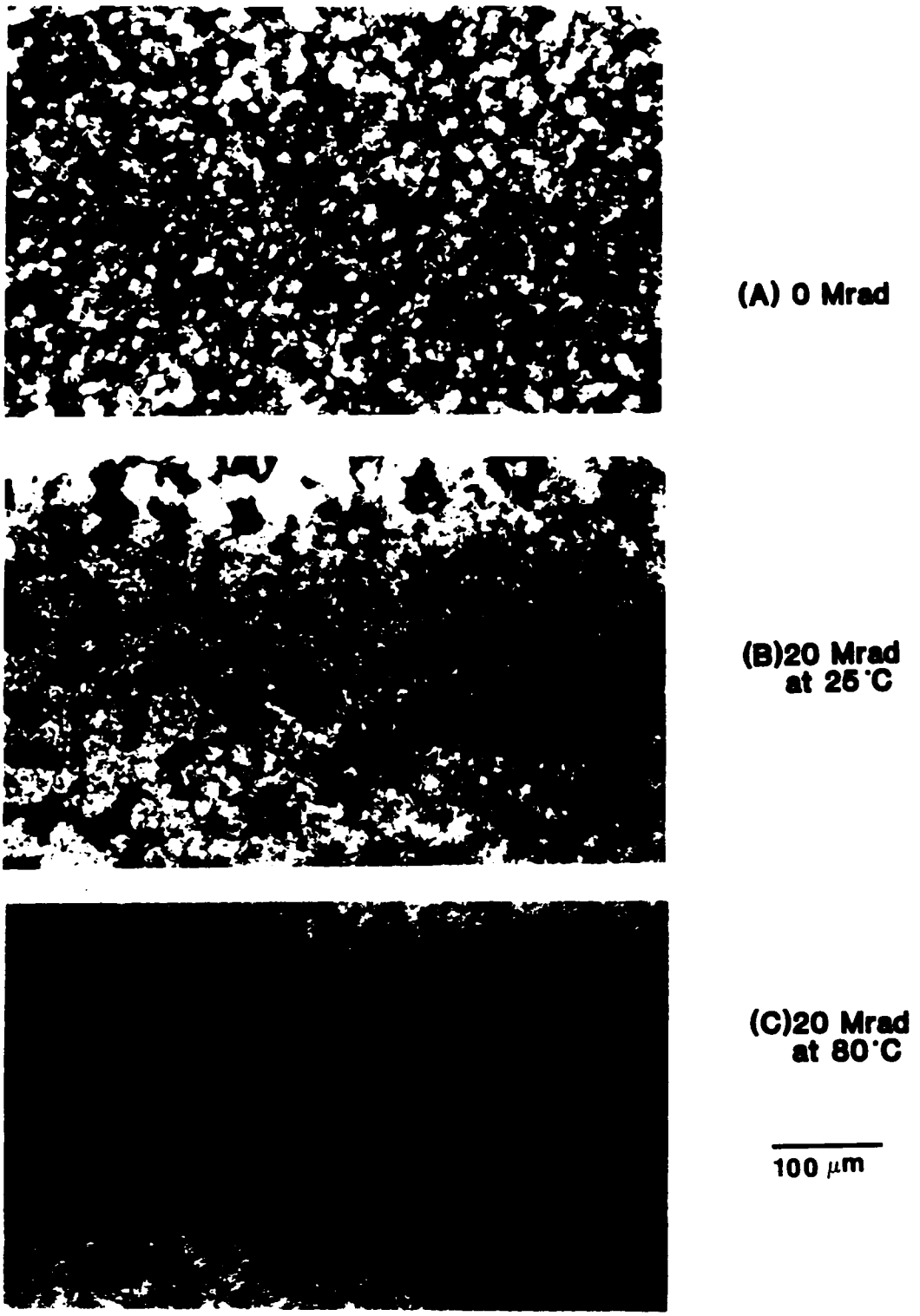

Figure 4.7. Cross polarizer optical micrographs taken for the CL-AGE copolymers at 25C.

ing **during** the irradiation process with 20 Mrad. In contrast, the initial spherulitic structure was almost destroyed for the case of the sample irradiated with 20 Mrad at 80 °C indicating that the formation of the spherulite was greatly hindered due to the random introduction of crosslinking in the melt state.

As indicated earlier, irradiation with 20 Mrad can induce some heating of the samples. An approximate calculation of the temperature rise due to electron beam irradiation process should be useful in this regard. In brief, an energy balance based on a unit volume element of the medium provides the following equation:

$$\rho Cp(\frac{dT}{dt}) = k\nabla^2 T + S \qquad [4.1]$$

where ρ is density, Cp is the heat capacity, k represents the heat conductivity, T is the temperature, S is the heat generation term. If the adiabatic conditions are assumed and if energy deposition is only by penetrating electrons i.e. no consideration of the exothermic reaction, the above equation can be reduced to the following simple relation:

$$\Delta T = \frac{E't}{Cp} \qquad [4.2]$$

where E′ is dose rate in Mrad per second and t is time in seconds. For the case of a 20 Mrad-irradiation which is equivalent to the process with 0.4 [sec] of exposure time and 50 [Mrad/sec] of dose rate assuming 0.5 [cal/gK] as heat capacity, a maximum temperature increase of about 96°C can be calculated for the irradiation process. Although this is a rough estimation with some simplifications, it implies that the sample temperature could be rapidly and easily increased above the melting point in the irradiation process. Thus, this temperature rise can induce, at least, melting and subsequent

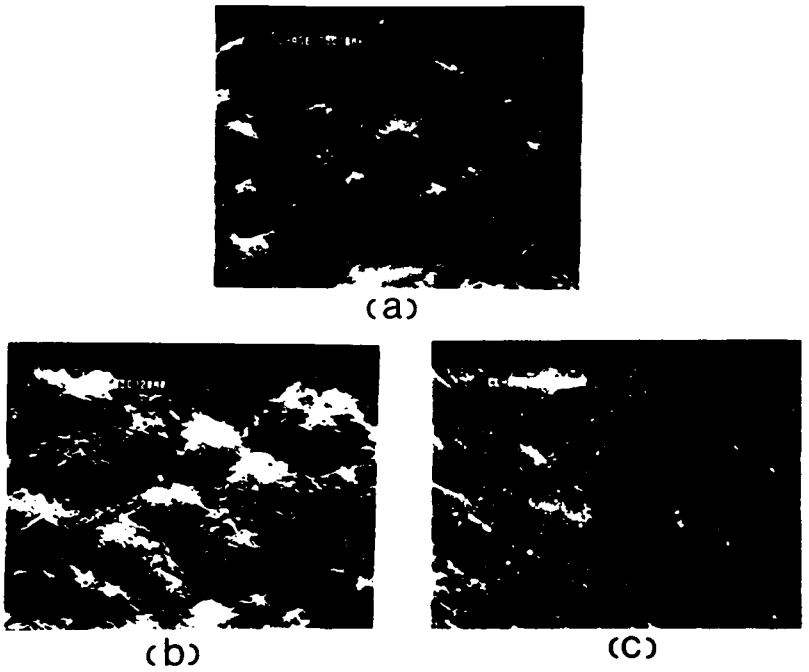

Figure 4.8. Scanning electron micrographs of the CL-AGE(6 mol% AGE) copolymers.: (a)unirradiated; (b)irradiated(20 Mrad) at room temperature; (c)irradiated(20 Mrad) at 80°C.

recrystallization when the sample is cooled down to room temperature after the irradiation process.

4.3.3 Thermal Properties

The crystalline melting transition behavior of the first and second DSC scans of the irradiated copolymers are shown in Figure 4.9 and 4.10, respectively. The crystalline melting point and the heat of fusion of a pure polycaprolactone having a number average molecular weight of 30,000 have been reported to be 60°C and 33[cal/g], respectively. However, due to the random introduction of the 6 mole percent of allyl glycidyl ether units which generate steric hindrances for crystallization, a melting point depression is expected for the unirradiated CL-AGE copolymer comparing to the pure polycaprolactone of comparable molecular weight. As shown in the first DSC scan of the **unirradiated** sample also having 6 mole percent AGE units, a melting temperature of 56.3°C, which is equivalent to approximately a depression of 4°C, was measured as shown in Figure 4.9. For a truly random copolymer, a melting point depression can be approximated by using the well-known Flory relation(8) as shown by:

$$\frac{1}{Tm} - \frac{1}{Tm^{\circ}} = \left(\frac{-R}{\Delta Hu}\right) \ln(Xa) \qquad [4.3]$$

where Tm° is the melting point without non-crystallizable units in [K] under the same melting procedure, R is the gas constant, ΔHu is the enthalpy of fusion per repeating unit in [cal/mol] and Xa is the mole fraction of the crystallizable units. A Tm of 56°C was calculated from the above relation showing good agreement between theory and experiment for the unirradiated CL-AGE copolymer.

In the first DSC scans as shown in Figure 4.9 & 4.10, the melting points of the samples irradiated at room temperature do not appear to be greatly affected by radiation-induced crosslinking up to 10 Mrad. However there is a relatively abrupt melting point depression observed for the samples irradiated with 20 and 40 Mrad. The abrupt melting temperature depression for the samples irradiated at room temperature with 20 and 40 Mrad is again believed to be due to the heating effect of the EB irradiation process as discussed previously. In contrast, there is a distinct gradual melting point depression shown for the samples irradiated at 80°C over the entire dose range. As can be seen in the DSC data, the melting points are depressed further and the peaks become broader and less steep with increasing irradiation dose for both room temperature and 80°C irradiation suggesting that irradiation introduces imperfections, and crosslinks which induce a molecular weight increase. The general trend of decreasing sharpness of the melting peaks with increasing irradiation dose is in good agreement with increasing gel contents with dose as previously shown in Figure 4.4.

The second DSC scans, as shown in Figure 4.11 & 4.12, indicate a crystalline melting behavior which is similar to that of the first scans except the disappearance of the abrupt depression of the melting point for the samples irradiated with 20 and 40 Mrad at room temperature. This can be expected since all the samples of room-temperature-irradiation are recrystallized by cooling down to room temperature after the first DSC scan(heating). That is, the abrupt melting point depression shown in the first scans induced by the EB heating for irradiation with 20 and 40 Mrad may well be nullified in the second scan.

The melting point depression behaviors with increasing irradiation dose for the first and second DSC scans are summarized as shown in Figure 4.13. The effects of EB heating

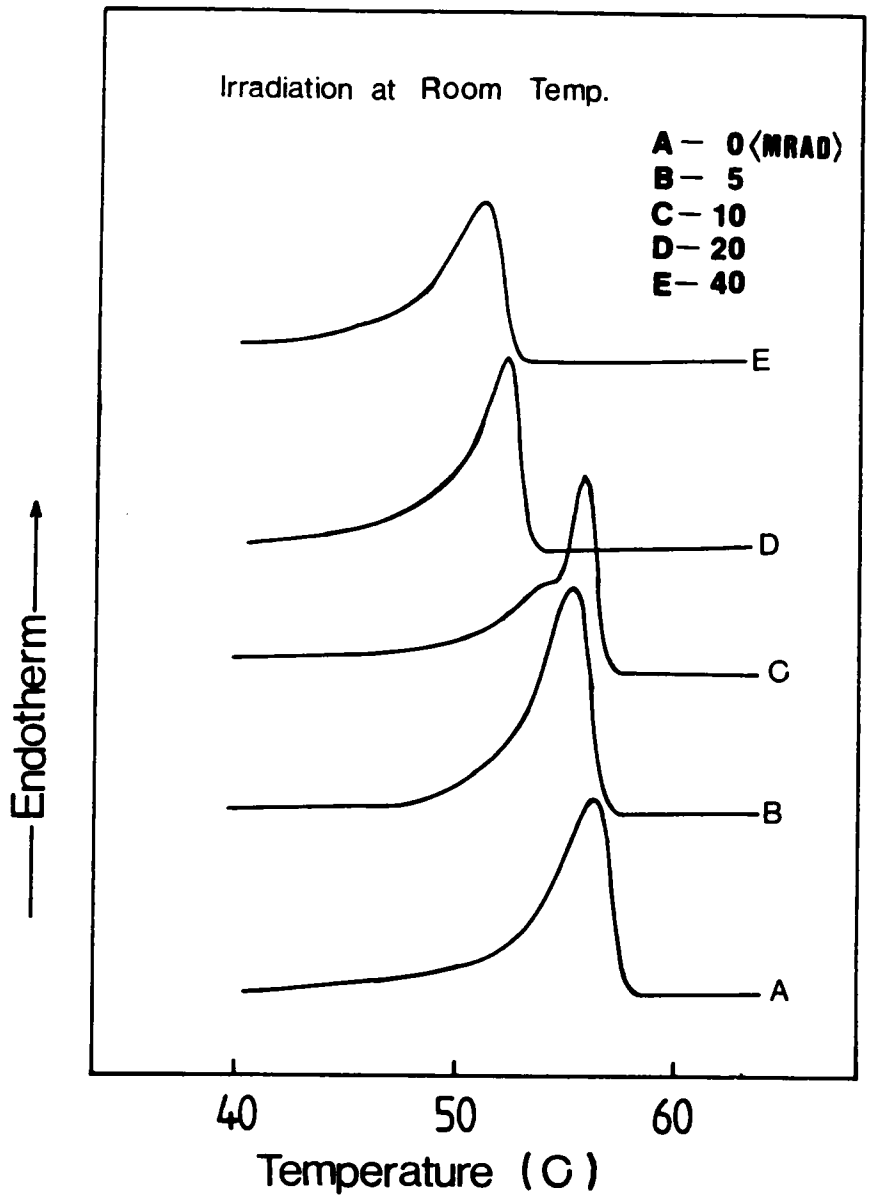

Figure 4.9. Crystalline melting transitions shown by the first DSC scan for the CL-AGE copolymers irradiated at 25C.

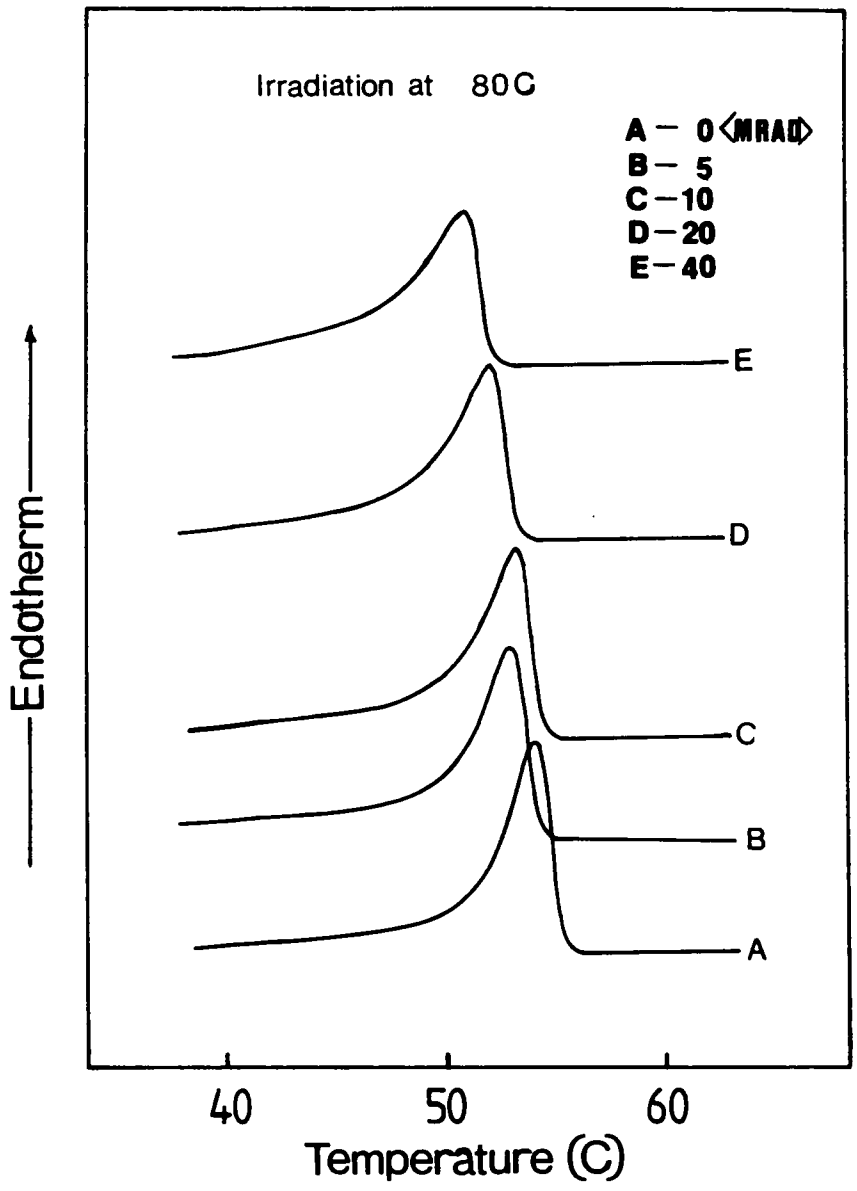

Figure 4.10. Crystalline melting transitions shown by the first DSC scan for the CL-AGE copolymers irradiated at 80C.

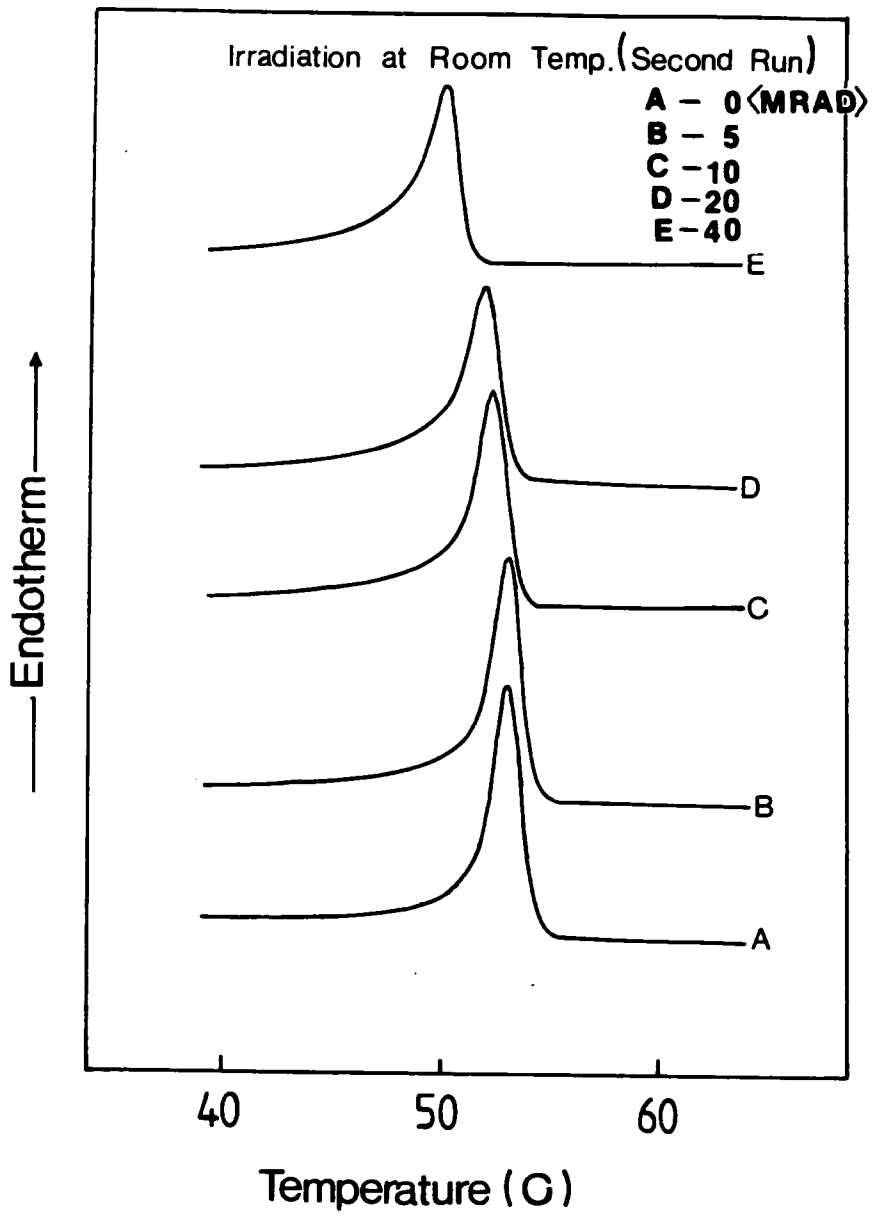

Figure 4.11. Crystalline melting transitions shown by the second DSC scan for the CL-AGE copolymers irradiated at 25C.

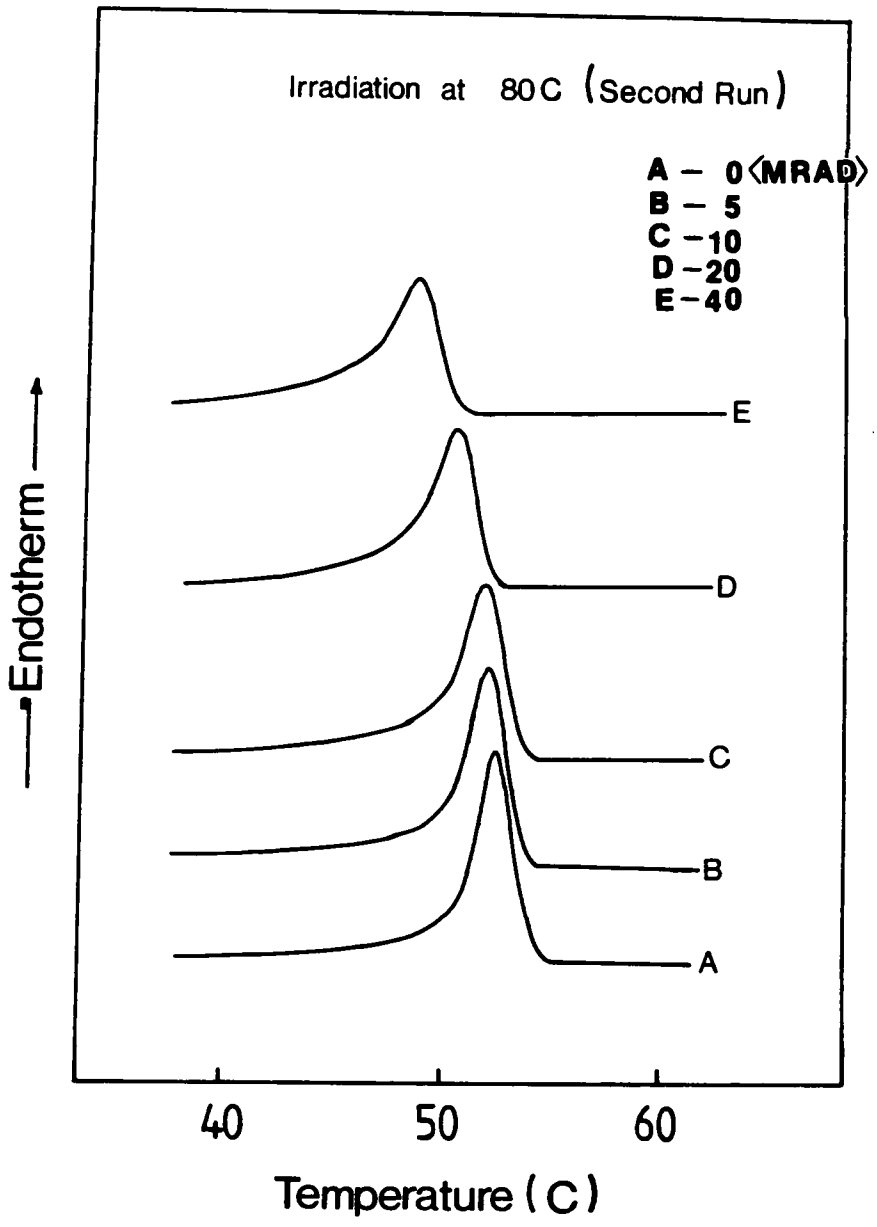

Figure 4.12. Crystalline melting transitions shown by the second DSC scan for the CL-AGE copolymers irradiated at 80C.

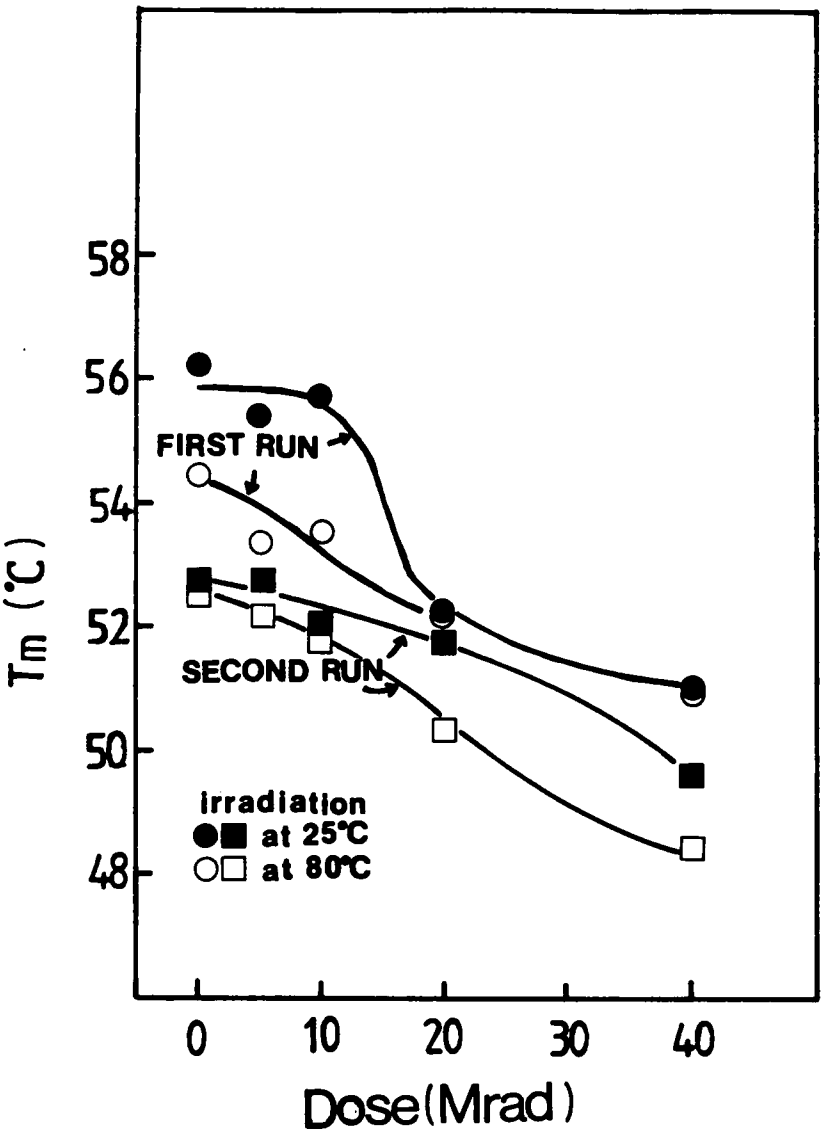

Figure 4.13. Crystalline melting temperatures of the irradiated CL-AGE copolymers with increasing dose for the first and second DSC runs.

and thermal "history" of the CL-AGE copolymers on the crystalline melting transition are well demonstrated in these plots. In the first DSC scan, the melting point of the room-temperature-irradiated sample shows abrupt depressions for the doses of 20 and 40 Mrad. In contrast, irradiation in the melt state resulted in a gradual melting point decrease showing Tm values lower than that for the sample irradiated in the semicrystalline state up to 10 Mrad but similar melting points for the 20 and 40 Mrad dosages. It should be emphasized that the melting point differences up to 10 Mrad in the first DSC run up to 10 Mrad are likely attributed to the difference in the thermal "history." Specifically, the material irradiated in the melt state was first heated to 80°C followed by irradiation and, subsequently cooled down to room temperature whereas the samples irradiated at 25°C had not undergone any significant thermal heat treatment except by EB heating effect for 20 and 40 Mrad irradiation. After the first DSC run, all the materials were recrystallized at room temperature and, hence, the effects of the thermal "history" which includes EB heating effects during the irradiation process were expected to be minimized in the following thermal test. In the second scan as shown in Figure 4.11& 4.12, the differences in the melting point between the samples irradiated at 25°C and 80°C for doses up to 10 Mrad were decreased in contrast to the case of the first run thereby supporting our discussion. Hence, the difference in the melting point depression behavior in the second run is somewhat widened with increasing irradiation dose showing only the effects of the difference in the degree of crosslinking.

The crystallization processes, as shown by the DSC peaks in Figure 4.14 and 4.15, appear to be more sensitive to the degree of crosslinking and the morphological state at the time of irradiation. These data show that the crystallization is delayed to a higher degree for the samples irradiated at a temperature above the melting point.

In addition, this effect becomes more noticeable as the irradiation dose is increased as well be expected.

4.3.4 Mechanical Properties

Limited mechanical testing was performed at room temperature on the EB-irradiated CL-AGE copolymers. As shown in Figure 4.16, the modulus of the room-temperature-irradiated sample increases slightly up to 10 Mrad and, upon further irradiation, it decreases abruptly. The increase in modulus of the room-temperature-irradiated sample up to 10 Mrad is believed to be due to the increase in crosslinking mainly occurring at the AGE units which are excluded from the crystallites. The decrease in modulus of the room-temperature-irradiated sample above 10 Mrads is caused by a slightly lower crystalline content due to the EB heating effect with crosslinking-this remark being indirectly supported by the previous DSC and microscopy data.

In summary, the irradiation process carried out below the melting point should be differentiated from that above the melting point for several reasons. First, radiation- induced crosslinking in the semicrystalline state results in a relatively high gel percent and a locked-in molecular anisotropy resulting which will persist the melt state. Second, crosslinking events induced by irradiation below the melting temperature may not be expected to occur in a random fashion as may well be the case in the irradiation process above melting point. Third, for irradiation below the melting point, the crystalline melting transition can occur if sufficient EB heating occurs with crosslinking reactions occurring at the same time. Finally, for irradiation above the melting point, the crosslinking reaction proceeds in the liquid state above the melting temperature and likely in

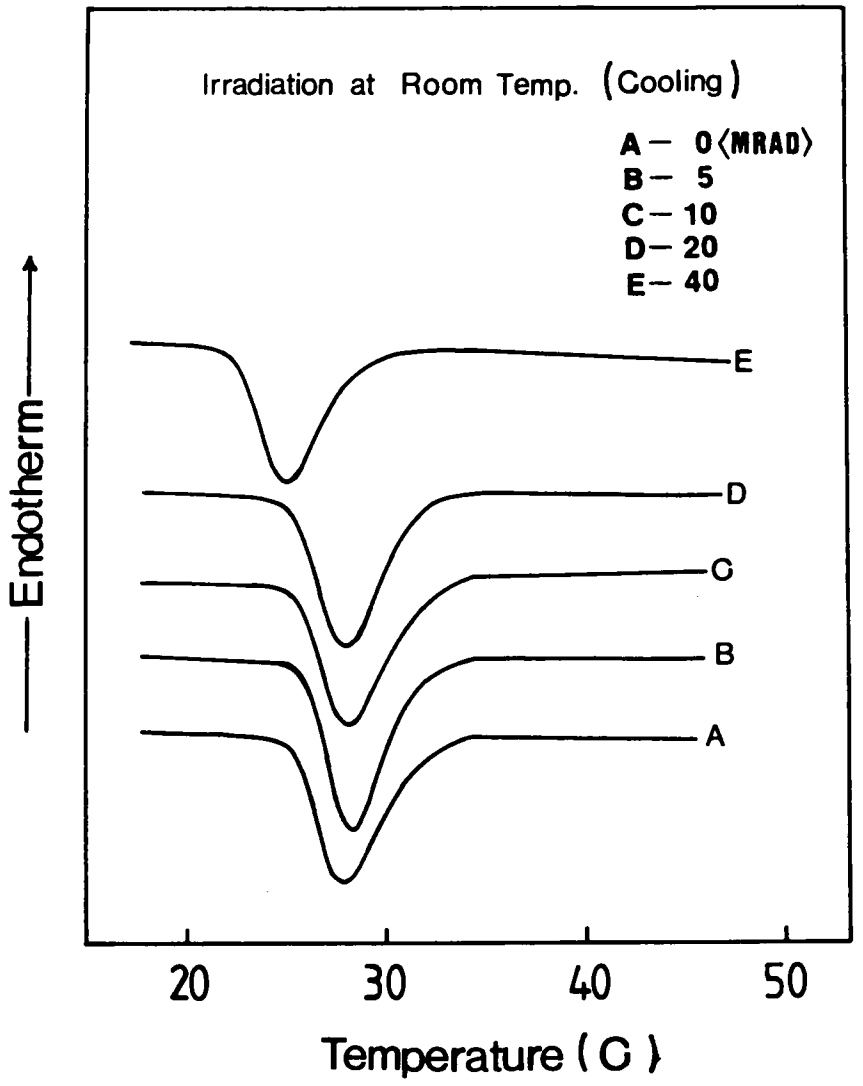

Figure 4.14. Crystallization peaks shown by DSC for the CL-AGE copolymers irradiated at 25C.

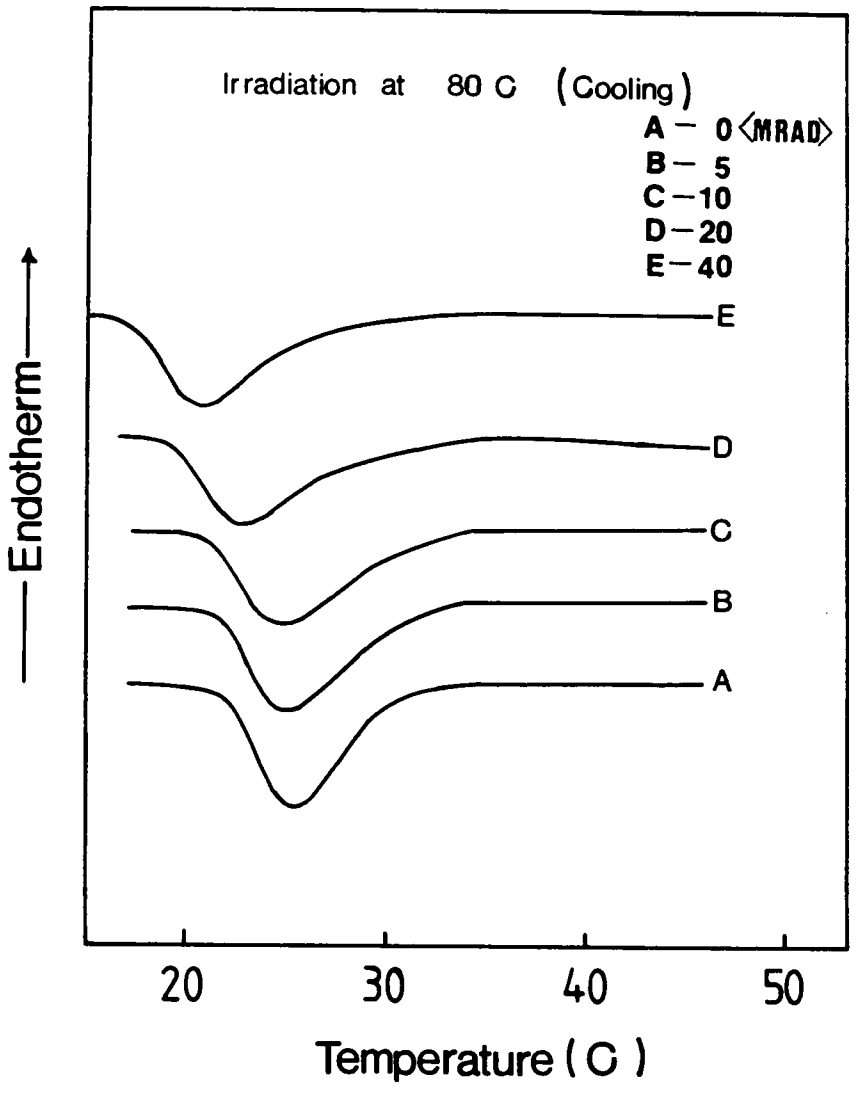

Figure 4.15. Crystallization peaks shown by DSC for the CL-AGE copolymers irradiated at 80C.

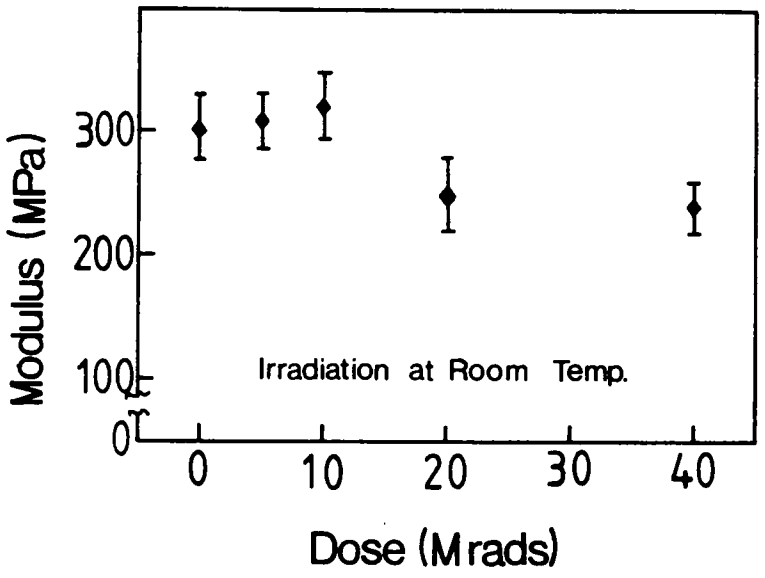

Figure 4.16. Modulus vs. irradiation dose for the CL-AGE copolymer irradiated at room temperature.

a random fashion thereby more distinctly influencing the recrystallization behavior upon cooling.

4.4 Conclusions

A number of conclusions can be made from this study on the effect of electron beam irradiation on the CL-AGE copolymers. Gel fraction of the CL-AGE copolymers increases with irradiation dose up to 40 Mrad. Crosslinking in the melt state results in slightly higher gel contents than irradiated in the semicrystalline state, although both values are quite high. Direct microscopic observations show that the polymer crosslinked in the semicrystalline state produces a stable spherulitic pattern which persists through the molten state. However, for the unirradiated sample the birefringent spherulitic pattern disappears at the temperature of the crystalline melting transition. In contrast, introduction of crosslinks into the CL-AGE copolymer in the molten state leads to restriction on the development of ordered spherulitic superstructure. Thermal and mechanical behavior was found to indirectly support the microscopic observations. It was concluded that the final solid state properties of the EB- irradiated CL-AGE copolymers are strongly dependent on the morphological state of the material at the time of irradiation process.

References

1. Chapiro, A. *Radiation Chemistry of Polymer Systems* Interscience, New York, 1962.

2. Charlesby, A. *Atomic Radiation and Polymers* Pergamon Press, New York, 1960.

3. Patel, G. N.; Keller, A. *J. Polym. Sci. Polym. Phys.* 1975, *13*, 303.

4. D'Alelio, G. F.; Haberli, R.; Pezdirtz, G. F. *J. Macromol. Sci. Chem.* 1968, *A2*, 501.

5. Narkis, M.; Sibony-Chaouat, S.; Siegmann, S.; Shkolnik, S.; Bell, J. P. *Polymer* 1985, *26*, 50.

6. Aida, T.; Inoue, S. *Macromolecules* 1981, *14*, 1166.

7. Yoo. Y. *Ph.D. Thesis* VPI&SU, 1988.

8. Mandelkern, *Crystallization of Polymers* McGraw-Hill, 1964.

5.0 Time-Temperature-Energy(TTE) Diagram of EB Radiation Curing Systems

Temperature variation of the reacting system in an electron beam(EB) radiation curing process often influences the extent of polymerization as well as the final solid state properties. Therefore, in order to control the EB curing process of monomeric resin materials, recognition of the temperature increase with regard to the absorbed EB energy(dose rate) and the EB exposure time should be considered. Example adiabatic time-temperature-energy(TTE) diagrams have been suggested to help provide a conceptual understanding of the relationship between the temperature increase, EB dose rate and exposure time. Three general adiabatic cases are presented with increasing degree of complexity: the first considers only heating through EB energy dissipation, while the second and third attempt to include a kinetic exotherm for polymerization and the effects of glass transition and vitrification behavior of the reaction, respectively. Some final remarks concerning the reality of non-adiabatic behavior are also provided. Similar concepts could also be applied to other types of radiation curing with some modification.

5.1 Introduction

High energy radiation such as electron beam(EB) offers excellent features as an alternative to the thermal process in the curing of low molecular resinous coatings. Among these features are the absence of solvents and initiators, low energy cost and the relatively high speed of the process, etc. Recently, pollution standards and increasing energy costs have accelerated the utility of the EB radiation process and the number of available EB radiation curable materials. In addition, a relatively low temperature nature of the cure has been regarded as an important feature compared to conventional thermal processes.

However, due to the highly exothermic curing reaction and generally low thermal conductivities of resin coatings, a substantial variation of temperature may be induced by the EB curing process and, subsequently, this can often influence the desired end properties of the final coating. EB radiation dose rate and exposure time, which are sensitive factors in changing the coating temperature, have been major concerns in industrial applications of the EB process since high processing rates should be profitable. Therefore, in order to efficiently control the EB curing process, performing a systematic estimation of the coating temperature is obviously important.

Several studies(1,2) on the temperature changes in EB cured resinous coatings have shown that the temperature increase is proportional to the total radiation dose absorbed by the target materials and 1 Mrad is generally equivalent to a 5-10K temperature increase. However, these observations have been strictly based on the assumptions that no chemical reactions are involved in the EB curing system and all the absorbed radiation energy is converted to thermal energy without any transfer to the

environment(adiabatic system). Although an adiabatic condition can often be assumed for an approximate temperature estimation in consideration of the relatively low thermal conductivities of the EB curable resins, an assumption of a non-reactive system might well lead to erroneous results. In addition, the viscosity changes significantly with temperature, thus affecting the reaction kinetics. And, due to molecular weight build-up, the system's glass transition may rise and lead to potential vitrification. At the vitrification point, the glass transition temperature of the partially cured reactants reaches the curing temperature and the reaction is retarded due to diffusion-limitations of the network segments(3).

The objective of this work is to semi-quantitatively predict some general relationships between EB exposure time, temperature increase of the coating and dose rate in an EB curing system. Three general adiabatic cases are investigated to consider the following effects: (I)EB energy dissipation; (II)kinetic exotherm; (III)glass transition and vitrification. Closing remarks will address more complex systems with particular emphasis on the reality of non-adiabatic systems.

5.2 Case I. Temperature Increase by EB Energy Dissipation

Charged particles such as electrons, upon penetration into a medium, interact with molecules, lose energy and slow down. They lose their energy by interacting either with the electrons or with the nuclei of the medium. As indicated by Pacansky(4), the EB exposure process can be divided into three sub-stages which correspond to the "physical stage," the "physiochemical stage" and the "chemical stage." The slowing down process

of the penetrating electrons is especially important in the first two stages since, in these stages, the electron energy is transferred to the medium and produces excited states for ultimate chemical reactions. Although the mechanisms of the electron energy transfer to the medium are typically complex, the amount of the energy transfer has been often represented by thermal energy for simplicity. Therefore, an approximate calculation of the temperature rise of the target material due to an EB irradiation process should be useful in this regard. In brief, an energy balance based on a unit volume element of the medium provides(5) the following equation:

$$\rho C_p(\frac{dT}{dt}) = k\nabla^2 T + S \qquad [5.1]$$

where ρ is density, C_p is the heat capacity, k represents heat conductivity, T is the temperature, and S is the heat generation term. If adiabatic conditions are assumed and if energy deposition is only by penetrating electrons i.e. no consideration of the exothermic reaction, the heat generation term can be defined by:

$$S = \rho E' \qquad [5.2]$$

where E′ is dose rate. Consequently, a solution of the adiabatic energy balance equation [5.1] leads to the following simple relation:

$$\Delta T = \frac{E't}{C_p} \qquad [5.3]$$

For an example of using the above expression, an irradiation process with the dose rate of 20[Mrad/sec] and the EB exposure time of 0.5[sec] can result in the temperature increase of approximately 48K. This example calculation is based on the premises that 1 Mrad is equivalent to 2.4[cal/g] and the heat capacity is independent on the temperature

and is 0.5[cal/gK] which is a value relatively typical of organic systems. On the other hand, heat capacities of high polymers range typically from 0.2 to 1 [cal/gK] resulting in the temperature increase of 24 to 120K according to the above mentioned relation, dose rate and EB exposure time. In addition, the heat capacity variation with changing temperature, which is assumed to be constant for simplicity, should also be examined in order to obtain more precise temperature approximation. A three-dimensional relation between time, temperature and energy(TTE) for this case is represented as shown in Figure 5.1 and hereafter is known as a TTE diagram.

5.3 Case II. Effects of EB Energy Dissipation and Kinetic Exotherm

The polymerization reaction for many EB curable resin coatings is highly exothermic and, due to their relatively low thermal conductivities, the exothermic heat of reaction plays a major role in influencing the coating temperature. The temperature increase in the irradiation process of resinous coatings is investigated in this section with an emphasis on the effects of a kinetic exotherm as well as the additional temperature rise from EB energy dissipation. In order to account for these two factors, the heat generation term in equation [5.1] should be re-defined as:

$$S = \rho E' + \rho \Delta H_{rxn} \frac{dx}{dt} \qquad [5.4]$$

where ΔH_{rxn} is the heat of reaction and x is the fraction of the remaining reactive functional groups, the latter of which is related to the degree of cure. This provides an adiabatic energy balance equation as follows:

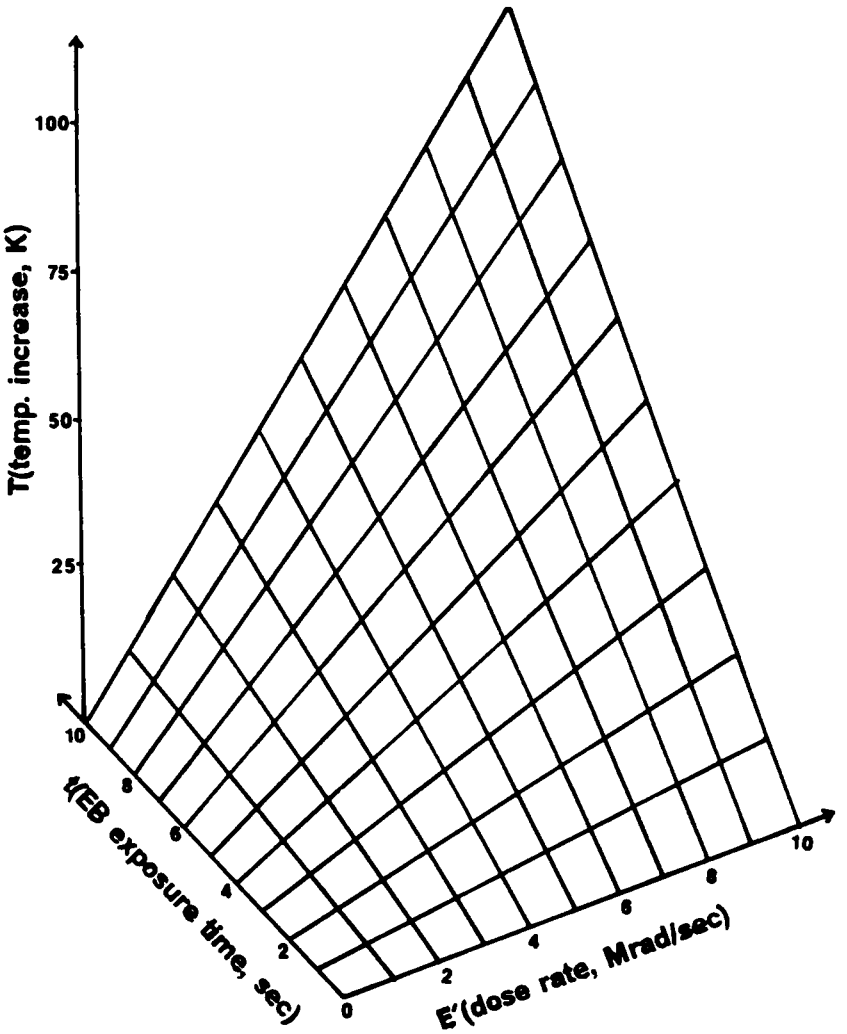

Figure 5.1. An example plot of the TTE relation for the case I.

$$C_p \frac{dT}{dt} = E' + \Delta H_{rxn} \frac{dx}{dt} \qquad [5.5]$$

It is obvious that, in majority of cases, EB radiation-induced polymerizations take place predominantly by free radical mechanisms although ionic mechanisms might be applicable depending on the type of material and dose rate range, etc.(6) Applications of the kinetics of free radical polymerization to a number of processes have been proven to be successful(7). Taking the latter approach, the kinetic expression for the rate of free radical polymerization can often be described(8) as follows:

$$\frac{dx}{dt} = -A \exp(\frac{-E_a}{RT}) E'^{0.5} x \qquad [5.6]$$

where E′ is the dose rate, E_a the activation energy, A the Arrhenius constant and R the molar gas constant. In order to develop a relation between time, temperature and energy(dose rate), the fraction of residual functional groups, x, should be represented as a function of the time and the energy(dose rate). Therefore, a relation between the total irradiation dose(E′t) and the fraction of residual functional groups, x, is suggested for this example as follows:

$$x = \frac{1}{kE't + 1} \qquad [5.7]$$

where k is an adjustable constant. *The purpose of suggesting this particular equation is primarily to establish a simple correlation between experimental behavior and a mathematical relationship to permit a reasonable numerical solution.* Accordingly, a number of different mathematical forms could be applied for this specific purpose depending on the type of the radiation curable system. One example of utilizing equation [5.7] is shown in Figure 5.2 where several values for the constant(k) have been related.

A combination of equations [5.5], [5.6] and [5.7] leads to the following relation:

$$C_p \frac{dT}{dt} = E' - \Delta H_{rxn} A \exp\left(\frac{-E_a}{RT}\right) E'^{0.5} \left(\frac{1}{kE't + 1}\right) \qquad [5.8]$$

which has three variables(t, T, E′) and five unknown property constants(C_p, ΔH_{rxn}, A, E_a, k). Therefore, if these property constants and a possible correlation between the fraction of residual functional groups and the total dose are known for a specific EB curable resin coating, an equation such as equation [5.8] can be utilized to illustrate the time-temperature-energy(TTE) behavior. In order to demonstrate this concept, a set of numerical values for the property constants which might be relatively close to those of practical radiation curable resins were selected as follows and substituted into equation [5.8]:

C_p = 0.5 [cal/gK]

ΔHrxn = - 50 [cal/g]

A = 10,000 $[\text{Mrad sec}]^{-0.5}$

E_a = 5,000 (cal/molK)

k = 200 [1/Mrad]

Due to the non-linearity of equation [5.8], a numerical solution was obtained instead of an analytical solution(9). This result is represented in a three-dimensional TTE diagram with axes of t, T and E′ as shown in Figure 5.3. As illustrated in this example, at a given dose rate, the temperature initially increases rapidly with increasing exposure time followed by a slower increase as the reactive functional groups are depleted by the curing reaction. Also, the rate of temperature rise increases as the dose rate increases due to the adiabatic system.

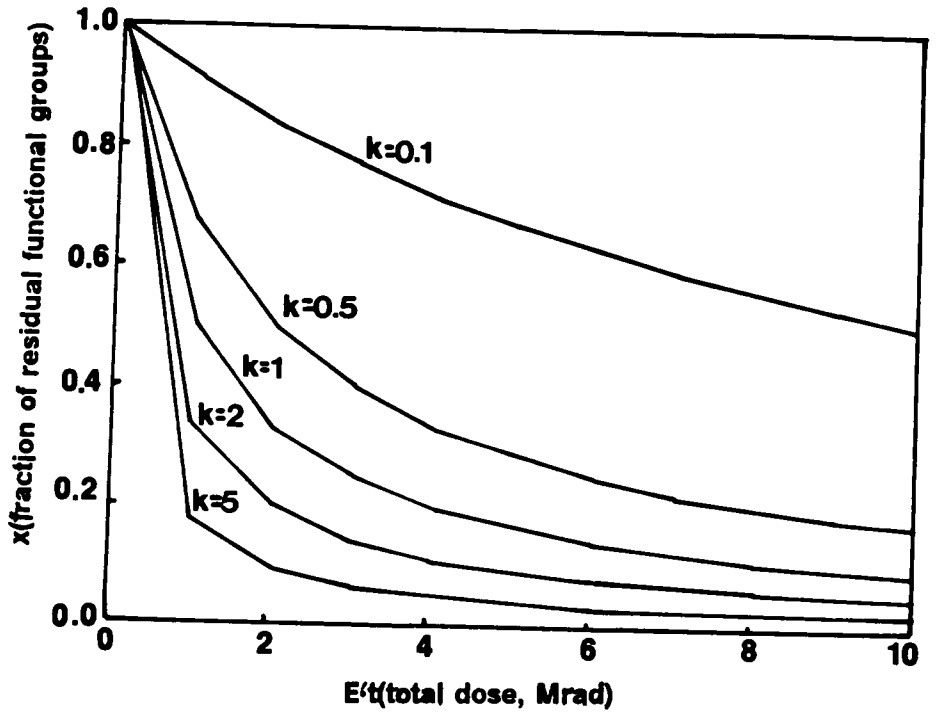

Figure 5.2. Example plots of the suggested equation [5.7].

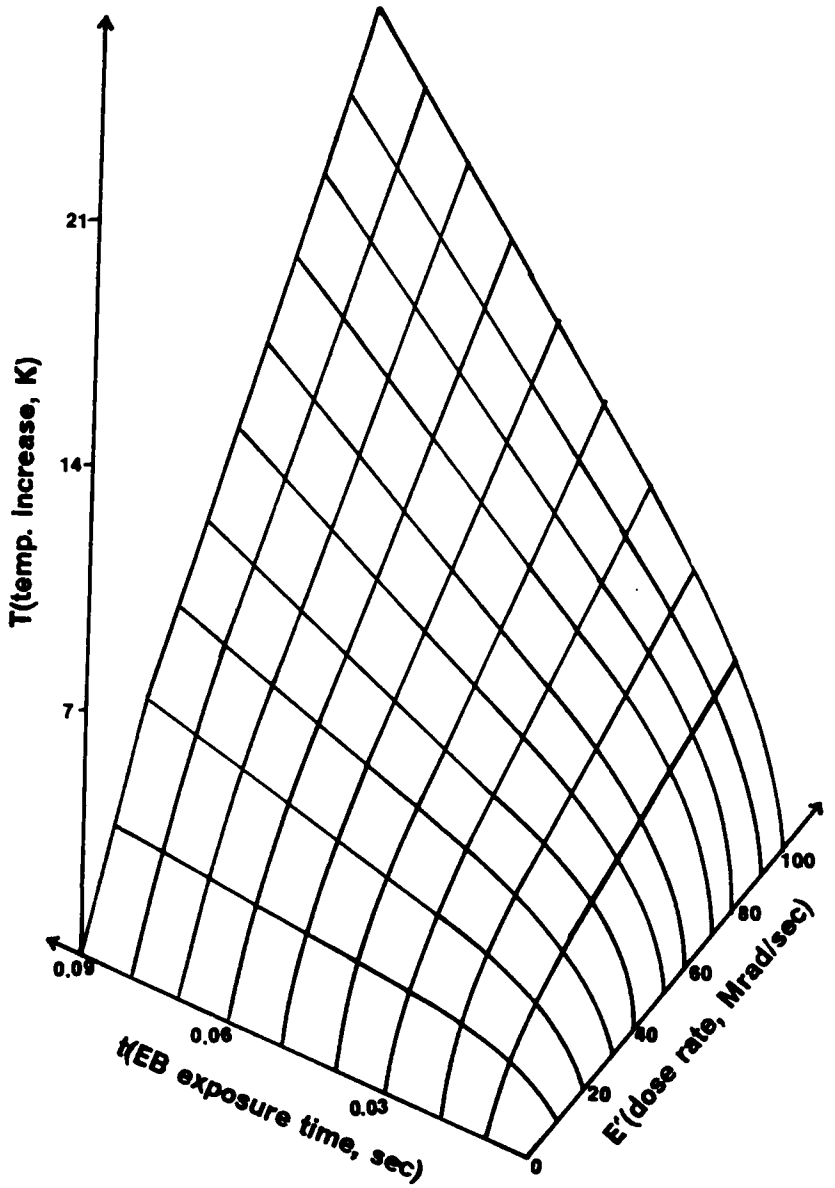

Figure 5.3. An example plot of the TTE relation for the case II.

5.4 Case III. Effects of Glass Transition and Vitrification

Curing of reactive resin coatings by electron beam irradiation may often be accompanied by a significant increase in the glass transition temperature, Tg, of the reacting system. As the Tg approaches the curing temperature during the proceeding polymerization, the segmental mobility of the reactive species is reduced and the curing reaction may start being controlled by diffusion limitations instead of being controlled by the reaction kinetics. Once the Tg of the reacting system exceeds the curing temperature, the reaction is retarded and, subsequently, ceases to proceed due to vitrification as has been well discussed by Gillham et al(3). In this section, *a qualitative relation* between time, temperature and energy in an adiabatic system is introduced which is based on the relationship between the polymerization reaction rate and the curing temperature.

As previously indicated in the discussion with regard to equation [5.5], the rate of temperature increase is controlled by two factors-the EB energy dissipation and the kinetic exotherm. In an adiabatic system, which is a simplifying assumption in this study, the EB energy dissipation factor contributes to raise the temperature with a constant rate. In other words, the temperature increase due to EB energy dissipation is proportional to the exposure time based on the assumption that the heat capacity is independent on the temperature and the physical state of the resinous coating. Therefore, in order to develop a time-temperature relationship at a constant dose rate, a pattern of polymerization reaction rate with regard to time or temperature should be derived including the consideration of the effects of glass transition and vitrification. Based on the free radical polymerization kinetics, a possible qualitative relationship between polymerization reaction rate and temperature has been proposed as illustrated in Figure 5.4.

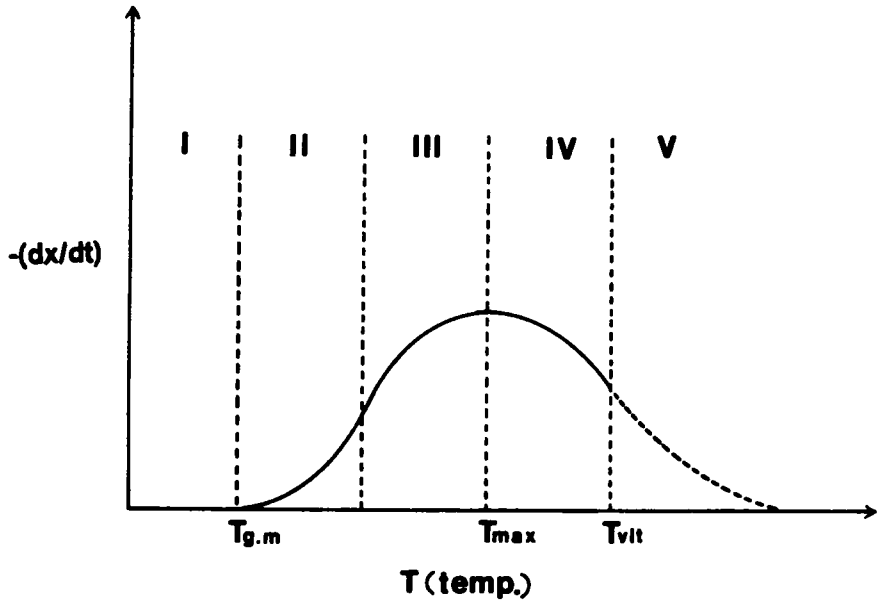

Figure 5.4. A suggested behavior of polymerization reaction rate vs. temperature.

In the temperature range(I) below the glass transition temperature of monomeric species, Tg,m, the temperature is low enough to hinder any polymerization reaction and hence this region is of little interest to this discussion. In the following range shown as region(II), the reaction rate starts increasing due to the rapidly decreasing viscosity of the reacting system. According to the well-known WLF equation(10) such as:

$$\log(\frac{\eta}{\eta_{To}}) = \frac{-C_1(T - T_o)}{C_2 + T - T_o} \qquad [5.9]$$

where η_{To} is the viscosity coefficient at reference temperature T_o, and C_1, C_2 are the WLF parameters, the viscosity dependence on the temperature suggests that the viscosity decreases exponentially with increasing temperature in an appropriate temperature range above Tg,m. Therefore, it is reasonable to indicate that the reaction rate also increases exponentially with increasing temperature in this temperature range. In temperature region(III), the exponentially increasing polymerization rate continues to rise due to the decreasing rate of termination reaction until it reaches a maximum value where the rate of propagation starts to control the reaction rate. The rate of propagation reaction in the temperature range(III) is affected much less than the rate of termination reaction. As the viscosity starts increasing with the increasing conversion, the termination process is increasingly hindered due to the reduced mobility of macroradicals, which is also known as the Tromsdorff effect, while the propagation involving a large radical with a small monomer has not changed significantly.

To more semi-quantitatively address this case, suppose the generalized expression for the polymerization rate is as follows:

$$-\frac{d[M]}{dt} = (\frac{k_p}{k_t^{0.5}})[M]E'^{0.5} \qquad [5.10]$$

which is an alternative for equation [5.6]. Here k_p is the rate constant of propagation, k_t the rate constant of termination and [M] the monomer concentration. A decrease in k_t contributes to raise the reaction rate further up to the maximum value(11). Upon reaching the temperature of the maximum reaction rate, Tmax, the kinetics start being controlled by the effect of decreasing propagation rate as illustrated by the decreasing k_p value in equation [5.10]. In the temperature region(IV), the propagation reaction proceeds under the control of diffusion until it reaches the temperature of vitrification, Tvit. Vitrification significantly reduces the molecular and submolecular mobilities, and hence the polymerization reactions are quenched. Typically, the vitrified material will contain both sol and gel fractions. In region(V), since the temperature continues to rise by EB energy dissipation in the adiabatic system which is an assumption in this study, further curing beyond the vitrification point might well be possible depending on the EB exposure time and the chemistry of the system, etc. **As an example** for the curing beyond the initial vitrification point, it can be suggested that the cure temperature and the temperature of vitrification increase coincidentally until the reactions are extinguished in principle. Therefore, the generalized polymerization rate vs. temperature behavior as illustrated in Figure 5.4 at least suggests that there should be a maximum point for the polymerization rate between Tg,m and Tvit as indicated by Tmax. For the adiabatic system where the temperature continues to rise due to EB energy dissipation, the time-temperature behavior with different energy(dose rate) can be schematically shown(no absolute units) such as in Figure 5.5 which is based on the above discussion. As represented three- dimensionally in terms of a time-temperature-energy(TTE) diagram in Figure 5.6, the increasing dose rate results in a higher rate for temperature increase and accelerates the process to reach Tmax and Tvit, although these temperatures might be slightly different depending on the dose rate level. In general, the TTE behavior in Figure 5.6 shows that, with increasing EB exposure time at a certain dose rate, the

temperature of the system reaches the Tg of the unreacted resin followed by Tmax, where the rate of the temperature increase is at a maximum due to the effects of viscosity and propagation rate. When the system reaches the vitrification point(Tvit), the rate of temperature increase is slowed down although a relatively small amount of residual reaction might proceed further due to the continuous temperature rise in the adiabatic system, which is directly dependent on dose.

Attempts to establish a relationship between the Tg and the conversion of the network-forming epoxy resin system have shown to be relatively complex and strongly dependent on the type of the system. One of the noticeable developments with respect to this relationship was proposed by Di Benedetto(12) who presented a theory relating the glass transition temperature with conversion. However, due to the complexity of the epoxy curing system, studies have been limited to a case of isothermal process and curing of linear high polymers which is highly simplified situation in comparison to our study of the TTE relationship. In addition, as the viscosity increases and the system approaches vitrification point, the curing reaction becomes controlled by diffusion limitation suggesting another complicating factor. Hence, our semiquantitative study on TTE relationship offers a reasonable approach showing the overall behavior of EB curing systems.

In this study, some example time-temperature-energy(TTE) diagrams have been suggested based on the conceptual features for the EB curing of reactive resin coatings. In order to explore the possibilities of numerical solutions and schematic representations of the TTE relationships, several simplifying assumptions have been made. In reality where adiabatic and stationary systems are no longer applicable, additional important factors should include: a) temperature variation inside the resin coating due to the con-

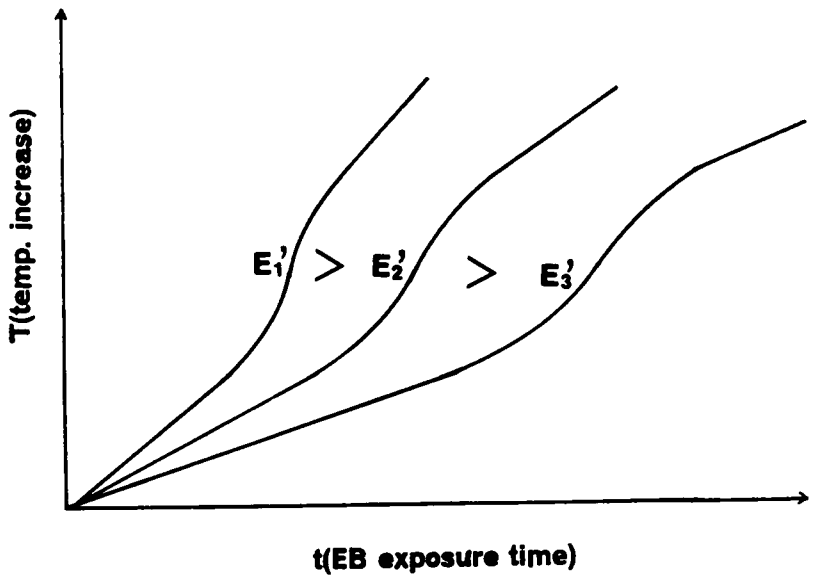

Figure 5.5. Plots of the temperature vs. time with different dose rates.

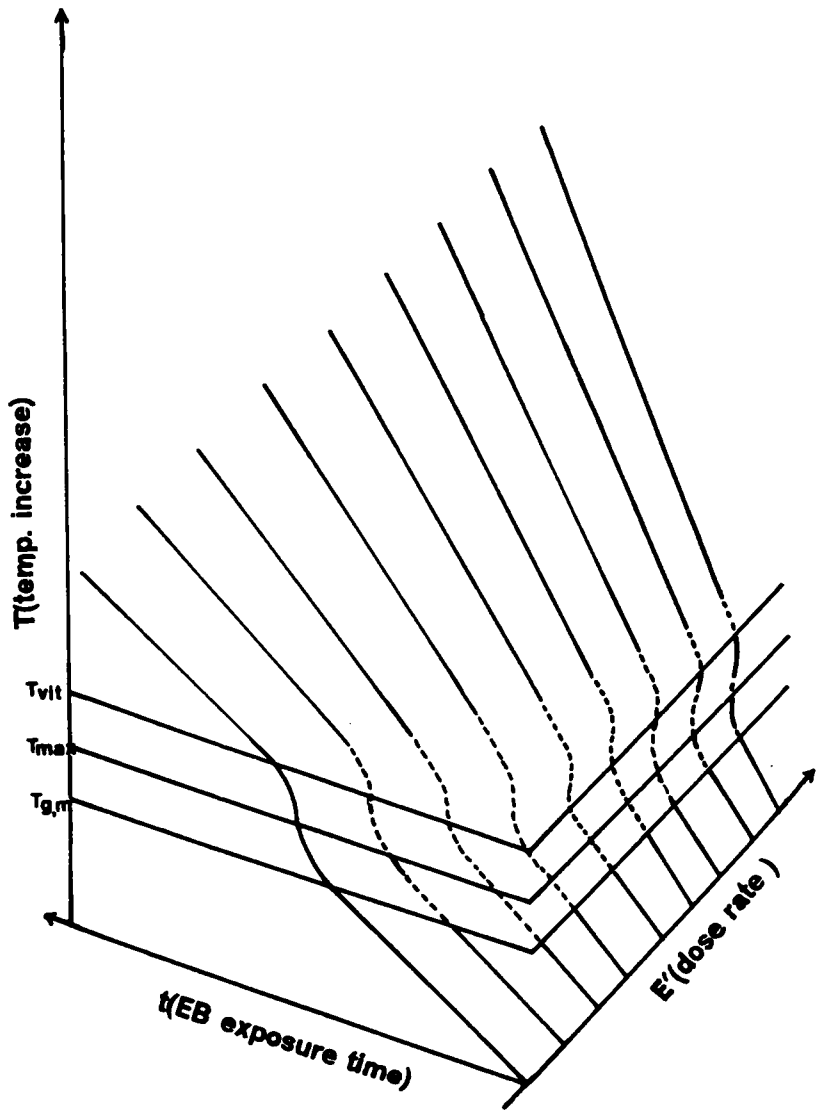

Figure 5.6. An example plot of the TTE relation for the case III.

vection and conduction heat transfer to substrates and continuously purged inert gas; b) dependences of the physical properties of the EB reactive material on cure temperature, degree of cure, glass transition and vitrification; c) effects of a non-stationary system, etc. Our discussion here of these three idealized TTE relationships is believed to have addressed some of the important fundamental variables in order to help establish a better semiquantitative understanding of an electron beam curing process.

5.5 Summary

Three general adiabatic cases in EB curing of resinous coatings have been investigated in consideration of the temperature increase by EB energy dissipation, kinetic exotherm, and effects of glass transition and vitrification. In the first case where the temperature increase occurs only by EB energy dissipation, an energy balance shows that the rate of temperature increase is proportional to the energy(dose rate). In the second case, the kinetic exotherm for polymerization has been considered in addition to the EB energy dissipation. An attempt has been made to suggest a time-temperature-energy(TTE) relation by numerically solving the mathematical equations for a generalized free radical polymerization scheme with an example calculation. It has been found that the trend of the temperature change is dependent on the properties of the resin- these being the activation energy, exothermic heat, radiation sensitivity, and functionality, etc. In the third case, the effects of glass transition and vitrification are introduced in addition to the considerations in the previous cases. A qualitative TTE diagram was suggested with regard to the free radical polymerization process and the effects of viscosity change and the diffusion limitation. Although each case was strictly based on the idealized adiabatic

system, these TTE analyses provide valuable conceptual features for the EB curing of reactive resin coatings. In addition, it is our hope that this discussion, which introduces the TTE diagram, will serve as important background for further experimental studies in the future with regard to the effects of non- adiabatic, non-stationary cases, etc.

References

1. Davidson, W. H. T. *J. Oil Col. Chem. Assoc.* 1963, *52*, 946.

2. Bailey, D. R. *Paint Technol.* 1971, *35*, 12.

3. Chan, L. C.; Nae, H. N.; Gillham, J. K. *J. Appl. Polym. Sci.* 1984, *29*, 3307.

4. Pacansky, J. *J. Radiat. Curing* 1983, *10*, 4.

5. Kim, H. C.; Elnaggar, A. M.; Wilkes, G. L. *Polym. Prep. Div. Polym. Mat. Sci. Eng.* 1989, *60*, 468.

6. Hayashi. K.; Okamura, S. *Radiat. Phys. Chem.* 1981, *18*, 1133.

7. Ausloos, P. *Fundamental Processes in Radiation Chemistry* Intersciences, New York, 1968.

8. Degnan, T. *Radiat. Phys. Chem.* 1982, *19*, 393.

9. Carnahan, B.; Luther, M. A.; Wilkes, J. O. *Applied Numerical Methods* Wiley, New York, 1969.

10. Williams, M. L.; Landel, R. F.; Ferry, J. D. *J. Am. Chem. Soc.* 1955, *77*, 3701.

11. Rudin, A. *The Elements of Polymer Science and Engineering* Academic Press, 1982.

12. Nielson, L. E. *J. Macromol. Sci. Rev. Macromol. Chem.* 1969, *C3*, 69.

6.0 Mechanical and Thermal Properties of EB Irradiated Poly(phenylene Sulfide)(PPS)

The effect of electron beam(EB) irradiation on the mechanical and thermal properties of initially amorphous and semicrystalline poly(phenylene sulfide)(PPS) films has been investigated. Irradiations were carried out either in a nitrogen or air atmosphere. Subsequent mechanical testing carried out at 23°C suggested that oxidative degradation occurs in air for high radiation doses. However, modulus and tensile strength were not greatly affected by irradiation level. Moreover, it was found that elongation by yielding no longer occurs at doses higher than 1000 Mrad for initially amorphous materials and above 500 Mrad for the initially semicrystalline materials. Differential scanning calorimetry(DSC) measurements utilized to determine crystallinity and melting behavior suggest the likely occurrence of some crosslinking with high irradiation levels. Scanning electron microscopy(SEM) of the irradiated PPS surface suggest the possible occurrence of gas evolution-at least for high dose levels.

6.1 Introduction

Chemical and physical changes of polymers caused by ionizing radiation are of considerable continuing concern because of the utility of polymeric systems in applications

where exposure to irradiation occurs. In particular, polymers containing various aromatic rings in the main chain have received much attention. This is because the aromatic character of these polymers tends to make these systems more resistant to radiation damage; therefore, these systems are often utilized in the field of nuclear energy, in outer space, and related applications where potential exposure to high energy radiation exists. The influence of electron beam irradiation on the degradation of tensile properties as well as the general mechanical relaxation of several aromatic polymers has been investigated by Sasuga and others(1,2,3). According to the limited studies carried out in air at 23°C, the radiation stability of selected polymers was in the following order: Polyimide > PEEK > polyamide > polyetherimide > polyarylate > polysulfone > poly(phenylene oxide)(PPO). However, this latter classification is not rigorous and will be system dependent.

Poly(phenylene sulfide)(PPS) is a highly aromatic high- temperature engineering thermoplastic that has a number of beneficial properties(4). One of its outstanding properties is that it has a particularly strong resistance to chemical(solvent) environments. Recently, films of initially amorphous PPS were irradiated with high energy Li, F, and I ions to produce electrically conductive materials(5). Based on this study, it was found by differential scanning calorimetry(DSC) that there was some crystallinity induced in the irradiated material. Moreover, results of infrared(IR) and electron spin resonance(ESR) spectroscopies show the creation of free carriers at high doses thereby promoting conductivity and the existence of free radicals in the irradiated material. Similarly, Mazurek et al.(6) reported that ion implantation of arsenic, krypton, and bromine onto thin films of PPS increased the conductivity of the material by up to 12 orders of magnitude. Moreover, infrared spectra of the films before and after implan-

tation showed that crosslinking might have occurred in the implanted films. The response of PPS to EB radiation, however, has not been distinctly investigated.

The objective of the present work is to study the effect of EB irradiation on the mechanical and thermal properties of initially amorphous and semicrystalline PPS in the presence of either an air or nitrogen atmosphere.

6.2 Materials and Experiments

6.2.1 Materials

Amorphous PPS films were supplied by the Phillips Petroleum Company in the form of unoriented amorphous tape having an average thickness of $9x10^{-3}$ cm and a width of 3.9 cm. Semicrystalline films were prepared by heating these tapes at 120°C for 10 min under vacuum conditions.

6.2.2 Electron Beam Irradiation

Irradiation was performed with an electrocurtain-type accelerator manufactured by Energy Science, Inc. model CB/150/15/180. Samples for irradiation were cut into dumbbell shape and exposed to EB irradiation with a dose rate of 50 Mrad/sec. The maximum available dose was 20 Mrad per pass, hence, several passes under the electrocurtain were required for higher dose levels. The materials were placed on a stainless steel plate to

minimize the rise in the temperature of the samples during irradiation. As will be discussed, however, use of this metal substrate does not inhibit a considerable short-term rise in film temperature at the high dose rate used.

6.2.3 Mechanical Properties

Mechanical tests including tensile strength, elongation and Young's modulus were made at room temperature using an Instron(Model 1122) employing a crosshead speed of 0.5 mm/min. Samples were cut with a die in a dog-bone shape of initial dimensions(10 mm in gauge length and 2.8 mm in width). Young's modulus was calculated from the initial slope of the stress- strain curves. The yield stress and tensile strength were obtained at the yield point and at break, respectively. The elongations at yield and break were calculated on the same basis mentioned above. Dynamic storage and loss moduli(E′ and E″), as well as tanδ were determined as a function of temperature using an Autovibron Dynamic viscoelastometer. These samples were run from 0°C to 200°C to investigate glass transition(Tg) behavior with a scanning rate of 2°C/min at a frequency of 11 Hz.

6.2.4 Thermal Properties

Differential scanning calorimetry(DSC) measurements were performed using a Perkin-Elmer DSC-4 calorimeter equipped with a TADS data station. The melting points of initially amorphous and semicrystalline PPS were determined as a function of radiation dose. A heating rate of 10°/min was utilized and the determinations were performed under a nitrogen atmosphere. The melting points determined for each sample after

irradiation were labeled "first run." After melting the samples at 320° for 5 min, they were cooled to room temperature and then the melting point was determined again. These data were labeled "second run." These two kinds of data allowed the determination of the effect of EB irradiation on the melting point of PPS(first run), and recrystallization of PPS(second run). Similarly, the heat of fusion was determined from the area under the fusion peak of the DSC scans. The results of melting points and heat of fusion determinations are the average of two measurements per data point.

6.2.5 Scanning Electron Microscope Analysis

The surface of initially amorphous and semicrystalline PPS before and after EB irradiation were observed via scanning electron microscopy to look for evidence of damage or gas evolution as a result of EB irradiation. The samples were first metallized by sputter coating and left overnight in a vacuum oven. A scanning electron microscope(Cambridge Stereoscan 200) was utilized for this investigation.

6.3 Results and Discussion

6.3.1 Mechanical Properties

Mechanical response of either initially amorphous or semicrystalline PPS as calculated from the load-elongation curves before EB irradiation show that the elongation occurs by necking. Initially amorphous and semicrystalline PPS were subjected to a

radiation dose of 1000 Mrads in the presence of either nitrogen or air. It was found that at this level of electron beam dose, irradiation in the presence of nitrogen had little effect on the mechanical properties of either amorphous or semicrystalline PPS. However, when initially semicrystalline PPS was exposed to the same dose in the presence of air, the occurrence of distinct yielding disappeared at dosages above 500 Mrad but was still observed for the initially amorphous PPS as shown by the data in Table 6.1.

Figures 6.1-3 show the effect of electron beam irradiation on the tensile strength at break, σ_B, Young's modulus, and elongation at break as a function of dose in air for both initially amorphous and semicrystalline PPS, respectively. It is evident that EB irradiation has a distinct effect on the tensile strength of both materials. At low doses there is a tendency for the tensile strength of the initially amorphous PPS to increase up to a dose value of 1500 Mrads after which it rapidly decreases. The increase in tensile strength at lower dose is due to the change in structure from amorphous to that of semicrystalline as result of rising temperature of the material during the irradiation steps. Although the samples were placed on stainless steel plates, which was expected to minimize the increase in sample temperature during irradiation, it still permitted a considerable rise in the sample temperature due to the rapid energy deposition of the EB into the substrate. In fact, using the energy equivalent of 2.4 cal/g per Mrad and a general heat capacity value of 0.4 cal/g per °C, gives a rise in temperature of ca. 6°C/Mrad if adiabatic conditions are assumed. Hence, for a rapid dose of 20 Mrads and for several passes, the material is distinctly brought to temperature above Tg(85°C) for sufficient time to allow some crystallization to occur before cooling. Indeed, visual inspection of the initially amorphous materials showed the development of turbidity as multiple pass dosage increased. The use of light transmission through

Table 6.1. Mechanical properties of EB irradiated initially amorphous and semicrystalline PPS in air.

Radiation dose (Mrad)	Tensile strength (MPa)	Elongation at yield (%)	Young's Modulus (GPa)	Tensile strength at break(MPa)	Elongation at break (%)
Initially amorphous PPS					
0	59	3.0	2.1	45	23
500	61	4.7	2.5	46	20
1000	80	4.7	2.5	63	7
Initially semicrystalline PPS					
0	85	4.9	2.7	70	18
500	90	5.4	2.6	79	9
1000	-	-	2.8	75	4

crossed polarizers also supported this view. It is noted that for the initially semicrystalline PPS, the general behavior of the tensile strength decreases with dosage but less so than for the initially amorphous system, thereby suggesting that the crystalline phase is less prone to radiation effects as has been observed for several polymers.

Figure 6.2 shows the modulus response of initially amorphous and semicrystalline PPS to EB irradiation. As shown, the modulus of initially amorphous PPS and semicrystalline PPS seems to increase with increasing dose up to 100 Mrad. This initial rise is caused by the induced crystallinity from radiation heating. Following the rise, subsequent loss of modulus occurs, suggesting degradation. On the other hand, the modulus of the initially semicrystalline PPS tends to decrease by increasing dose to 100 Mrad. Interestingly, this material still maintains a somewhat higher modulus than the initially amorphous material, again suggesting a greater radiation resistance of the crystalline phase.

In Figure 6.3, it is clear that the elongation at break is very much affected by EB irradiation regardless of whether the initial structure of PPS is amorphous or semicrystalline. One notes that even below about 500 Mrad, there is a considerable decrease in elongation and it nearly plateaus in value above 1000 Mrad. This behavior in elongation at break, together with the deterioration in tensile strength, display the increase in brittleness of the materials. The results are believed to be due to the occurrence of oxidative degradation due to EB irradiation.

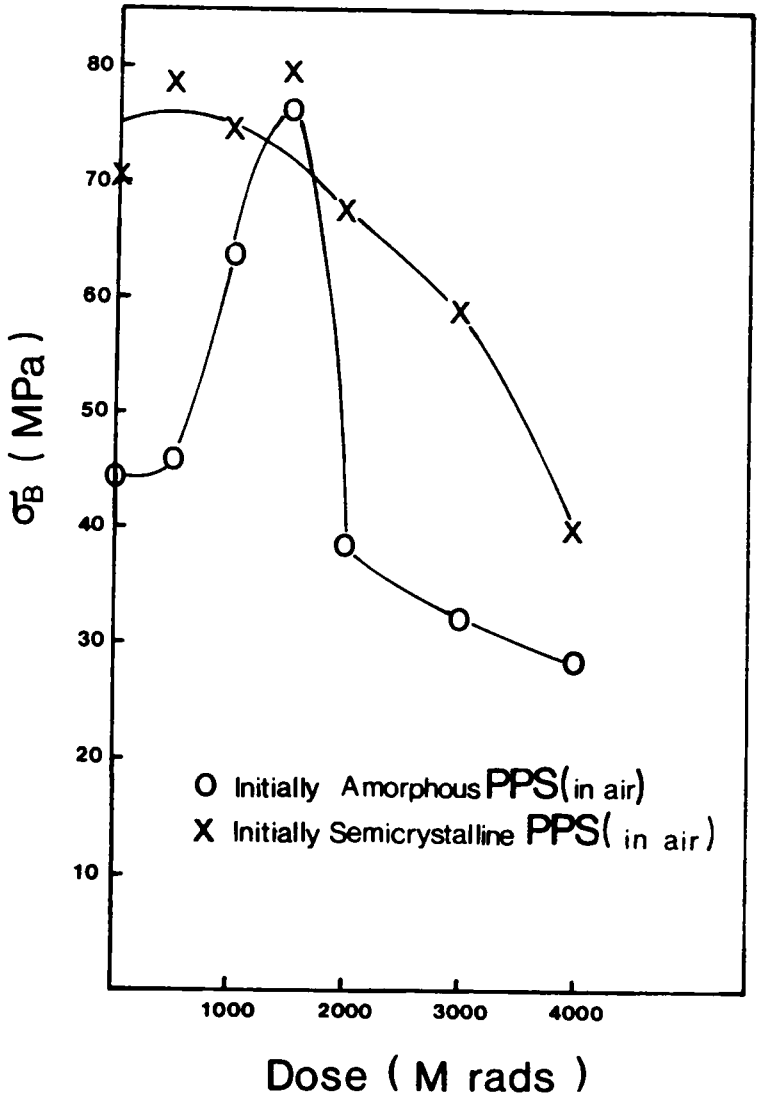

Figure 6.1. **Effect of EB irradiation in air on the tensile strength.:** initially amorphous(o) and initially semicrystalline(x) PPS.

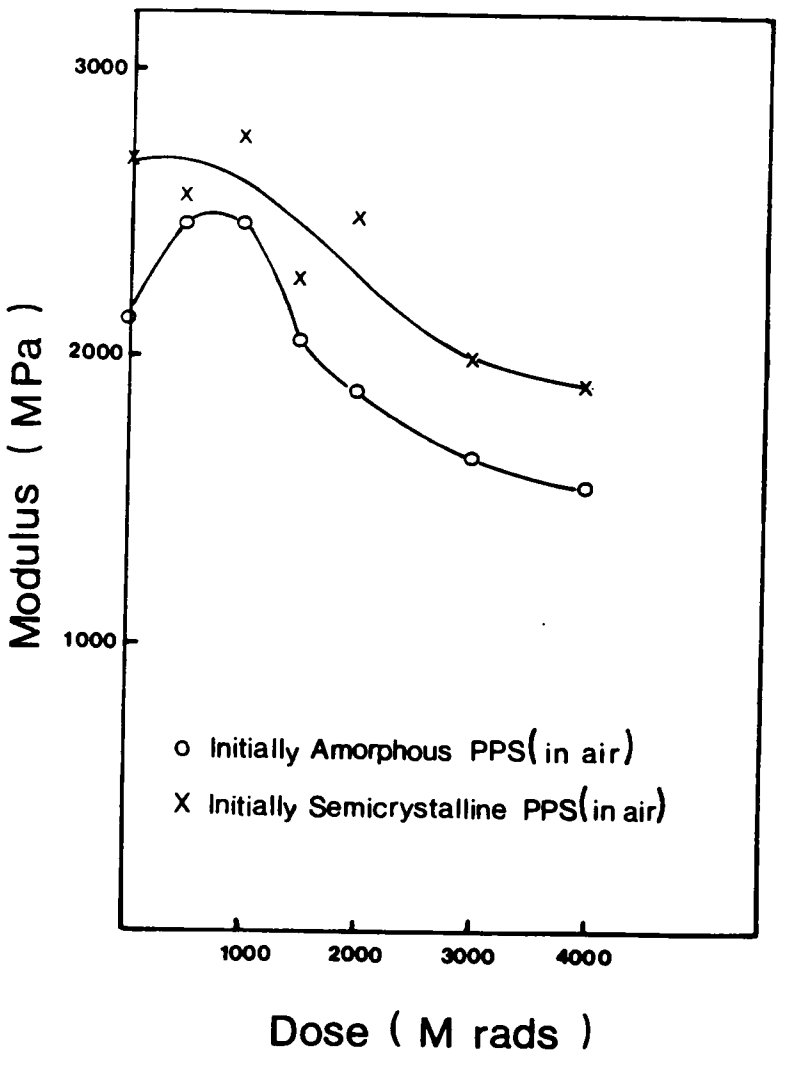

Figure 6.2. **Effect of EB irradiation in air on the modulus.:** initially amorphous(o) and initially semicrystalline(x) PPS.

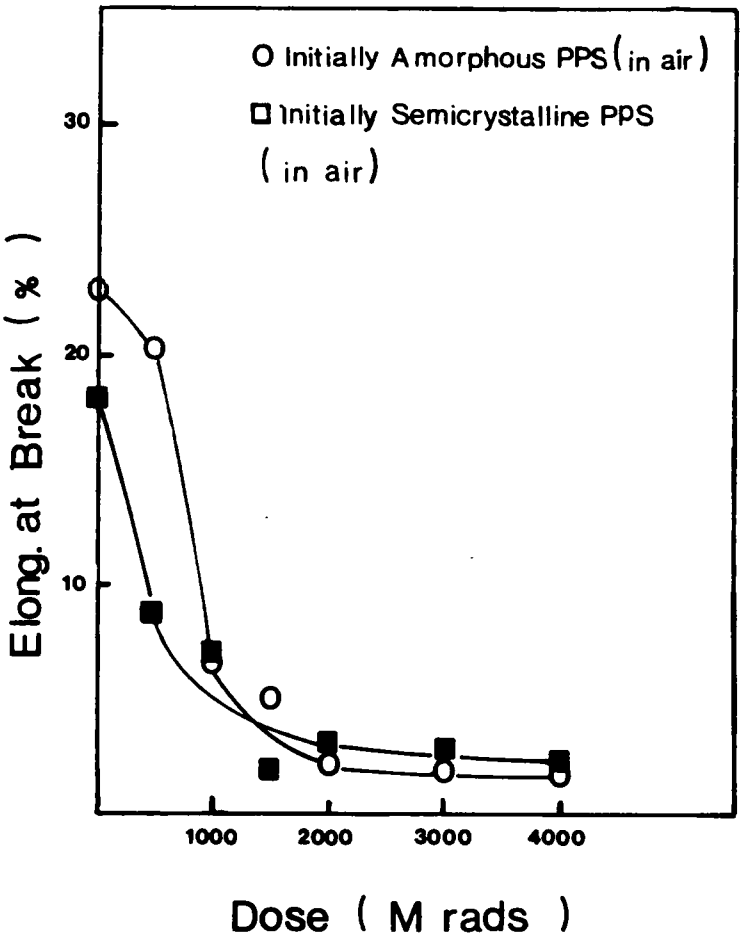

Figure 6.3. **Effect of EB irradiation in air on the elongation at break.:** initially amorphous(o) and initially semicrystalline(■) PPS.

6.3.2 Dynamic Mechanical Properties

Figure 6.4 shows typical curves of the logarithm of storage modulus as a function of temperature obtained for initially amorphous PPS before and after irradiation to 1500 Mrad. It is observed that before irradiation, initially amorphous PPS shows a decrease in the modulus at about 90°C indicating the onset of the glass transition temperature of PPS. Following this drop, the modulus increases at about 120°C as a result of crystallization. The glass transition and crystallization temperatures observed by the change in storage modulus are in good agreement with the values obtained by differential scanning calorimetry shown later in Figure 6.5. Furthermore, the irradiated PPS does not present the typical decrease in modulus at the glass transition temperature as seen in the unirradiated PPS, but there is a slight decrease in modulus noticed at 115°C. As discussed earlier, this difference is attributed to the fact that with a sufficient irradiation dosage, the initially amorphous PPS crystallizes and hence the modulus drop at Tg is no longer as distinct.

6.3.3 Thermal Properties

Figure 6.5 shows a DSC scan for an amorphous unirradiated PPS sample. The typical thermal transitions of the amorphous polymer are observed. First is the Tg of PPS at ca. 85°C, followed by a crystallization peak with its maximum at 130°C, and finally a melting transition, Tm, that peaks at 278°C. Figures 6.6 and 6.7 present plots of the melting point of the irradiated samples as a function of radiation dose for initially amorphous and semicrystalline PPS, respectively. The melting points have been defined as the maximum in the crystallization peak as shown in figure 6.5. It is observed that

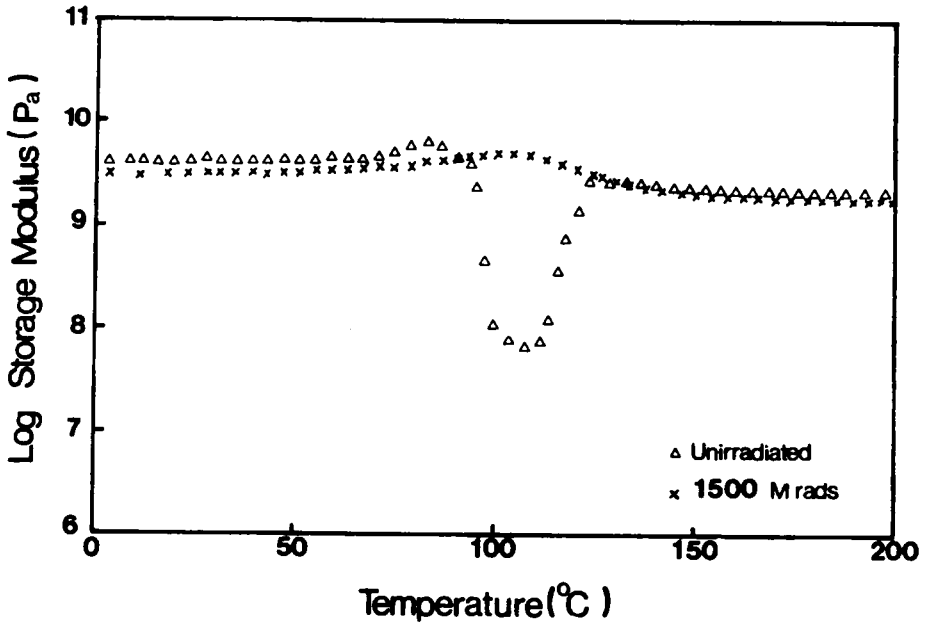

Figure 6.4. **Plot of storage modulus as a function of temperature for initially amorphous PPS.:** before(Δ) and after(x) irradiation(1500 Mrad) in air.

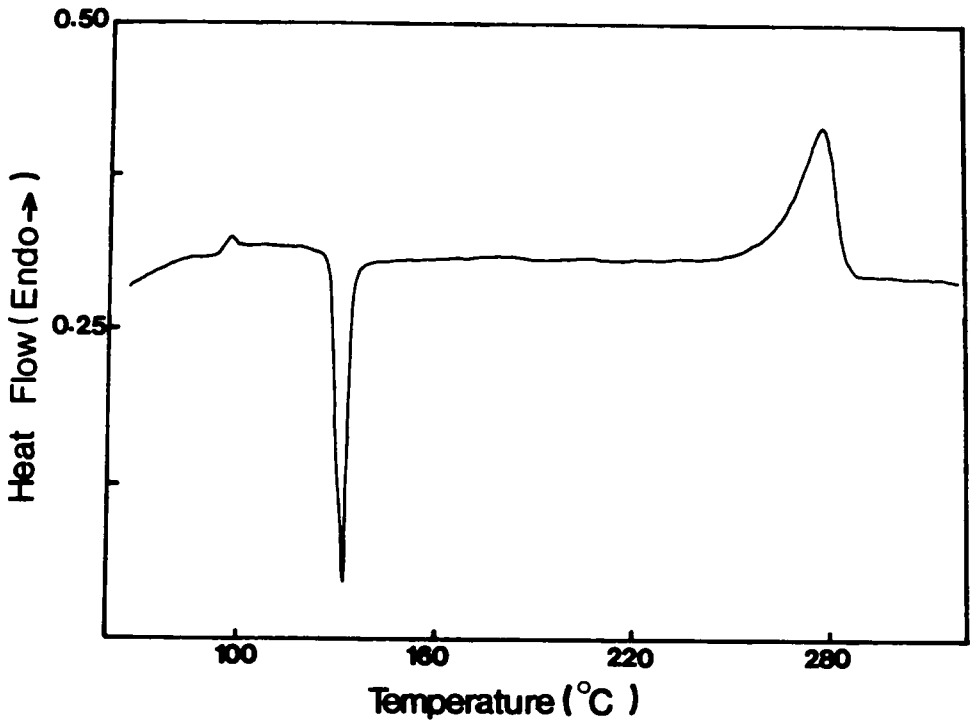

Figure 6.5. DSC scan of unirradiated initially amorphous PPS.

the melting point of initially amorphous PPS decreases form 276°C for unirradiated to ca. 270°C at 4000 Mrad.(Recall it crystallizes during the DSC scans.) Similarly, the melting point of initially semicrystalline PPS deceases from 281°C after a dose of 4000 Mrad. In addition, PPS irradiated in the amorphous state shows a lower melting point than that irradiated in the initially semicrystalline state. Also, upon recrystallization after melting(second run), the melting point is further depressed for both irradiated PPS that initially had been in either the amorphous or in the semicrystalline state. This indicates that the ability of the polymer to recrystallize is decreased by the earlier electron beam irradiation. Since the melting point is an indication of the crystallite size and perfection, a decrease in the melting point implies a smaller crystallite size and/or a less perfect crystal formed after irradiation. Two possible explanations can be forwarded, the first would consider a chain scission mechanism; i.e., a decrease of molecular weight due to irradiation. This is in accordance with previous studies performed on the crystallization behavior of PPS which showed that the melting point of PPS decreases with decreasing molecular weight(7). The second argument implies the occurrence of branching and/or possibly crosslinking. Previous studies have indicated that branching decreases the melting point of PPS(8). Moreover, it has been reported that curing or crosslinking of PPS decreases the crystallizability of PPS, i.e., its ability to crystallize(9). Crosslinking of thin film of PPS upon ion implantation has been previously suggested by Mazurek et al.(6). While either argument(or both) might be applicable to our data, the small increase in Tm and ΔH_f suggests that if crosslinking occurs, it is not extreme even at these high dosages and, for this reason, gel fractions were not measured.

The heat of fusion, ΔH_f, provides another important piece of information. Figure 6.8 and 6.9 show the heat of fusion of irradiated PPS as a function of dose. For initially semicrystalline PPS, irradiation does not seem to produce any systematic vari-

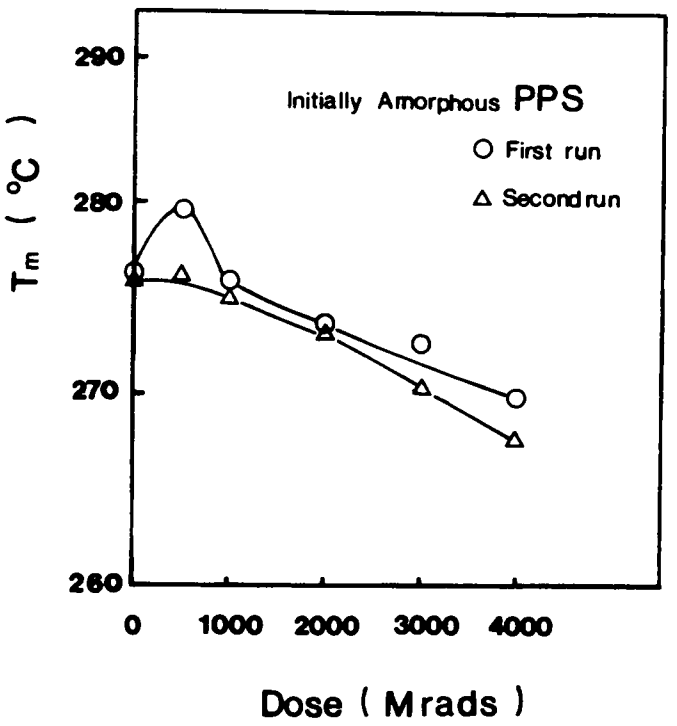

Figure 6.6. **Effect of EB irradiation in air on the melting point of initially amorphous PPS.:** first run(o) and second run(Δ).

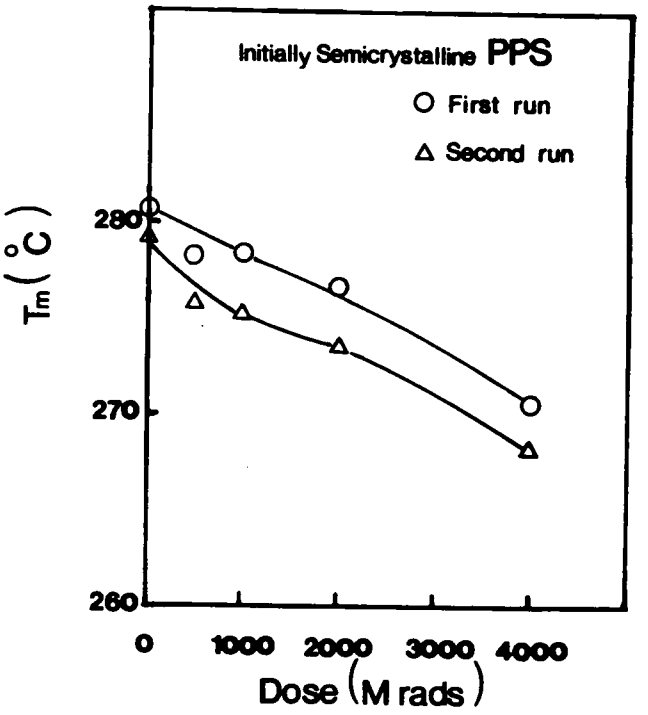

Figure 6.7. Effect of EB irradiation in air on the melting point of initially semicrystalline PPS.: first run(o) and second run(Δ).

ation in ΔH_f. In addition, there is no difference in ΔH_f obtained in the first or second heating. However, the heat of fusion for initially amorphous PPS presents a clear trend. The ΔH_f decreases from 11.0 cal/g for the unirradiated PPS to 9.0 cal/g at 1000 Mrad. Irradiation to doses of 4000 Mrad does not appear to decrease ΔH_f any further. Also, there is no difference in ΔH_f obtained from the first or second heating. The heat of fusion is, of course, proportional to the crystalline content of a semicrystalline polymer. Therefore, these data indicate that irradiation of initially amorphous PPS only slightly decreases the crystalline content achievable during a DSC scan at 10°C/min, suggesting a lower radiation resistance of the amorphous phase. Previous investigations on the crystallization behavior of PPS(7) have shown that lower molecular weight PPS($< Mw > = 24,000$) presents a higher heat of fusion than higher molecular weight PPS($< Mw > = 63,000$) for the same thermal treatment. Furthermore, it was observed that the introduction of branches(8) or crosslinking(9) in PPS decreases the heat of fusion. Consequently, the present data on heat of fusion seem to indicate the occurrence of branching and possibly very light crosslinking upon irradiation of amorphous PPS rather than a decrease in molecular weight.

6.3.4 Scanning Electron Microscopy(SEM) Tests

Scanning electron micrographs of unirradiated and EB(2000 Mrad) irradiated PPS surfaces are shown in Figure 6.10. These samples were crystallized at 120°C for 10 minutes. As shown in Figure 6.10(a), the unirradiated surface is relatively smooth with small size(less than 1 μm) imperfections. However, the surface of a PPS film irradiated at 2000 Mrad shows some evidence of gas evolution[figure 6.10(b)], as indicated by random

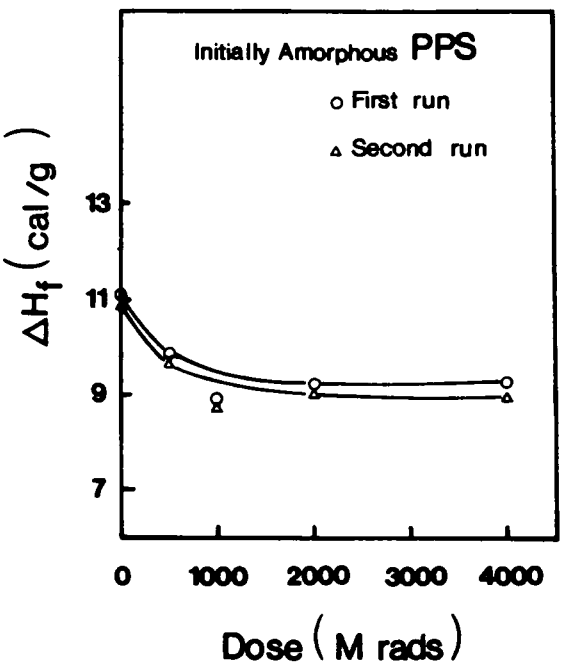

Figure 6.8. **Heat of fusion of initially amorphous PPS as a function of radiation dose in air.:** first run(o) and second run(Δ).

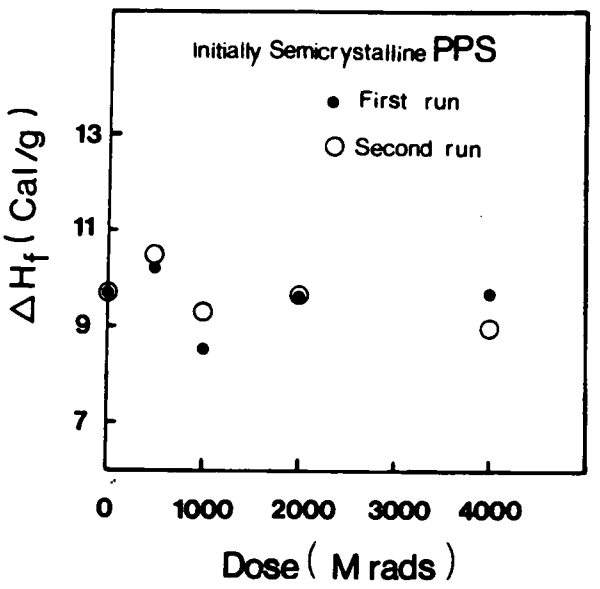

Figure 6.9. **Heat of fusion of initially semicrystalline PPS as a function of radiation dose in air.:** first run(•) and second run(o).

pore-like structures. These are somewhat consistent with results previously reported as H_2 evolution in the irradiated PPS samples(10). Our results suggest an off-gassing caused by chemical changes induced by radiation. While the extent of change was not investigated in depth, it was noted that the infrared spectrum of the materials showed no significant change after exposure to high irradiation dosage. This indirectly suggests that little chemical change occurs at these dosage levels. This, of course, is in agreement with the results resented earlier(little change in Tm, ΔH_f, etc.). Our earlier suggestion of some partial oxidative degradation would still be reasonable to apply to these observations. If solution nuclear magnetic resonance(NMR) could be applied, possibly a more complete answer could be provided, however, as pointed out earlier, this technique has not been utilized due to the inability of obtaining a sufficiently good solution at temperatures where NMR spectra can be obtained.

6.4 Conclusions

Initially amorphous and semicrystalline films of PPS have been exposed to high doses of electron-beam radiation in either air or nitrogen atmosphere. The electron beam irradiated materials were evaluated by mechanical tests, dynamic mechanical tests, differential scanning calorimetry, and scanning electron microscopy. Irradiation results in the presence of nitrogen revealed no noticeable change in mechanical or thermal properties of PPS at least up to 1000 Mrad. On the other hand, at the same level of dosage in air instead of nitrogen, the data show change in both the mechanical and thermal properties. In general, based on the experimental results obtained from mechanical tests several points can be stated:

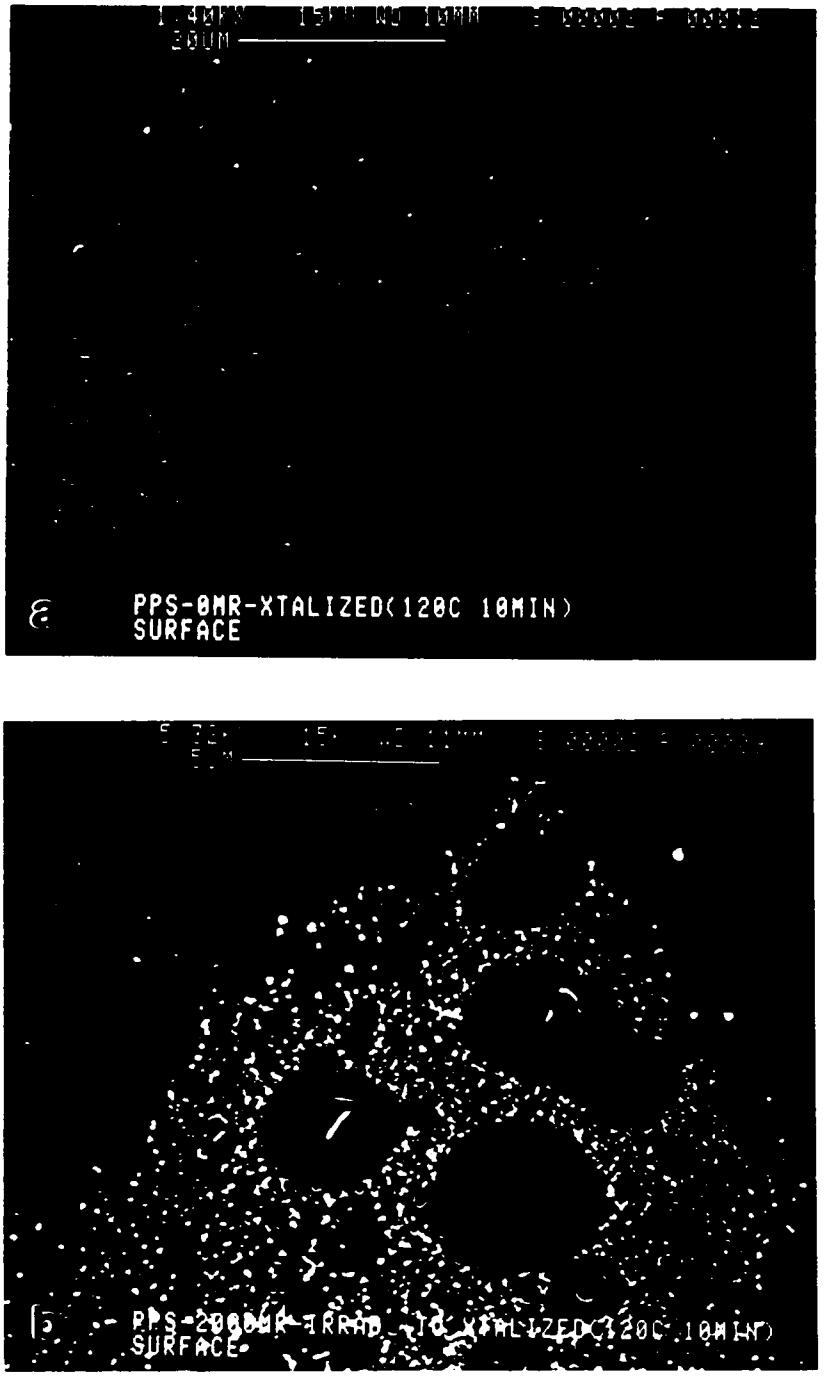

Figure 6.10. SEM micrographs of the surface of initially semicrystalline PPS.: (a)unirradiated PPS and (b)PPS irradiated in air to 2000 Mrad.

1.Elongation at break is much more affected by electron beam irradiation than the other stress-strain properties reported.

2.At higher doses(4000 Mrad), the initially amorphous PPS loses about 62% of its original tensile strength while the initially semicrystalline PPS loses about 57%.

3.Initially amorphous PPS is more susceptible to damage than initially semicrystalline PPS upon electron beam irradiation as determined from mechanical properties as well as DSC results.

4.In general, PPS shows considerable resistance to degradation by electron beam radiation-at least under the irradiation conditions addressed here.

5.Scanning electron microscopy observations of the surfaces of PPS irradiated at high dosage suggest the occurrence of gas evolution following high dosages of irradiation.

References

1. Sasuga, T.; Hayakawa, N.; Yoshida, K.; Hagiwara, M. *Polymer* 1985, *26*, 1039.

2. Sasuga, T.; Hagiwara, H. *Polymer* 1986, *27*, 821.

3. Sasuga, T.; Hayakawa, N.; Yoshida, K. *Polymer* 1987, *28*, 236.

4. Hill, H. W.; Brady, D. G. *Polym. Eng. Sci.* 1976, *16*, 832.

5. Schoch, K. F.; Bartko, J. *Polymer* 1987, *28*, 556.

6. Mazurek, H.; Day, D. R.; Maby, E. W.; Abdel, J. S.; Senturia, S. D.; Dresselhaus, M. S.; Dresselhaus, G. *J. Polym. Sci., Polym. Phys. Ed.* 1983, *21*, 539.

7. Lopez, L. C.; Wilkes, G. L. *Polymer* 1988, *29*, 106.

8. Lopez, L. C.; Wilkes, G. L. *Polymer* in press.

9. Brady, D. G. *J. Appl. Polym. Sci.* 1976, *20*, 2541.

10. Wasserman, B.; Dresselhaus, M. S.; Braunstein, G.; Wnek, G. *MRS symposium on Ion Implantation and Ion Beam Processing Materials* Materials Research Society, Boston, 1983.

7.0 Symmetric and Asymmetric Systems based on the Controlled Distribution of bis-GMA into NBR Film

Two systems based on the controlled distribution of the methacrylic acid derivative of the diglycidyl ether of bisphenol-A (bis-GMA) into crosslinked acrylonitrile-butadiene copolymers, commonly called nitrile rubber(NBR), were prepared utilizing electron beam(EB) radiation. In the system called "symmetric," the EB crosslinked NBR was swollen to equilibrium in solutions containing different concentrations of bis-GMA. The swollen NBR film was then EB irradiated to different dosage levels. The other system called "asymmetric" or "gradient" was prepared by applying the solutions containing bis-GMA to **one surface** of the EB crosslinked NBR film in a controlled time that was less than the time to achieve an equilibrium concentration across the thickness or "swelling" dimension. This asymmetrically swollen NBR film was then immediately EB irradiated using different dose levels. The prepared "symmetric" and "asymmetric" NBR systems were investigated by thermal and mechanical as well as microscopic analyses. The mechanical responses were shown to be strongly dependent on the bis-GMA content in the NBR film and the type of preparation history. The dynamic mechanical spectra showed the presence of two transitions indicating some level of phase separation which was supported by scanning electron microscopy of fracture surfaces for symmetric and asymmetric systems. The distribution of the imbibed(cured) monomer in the asymmetric system was also studied by FTIR and optical microscopy analyses.

7.1 Introduction

In the last decade, attention has been drawn to the area of polymeric material modification by blending to give a new material retaining some of the desirable features of each constituent polymer. Chemical modification based on various copolymerization methods leading to polymer blends or interpenetrating networks(IPN) have also been regarded as major directions in both the academic and industrial communications. Each modification method can be utilized to sometimes achieve a homogeneous verses a multi-phase system depending on the type of the desired ultimate applications. Numerous methods based on the chemical and physical modifications have been developed to generate multicomponent polymeric systems. Particularly, in recent years, the concept of interpenetrating polymer networks(IPN) offers unique potential features which provide a combination of various chemical networks and possibly a control of morphological structures(1).

Interpenetrating polymer networks(IPN) provide a new way of generating a multicomponent polymeric system. An IPN is defined as an alloy of two polymers produced by separate reactions and it can be prepared by two methods-these being sequential IPN's and simultaneous IPN's. For a sequential IPN, a prereacted network is swollen by another reactive monomer or functionalized oligomeric species and this system is then placed under conditions to polymerize the added monomer. A simultaneous IPN however is generated from two networks formed by simultaneous polymerization(2). Both types of IPN's have been utilized in producing toughened elastomers and reinforced plastics. The sequential IPN method can produce heterogeneous domains of various

sizes depending on the system variables such as the compatibility of the chemical components and the process conditions, etc.(3). In this latter case which is of interest in our study, one polymeric material forms the matrix while the other constituent material may generate phase separated particles and/or an interpenetrating network through cross-linking reactions. In a similar context, there has been a growing interest in the concept of generating systems of "asymmetric" or "gradient" structures utilizing the above-mentioned methodology based on IPN techniques and radiation processes(4,5,6).

The gradient system, which was termed by Shen and Bever(7), can be defined as a system in which structure and properties vary continuously and gradually. If this concept is applied to polymer film and coating technology, the final product might be asymmetric in that the structure and properties are changing gradually across the "film thickness dimension." Possible applications of the asymmetric gradient polymer films can be envisioned for a number of different fields as illustrated by Shen and Bever(7) and the following examples are based on their discussion. Utilizing chemical properties, a reactive hydrophilic monomer could be diffused from one surface to the other through the hydrophobic polymer film generating a gradient concentration and subsequently polymerized. This method may result in a gradient of hydrophilicity across the hydrophobic polymer "film thickness." A possible application was suggested for the construction of gasoline tanks for aircraft or automobiles. A hydrophilic interior layer would help prevent the gasoline from swelling the material, while a hydrophobic exterior layer would be inert to water or moisture in the environment. As another example but now considering mechanical properties, if a relatively soft(rubbery) material is to be fastened to a rigid structure, the region where the fastener is to be applied requires higher mechanical strength. This can be achieved by obtaining a gradient of the glassy polymer across the rubbery polymer film. Other possible applications include utilizing surface

modification to enhance resistance to abrasion and indentation, biocompatibility for medical applications, barrier properties such as for membrane technology, etc. After the introduction of the concept of the gradient polymeric system, Shen and co-workers published on the preparation and characterization of this system using crosslinked polystyrene and poly(methyl methacrylate) as substrates and acrylic monomers as penetrants. In their studies, the polymer substrates were immersed in the monomer solutions for several days and exposed to UV radiation(4).

The objective of the study presented here is to prepare and characterize two different systems, "symmetric" and "asymmetric," based on crosslinked nitrile rubber as an initial matrix. In the symmetric system, the NBR in the crosslinked(gel) form was swollen to equilibrium in a solution of the methacrylic acid derivative of the glycidyl ether of bisphenol-A(commonly called bis-GMA) followed by electron beam(EB) radiation. The obtained distribution of crosslinked bis-GMA inside the NBR matrix will be referred to as "symmetric" distribution even though, on a localized basis, some phase separation may occur. In the case of the "asymmetric" distribution, a solution of bis-GMA was allowed to partially penetrate the NBR films from one surface only for a limited time that was less than the time to achieve a uniform concentration in this same direction. The asymmetrically swollen NBR film was then immediately exposed to EB irradiation. This asymmetric system can be also called a gradient structure as previously mentioned. Schematic illustrations of the morphological textures one might expect for some possible symmetric and asymmetric distribution of bis-GMA into the NBR matrix, or any other related two component systems prepared in a similar way, are shown in Figure 7.1 and 7.2. As illustrated, four possible sample morphological textures might result-these being discussed as follows. In the first case as shown in Figure 7.1(a), the addition of the bis-GMA system, which is glassy in nature following crosslinking, might result in phase

separation in the NBR matrix. The final properties would be dependent on the particle size, volume fraction, and size distribution of the dispersed glassy phase as well as the chemical nature of the matrix and the dispersed phase(8). One might expect that possibly the swollen unreacted system would be initially homogeneous, however at a certain conversion, bis-GMA rich domain could begin to form in the matrix if chemical immiscibility exists prior to possible vitrification of the bis-GMA component. In radiation curing, the phase separation process becomes more complicated and significantly system dependent. This is due to the fact that the reaction generally proceeds rapidly with a temperature increase(due to exothermic reactions and radiation energy dissipation) until the system reaches vitrification resulting from diffusion limitation. A second case is illustrated in Figure 7.1(b) which exhibits a similar phase separation morphology except that the second polymerized particulate phase is interconnected by a network of its own kind. On the other hand, depending on the volume fraction of the dispersed glassy phase and/or the variables of the radiation curing process such as dose rate, a morphological structure similar to that shown in Figure 7.1(c) might result. In this case, the dispersed glassy phase is continuously connected by crosslinking but no distinct particulate regions occur. Finally, interpenetrating networks without significant phase separation might be obtained as schematically shown in Figure 7.1(d). The respective morphological structures of the symmetric system can be similarly modified as the asymmetric systems showing a concentration gradient across the thickness direction as represented in Figure 7.2.

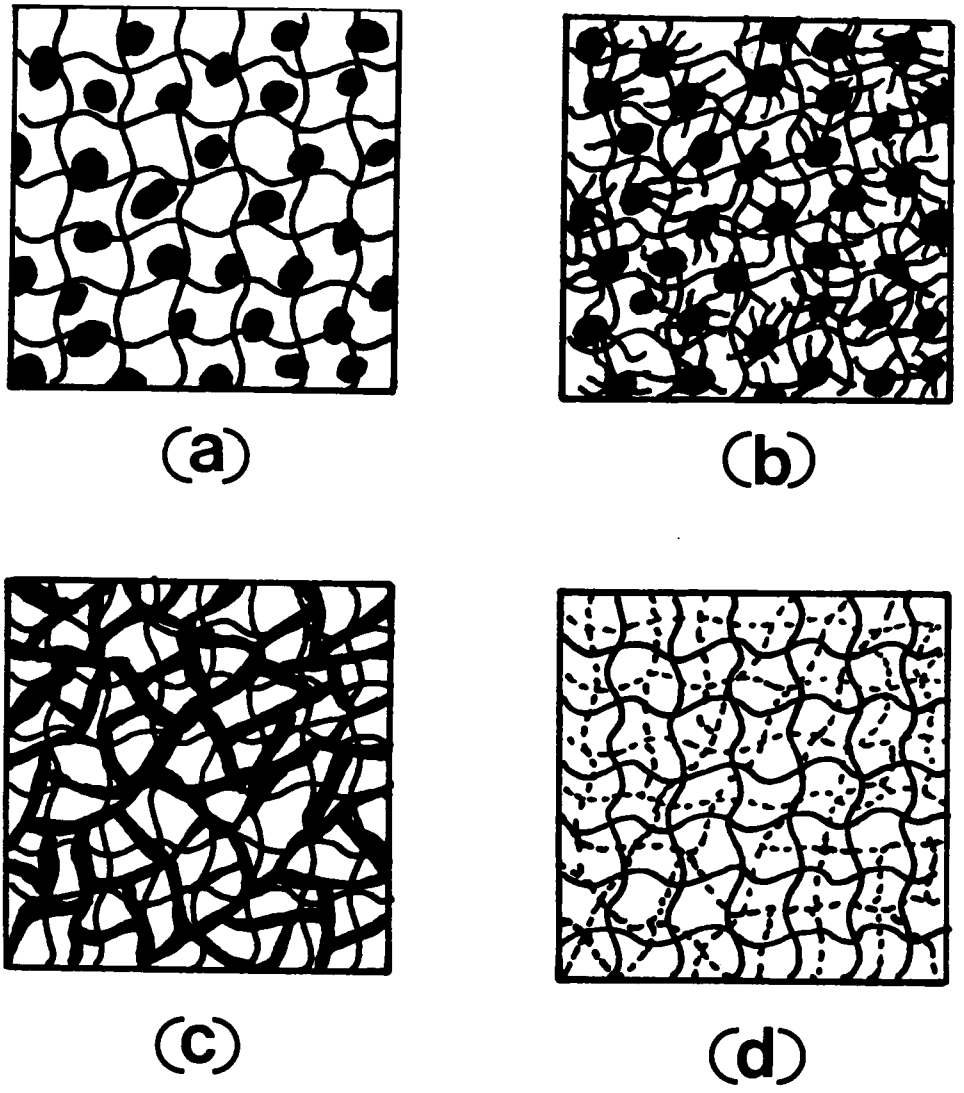

Figure 7.1. Schematic illustrations of possible morphological structures of NBR/bis-GMA symmetric systems.

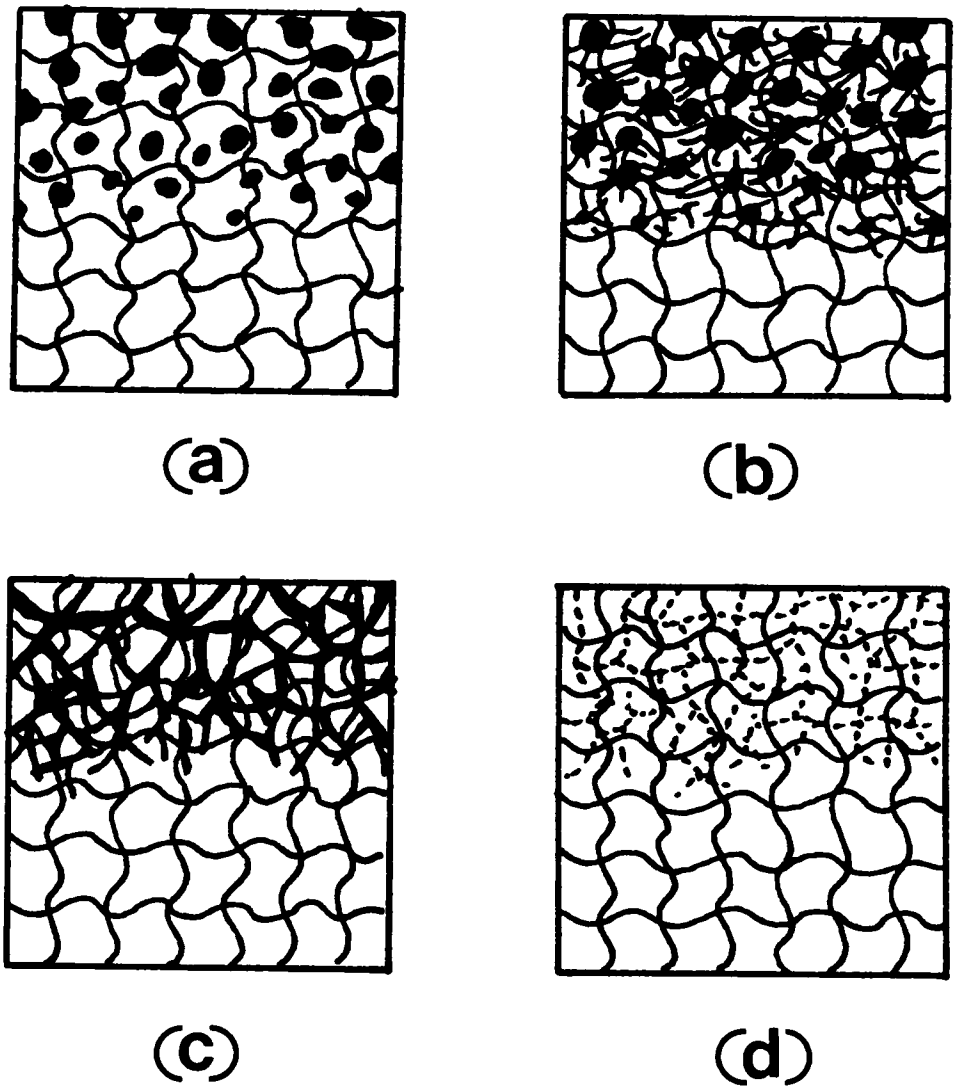

Figure 7.2. Schematic illustrations of possible morphological structures of NBR/bis-GMA asymmetric systems.

7.2 Materials and Experiments

7.2.1 Materials

Samples of a uncrosslinked acrylonitrile-butadiene copolymer(NBR, 40% acrylonitrile) were kindly provided by Dow Chemical Company. The number average molecular weight was 85,000 and its glass transition temperature was found to be ca. -20°C. This material was cured by EB irradiation and served as the crosslinked rubber matrix(the preparation of the crosslinked NBR is described later). Bis- GMA was obtained in the form of a viscous liquid from Freeman Chemicals(Nupol 46-4005). The chemical structures of these materials were shown in Figure 7.3. Tetrahydrofuran(THF) and acetone(HPLC grade) were purchased from Fisher Scientific.

7.2.2 Electron Beam Irradiation

Electron beam irradiation was carried out at room temperature under a nitrogen atmosphere with a maximum dose rate of 50 Mrad/sec. An electrocurtain accelerator manufactured by Energy Science, Inc. (model CB/150/115/180) was used throughout this study. The samples were placed on steel plates in aluminum trays and passed through the conveyor system of the electron beam instrument. The maximum available dose per pass was 20 Mrad, hence for the highest dosage used in this study(40 Mrad) two passes were required.

7.2.3 Preparation of Crosslinked NBR Film Samples

Thin films(4-5 mil in thickness) of the initially uncrosslinked NBR were prepared by first dissolving the NBR linear polymer in THF and casting at room temperature. These NBR films were then EB irradiated following the procedure mentioned above. The gel formation was evaluated by immersing and stirring the irradiated NBR film in THF for 72 hours and subsequently drying under vacuum for 72 hours. Figure 7.4 shows the influence of irradiation dose on the gel formation. It can be seen that, over the dose range studied, the gel percent reaches a value of approximately 90% at 30 Mrad. A further dose to 40 Mrad causes little increment in gel content. Hence, in this study, NBR film samples cured by an EB dose of 40 Mrad were utilized as the crosslinked rubber matrix without further extraction of the sol fraction(ca. less than 10%).

7.2.4 Swelling Procedures.

The dry extracted NBR gels were then immersed in bis-GMA solutions(in acetone) for controlled lengths of time. The swollen NBR samples were then removed from the solutions, gently wiped and dried under vacuum to a constant weight to remove the acetone. The weight uptake of bis-GMA was determined as follows:

$$\% \text{ wt. uptake} = \frac{\text{dried NBR wt. after swelling} - \text{initial NBR wt.}}{\text{initial NBR wt.}} \text{x100} \qquad [7.1]$$

This procedure was applied to the symmetrically swollen NBR films. The swelling behavior of these NBR gels in the bis-GMA solution(in acetone) as a function of time is

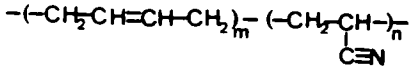

(a)

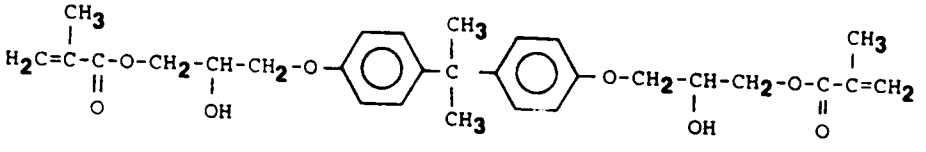

(b)

Figure 7.3. Chemical structures of acrylonitrile-butadiene copolymer(NBR) and bis-GMA.

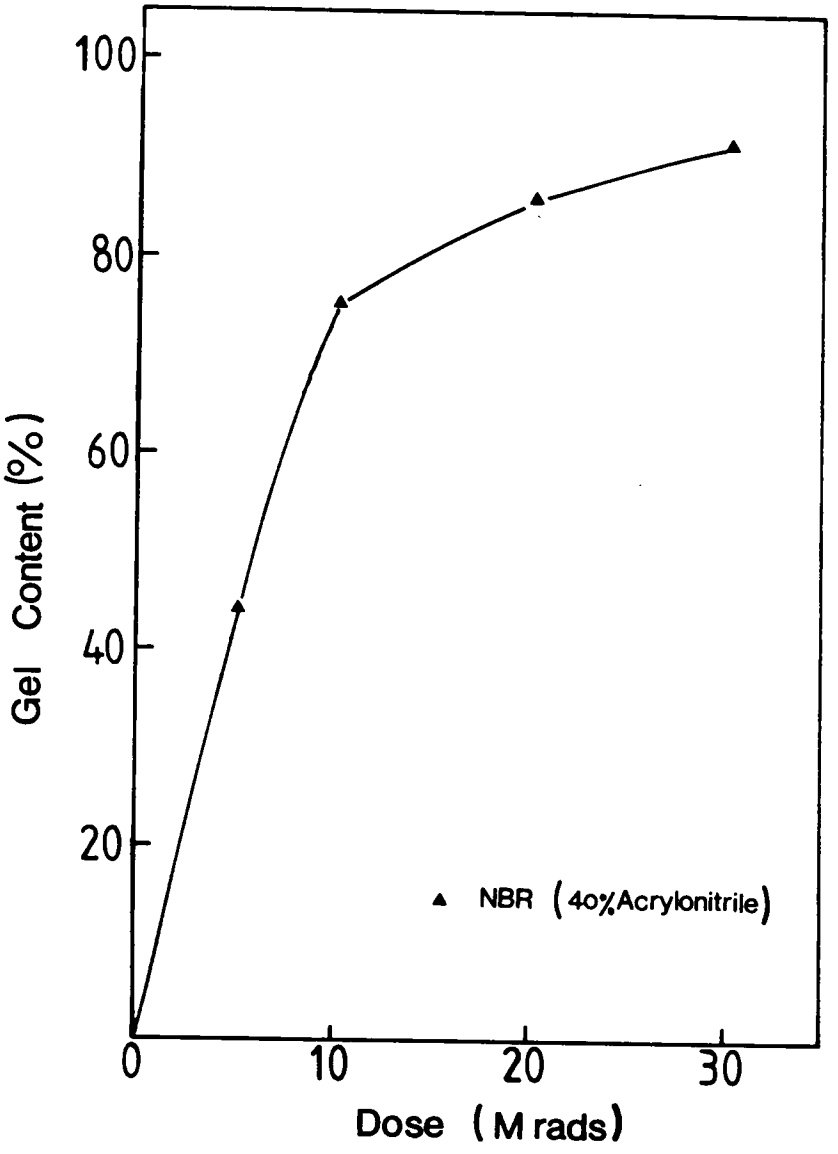

Figure 7.4. Effect of EB radiation dose on the gel formation of NBR.

presented in Figure 7.5 It is seen that the bis-GMA weight uptake by NBR gel film increases significantly by increasing the bis-GMA concentration in acetone up to 50%.

It is apparent that the time for equilibrium swelling of the NBR gel depends on the bis-GMA concentration. The equilibrium swelling time was found to increase from 5 minutes for the 5% bis-GMA solution to 120 minutes for the 50% solution. Based on the results presented in Figure 7.5, NBR films carrying 17%, 36%, 79% and 117% weight uptake of bis-GMA(these values based on the initial dry NBR weight) were prepared to be irradiated for the symmetric systems.

An asymmetric distribution or gradient structure of the bis-GMA through the NBR film was prepared by allowing the swelling solution to contact **only** the upper surface. The penetration(swelling) of the bis-GMA solution was controlled by leaving the bis-GMA solutions for a limited time that was less than the time to achieve equilibrium swelling. This controlled time is also dependent on the concentration of the swelling bis-GMA solution as shown previously in Figure 7.5. As an example, swelling times of 5 minutes for the 25% solution or 10 minutes for the 10% solution were utilized to obtain the asymmetric concentration gradient based on the results in Figure 7.5. The partially swollen NBR film was immediately exposed to EB irradiation after the excess solution on the upper film surface had been gently wiped away.

7.2.5 Mechanical Properties

The irradiated samples were tested to determine Young's modulus, elongation and tensile strength at break at ambient temperature. Samples were cut with a die in a dog-bone

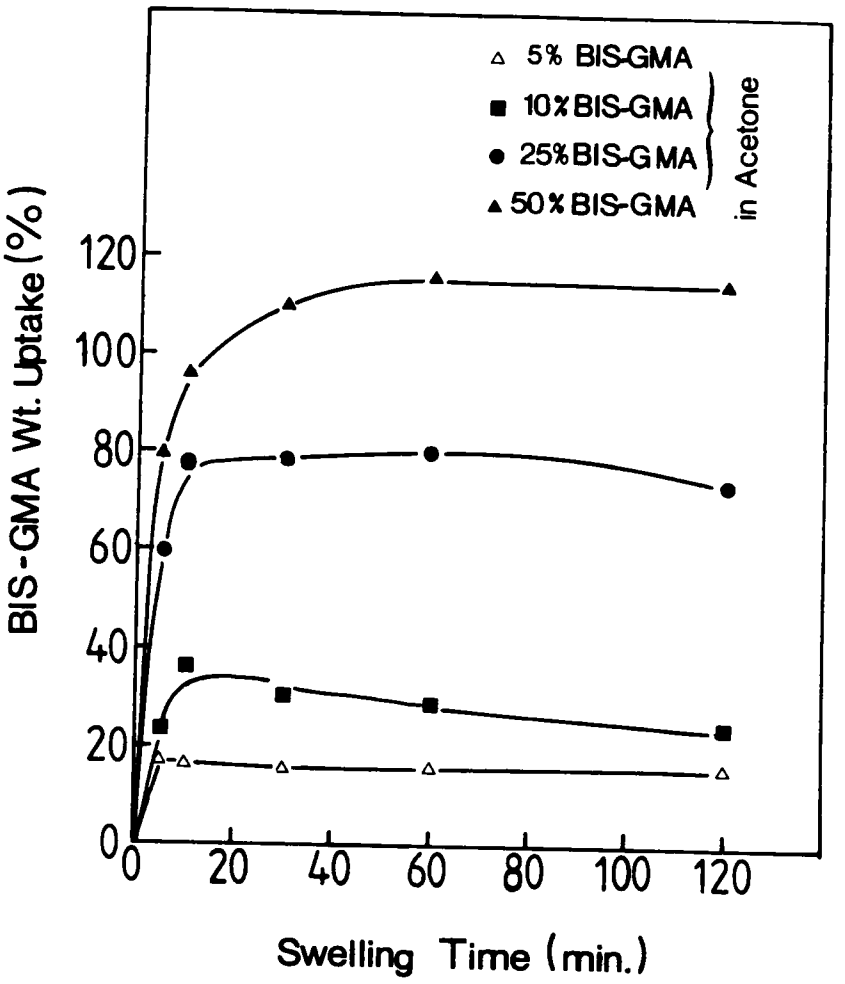

Figure 7.5. Swelling behavior of crosslinked NBR in solutions containing different concentrations of bis-GMA.

shape with the initial dimensions being 10 mm in gauge length and 2.8 mm in width. An Instron tensile tester(model 1122) was used with an extension rate of 50% per minute based on the initial sample length. Young's modulus was calculated from the initial slope of the stress-strain curves. The tensile strength was obtained at the break point. Dynamic storage and loss moduli(E′ and E″) as well as tanδ were determined as a function of temperature using an Autovibron Dynamic Viscoelastometer. These samples were run from - 40°C to 200°C to investigate the thermal transition behavior with a scanning rate of 2°C per minute at a frequency of 11 Hz.

7.2.6 Thermal Properties

Differential Scanning Calorimetry(DSC) measurements were performed using a Perkin-Elmer DSC-4 Calorimeter equipped with a TADS data station. An indium standard was utilized to calibrate the temperature scale. A heating rate of 10°C/min was used and the determinations were performed under a nitrogen atmosphere. A given sample was run from 15°C up to 75°C-this initial scan being labelled "first run." After that sample was cooled to 15°C with a cooling rate of 10°C/min, the sample was reheated to 75°C at the same scan rate. This scan was labelled "second run."

7.2.7 Scanning Electron Microscopy(SEM) Analysis

The morphological structure of the EB irradiated NBR systems was investigated using scanning electron microscopy(SEM) of fractured surfaces. The SEM micrographs were taken with a Cambridge Stereoscan 200 instrument. The EB irradiated NBR/bis-GMA

samples were first fractured in liquid nitrogen and then sputter coated with gold. The SEM technique was utilized as one means to investigate the symmetric and asymmetric distributions of crosslinked bis-GMA occurred inside the NBR matrix.

7.2.8 FTIR Microscopy Analysis

Symmetric and asymmetric distributions of bis-GMA inside the NBR film were investigated using a FTIR spectrometer(Nicolet model 5DXB) equipped with a Spectra-Tec IR-PLAN infrared microscope. The movable apertures were set to 40 microns by 40 microns in size. First, a NBR film was precisely cut in a direction perpendicular to the film surface resulting in a strip which is 125 microns(5 mils) in the original film thickness and a thickness(125 microns) in the direction perpendicular to the cross-section surface. Next, the original film thickness of the NBR film(ca. 125 microns)was divided into three regions(ca. a 40μ x 40μ square for each region)-these being called "lower," "middle," and "upper" regions in an order moving from the bottom to the top of the NBR film facing the cross-section. A schematic of the NBR film prepared for FTIR microscopy is shown in Figure 7.6 which illustrates the details of the analysis. A FTIR spectrum was obtained for each region and analyzed for the relative concentration distribution of bis-GMA throughout the thickness of NBR film. The phenyl peaks(1583 and 1608 cm^{-1}) from the presence of bis-GMA were normalized to the nitrile peak(2235 cm^{-1}) to account for variations in sample thickness.

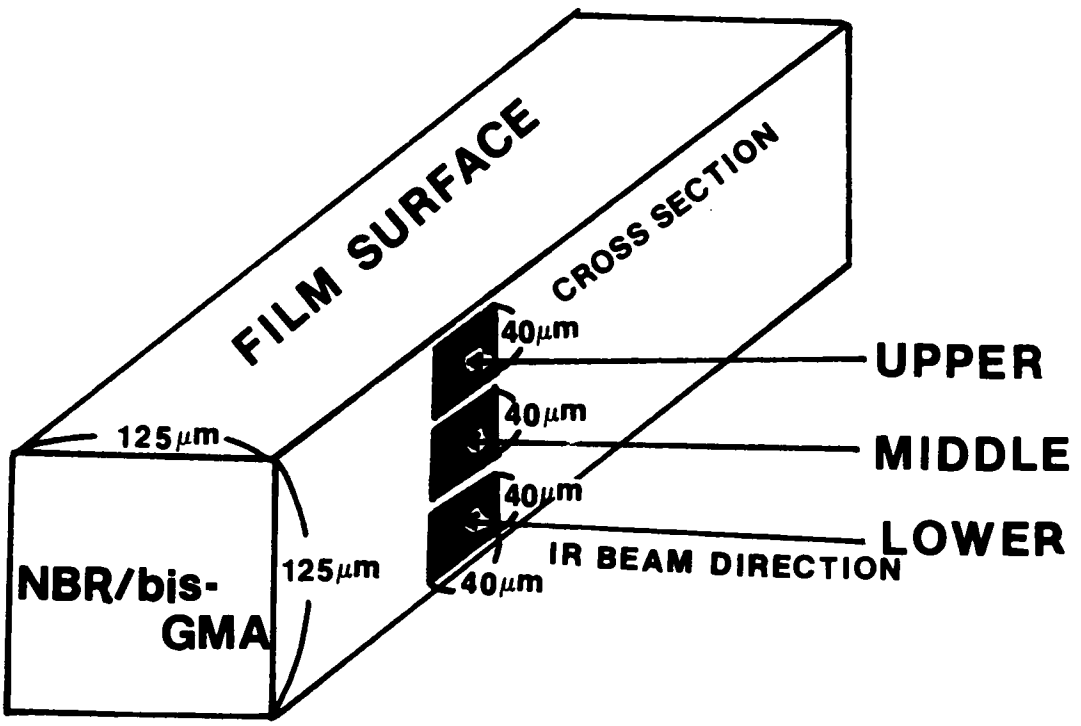

Figure 7.6. A schematic of the NBR sample prepared for the FTIR microscopy analysis.

7.2.9 Optical Microscopy Analysis

A Zeiss polarizing microscope equipped with a 35 mm camera was utilized to investigate the symmetric and asymmetric distributions of bis-GMA inside the NBR film. Thin strip samples of 5 mils in the original film thickness and 5 mils in the thickness perpendicular to the cross-section surface(as described in Section 7.2.8) were stretched to 30% elongation using the Instron. The stretched samples were then immediately released relieving the mechanical strain on the NBR samples. The cross-section of the sample prepared as above was investigated with a cross-polarized microscope.

7.3 Results and Discussion

7.3.1 Symmetric Distribution of bis-GMA

7.3.1.1 Mechanical Properties

The mechanical properties of the EB radiation prepared NBR/bis-GMA films are shown in Figures 7.7, 7.8 and 7.9. Figure 7.7 presents the tensile strength of NBR/bis-GMA systems as a function of bis-GMA content. In this plot, the zero point in the x-axis represents 100% NBR. It is clear that the tensile strength of the prepared material is significantly enhanced by increasing the bis-GMA content in the material. On the other hand, the elongation at break decreases dramatically as might be expected by increasing bis-GMA content as shown in Figure 7.8. Moreover, Young's modulus is markedly increased by increasing bis-GMA content in the prepared material as illustrated in Figure

7.9. The increase in tensile strength and modulus upon increasing bis-GMA content can be explained on the basis of increasing the level of crosslinked bis-GMA material in the NBR matrix. This increased content reinforces the rubber phase and causes the decrease in elongation at break.

7.3.1.2 Dynamic Mechanical Properties

The EB curing process of an initially homogeneous mixuture of epoxy resin(bis-GMA) and rubber(NBR matrix) can be generally represented by the sequential processes-these being phase separation, gelation and vitrification. As the molecular weight of bis-GMA increases, the system undergoes in-situ phase separation due to the lowered compatibility between the NBR and the bis-GMA. Phase separation is generally terminated due to vitrification by which the crosslinking reaction becomes diffusion limited. These phenomena can be discussed in terms of the well-known time-temperature-transformation(TTT) diagram(9) with the concept being applied in this laboratory to radiation curing(10). These latter studies suggest that the free radicals trapped in the reacting network(bis-GMA) due to vitrification exhibit a finite lifetime. When a dynamic mechanical test is performed on a pure EB cured(5 Mrad) bis-GMA with an aging time of a relatively short period(eg. one hour), two tanδ peaks may exist-a weak one at about 55°C and the other at ca. 160°C(10). This can be explained in terms of the TTT diagram as mentioned above. As the temperature scan proceeds in the dynamic mechanical tests, the cure temperature from the EB radiation process is surpassed. At this point, the material physically softens and simultaneously the bis-GMA molecules acquire chain mobility such that that the activated species(e.g. trapped free radicals) can continue the crosslinking reaction-the combination of these two processes resulting in a

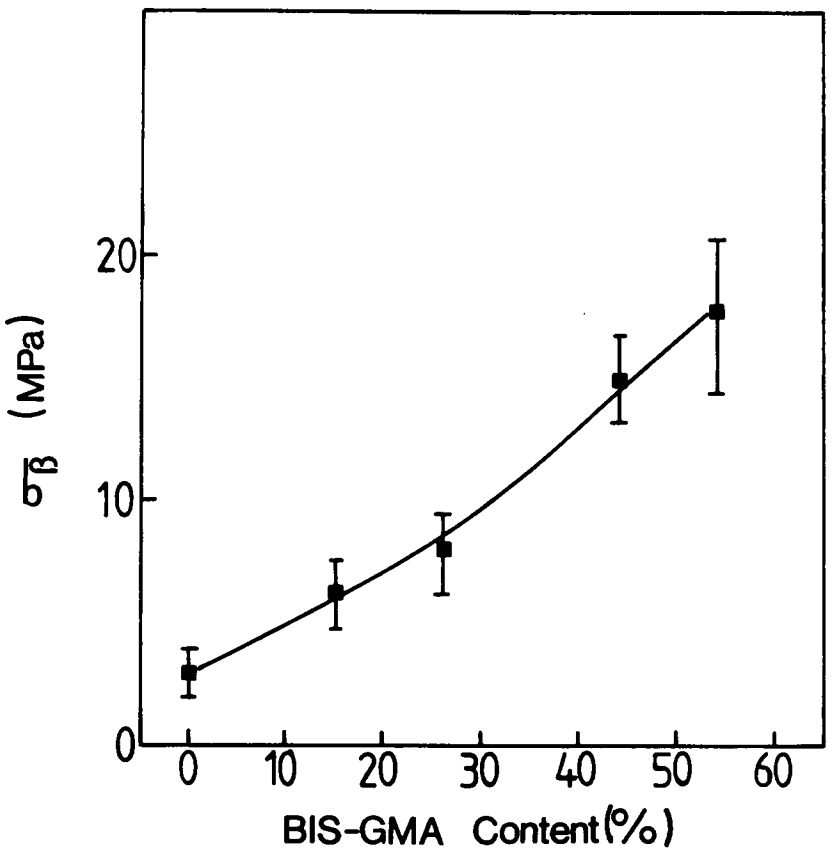

Figure 7.7. Tensile strength at break as a function of bis-GMA content in the NBR/bis-GMA symmetric system.

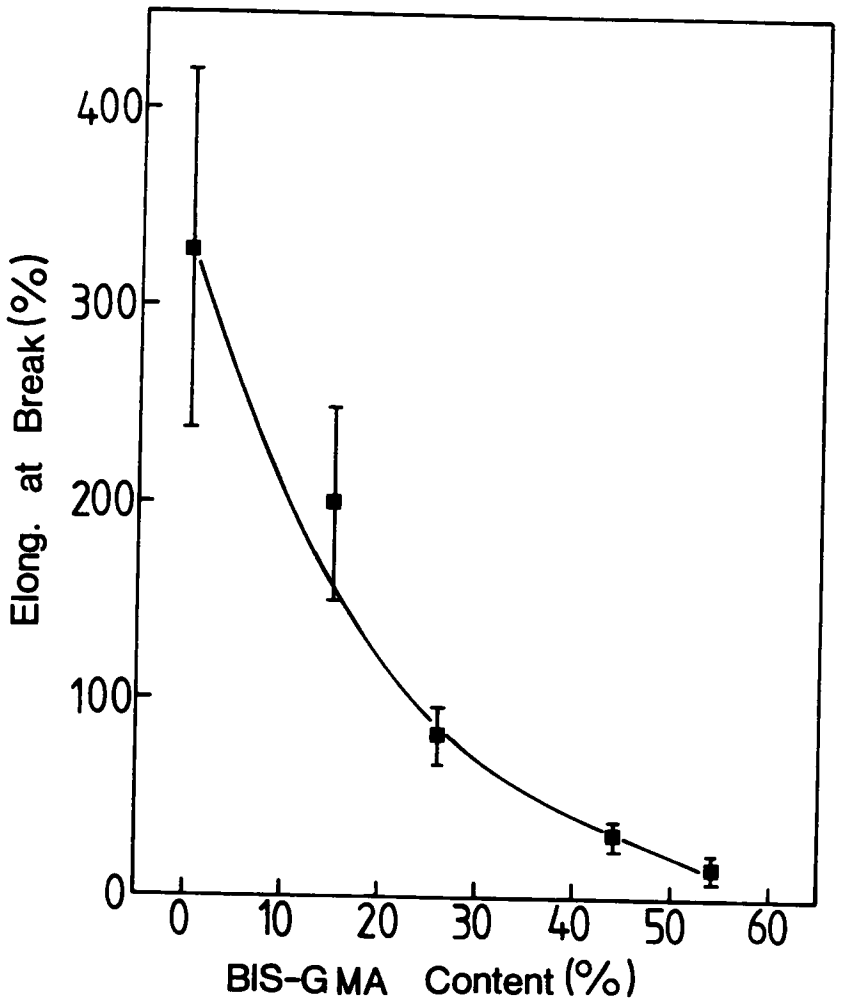

Figure 7.8. Elongation at break as a function of bis-GMA content in the NBR/bis-GMA symmetric system.

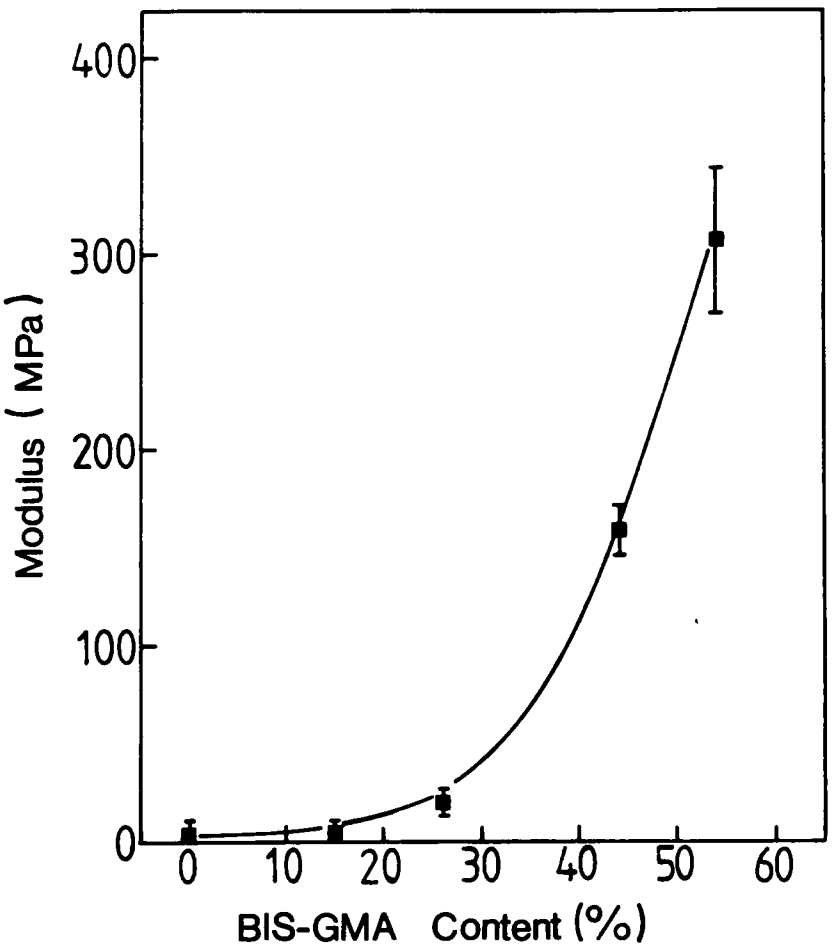

Figure 7.9. Young's modulus as a function of bis-GMA content in NBR/bis-GMA symmetric system.

weak tanδ peak. Another tanδ peak exists at a higher temperature. That is, the continued chemical crosslinking after the initial softening point(ca. 55°C) during the relatively slow temperature scan(e.g. 2°C per minute) provides the bis-GMA with a near glassy modulus until the rate of reaction slows down at a higher temperature(ca. 160°C) where another tanδ peak occurs. This decrease in reaction rate is caused by the depletion of a sufficient concentration of reactive moieties(bis-GMA) in close proximity. However, in the case of longer aging times after EB irradiation(eg. 120 hours), the trapped free radicals recombine and/or are scavenged(likely by oxygen) such that the amount of further crosslinking during the temperature scan is reduced resulting in the second tanδ peak at lower temperature in comparison to the case of the sample without aging. Details on these aspects were shown in a previous study from this laboratory(10,11). The NBR/bis-GMA material for the dynamic mechanical analysis in this study were aged at least for several days, and therefore the material may soften(the second transition) at a slightly lower temperature(< 160°C for the 5 Mrad irradiated sample). This second Tg(maximum in tanδ peak) hereafter is referred as the Tg of the EB cured bis-GMA component in the NBR/bis-GMA system.

Dynamic mechanical tests were performed on the EB prepared NBR systems to illustrate the existence of a symmetric distribution and possible phase separation of bis-GMA in the NBR matrix. Figures 7.10 and 7.11 show the temperature dependence of the storage modulus and tanδ for the systems containing different contents of bis-GMA prepared at 5 and 10 Mrads, respectively. From these dynamic mechanical spectra, two principal transitions can be identified. The lowest is due to the NBR glass transition which occurs around 0°C(maximum in tanδ). This transition is in agreement with the Tg obtained for crosslinked pure NBR as shown in Figure 7.10. A second transition occurs between 120 °C and 150°C(the location of this transition depends on the exact preparation condition

as discussed earlier) which is attributed to the glass transition temperature of the irradiated pure bis-GMA.

The observation of two distinct transitions clearly suggests the occurrence of considerable phase separation of bis-GMA from the NBR phase during the EB curing process. It is obvious from the storage modulus plots(Figure 7.10) that pure NBR initially shows a lower modulus in comparison to the bis-GMA/NBR systems and, above the lower Tg(NBR), all samples display a rubbery plateau value. The modulus value for the rubbery plateau tends to increase with increasing bis-GMA content as can be expected. It was shown that the NBR system containing 26% bis-GMA does not show distinct Tg characteristics for the bis-GMA component but rather displays a peak-broadening as shown in Figures 7.10 and 7.11. This significant broadening of the transition at the higher temperature in the NBR system may arise from some degree of grafting reaction between NBR and bis-GMA and/or mixing of the two component networks. If grafting occurs, it likely occurs simultaneously with the crosslinking of bis-GMA component within the NBR matrix. The Tg(tanδ peak) of NBR is found to increase from -8°C at 5 Mrad to 2°C at 10 Mrad for the NBR sample of 26% bis-GMA. Also, the glass transition of the bis-GMA component in the systems having bis-GMA contents of 44% and 54% was found to increase with increasing radiation dose indicating that the amount of cure of the bis-GMA is proportional to radiation dosage-again, an expected outcome. A summary of these results is presented in Table 7.1 showing the effects of radiation dose and bis-GMA content on the dynamic mechanical properties.

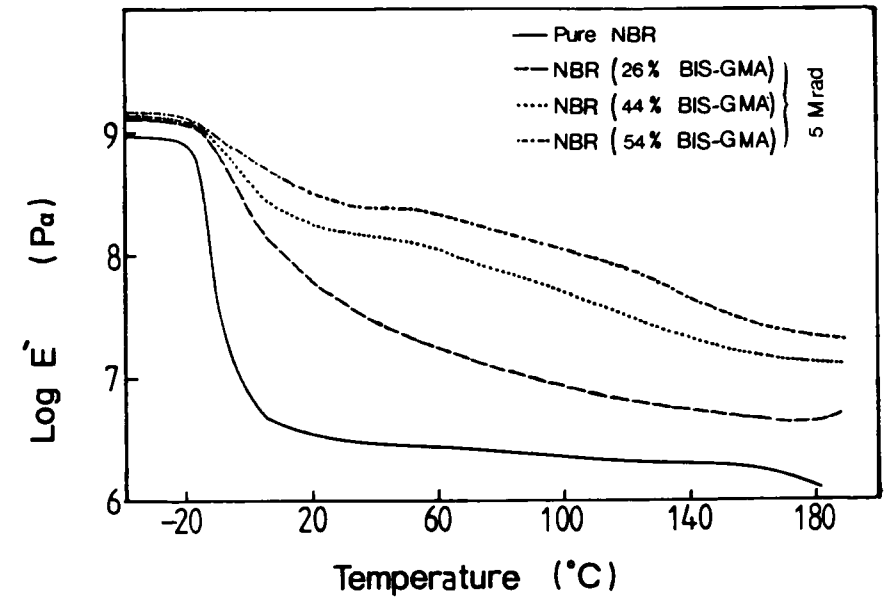

(a)

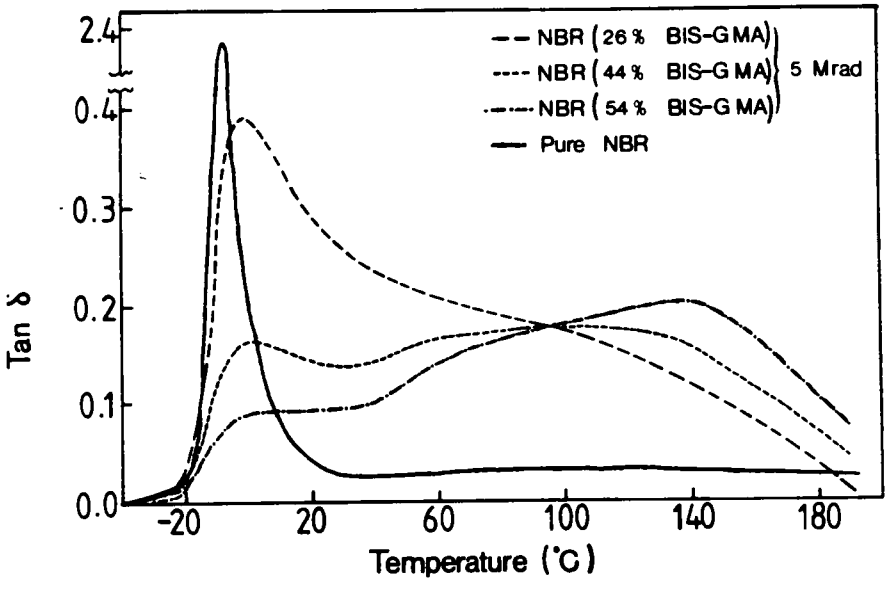

(b)

Figure 7.10. **Dynamic mechanical analysis of the symmetric NBR/bis-GMA(5 Mrad) system.:** Temperature dependence of (a)storage modulus(E') and (b)tanδ.

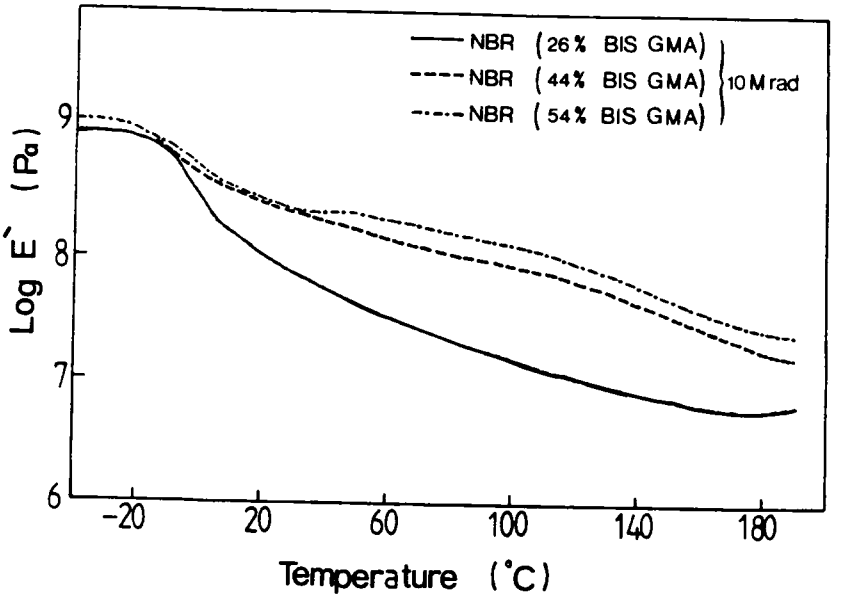

(a)

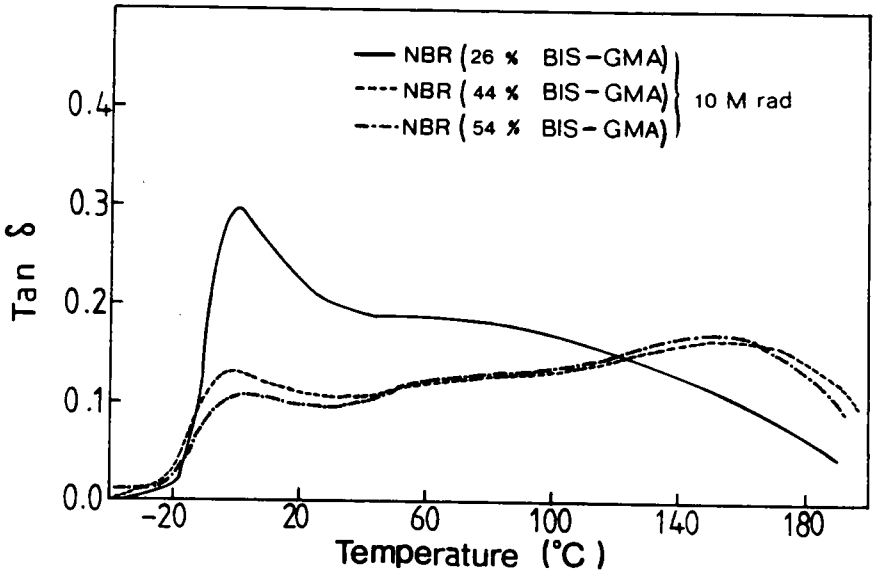

(b)

Figure 7.11. Dynamic mechanical analysis of the symmetric NBR/bis-GMA(10 Mrad) system.: Temperature dependence of (a)storage modulus(E′) and (b)tanδ.

Table 7.1. Dynamic mechanical and thermal properties of NBR/bis-GMA symmetric systems.

bis-GMA content(%)	EB radiation dose(Mrad)	NBR glass transition(C)	bis-GMA glass transition(C)	Exothermic heat,ΔH(cal/g)
26	5	-8	--	79.3
	10	2	--	53.0
44	5	0	117	290.9
	10	-2	156	249.1
54	5	0	136	484.2
	10	2	156	351.0

7.3.1.3 Thermal Analysis

Figure 7.12 represents the DSC thermograms for pure NBR(40 Mrad) and NBR systems with different bis-GMA contents. All samples were aged at room temperature for 1 hour prior to the DSC test. In general, the exothermic behavior is only observed for samples having higher bis-GMA contents than 15%. Table 7.1 also shows the heat of the exotherm, ΔH, as calculated from the exothermic peak area for NBR/bis-GMA systems prepared at 5 and 10 Mrad. It is obvious that the total area increases by increasing the bis-GMA content and decreases by increasing the dosage from 5 to 10 Mrad as shown in Table 7.1. This exotherm can be easily explained as a result of the further crosslinking of bis-GMA which occurs from trapped free radicals formed during EB irradiation and crosslinking from thermally induced opening of double bonds during the DSC experiments. These findings were confirmed by a second DSC scan which shows no exothermic peak but only a "flat" response. Moreover, these results are in accordance with a previous study from this laboratory which showed that the exotherm at higher temperature occurs from the thermally induced reaction of residual double bonds in bis-GMA(11).

7.3.1.4. Scanning Electron Microscopy(SEM) Analysis

A SEM micrograph of the fractured surface of the NBR/bis-GMA material having 20 percent of bis-GMA content is shown in Figure 7.13. Small particles dispersed throughout the fractured surface of NBR matrix indicating that some amount of the bis-GMA has phase-separated although the volume percent of the particles by themselves clearly do not appear to represent the amount of 20% bis- GMA content. As can be expected, some portion of bis-GMA which may not have participated in the phase separation

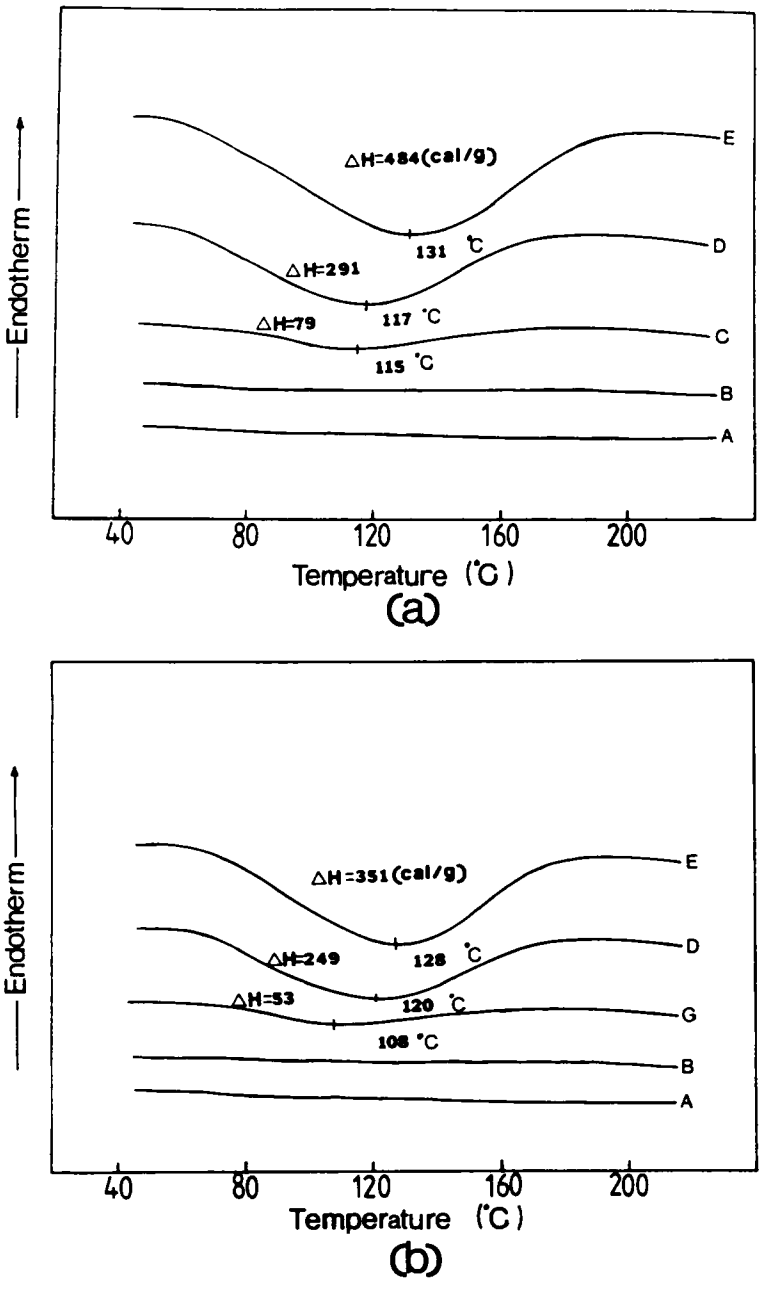

Figure 7.12. DSC scans of NBR/bis-GMA symmetric systems prepared at (a)5 Mrad and (b)10 Mrad.: (A)pure crosslinked NBR and NBR/bis-GMA containing (B)15%, (C)26%, (D)44%, and (E)54% bis-GMA.

would remain dispersed as might be suggested by the morphological texture given earlier in Figure 7.1(b).

7.3.2 Asymmetric Distribution of bis-GMA

7.3.2.1 Mechanical Properties

Mechanical properties of the asymmetric or gradient NBR/bis- GMA systems having different bis-GMA content(10%, 20%, 35%) are shown in Table 7.2. These materials were prepared by subjecting one surface of the NBR film to bis-GMA solution for 5 minutes, quickly removing any excess solution from the surface, followed immediately by EB irradiation at a 10 Mrad dose. As expected, the tensile strength at break as well as the Young's modulus again increased by increasing bis-GMA content, while the elongation at break decreases.

7.3.2.2 Dynamic Mechanical Properties

Figures 7.14 (a) and (b) show the temperature dependence of the storage modulus and damping(tanδ) for three asymmetric NBR/bis-GMA samples having different contents of bis-GMA. The transition at lower temperatures(-10°C to 0°C) is distinct and it arises from the NBR phase as previously discussed. On the other hand, the second transition which is due to the presence of bis-GMA in the NBR material occurs from 50°C to 120 °C. In comparison to the dynamic mechanical spectra of the symmetric system(Figure 7.11), the tanδ peaks of the higher or second transition are significantly broadened and somewhat shifted to lower temperature. In order to explain this, the anticipated

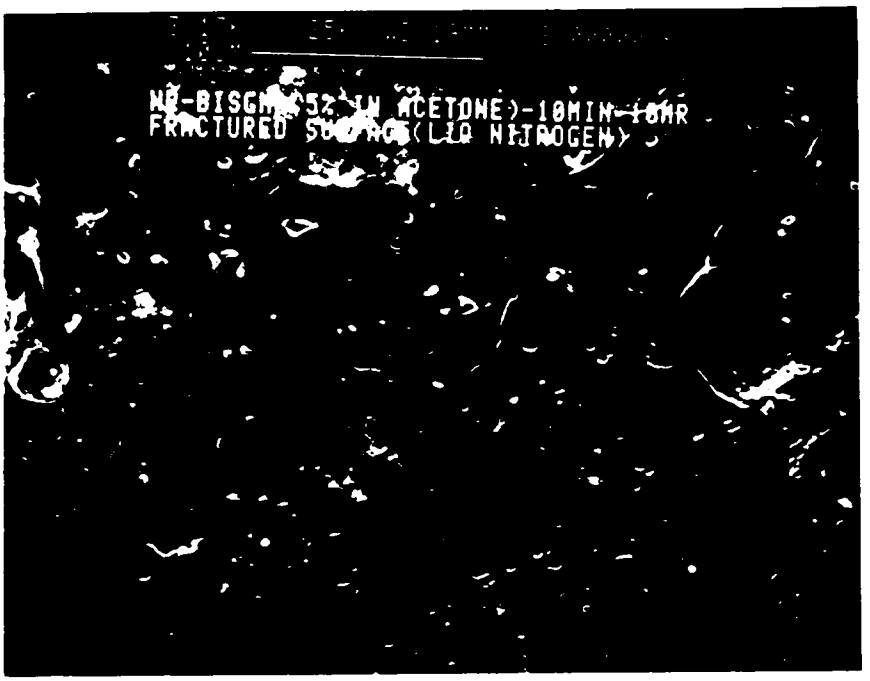

Figure 7.13. SEM photograph of fractured cross-section of the NBR/bis-GMA symmetric system.

Table 7.2. Mechanical properties of NBR/bis-GMA asymmetric systems.

bis-GMA content(%)	Tensile strength(MPa)	Young's modulus(MPa)	Elongation at break(%)
10	3.4	6.7	117
20	3.6	12.5	61
35	4.9	13.1	73

morphological structure of the NBR/bis-GMA should be described. In any of these films, it is expected to have a concentration distribution of bis-GMA across the NBR matrix. At the upper surface where the bis-GMA solution was initially introduced, both NBR and bis-GMA phases should be present and then gradually the concentration of bis-GMA should decrease in the direction as the bottom surface is approached. Therefore the significant broadening of the second transition shown in Figure 7.14 is tentatively attributed to the gradient structure in sample morphology. However, further support for this speculation will be provided later.

7.3.2.3 Scanning Electron Microscopy Analysis

Shown in Figure 7.15 is a SEM of the fractured surface of a NBR/bis-GMA samples possessing a asymmetric distribution. Small particles dispersed near the upper surface of the NBR matrix indicate that a considerable amount of the bis-GMA has phase-separated. It also shows a "concentration gradient" distribution of the phase-separated bis-GMA particles across the NBR film "thickness" supporting the earlier discussion. Therefore, this SEM micrograph strongly indicates that an asymmetric distribution of bis-GMA phase has resulted with a certain degree of phase- separation as proposed previously.

7.3.2.4 FTIR Microscopy Analysis

Table 7.3 shows the results obtained from the FTIR microscopy investigation which clearly illustrates the distribution of the bis-GMA in the NBR/bis-GMA material. Two peaks at the respective wavelengths of 1583 and 1608 cm^{-1} due to the presence of the

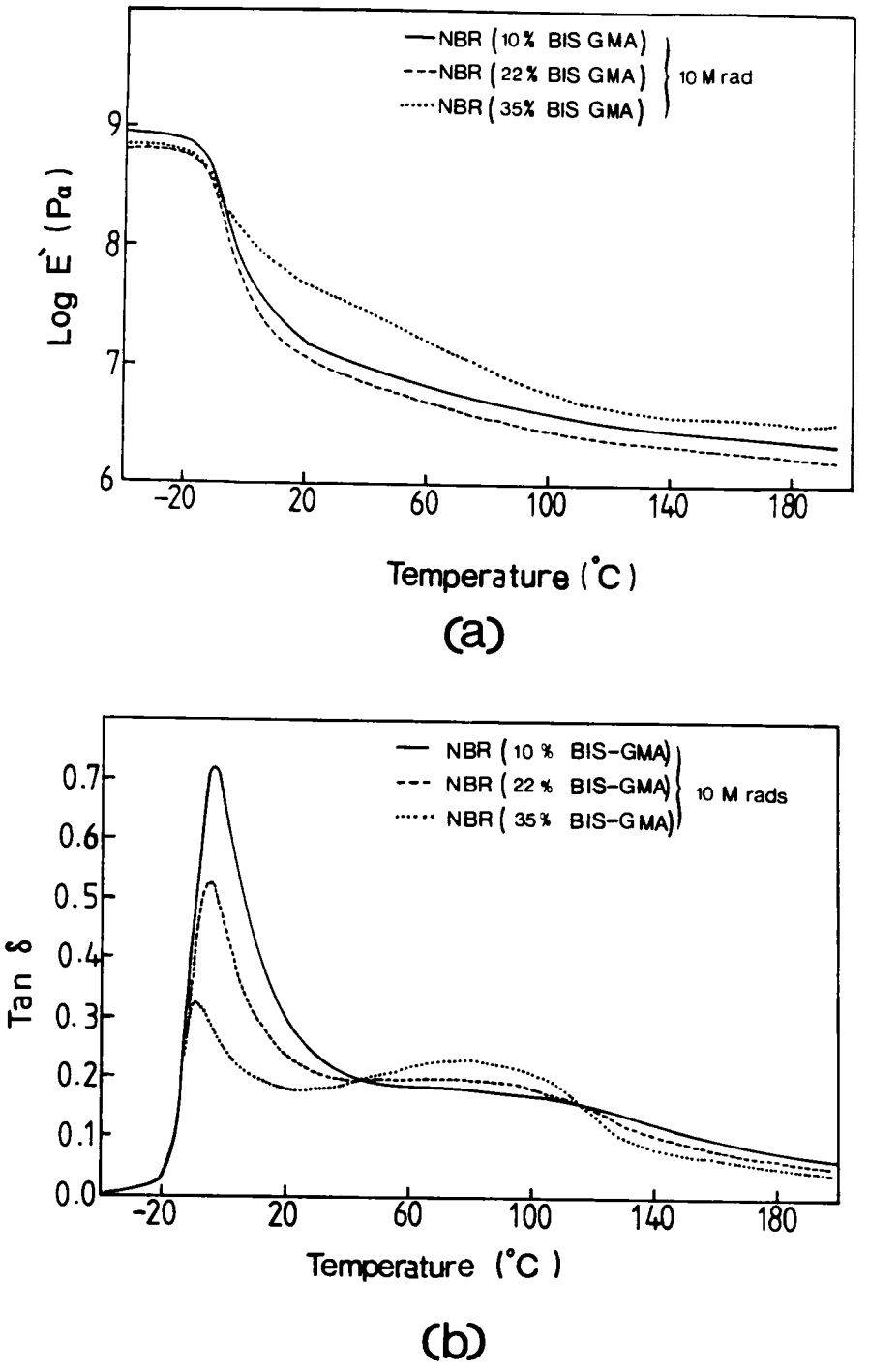

Figure 7.14. Dynamic mechanical analysis of the asymmetric NBR/bis-GMA(10 Mrad) system.: Temperature dependence of (a)storage modulus(E′) and (b)tanδ.

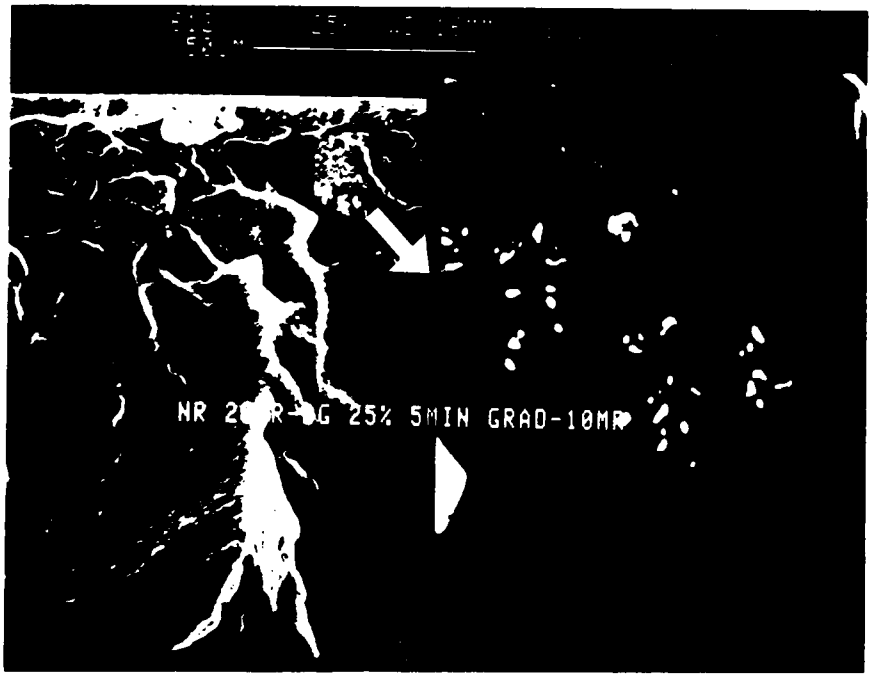

Figure 7.15. SEM photograph of fractured cross-section of the NBR/bis-GMA asymmetric system.

phenyl ring in bis-GMA were normalized to the peak at 2235 cm^{-1}(-CN) from the NBR material and these ratios are shown for the three regions, "upper," "middle," and "lower"-these being schematically shown in Figure 7.5 and explained earlier.

For the asymmetric systems, the concentration of bis-GMA decreases gradually from the upper(near surface) region to the lower region(near bottom) as demonstrated by a decreasing phenyl ring content. This decreasing tendency was shown from both peaks at 1583 and 1608 cm^{-1}. These data from FTIR microscopy analysis affirm the earlier more indirect dynamic mechanical as well as SEM results supporting our discussion that a gradient or asymmetric distribution in the NBR film was present.

7.3.2.5 Optical Microscopy Analysis

Cross-polarized optical micrographs were taken to observe the cross-sections of the symmetric and asymmetric NBR/bis-GMA films. As discussed earlier in Section 7.2.9, the samples were stretched to 30% elongation followed by immediate release of the strain prior to the microscopy studies. The purpose of this stretching and releasing procedure was to generate mechanically induced residual anisotropy(chain orientation) in the NBR/bis-GMA systems. Pure NBR material displays optical anisotropy when it is stretched, however this ansotropy disappears immediately after the mechanical strain is released reflecting the loss of orientation. In contrast, the NBR/bis-GMA retains the optical anisotropy after the mechanical strain is released due to the glassy nature of the EB cured bis-GMA distributed inside the NBR film which prevents the NBR matrix from recovering its initial dimension in a relatively short time period. This preparation procedure generating the mechanically induced residual anisotropy was ex-

Table 7.3. FTIR microscopy data for the NBR/bis-GMA systems.

sample	analysis region	peak1(2235/cm)	peak2(1583/cm) (peak2/peak1)	peak3(1608/cm) (peak3/peak1)
asymmetric	upper	1.73	0.29 (0.17)	0.83 (0.48)
	middle	2.25	0.23 (0.10)	0.61 (0.27)
	lower	2.42	0.17 (0.07)	0.42 (0.17)

pected to help demonstrate the symmetric and asymmetric distribution pattern of bis-GMA in the NBR matrices.

Figure 7.16(a) and 7.16(b) show the cross-polarized optical micrographs of the cross-sections of the symmetric and asymmetric NBR films, respectively. The symmetric sample(Figure 7.16(a)) shows a brightness(anisotropy) evenly distributed across the NBR film indicating that bis-GMA is symmetrically distributed. In striking contrast, the asymmetric sample shown in Figure 7.16(b) resulted in a gradient of the induced anisotropy across the NBR film.

The bright surface region and the decreasing brightness toward the bottom surface obviously demonstrate that a gradient concentration distribution of bis-GMA was obtained for the asymmetric system. Although these observations on the distribution of the mechanically induced anisotropy are qualitataive, they clearly represent the distribution pattern of bis-GMA inside the NBR matrix. Hence, the results of this investigation are in strong agreement with thermal, mechanical, SEM as well as FTIR microscopy analysis.

7.4 Conclusion

"Symmetric" and "asymmetric" systems based on the controlled distribution of the bis-GMA into a network acrylonitrile-butadiene copolymer(NBR) were prepared utilizing electron beam(EB) radiation. In the symmetric system, the crosslinked NBR was swollen to equilibrium in bis-GMA solution followed by EB irradiation. In the case of asymmetric system, only one surface of the EB crosslinked NBR film was exposed to a

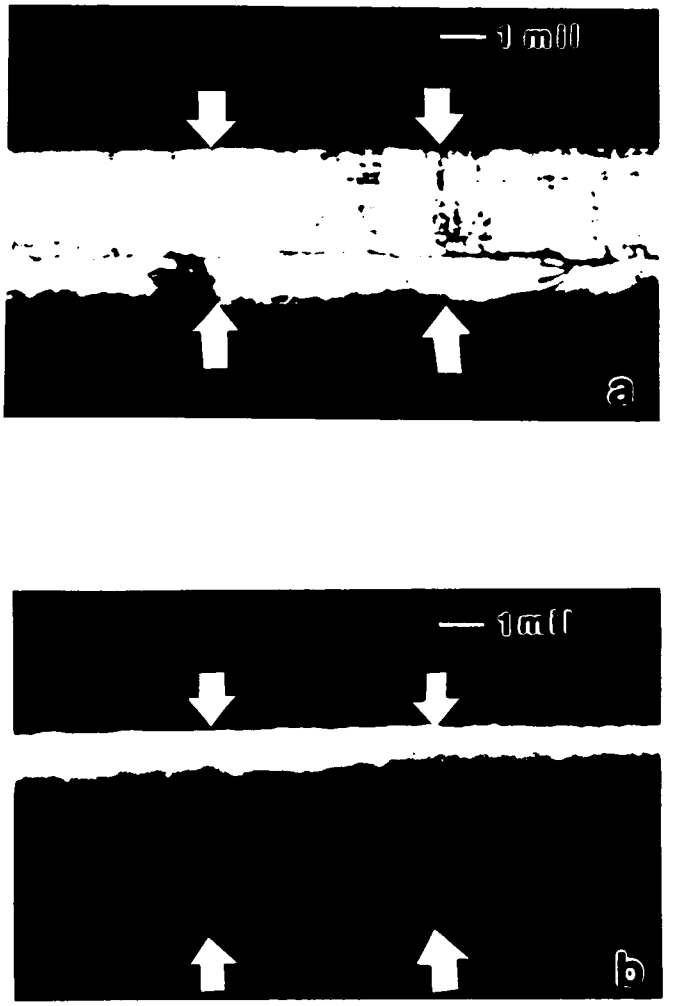

Figure 7.16. Cross-polarized optical micrographs showing the cross-sections of (a)symmetric and (b)asymmetric NBR/bis-GMA samples.

bis-GMA solution for a limited time that was less than the time to achieve a uniform concentration profile in the swelling direction. The asymmetrically swollen NBR film was then immediately cured by EB irradiation. The mechanical tests showed that the final properties were strongly dependent on the bis-GMA content of NBR/bis-GMA systems. The dynamic mechanical studies showed the presence of two major transitions suggesting a considerable degree of phase separation of bis-GMA inside the NBR matrix for both symmetric and asymmetric systems. The prepared symmetric and asymmetric distributions of bis-GMA in the NBR/bis- GMA systems were demonstrated by dynamic mechanical tests as well as by FTIR, SEM and optical microscopy analyses.

References

1. Frisch, K. C.; Frisch, H. L.; Klempner, D.; Mukherjee, S. K. *J. Appl. Polym. Sci.* 1974, *18*, 689.

2. Sperling, L. H. *Interpenetrating Polymer Network and Related Materials* Plenum, New York, 1982.

3. Yeo, J. K.; Sperling, L. H.; Thomas, D. A. *Polymer* 1983, *24*, 307.

4. Akovali, G.; Biliyar, K.; Shen, M. *J. Appl. Polym. Sci.* 1976, *20*, 2419.

5. Yamakawa, S.; Yamamoto, F. *J. Appl. Polym. Sci.* 1978, *22*, 2459.

6. Yamamoto, F.; Yamakawa, S. *J. Polym. Sci., Polym. Phys. Ed.* 1979, *17*, 1581.

7. Shen, M.; Bever, M. B. *J. Mater. Sci.* 1972, *7*, 741.

8. Riew, C. K. *Rubber Chem. Technol.* 1981, *54*, 374.

9. Chan, L. C.; Nae, J. K.; Gillham, J. K. *J. Appl. Polym. Sci.* 1984, *29*, 3307.

10. Thompson D. *Ph.D. Thesis* VPI&SU, 1986.

11. Thompson, D.; Song, J. H.; Wilkes, G. L. *J. Appl. Polym. Sci.* 1987, *34*, 1063.

Appendix A. Relationship between Glass Transition Temperature(Tg) and Degree of Crosslinking Reaction

Glass transition temperature(Tg) of a polymeric system generally increases with an increasing number of crosslinks. Studies to establish a relationship between the Tg and the degree of crosslinking reaction have shown to be relatively complex and strongly dependent on the type of the system. Especially, in radiation crosslinking processes, complicating factors include the chemical compositions and the reaction mechanisms of the prepolymer, polymer and additives such as crosslinking agents, etc. In the earlier stages of crosslinking reaction, the increase of Tg may not be significant in most cases, however in the later stages of polymerization the system includes an appreciable amount of the generated polymeric species resulting in continuous Tg increase with conversion.

Kelly and Bueche(1) proposed a relation based on the free volume theory as follows:

$$T_g = \frac{\alpha_p \phi_p T_{g,p} + \alpha_m (1 - \phi_p) T_{g,m}}{\alpha_p \phi_p + \alpha_m (1 - \phi_p)} \qquad [A.1]$$

where

T_g = glass transition temperature of the reacting system

$T_{g,p}$ = glass transition temperature of polymer

$T_{g,m}$ = glass transition temperature of monomer

ϕ_p = volume fraction of polymer

ϕ_m = volume fraction of monomer

α_p = difference in volume expansion coefficient above and below Tg of polymer

α_m = difference in volume expansion coefficient above and below Tg of monomer

Utilizing the conversion of polymerization, (1-x), where x is the fraction of residual functional groups as discussed in Chapter 5, the volume fraction of polymer can be expressed as follows:

$$\phi_p = \frac{d_m(1-x)}{d_p x + d_m(1-x)} \qquad [A.2]$$

$$1 - \phi_p = \frac{d_p x}{d_p x + d_m(1-x)} \qquad [A.3]$$

where

d_p = density of polymer

d_m = density of monomer

A combination of Eqs. (A.1), (A.2) and (A.3) leads to the following relation:

$$T_g = \frac{\alpha_p d_m(1-x)T_{g,p} + \alpha_m d_p x T_{g,m}}{\alpha_p d_m(1-x) + \alpha_m d_p x} \qquad [A.4]$$

The above relation was derived based on the nature of linear free radical polymerization. In this approach, the reacting system is assumed to be a two-phase binary mixture composed of monomer and high polymeric species. This two-phase system might be applicable to a number of radiation curing processes since the free radical

polymerization model is known to produce spatial inhomogeneity such as for the curing of diacrylates as discussed in the section 2.3. Although the quantitative derivation described above with regard to Tg and degree of polymerization might be one of several possible approaches, the consideration of this relationship in the theoretical and experimental aspects may aid in further understanding of time-temperature-energy(TTE) relation of electron beam radiation curing system.

References

1. Kelly, F. N.; Bueche, F. J. *J. Polym. Sci.* 1961, *50*, 549.

2. Kloosterboer, J. G.; Van de Hei, G. J. M.; Boots, H. M. J. *Polym. Comm.* 1984, *25*, 354.

The vita has been removed from the scanned document